# Fault Diagnosis and Fault Tolerant Control of DFIG Based Wind Turbine System

A THESIS SUBMITTED TO THE UNIVERSITY OF MANCHESTER

FOR THE DEGREE OF DOCTOR OF PHILOSOPHY

IN THE FACULTY OF ENGINEERING AND PHYSICAL SCIENCES

2011

By

Qian Lu

School of Electrical and Electronic Engineering

# Contents

Word Count: 35784

# List of Tables



# List of Figures

# Abstract

Wind energy is the fastest-growing energy source in the world nowadays and most wind turbines are installed at remote areas, e.g. country side, off sea-shore. Having a reliable fault diagnosis and fault tolerant control (FTC) scheme is crucial to improve the reliability of wind turbines and reduce expensive repair cost. This PhD work is motivated by this fact and a model-based fault diagnosis and FTC scheme is developed for a doubly fed induction generator (DFIG) based wind turbine system. In particular, an electrical and a mechanical fault scenarios, the DFIG winding short circuit and drive train faults, are considered due to their high occurrence rates.

For the DFIG winding short circuit fault, two mathematical models of DFIG with respect to two types of faults, i.e. single-phase and multi-phase faults, are proposed which can represent all possible cases of the faults. Moreover, the state-space representations of these models are derived by using reference frame transformation theory, such that the faults are represented by some unknown variables or parameters. Based on these models, an adaptive observer based fault diagnosis scheme is proposed to diagnose short circuit faults via online estimation of unknown variables or parameters. By dong this, the fault level and location can be online diagnosed. To consider the effects of model uncertainties, two robust adaptive observers are proposed based on the $H_\infty$ optimization and high-gain observer techniques, respectively, which can ensure the accuracy and robustness of fault estimations. In addition, a self-scheduled LPV adaptive observer is developed with consideration of rotor speed variations, which is suitable for the fault diagnosis under non-stationary conditions. In the context of FTC, a fault compensator is developed based on fault information provided by the fault diagnosis scheme, and it incorporates with a traditional controller (i.e. stator flux oriented controller) to provide an online fault compensation of winding short circuit faults.

For the mechanical drive train fault, the work focuses on FTC rather than diagnosis. Without using an explicit fault diagnosis scheme, an active FTC scheme is directly designed by employing an adaptive input-output linearizing control (AIOLC) technique. It provides a perfect reference tracking of the torque and reactive power no matter whether the fault occurs. In addition, a robust AIOLC is proposed in order to ensure FTC performance against model uncertainties.

# Declaration

No portion of the work referred to in this thesis has been submitted in support of an application for another degree or qualification of this or any other university or other institute of learning.

# Copyright Statement

I. The author of this thesis (including any appendices and/or schedules to this thesis) owns any copyright in it (the "Copyright") and s/he has given The University of Manchester the right to use such Copyright for any administrative, promotional, educational, and/or teaching purposes.

II. Copies of this thesis, ether in full or in extracts, may be made only in accordance with the regulations of the John Rylands University Library of Manchester. Details of these regulations may be obtained from the Librarian. This page must form part of any such copies made.

III. The ownership of any patents, designs, trade marks and any and all other intellectual property rights except for the Copyright (the "Intellectual Property Rights") and any reproductions of copyright works, for example graphs and tables ("Reproductions"), which may be described in this thesis, may not be owned by the author and may be owned by third parties. Such Intellectual Property Rights and Reproductions can not and must not be made available for use without the prior written permission of the owner(s) of the relevant Intellectual Property Rights and/or Reproductions.

IV. Further information on the conditions under which disclosure, publication and exploitation of this thesis, the Copyright and any Intellectual Property Rights and/or Reproductions described in it may take place is available from the Head of the School of Electrical and Electronic Engineering.

# Acknowledgements

I would like to express my gratitude to my first supervisor Dr. Timofei Brekin, who guided me throughout the first and second years of my PhD course. He introduced me to this research field, and gave me thoughtful supervision, sincere advice and tremendous assistance, which helped me lay a solid foundations for my following PhD studies.

I would like to thank my advisor Prof. Hong Wang, who is also my supervisor for the third year of my PhD course. He has guided, tutored, questioned, challenged and cheered me throughout entire time of my PhD study.

Further sincere thanks should be given to Dr. Zhengtao Ding for his enthusiasm and encouragement; Thanks are also given to all my dear friends in Control System Centre, specially Xuejiao. Yang, XiaFei. Tang, for their great supports, valuable discussion, and nice time we spend together.

My special thanks to my dear parents Mingzhe. Lu and Guijian.Gao for their understanding and supports throughout my entire life. I also would like to thank my dear boyfriend Fei He for his patient and supports for all these years. To them I dedicate this thesis.

Finally, I appreciate the financial support from the Scholarships for Excellence funded by CSC (China).

# Nomenclature

## Symbols

In this thesis, the bold letters denote matrices or vectors.

### Electrical & Magnetic Symbols

| | |
|---|---|
| $\mu$ | Fault level parameter (percentage of the shorted turns) |
| $\boldsymbol{\mu}$ | Fault level parameter matrix |
| $\mathbf{f}_x$ | Fault position vector |
| $i$ | Instantaneous phase current |
| $\mathbf{i}$ | Current vector |
| $\tilde{I}$ | Current phasor |
| $v$ | Instantaneous phase voltage |
| $\mathbf{v}$ | Voltage vector |
| $\tilde{V}$ | Voltage phasor |
| $\psi$ | Instantaneous phase flux |
| $\boldsymbol{\psi}$ | Flux vector |
| $\tilde{\Psi}$ | Flux phasor |
| $r$ | Resistance |
| $\mathbf{R}$ | Resistance matrix |
| $L$ | Inductance |
| $\mathbf{L}$ | Inductance matrix |
| $M$ | Mutual inductance |
| $\theta$ | Angle (rotating position) |
| $T$ | Torque |
| $p$ | Number of pole pair |

| | |
|---|---|
| $\omega_s$ | Synchronous speed |
| $\omega_r$ | Electrical rotor speed of generator |
| $\omega_{wt}$ | Wind turbine speed |
| $\omega_g$ | Mechanical rotor speed of generator |
| $f$ | Frequency |
| $P$ | Instantaneous active power |
| $Q$ | Instantaneous reactive power |
| $\upsilon_w$ | Wind speed |
| $\upsilon_{w\_rat}$ | Rated wind speed |
| $\upsilon_{w\_cin}$ | Cut in wind speed |
| $\upsilon_{w\_cout}$ | Cut out wind speed |
| $\rho$ | Air density |
| $R_{wt}$ | Wind turbine radius |
| $\lambda$ | Tip-speed ratio |
| $\beta$ | Blade pitch angle |
| $J$ | Moment of inertia |
| $B$ | Torsion damping coefficient |
| $N_g$ | Drive train gear ratio |
| $K$ | Stiffness |
| $\mathbf{T}_{32}$ | Transformation matrix (from abc to dq) |
| $\mathbf{T}_{23}$ | Inverse transformation matrix (from dq to abc) |
| $\mathbf{I}_n$ | Identity matrix with dimension $n$ |
| $\mathbf{0}_{n\times m}$ | Zero matrix with dimension $n\times m$ |

| | |
|---|---|
| $j$ | $\sqrt{-1}$ |

## Mathematical Symbols

| | |
|---|---|
| $\mathbb{R}$ | Space of real numbers |
| $\mathbb{R}^n$ | N-dimensional real space |
| $\mathbb{R}^{n\times n}$ | n$\times$n dimensional real space |
| $A^T$ | Transpose of vector or matrix $A$ |
| $A^{-1}$ | Inverse of matrix $A$ |
| $\lvert A\rvert$ | Absolute value of number $A$ |
| $\lambda_{\max}(A)$ | Maximum eigenvalue of matrix $A$ |
| $\lambda_{\min}(A)$ | Minimum eigenvalue of matrix $A$ |
| $A_i$ | i-th element of vector $A$ |
| $\hat{x}(t)$ | Estimate of variable $x(t)$ |
| $\lVert T(s)\rVert_\infty$ | $H_\infty$ norm of transfer function $T(s)$ |
| $\lVert x(t)\rVert$ | $L_2$ norm of signal $x(t)$ |
| $\sup f(x)$ | Supreme of function $f(x)$ |
| $\frac{\partial(\bullet)}{\partial\theta}$ | Partial differential operator |
| $\times$ | Cross product |

# Subscripts

| | |
|---|---|
| $s$ | Stator |
| $r$ | Rotor |
| $m$ | Mutual |
| $a, b, c$ | abc reference frame |
| $d, q$ | dq reference frame |

| | |
|---|---|
| $u$ | Un-faulted quantities |
| $f$ | Faulted quantities |
| $\sigma$ | Leakage |
| $g$ | Generator |
| $wt$ | Wind turbine |
| $w$ | Wind |
| $rated$ | Rated value |
| $ls$ | Low speed shaft |
| $hs$ | High speed shaft |

## Superscripts

| | |
|---|---|
| $h$ | Healthy component |
| * | Reference value |
| +, - | Positive and negative sequence components |

## Abbreviations

| | |
|---|---|
| VSCF: | Variable Speed Constant Frequency |
| FDD: | Fault Detection and Diagnosis |
| FTC: | Fault Tolerant Control |
| MCSA: | Machine Current Signature Analysis |
| VFC: | Variable Frequency Converter |
| DFIG: | Doubly Fed Induction Generator |
| PNSC: | Positive Negative Sequence Components |
| UIO: | Unknown Input Observer |
| LS: | Least Square |
| LMS: | Least Mean Square |
| RLS: | Recursive Least Square |
| LIT: | Linear Time Invariant |

| | |
|---|---|
| LPV: | Linear parameter varying |
| SPR: | Strictly Positive Real |
| PI: | Proportional Integer |
| ARE: | Algebraic Riccati Equation |
| LMI: | Linear Matrix Inequality |
| AIOLC | Adaptive input-output linearizing control |

# Publications

## Journal Papers:

1. Q. Lu and T. Breikin, “Fault detection for stator inter-turn short circuit in doubly fed induction generators using adaptive observers,” *International Journal of Advanced Mechatronic Systems*, vol. 3, no. 1, pp. 44-53, 2011.

## Conference Papers:

1. Q. Lu and T. Breikin, “Observer based fault detection for stator inter-turn short circuit in wind turbine DFIGs,” *International Conference on Modelling identification and Control*, Okayama, Japan, July 17-19, 2010.

2. Q. Lu, T. Breikin, and H. Wang, “Modelling and fault diagnosis for DFIGs with multi-phase inter-turn short circuit,” *International Conference on Advanced Mechatronic Systems*, Zhengzhou, China, August 11-13, 2011.

3. Q. Lu, T. Breikin, and H. Wang, “Modelling and fault diagnosis of Stator inter-turn short circuit in doubly fed induction generators,” *18$^{th}$ IFAC World Congress*, Milano, Italy, August 28-September 2, 2011.

# 1. Introduction

## 1.1. Overview

Wind energy, considered as a nonpolluting, renewable and economical energy, has experienced a rapid increase in its share in power generation all over the world. Particularly in the United States and Europe, wind power capacity has grown at a rate of 20%-30% per year over the past decade [11]. In order to capture the maximum wind power, many new wind farms have employed DFIG for power generation, which offers many advantages over other generators, such as variable speed constant frequency (VSCF) operation, low mechanical stresses, high system efficiency [1], [3].

Wind turbines are usually constructed in mountainous or off-shore regions with harsh environmental conditions. Because of the temperature variation, material corrosion, mechanical stress, and voltage stress, etc., faults may occur at any components of wind turbine systems. Hence a reliable online fault detection and diagnosis (FDD) system is requisite to prevent further failures and deteriorating other parts of the wind turbine via early detection [12]. In addition, most existing control algorithms of DFIG based wind turbine systems are designed based on the nominal conditions. Nevertheless, when a fault occurs, the system performances could be severely deteriorated by using standard nominal control scenario. Therefore, introducing FTC scheme is important to maintain appropriate operations from the time a fault is detected to the next planned service [14].

It has been reported that most failures in wind turbine systems are linked to two components: the DFIG and drive train [13], [15]. Additionally, the majority of the DFIG failures are caused by winding faults [16]. Therefore, in this PhD study, we mainly focus on these two types of faults (i.e. DFIG winding and drive train faults) and aims to develop FDD and FTC schemes to diagnose and tolerate these faults.

Within the last two decades, the theoretical background of fault diagnosis algorithms

has been established, which has been widely applied to cope with faults in many industrial systems including wind turbine systems [12], [22], [18]-[31]. The common approaches can be classified into three categories: signal-based approach, knowledge-based approach, and model-based approach. Signal-based approaches are the most commonly used technique in wind turbine systems [12]. The approaches such as motor current signature analysis (MCSA) [70], [71] and vibration monitoring [17] [81], have been extensively used to diagnose electrical and mechanical faults in the generator, drive train, and other important components in wind turbine systems. However, these signal-based approaches require explicit priori knowledge of the relationship between signal symptoms (e.g. spectrum) and faults, and most of existing studies mainly focus on fault detection rather than diagnosis. In addition, most traditional signal-based methods (e.g. MSCA) are not suitable for the non-stationary analysis [14]. The knowledge-based approaches employ the historical data in both nominal and faulty conditions to train qualitative models built by artificial intelligent techniques (e.g. neural network, or fuzzy system), in order to capture the fault patterns, The research in this area is very active recently and it has many applications in wind turbine systems [96], [97]. However, it only focuses on identifying the current system condition, without necessarily providing detailed information of the faults. As long as an accurate mathematical model can be constructed, model-based approach is often considered as a preferable method, which allows to diagnose the fault (i.e. level and location) quantitatively and it can be applied to both stationary and non-stationary conditions [23]. The latter characteristic is especially suitable for wind turbine systems, as it predominately operates under non-stationary conditions [70]. For this reason, in this PhD work, we aim to develop a model-based FDD scheme with application to DFIG based wind turbine systems.

In the field of model-based FDD, a large amount of results have been reported recently with different applications [18]-[20], [26]-[33]. Many different approaches have been proposed such as parity relation, parameter estimation, state estimation, and joint state/parameter estimation based approaches. Parameter estimation is considered as a direct and simple approach, whenever the fault can be reflected through parameter

changes (e.g. multiplicative fault) [27]. However, sometimes the unknown states of the post-fault system are also required to reconstruct or modify the controller in order to tolerate the fault. Therefore, a combination of state and parameter estimation based approach is probably more appropriate in the context of both fault diagnosis and fault tolerance. Some recent results of fault diagnosis by using adaptive observers have been proposed in [43]-[46], [49], [78]. This approach belongs to the field of joint state and parameter estimation, which is able to provide an online estimation of constant or slowly varying faults, and simultaneously estimate system states for the purpose of control reconfiguration. In this PhD study, we attempt to employ adaptive observer techniques to diagnose DFIG winding short circuit faults, and also use the estimated states to reconstruct the controller so as to compensate the effects of faults.

In many cases, the degradation of system performance in faulty condition can be avoided by applying appropriate FTCs. In general, FTC can be achieved by two approaches: the passive approach and the active approach [51]. In passive approach, a fixed controller is applied throughout the normal and faulty conditions, which can maintain acceptable performance against a limited numbers of faults. However, as the number and level of faults increase, the passive controllers become more conservative, and attainable control performance may be deteriorated [55]. In active approaches, faults are compensated either by switching to a pre-designed control algorithm or by online synthesizing a new control algorithm. For the latter method, adaptive control is commonly employed, which has been extensively used to accommodate the fault [54], [55], [60]-[64]. In comparison with other methods, it does not heavily rely on the fault diagnosis decision and no explicit knowledge of the faults is needed to reconstruct the controller. In this thesis, the active FTC approach is employed to compensate the DFIG winding short circuit and drive train faults. The first fault is compensated based on the information from fault diagnosis systems, and then the controller is switched from the nominal to faulty mode. The second one is accommodated by a parameter adaptive controller which can ensure the closed-loop system performance in the presence of fault-induced parameter variations.

## 1.2. Thesis Objectives

The primary objective of this work is to develop an online model-based fault diagnosis and FTC scheme for DFIG based wind turbine systems. In particular, two fault scenarios are considered: DFIG winding short circuit fault and drive train fault. To facilitate the design of model-based fault diagnosis and FTC schemes, and also to provide a simulation environment to test the schemes, a mathematical model of DFIG based wind turbine system subject to such two fault scenarios are expected to be developed. The detailed objectives can be listed as follows.

1. Investigate the characteristics of DFIG winding short circuit faults, and develop a mathematical model of the DFIG which can generally represent all possible scenarios of this fault.
2. Parameterize the model in terms of DFIG winding short circuit faults and develop a model-based fault diagnosis scheme in order to online estimate the fault-related parameters.
3. Improve the robustness of developed diagnosis schemes against model uncertainties.
4. Develop a FTC scheme for the DFIG winding short circuit fault based on the information obtained from fault diagnosis scheme.
5. Build a mathematical model of drive train system, and parameterize this model in terms of drive train fault.
6. Based on this model, develop a FTC strategy to accommodate drive train fault and maintain closed-loop performance.
7. Enhance the robustness of the developed FTC scheme against model uncertainties.

## 1.3. Thesis Contributions

The main contributions of this PhD work are summarized as follows:

1. *Modeling of DFIG with winding short circuit faults.*

   Two mathematical models of the DFIG with respect to winding short circuit faults

are proposed. One is used to represent the fault in a single phase (i.e. single-phase short circuit fault), and the other is used to represent the faults in several phases simultaneously (i.e. multi-phase short circuit fault). By using these two models, the short circuit faults at any levels and in any phases can be quantitatively represented. In addition, the state-space representations of these two models are developed by using the reference frame transformation theory, which largely facilitate the digital simulation and the development of fault diagnosis schemes. Equivalent circuits of DFIG with respect to short circuit faults are also derived from the proposed mathematical models, based on which the properties of the short circuits are analyzed. These proposed models provide a base for the studies of model-based fault diagnosis and FTC approaches, and also provide a model test bench for evaluating other approaches.

2. *Fault diagnosis and compensation of winding short circuit faults*

Based on these proposed fault models, an adaptive observer based fault diagnosis scheme is proposed which allows online diagnosing the fault level and location. To consider the effects of model uncertainties, two robust adaptive observers are proposed by using $H_\infty$ optimization and high-gain observer techniques, respectively. These observers can ensure accurate fault diagnosis in the presence of model uncertainties. In addition, a self-scheduled LPV adaptive observer is developed with consideration of the rotor speed variation, which is suitable for the fault diagnosis under non-stationary conditions. This characteristic is especially significant for the wind turbine system as it predominantly operates under such conditions.

Based on the proposed fault diagnosis scheme, a fault compensator is developed and integrated with a traditional control algorithm (i.e. stator flux oriented control), which is able to provide online compensation of any possible winding short circuit faults, regardless their level and location. The simulation studies show that this fault compensator can highly reduce the oscillations in the electromagnetic torque, output power and some other electrical quantities in the presence of short circuit faults.

3. *FTC of DFIG based wind turbine system subjected to drive train fault*

An active FTC scheme is proposed based on adaptive input-output linearizing

control technique, which can ensure perfect reference tracking of the torque and reactive power in the presence of drive train fault. In addition, a robust adaptive control algorithm is proposed, which can ensure desired control performance against model uncertainties.

## 1.4. Thesis Outline

In this section, a general overview of this thesis is presented.

Chapter 2: **Literature Review** gives a brief introduction to the field of fault diagnosis and FTC. Additionally, their applications to wind turbine system are investigated. This chapter starts with Section 2.1 on a general description of DFIG based wind turbine system. Section 2.2 summaries the available methods used in the field of fault diagnosis and FTC. Section 2.3 introduces the current status and some existing methods of fault diagnosis and FTC in wind turbine systems.

Chapter 3: **Modeling of DFIG with winding short circuit Fault** proposes two mathematical models of DFIG for the single-phase and multi-phase short circuit faults respectively. These models are initially developed in the natural a-b-c coordinate, and then transformed into the d-q coordinate. Finally, the equivalent circuit diagrams of DFIG with respect to short circuit faults are provided based on which an explicit analysis of the fault characteristics and its effects on the DFIG behaviour is provided.

Chapter 4: **Diagnosis of Single-Phase Short Circuit Fault in DFIG** proposes an adaptive observer based fault diagnosis scheme for the short circuit fault in a single phase. In Section 4.2, a common sinusoidal signal decomposition technique, i.e. sequence component decomposition, is introduced. In Section 4.3, by using this technique, the single-phase fault model proposed in Section 3.2 is transformed into a state-space model representation and the fault is formulated into an additive fault represented by two unknown variables. In Section 4.4, a conventional adaptive observer is firstly applied to estimate these unknown variables so as to diagnose the fault. In Section 4.5, the effects of model uncertainties are considered and a robust adaptive observer is proposed based on $H_\infty$ optimization technique. In Section 4.6, the

effects of the speed variation are considered and a self-scheduled LPV adaptive observer with guaranteed $H_\infty$ performance is proposed which can cope with both model uncertainties and speed variations.

Chapter 5: **Diagnosis of Multi-Phase Short Circuit Fault in DFIG** proposes a fault diagnosis scheme for short circuit faults in multiple phases simultaneously. Similar to Chapter 4, it is also based on adaptive observers. A state-space representation of the DFIG model with respect to multi-phase fault is presented in Section 5.2. In this model, faults are quantitatively represented by a set of unknown model parameters. In Section 5.3, a conventional adaptive observer is firstly applied to estimate the unknown parameters so as to diagnose the fault. In Section 5.4, a modified adaptive observer is designed to relax the SPR condition required by the conventional adaptive observer. In Section 5.5, the effects of model uncertainties are considered and a robust adaptive observer is proposed based on high gain estimation technique. In Section 5.6, the effects of speed variations are considered and a LTV adaptive observer is designed to cope with speed variations.

Chapter 6: **Fault Compensation for Short Circuit Fault in DFIG Wind Turbine Systems** proposes a fault compensator to compensate the effects of winding short circuit faults in a closed-loop controlled DFIG wind turbine system. This fault compensator is based the adaptive observer proposed in Chapter 5. In Section 6.2, a traditional control strategy: stator flux oriented control, is firstly introduced. And then in Section 6.3 a fault compensator is developed and incorporates with this traditional control strategy to maintain a continued operation of DFIG in the presence of winding short circuit faults.

Chapter 7: **Adaptive Nonlinear Control of DFIG Wind Turbine System with Drive Train Fault** proposes a FTC strategy for DFIG wind turbine system to tolerate the drive train fault. In Section 7.2, a one-mass model of the drive train is presented and the faults are considered as the unexpected change of the parameter in this model. In Section 7.3, an adaptive input-output linearizing control algorithm is developed for the adaption of the parameter variations and the decoupled control of the torque and reactive power. In Section 7.4, a robust control algorithm is developed to ensure the

desired reference tracking of the torque and reactive power in the presence of model uncertainties.

Finally, concluding remarks are made in Chapter 8.

# 2. Literature Review

This chapter gives a brief introduction to the field of fault diagnosis and FTC. Additionally, its application to wind turbine systems is investigated. This chapter starts by Section 2.1 on a general description of DFIG based wind turbine systems. Section 2.2 summaries the available methods used in the field of fault diagnosis and FTC. Section 2.3 introduces the current status and some existing methods of fault diagnosis and FTC in wind turbine systems.

## 2.1. DFIG Based Wind Turbine System Description

A brief description of DFIG based wind turbine system is given in this section. Figure 2.1 presents the basic configuration of a DFIG based wind turbine system [1]. The wind turbine is connected to DFIG through a drive train system, which contains high and low speed shafts, bearings and a gearbox. The DFIG is constructed from a wound rotor induction machine [2]. Its stator is directly connected to the grid while its rotor is fed by a bi-directional variable frequency converter (VFC). The generator and converters are protected by a crowbar from over-current by disconnecting the rotor side converter. The main components of the DFIG based wind turbine system, i.e. wind turbine, DFIG, driven train and VFC, which will be introduced in the following subsections, respectively.

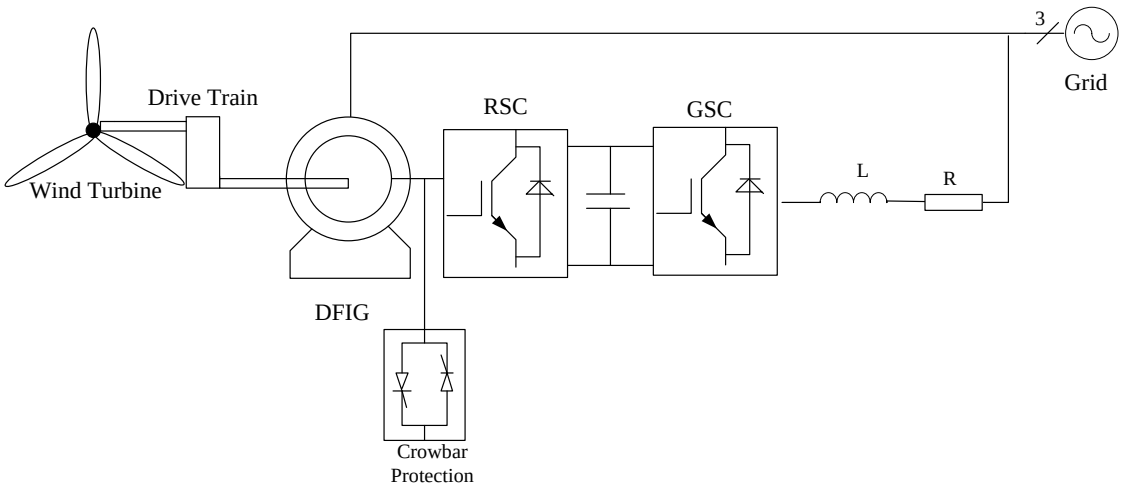


Figure 2.1. Configuration of a DFIG wind turbine system.

### 2.1.1. Wind Turbine

The wind turbine is the key device in wind power generation systems, whose basic functionality is to transfer the wind power into the mechanical power on the rotor shaft. The amount of captured wind power is controlled by adjusting blade angle and rotational speed of wind turbine.

The wind turbine is designed to perform different behaviours on different regions of the wind speed [3]. The wind turbine starts running as soon as wind speed exceeds the lower bound (i.e. cut-in speed), usually around 5m/s. While when the wind speed exceeds the upper bound (i.e. cut-out speed) usually around 25m/s, the wind turbine stops running to avoid damages. Additionally, when the wind speed is higher than a certain value (i.e. rated speed) at which the generator achieves its rated power, the blade angle of wind turbine is changed to release a part of excess wind energy in order to protect the generator. The wind turbine mostly operates at the region between cut-in speed and rated speed. At this region the mechanical power captured from the wind can be calculated by the following formula [4].

$$P_{wt}(\upsilon_w) = \frac{1}{2}\rho\pi R_{wt}{}^2 C_p(\lambda,\beta)\upsilon_w{}^3 \tag{2.1}$$

where, $\rho$ is the air density. $R_{wt}$ is the wind turbine radius. $\upsilon_w$ is the wind speed. $C_p(\lambda,\beta)$ is called the power coefficient, which is a function of the tip-speed ratio ($\lambda$)

and the blade pitch angle ($\beta$). The power coefficient is given by the wind turbine manufacturer depending on the blade design. According to Betz's law [7], the ideal power coefficient is 59%. However, in practice, a wind turbine with good blade profile can only reach to 50%. The output power of wind turbine on different regions of wind speed is given as follows:

$$P_{wt} = \begin{cases} P_{rated} & ;\ \upsilon_{w\_rat} \le \upsilon_w \le \upsilon_{w\_cout} \\ P_{wt}(\upsilon_w) & ;\ \upsilon_{w\_cin} \le \upsilon_w \le \upsilon_{w\_rat} \\ 0 & ;\upsilon_w \le \upsilon_{w\_cin} \text{ and } \upsilon_w \ge \upsilon_{w\_cout} \end{cases} \tag{2.2}$$

where $P_{rated}$, $\upsilon_{w\_rat}$, $\upsilon_{w\_cin}$ and $\upsilon_{w\_cout}$ are the rated power, rated wind speed, cut-in wind speed and cut-out wind speed, respectively.

In Chapter 6, the characteristic of the output power is further investigated, based on which an optimum power control strategy (i.e. Maximum Power Point Tracking) is introduced and employed to the control of DFIG based wind turbines.

### 2.1.2. DFIG

DFIG is the most commonly used generator in wind power generation systems [1]. Since it is constructed from a wound rotor induction machine, its stator and rotor both have winding structures. The stator windings are directly connected to the three-phase grid, while the rotor windings are connected to the rotor side converter by slip rings and brushes. A voltage is injected into the rotor circuit through slip rings in order to control the rotational speed of the DFIG [2]. The DFIG operates in two speed regions: super-synchronous and sub-synchronous regions [8], which are decided by the rotor voltages. The effects of the rotor voltages can be observed from the torque-slip characteristic plot as given in Figure 2. In this figure, 'pu' stands for per unit. Curve (1), (2) and (3) correspond to zero, negative and positive rotor voltages, respectively. Assume that DFIG initially operates at synchronous speed with slip $s = 0$. The speed can be increased to super-synchronous speed (A point) by injecting a negative rotor voltage, or decreased to sub-synchronous speed (B point) by injecting a positive rotor voltage.

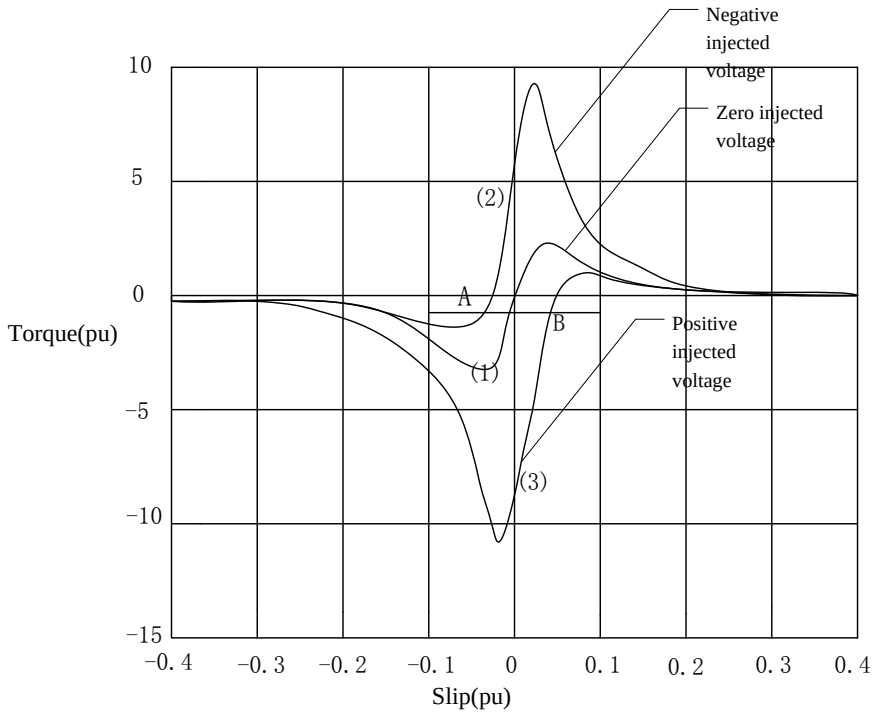


Figure 2.2. Torque-Slip Characteristic of the DFIG.

The power flow of DFIG at super-synchronous and sub-synchronous regions is given in Figure 2.3. As it is shown, when DFIG operates at super-synchronous region, the rotor produces power and the power is delivered to the grid through converters. On the other hand, if DFIG runs at sub-synchronous region, the rotor absorbs power and a part of stator power enters into the rotor circuits. Neglecting the losses, the power delivered by the stator and rotor can be calculated as [1]

$$P_r \approx -sP_s \tag{2.3}$$

$$P_s \approx \frac{P_{grid}}{1-s} \tag{2.4}$$

where $P_s$ is the power delivered by the stator, $P_r$ is the power delivered by the rotor, $P_{grid}$ is the total power generated and delivered to the grid. $s$ is the slip.

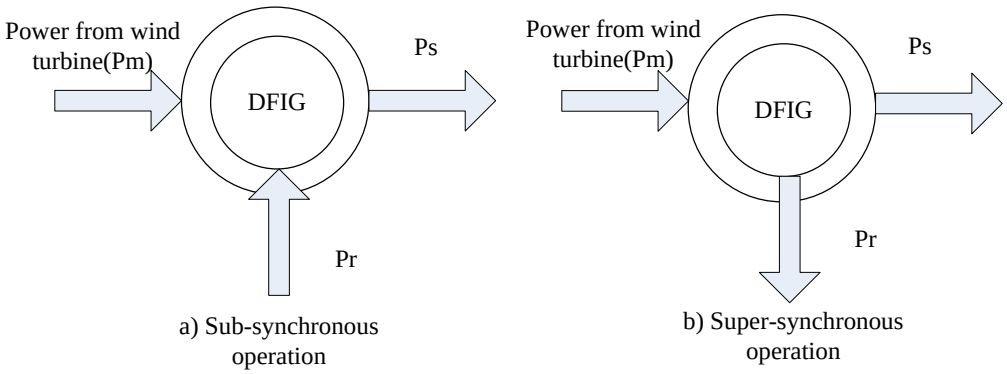


Figure 2.3. Power flow of DFIG.

In this PhD work, we focus on investigating the behaviours of DFIG in the presence of a common electrical fault, i.e. winding short circuit fault. In this following chapters, a mathematical model of DFIG subjected to this type of fault is developed, and based on this model the fault diagnosis and FTC schemes are proposed, respectively in Chapter 4, 5, and 6.

### 2.1.3. Drive Train

The drive train is an important component of DFIG wind turbine systems. It connects wind turbine with DFIG and transfers the aerodynamic mechanical power to DFIG. The drive train system consists of the low and high speed shafts, gearbox, bearings and other mechanical components, which can be represented a two-mass model as shown in Figure 2.4 [6]. In this figure, the big mass is used to represent the low speed shaft, and the small mass is used to represent the high speed shaft. The connecting the resilient shaft is modeled as a spring-damper system. The gearbox is modeled as a gear ratio without any loss. Before presenting the dynamic equations of the whole drive train system, the motion equations of these four main components are given individually.

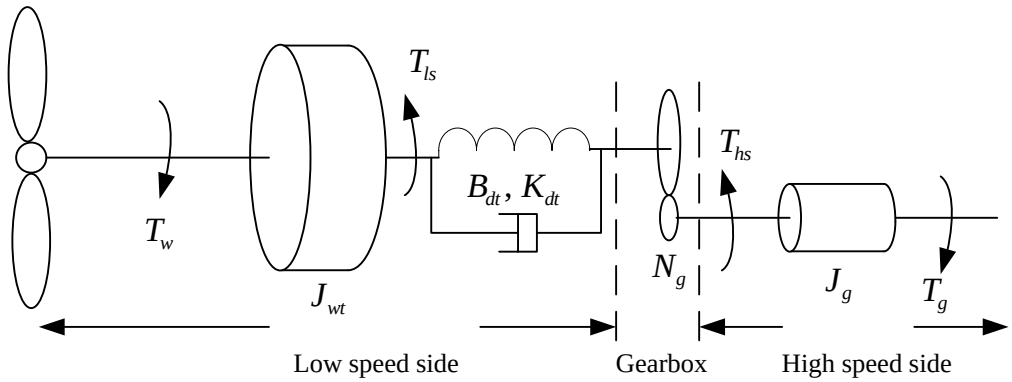


Figure 2.4. Two-mass model of the drive train.

The dynamics of the low speed shaft (bigger mass) is expressed as

$$J\ \dot{\omega}_{wt}(t) = T_{wt}(t) - T_{ls}(t) \tag{2.5}$$

where $J_{wt}$ is the moment of inertia of the low speed shaft.

$T_{wt}(t)$ is the aerodynamic torque from the wind turbine.

$T_{ls}(t)$ is the torque acting the on the low speed shaft.

$\omega_{wt}(t)$ is the angular speed of the low speed shaft.

The dynamics of the high speed shaft (small mass) is expressed as

$$J_g \dot{\omega}_g(t) = T_{hs}(t) - T_g(t) \tag{2.6}$$

where $J_g$ is the moment of inertia of the low speed shaft.

$T_g(t)$ is the electromagnetic torque from the generator.

$T_{hs}(t)$ is the torque acting the on the high speed shaft.

$\omega_g(t)$ is the mechanical angular speed of the high speed shaft, or called generator rotor speed.

The behaviour of the gearbox is modeled as a gear ratio defined as below.

$$T_{hs}(t) = \frac{T_{ls}(t)}{N_g} \tag{2.7}$$

where $N_g$ is the drive train gear ratio.

The dynamics of the resilient shaft (spring-damper system) can be expressed as

$$T_{ls}(t) = K_{dt}\Delta\theta(t) + B_{dt}\Delta\dot{\theta}(t) \tag{2.8}$$

where $\Delta\theta(t) = \theta_{wt}(t) - \frac{\theta_g(t)}{N_g}$

$B_{dt}$ is the torsion damping coefficient of the shaft.

$K_{dt}$ is the torsion stiffness of the shaft.

$\theta_{wt}(t)$ is the angle of the low speed shaft.

$\theta_g(t)$ is the angle of the high speed shaft.

Above equations are reorganized to obtain the dynamic equations for the whole drive train system.

$$\begin{cases} J_{wt}\dot{\omega}_{wt}(t) = T_{wt}(t) - K_{dt}\Delta\theta(t) - B_{dt}\omega_{wt}(t) + \frac{B_{dt}}{N_g}\omega_g(t) \\ J_g\dot{\omega}_g(t) = \frac{K_{dt}}{N_g}\Delta\theta(t) + \frac{B_{dt}}{N_g}\omega_{wt}(t) - \frac{B_{dt}}{N_g^2}\omega_g(t) - T_g(t) \\ \Delta\dot{\theta}(t) = \omega_{wt}(t) - \frac{\omega_g(t)}{N_g} \end{cases} \tag{2.9}$$

This first order differential equation group can represent the dynamics of the drive train system. In Chapter 7, a simpler model, i.e. one-mass model, is presented by only considering the dynamic of the high speed dynamics. Based on this model, a fault tolerant control algorithm is developed to control the DFIG wind turbine in the presence of drive train fault.

### 2.1.4. Variable Frequency Converter (VFC)

The VFC consists of two AC/DC IGBT based voltage source converters: grid side converter (GSC) and rotor side converter (RSC), connected back to back by a DC capacitor. GSC is used to maintain the DC link voltage constant and provide a channel for the power on rotor side [5]. RSC is used to yield voltage required by the DFIG controller. The configuration of VFC is given in Figure 2.5. As it is shown, the GSC and RSC both consist of six insulated gate bipolar transistors (IGBT). Pulse width

modulation (PWM) topology is implemented to control the gates of IGBT in order to change the amplitude and frequency of the output voltages [10].

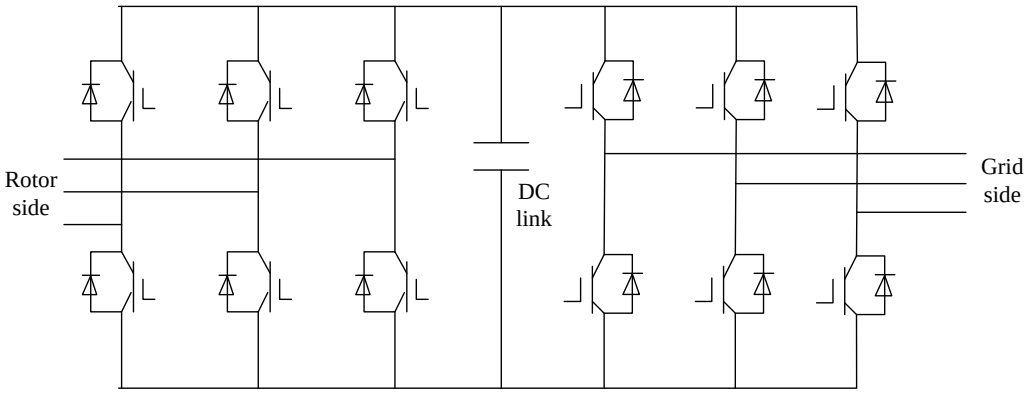


Figure 2.5. Configuration of VFC.

## 2.2. Fault Scenarios in Wind Turbine System

Wind turbines are usually built in mountainous and off-shore regions, where the working environment is very harsh. Because of the temperature variation, material corrosion, mechanical stress, and voltage stress, etc., faults can occur at any components of wind turbine systems. An overview of main components to be monitored is shown in Figure 2.6. These components can be generally classified into the following sub-systems: rotor blades, drive train, generator, yaw system, tower, and sensors.

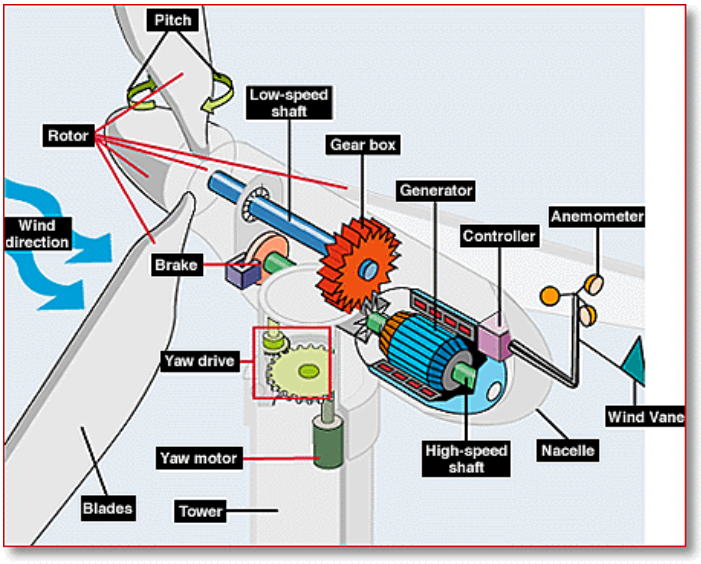


Figure 2.6. Main components of the wind turbine system.

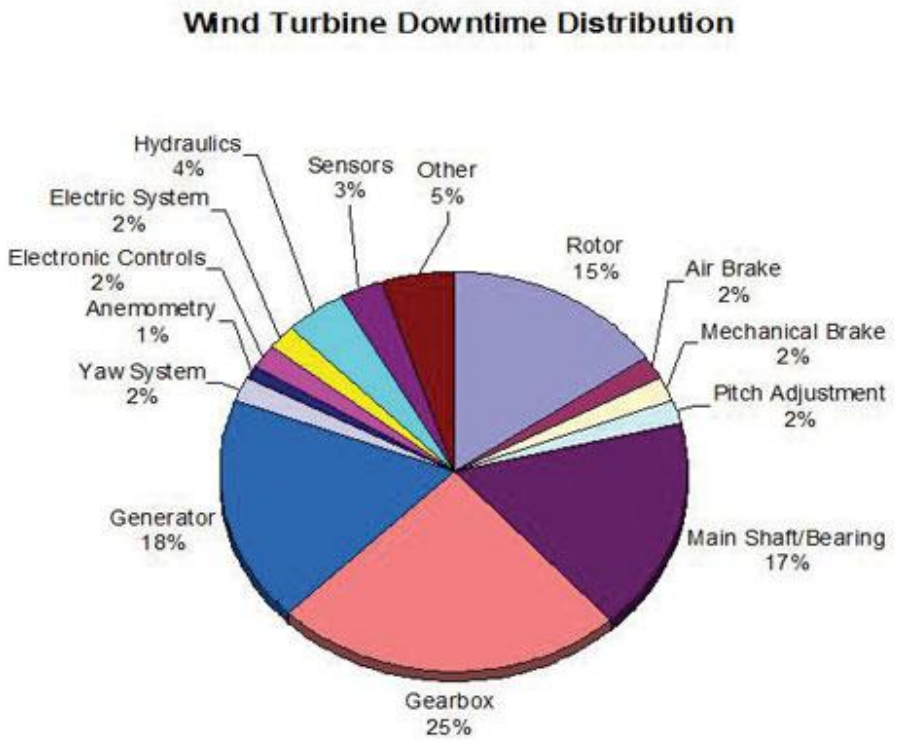


Figure 2.7. Wind turbine downtime distribution (extracted from [15]).

An investigation of the failure statistics from four wind farms: two separate wind farms from Sweden, one from Finland, and one from Germany is presented in [15]. The downtime distribution of the wind turbine system is given in Figure 2.7. According to their studies, faults in the generator and drive train (includes gear box, main shafts, and bearings) are the most crucial and widely observed failures, which dominate over 60% of the downtime in wind turbine systems.

It is also known that a major cause of generator failures is the windings short circuit, or called the inter-turn short circuit in some literatures [91], [94]. It has been stated in [16] that over 38% failures of the generator are caused by this type of fault. This fault is difficult to be detected, especially in the initial stage. However, undetected winding short circuit faults may lead to a catastrophic fault and bring an irreversible damage to the generator. Therefore, in recent years, a large amount of research efforts are attracted to study this type of electrical fault.

In this PhD study, the generator winding short circuit and drive train faults are explicitly investigated due to their high occurrence rates, for which model-based fault diagnosis and FTC schemes are developed in the following chapters.

## 2.3. Fault Diagnosis and Fault Tolerant Control Techniques

### 2.3.1. Fault Diagnosis

Due to the importance of safety and reliability in industrial systems, fault detection and diagnosis (FDD) algorithms and their industrial applications have been investigated extensively over the past two decades. The main tasks of a FDD algorithm consist of *fault detection* (indicate whether a fault occurs in the monitored system), *fault isolation* (determine the exact location of the fault), and *fault identification* (determine the shape and size of the fault) [27]. The last two tasks are usually referred as fault diagnosis according to [29]. Based on this classification, FDD often represent the functions including fault detection and diagnosis, or simply called fault diagnosis in some literatures [31].

Many different FDD approaches have been developed, which are summarized in some survey literatures [23]-[25]. According to different properties and applications, these approaches can be generally classified into three main categories:

- Signal-based approach.
- Knowledge-based approach.
- Model-based approach.

In this thesis, we focus on the model-based approach, as it is more suitable for online and non-stationary FDD. Therefore, the theoretical background of only the last approach is provided in later this chapter. However, a brief review of applications in wind turbines of all the three approaches are discussed in Section 2.4.1, since the first two approaches are still commonly used techniques in practice.

In model-based approaches, an accurate mathematical model is required to represent the system. Such a model runs in parallel to the system and is supplied with the same input signals. In an ideal situation, the model variables can well track the real system variables in the absence of fault and present an obvious derivation when fault occurs.

This derivation is measured in terms of a residual, which is obtained by subtracting the measured system variables with their estimates provided by the model. The residual contains important information with respect to the fault. The fault detection and diagnosis can be then achieved by observing and analyzing this residual. A schematic description of the model-based FDD scheme is given in Figure 2.8, which is accomplished by two steps: the residual generation and residual evaluation [32].

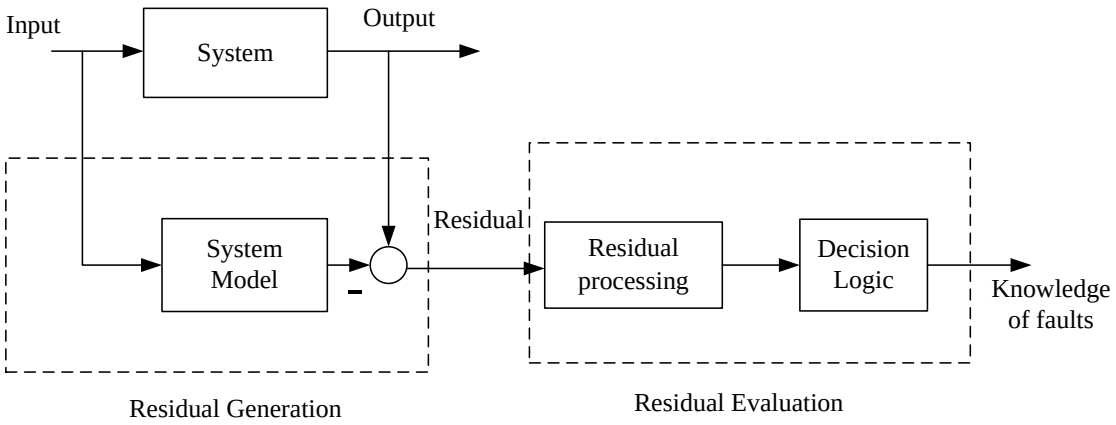


Figure 2.8. Schematic description of the model-based FDD.

Different model-based FDD approaches have been developed in the past two decades. The survey papers [18], [19], [23], [26]-[30] by Isermann, Frank, Patton, etc., provide a good overview of the development and achievements in the field of model-based FDD, and the book by Isermann [31] presents a clear framework of the model-based FDD. Four most commonly used approaches are

- State estimation (or called observer based approach)
- Parity relation
- Parameter estimation
- Joint state and parameter estimation

Based on this classification, several important and common model-based FDD algorithms are classified and summarized in Figure 2.9.

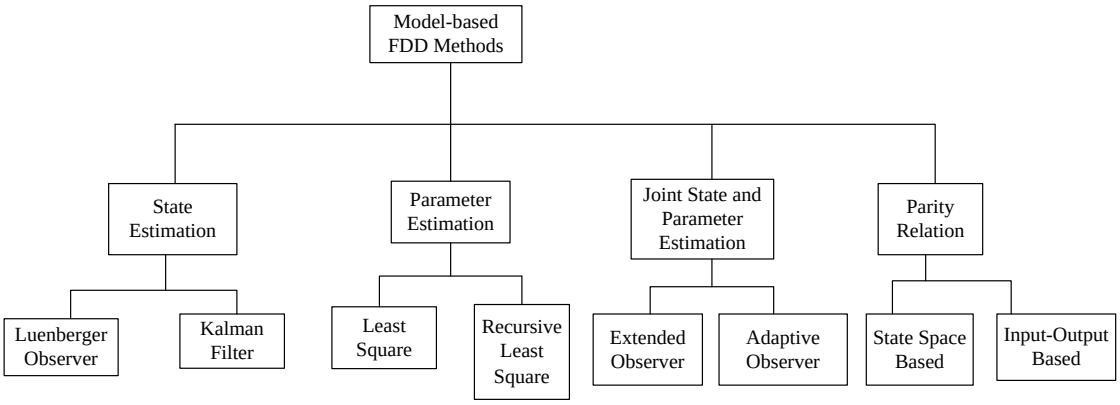


Figure 2.9. Classification of the model-based FDD approaches.

For the purpose of fault detection only, the first two approaches (i.e. state estimation, parity relation) are commonly used, which use the residual signal as fault indicator. As mentioned previously, this is simply due to that the residual remains at zero in the absence of fault, while runs away from zero when fault occurs. However, actually the residual is not only affected by fault, but also influenced by the model uncertainties, measurement noise and external disturbances. For these reasons, researchers have sought to develop a residual sensitive to fault but insensitive to disturbances. The dominate approaches can be divided into two classes. One strategy is to decouple the residual signals from the disturbances [33], [34]. The unknown input observer (UIO) is a typical method belongs to this sort of approaches [20], [21], [35]. The other sort of approaches aim at attenuating the effects of the disturbances on the residuals, which is usually applied to the situation that complete decoupling is impossible. The typical method is $H_\infty$ filter [36], [37].

Compared to fault detection, fault diagnosis is a much more challenging task, as it requires further estimating and quantifying the location and magnitude of the faults apart from simply reporting them [78]. The last two approaches listed above (i.e. parameter estimation, joint parameter/state estimation) are commonly used in the context of fault diagnosis, while they are applicable whenever the fault can be reflected through the parameter changes [38] (e.g. multiplicative fault). The basic idea of these two approaches is to estimate some fault-related parameters so as to obtain the information of the faults (i.e. location and level) by analyzing these estimated parameters. This idea is further illustrated as follows [39].

1. Construct a parametric model of a system under study.
2. Determine the relationship between the model parameter vector $\theta$ and physical parameter vector $p$.

$$\theta = f(p) \tag{2.10}$$

3. Estimate the model parameter vector $\theta$ using the input-output measurements.
4. Calculate the physical parameter vector from the estimated $\theta$.

$$p = f^{-1}(\theta) \tag{2.11}$$

5. Compare the $p$ with its nominal values, and obtain the deviation $\Delta p$.
6. Determine the fault location and size by exploiting the relationship between fault and $\Delta p$.

Some classical system identification techniques [27], [31], e.g. least squares (LS), least mean square (LMS), are commonly used to estimate unknown parameters so as to diagnose the fault. When online fault diagnosis is required, some recursive algorithm, e.g. recursive least squares, can be employed can be directly applied for fault diagnosis. However, such approaches are often implemented to the discretized input-output models and assume all the state variables are known. For a state-space model with unknown state variables, the parameter estimation problem becomes much more difficult. In such situations, two methods more suitable for the state-space models, i.e. extended and adaptive observers, are widely used. These methods belong to the field of the joint state and parameter estimation based approaches, which can simultaneously estimate the parameters as well as the unknown states online. Since sometimes the state variables of the system are required to reconstruct the controller after the fault occurs for the purpose of fault tolerance, these methods can not only provide the functionality of fault diagnosis, but also incorporate with the controller in the context of fault tolerance.

In extended observer based approaches, the unknown parameters (used to represent the faults) are regarded as extra states of the system, and then a state observer is

constructed to estimate all the extended states including the unknown parameters. A large amount of work on the extended observer has been reported in literatures [40]-[41]. In [40], an extended Kalman filter is applied to estimate the unknown parameters as well as the states for a linear system. In [41], descriptor observer approach is applied for a multivariable system simultaneously subjected to the actuator fault, senor fault, input disturbances and measurement noises. However, sometimes this approach might destroy the simple structure of the original system due to the nonlinearities and time-dependent terms can be introduced during the transformation of system parameters into the extra states. For instance, a linear time invariant system can be transformed into a nonlinear time varying system. Hence more advanced observer techniques (e.g. nonlinear or time-varying observer) are required to estimate the extended states.

An alternative approach is the adaptive observer based approach. Without destroying the simple system structure, it directly designs a simple observer (e.g. Luenberger observer) for the original system assuming that all the parameters are known, and tries to find some appropriate adaptive laws to estimate unknown parameters so as to keep the observer convergences. This approach does not need to employ complex observer algorithms, which make it easier to be implemented and computationally efficient in comparison with extended observers. A detailed comparison of these two methods is given in [42], and the connections between these two methods are presented in [43]. Various adaptive observer based fault diagnosis approaches have been proposed in literatures in different context. In [44], adaptive observer is used for fault diagnosis in order to deal with slowing varying or constant faults. In [45], a fast adaptive fault estimator is proposed to estimate time-varying faults. In [78], adaptive observer is first used for the diagnosis of the actuator faults in LTI systems. An extension of this research to both sensor and actuator faults is presented in [46].

In the classical adaptive observer designs [47], the state and parameter estimations both converge to their true values under assumption that the system model is a ‘true’ model which can perfectly represent the system. Nevertheless, problems will certainly arise when applying these approaches to practical systems, due to the existence of

model uncertainties. A typical problem is the so called parameter estimation drift (i.e. parameter estimation diverge to infinity). To prevent such drift, several techniques have been introduced to modify the observer structure, for instant the parameter projection, dead zone, dynamic normalization, etc. For more comprehensive introduction of these methods, readers can refer to [48]. Another important modification is to add a leakage term (i.e. σ-modification) to the parameter adaptive law, which is able to ensure bounded parameter estimations. However, inappropriate selection of observer parameters will still induce large estimation errors that certainly can not satisfy the accuracy requirements of fault diagnosis [49].

In this PhD study, the adaptive observer based approach is implemented for the fault diagnosis of the DFIG winding short circuit based on a state-space formed fault model. Due to the online property of adaptive observers, the fault location and level can be online diagnosed by estimating a set of fault related parameters. Meanwhile, the unknown states can be also estimated, which are used to reconstruct the controller in order to tolerate the fault. The effects of model uncertainties are considered in this work, the σ-modification is employed to ensure bounded parameter estimations, while in order to obtain enough small estimation errors for the sake of the accuracy of fault diagnosis, $H_\infty$ optimization and high gain observer techniques are implemented to synthesis a robust adaptive observer, which allows accurate estimations in the presence of model uncertainties.

### 2.3.2. Fault Tolerant Control

Fault tolerant control (FTC) is an advanced control technique that can accommodate system faults, assure system stability, and maintain system performance, not only under normal condition but also in the presence of faults. Several survey papers present a comprehensive review on development of FTC system since 1990s [50]-[52]. Some books on this subject have also been published recently [53], [54]. In these literatures, FTC approaches can be generally divided into two types: the passive and active approaches.

In the *passive FTC*, the same controller is used throughout the normal condition as well as the fault condition. Since only one fixed controller is used in the entire control process, the passive FTC is easily to be implemented. However, it can only tolerate a limited numbers of faults, which are assumed known prior to the controller design. Besides, as the number and level of the fault increase, this approach becomes very conservative, and attainable performance may become unsatisfactory. Most passive FTC algorithms are based on robust control techniques by treating the faults as model uncertainties or disturbances. For instant, the $H_\infty$ robust control theory integrated with the Algebraic Riccati Equation (ARE) [56], [57] or Linear Matrix Inequality (LMI) [58], [59] methods are usually employed in the passive FTC design to guarantee the stability and acceptable performance of the closed-loop system in the presence of faults.

The other approach is known as *active FTC*, the name indicates that it reacts to the system fault actively and allows online fault accommodation. An active FTC system can compensates the fault effects by either online selecting a pre-computed control law, or by online synthesizing a new control law. The general structure of an active FTC system is shown in Figure 2.10 [51], which has three subsystems: a reconfigurable controller, a FDD mechanism, and a control reconfiguration mechanism. An overview of existing active FTC methods with a detailed classification of different approaches has been provided in a recent review [51]. Among all these methods, adaptive control is one of the favorites and with wide applications recently. It principle is similar to the adaptive observer by considering the fault as some unknown variations of the plant parameters, and design a suitable parameter adaptive law to estimate such parameter variations so as to maintain consistent system performance in the presence of faults. In comparison with other methods, it does not heavily rely on the FDD decision and no quantitative knowledge of the fault is required to reconstruct the controller. Methods like direct and indirect parameter adaptive controller can ensure an acceptable performance of the closed-loop system in the presence of a wide range of unknown faults [54], [60], [61].

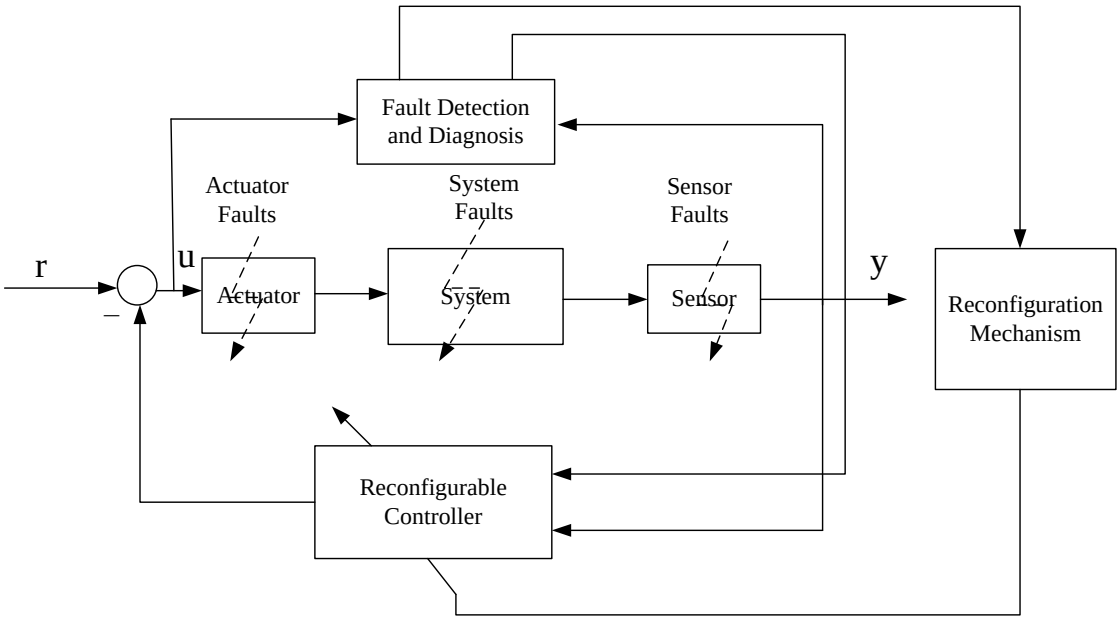


Figure 2.10. General structure of an active FTC system.

Adaptive control techniques have been applied to solve many FTC problems. In [54] and [60], a direct adaptive state feedback controller is developed for LTI system against actuator faults. A similar work using output feedback is given in [61]. Moreover, an adaptive fault tolerant $H_\infty$ controller is developed to cope with model uncertainties in [62]. All these studies focused only on linear systems and their applications are mainly related to the aircraft flight control. For nonlinear systems, an adaptive feedback linearization method is discussed in [63]. More recently, combing this method with sliding model control has been applied to induction motors to tolerant resistant variation and sensor faults [64]. However, so far very few case studies have been reported on the application to wind turbine systems.

In this PhD study, the active FTC strategy is employed to tolerate two common faults of wind turbine systems, i.e. DFIG winding short circuit and drive train fault. For the first fault, as an explicit fault diagnosis scheme is firstly developed in this work, thus the FTC for this fault is based on the fault information provided by this scheme. However, for the second fault, as no fault diagnosis scheme is provided in this work, we employ the adaptive control technique, specifically adaptive feedback linearization control, to synthesize the FTC, as it dose not rely the fault diagnosis scheme.

## 2.4. Fault Diagnosis and Fault Tolerant Control of Wind Turbine System

### 2.4.1. Fault Diagnosis of Wind Turbine System

A number of methodologies are available and applicable for the FDD of wind turbine systems, which have been briefly introduced in last section. Several review papers have been published recently [11]-[13], which present the state of the art achieved so far in the FDD of wind turbine systems. The results reviewed in these papers covers each component of the wind turbine system including drive train, rotor blades, generator, power electronics, etc. In this section, we only review the work relating to the generator and drive train faults, and the methods can be roughly classified into three categories.

- *Signal-based approach*

Signal-based approach is mainly based on the time and frequency domain analysis of some process measurements, such as generator currents, rotor speed, vibration, temperature. Fault indicators are then extracted from these process measurements by using various signal processing techniques. The most popular one is the spectrum analysis [70], [71], [85], [86]. The spectrum of the generator stator electrical quantities (e.g. stator voltage, line current [71], [85], instantaneous power [89]) is firstly extracted, and then the observation of some particular frequency components can be perceived as an indication of fault. Machine current signature analysis (MCSA) is a widely used spectrum analysis method, which is based on the steady-state line currents of the stator and is usually used to detect generator winding faults [71], [85]. In [87] and [88], the authors use rotor measurements (i.e. rotor modulating signal) to diagnose the fault. The experimental results show that this signal can provide a more clear evidence of the generator winding faults than using stator currents. Sequence component analysis has also been suggested as an effective approach of detecting generator winding faults by observing the negative sequence stator current [90], [91] or

sequence impedance matrix [92]. Nevertheless, these methods are sensitive to the machine inherent structure asymmetries and power supply imbalance, and thus they are not reliable on detecting the faults in such situations.

These methods mentioned above are mainly used in the steady-state analysis. In [70], the author raised an important feature of wind turbine systems, i.e. variable speed operation, and proposed a new problem, i.e. non-stationary fault diagnosis. To solve this problem, a new non-stationary analysis technique, i.e. wavelet analysis, has been extensively applied to wind turbine systems in the recent years [82], [95]. This technique can be also integrated with many traditional fault diagnosis methods. For instance, a combination of the wavelet analysis and power spectrum density analysis has been applied to detect generator winding faults in [80].

Drive train faults are usually diagnosed by observing the vibration signals or generator terminal currents (i.e. stator and rotor currents). Some of the methods mentioned above such as spectrum analysis and wavelets analysis, can be also applied for the diagnosis of drive train faults (i.e. gearbox fault, bearing fault and shaft fault). For instance, in [17] a new vibration spectrum analysis technique based on wavelet neural work is proposed for the diagnosis of gearbox faults. In [83], the wavelet analysis technique is applied to diagnose faults in a multistage gearbox by extracting the fault frequencies from the current signals through a discrete wavelet transform. In [84], the wavelet analysis technique is employed to analyze the stator currents so as to detect bearing defects.

- *Knowledge-based approach*

When a system is too complex to be modeled analytically, the knowledge-based approaches are usually employed to diagnose the faults. These techniques are based on qualitative models rather than quantitative mathematical model, which are developed by some artificial intelligence techniques, such as expert systems, neural network, and fuzzy systems. Different operation conditions including normal and faulty ones are treated as a family of patterns, then the neural network, fuzzy system or expert system is applied to evaluate the online measurements and map them into a known pattern

such that the current condition of the system can be identified. The research in this field becomes very active recently due to the fast development of artificial intelligence techniques and it also has many applications in wind turbine systems. For instance, a combination of neural network and fuzzy techniques [97] are applied to diagnose the generator winding faults through current and voltage measurements. An intelligent system for predictive maintenance based on artificial intelligent techniques has been recently developed and tested in wind turbine system to monitor the behaviour of wind turbine gearbox [98].

- *Model-based approach*

The model-based fault detection began in the early 1970s. This method requires a good analytical model of the system and fault. As most structural/internal faults are very complex, and difficult to be modeled analytically, model-based approach is usually applied to detect some external faults such as actuator or sensor faults (see [101], [102]). For wind turbine systems, there are also very few literatures relating to the structural/internal faults. Until recently several papers have been published, but only relating to the generator faults. The first paper appeared in 2006 [73], which is based on parameter estimation based approaches. In this paper, a new model of squirrel-cage induction machine (it is another common generator of wind turbine systems different from DFIG, its rotor is composed of longitudinal conductive bars) under stator and rotor faults is firstly developed, and some additional parameters are introduced to explain the faults in both stator windings and rotor bars. Fault detection is conducted by estimating these additional parameters by using two common identification techniques: equation error (EE) and output error (OE). A similar work of squirrel-cage induction machine fault detection was proposed in [74], which is also based on parameter estimation approach. In this work, instead of developing a new model to represent the faults, the author focused on finding the relationship between the faults and some physical parameters (e.g. resistance, mutual/self inductance). An adaptive Kalman filter is proposed to online estimate the parameters associated with faults. The observer based fault detection approaches are proposed in [75]-[77], which

only focus on detecting stator winding faults. In particular in [76], a state observer is constructed to generate a residual in form of vector, which allows for a fast detection of the faults independent of the phase where fault occurs. All this work mentioned above mainly focuses on fault detection rather than diagnosis. It is well known that the effectiveness of model-based fault diagnosis approaches highly rely on the model accuracy. Due to the saturation phenomenon and parameter variations during the operation process, model uncertainties generally exist in various generator models, which make robustness an important issue in the context of fault diagnosis. However, this issue is not discussed in this work mentioned above.

In this PhD work, the model based approach is employed to synthesize the fault diagnosis scheme of DFIG based wind turbines, as it allows for online and non-stationary FDD. The work is mainly concerned with fault diagnosis (i.e. identify the fault magnitude and location) as it is more challenging in comparison with fault detection. The effects of the model uncertainties are also considered in this work in order to improve the reliability of the fault diagnosis scheme.

### 2.4.2. Fault Tolerant Control of Wind Turbine System

Currently, FTC of wind turbine systems is mainly realized by hardware redundancy [14], but that leads to the problem of extra hardware costs and additional weight and space to accommodate the equipments. For this reason, it is necessary to develop analytical FTC approaches. However, limited studies are reported on analytical FTC for wind turbine system, especially for generator and drive train faults. Until recently, two papers relating to the FTC of wind turbine systems appear which both belong to the field of active FTC. The first work proposes a FTC for generator in the presence of both stator and rotor faults [99]. In this work, the possible faults are modeled as functions of time within a parameterized family. An internal model of this family is designed by using nonlinear output regulation theory, and embedded to the controller to offset the effects of all the possible faults. The second work is given in [100]. It addresses the fact that the fault development can be evaded or postponed by reducing

the torque stress. In this context, a demodulated torque control of the generator is proposed, Its basic idea is to reduce the torque whenever the magnetic flux moves to the areas affecting the damaged components, and increase the torque back to nominal value after the magnetic flux pass such areas. In this PhD study, we aim to develop an analytical FTC scheme for the DFIG based wind turbine system and mainly focus on the generator and drive train faults.

## 2.5. Summary

This chapter briefly reviewed the field of fault diagnosis and FTC and its application to wind turbine system. For the fault diagnosis of wind turbine system, most existing studies are based on signal or knowledge based approaches. These studies mainly focused on fault detection rather than fault diagnosis, and most of them are not suitable for non-stationary analysis. For the FTC of wind turbine systems, it is mainly realized by hardware redundancy, but that leads to the problem of extra hardware costs and additional weight and space to accommodate the equipments. For this reason, it is requisite to develop analytical FTC approaches. In this chapter, model-based fault diagnosis approaches and an analytical FTC approach, i.e. active FTC, are mainly reviewed, and their properties, advantages to other methods and applications in wind turbine systems are investigated.

Therefore, in this thesis, we focused on the model-based approaches and active FTC for the fault diagnosis and tolerant control of wind turbine systems, which are presented in the following chapters.

# 3. Modeling of DFIG with Winding Short Circuit Fault

## 3.1. Introduction

The winding short circuit fault is one of the most common faults in electric machines including DFIGs, which is caused by many reasons such as mechanical stress, insulation damage and transient over-voltages. This fault may occur within one phase or sometimes in several phases simultaneously. In this work, we denote the former case the single-phase fault and latter case the multi-phase fault. In this chapter, two mathematical models are developed with respect to these two types of faults. The modeling strategy is to consider the short circuit loops as some additional circuits placed in parallel to the original winding circuits of DFIG, and then represent the electrical and magnetic relationships among all these circuits by using circuit theory. This idea is firstly brought by Tallam in 2002 [91], where a simple model of induction motor was developed. A similar work for DFIG is presented in [69]. Both modeling results are supported by experimental data, whereas both of the work considers a special case that the short circuit only occurs at the stator phase 'a'. In this chapter, their work is extended to more general cases that the short circuits occur at an arbitrary phase or even multiple phases simultaneously. Additionally, two general mathematical models of DFIG (i.e. one for single-phase and the other for multi-phase fault) are proposed. For each model, it is firstly developed in the natural a-b-c coordinate (see in Figure 3.2), and then transformed into the d-q coordinate (see in Figure 3.2 and Figure 3.4) to simplify the model structure. A set of new model parameters ($\mu$ and $\mathbf{f}_x$ for the single-phase fault, and $\mu_{sa}$, $\mu_{sb}$, $\mu_{sc}$, $\mu_{ra}$, $\mu_{rb}$, $\mu_{rc}$ for the multi-phase fault)

are introduced to represent the fault quantitatively. Different fault scenarios can be then represented by defining these parameters properly. In this chapter, the models are all given in terms of the voltage and flux equations, which is a common representation of the DFIG model. In the next chapter, the state-space representations of these models are developed for the purpose of fault diagnosis.

This chapter is organized as follows. In Section 3.2, the models for the single-phase fault in the a-b-c and d-q coordinates are developed, respectively. In Section 3.3, the models for the multi-phase fault in the a-b-c and d-q coordinates are developed, respectively. In Section 3.4, the equivalent circuits of the DFIG are provided, based on which the characteristics of the short circuit fault and its effects on the DFIG are analyzed. In Section 3.5, some simulations of the proposed models are carried out to evaluate the behaviours of DFIG in the presence of winding short circuit faults. Finally, a summary is given in Section 3.6.

## 3.2. Modeling of DFIG with Single-Phase Fault

The aim of this section is to develop a mathematical model of DFIG with respect to the single-phase short circuit fault. First, a 3-phase model in the natural a-b-c coordinate is developed. In this model, the short circuit fault is represented by two parameters: fault level parameter $\mu$ (as in (3.1)) and fault position parameter $\mathbf{f}_x$ (as in (3.2)). By transforming this model into a stationary d-q coordinate, a d-q model is then developed, where a new fault position parameter $\mathbf{f}_{xdq}$ is defined (as in (3.23)). For both of these models, their corresponding electromagnetic torques are presented in (3.19) and (3.29), respectively.

### 3.2.1. Model in a-b-c Coordinate

Figure 3.1 shows the winding configuration of a DFIG with a short circuit fault in stator phase ‘a’. As shown in this figure, the fault splits the faulty phase into two parts: the shorted turns (as2) and un-shorted turns (as1). The shorted turns (as2) form a

closed-loop circuit, which can be modeled as a new phase of the stator. It is also known that the rotor of DFIG has three phase windings as well. Therefore, this faulty DFIG can be interpreted as a multi-phase induction machine with 4 stator phase windings and 3 rotor phase windings. Using this strategy, the mathematical model of the faulty DFIG can be easily obtained by representing the electrical and magnetic relationships among these phase windings using circuit theory. In this subsection, we will start with developing the model for a special case that the fault only occurs at stator phase 'a'. In the next, this model is generalized to represent the fault in any single phase of the stator. Before deriving the models, some assumptions have been made.

- Each stator phase of the machine has the same number of turns and uniform spatial displacement.
- The three phase stator and rotor windings are sinusoidally distributed.
- The machine is operating at an unsaturated point.
- The skin or slot effect is not considered.
- Insulation break resistance $r_f$ is negligible.

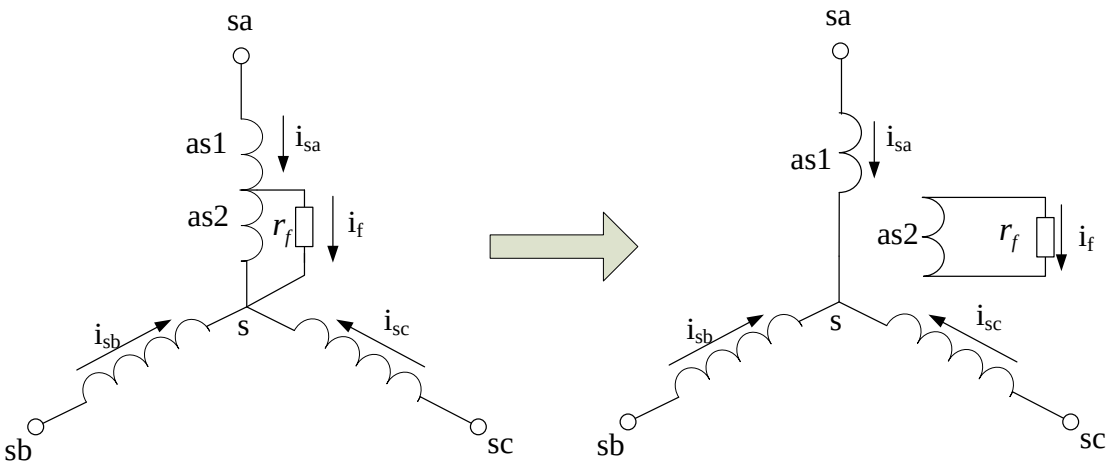


Figure 3.1. Stator winding configuration with a short circuit fault in stator phase 'a'.

### 3.2.1.1 Fault definition

The single-phase short circuit fault can be defined by two parameters: the fault level parameter $\mu$ and the fault location parameter $\mathbf{f}_x$. $\mu$ represents the percentage of

the shorted turns which is used to quantify the severity of the fault. It is calculated by the following formula [73].

$$\mu = \frac{\text{Number of shorted turns}}{\text{Total number of turns in a healthy phase}} \tag{3.1}$$

where $0 \le \mu \le 1$. $\mu = 0$ corresponds to the healthy condition.

The fault position parameter $\mathbf{f}_x$ is a vector and can take three different values which correspond to different fault in phase 'a', 'b' and 'c', respectively,

$$\mathbf{f}_a = [1\ 0\ 0]^T,\ \mathbf{f}_b = [0\ 1\ 0]^T,\ \mathbf{f}_c = [0\ 0\ 1]^T \tag{3.2}$$

These two parameters will be employed later to develop the model of DFIG with respect to single-phase short circuit fault.

### 3.2.1.2 DFIG model for a special case: short circuit only occurs at stator phase 'a'

As described earlier, a DFIG with a single-phase short circuit fault can be interpreted as a multi-phase induction machine with four stator phases and three rotor phases. By taking the case that fault in stator phase 'a' as an example, the relationship among these magnetically coupled phases can be expressed by the following voltage and flux equations.

Voltage equation:

$$\begin{bmatrix} v_{sa} \\ 0 \\ v_{sb} \\ v_{sc} \\ \hdashline v_{ra} \\ v_{rb} \\ v_{rc} \end{bmatrix} = \left[\begin{array}{cccc:ccc} r_{sa1} & & & & & & \\ & r_{sa2} & & & & & \\ & & r_{sb} & & & \mathbf{0}_{4\times 3} & \\ & & & r_{sc} & & & \\ \hdashline & & & & r_{ra} & & \\ & \mathbf{0}_{3\times 4} & & & & r_{rb} & \\ & & & & & & r_{rc} \end{array}\right] \begin{bmatrix} i_{sa} \\ i_{sa} - i_f \\ i_{sb} \\ i_{sc} \\ \hdashline i_{ra} \\ i_{rb} \\ i_{rc} \end{bmatrix} + \frac{d}{dt} \begin{bmatrix} \psi_{sa1} \\ \psi_{sa2} \\ \psi_{sb} \\ \psi_{sc} \\ \hdashline \psi_{ra} \\ \psi_{rb} \\ \psi_{rc} \end{bmatrix} \tag{3.3}$$

Flux equation:

$$\begin{bmatrix} \psi_{sa1} \\ \psi_{sa2} \\ \psi_{sb} \\ \psi_{sc} \\ \hdashline \psi_{ra} \\ \psi_{rb} \\ \psi_{rc} \end{bmatrix} = \left[\begin{array}{cccc:ccc} L_{sa1sa1} & L_{sa1sa2} & L_{sa1sb} & L_{sa1sc} & L_{sa1ra} & L_{sa1rb} & L_{sa1rc} \\ L_{sa2sa1} & L_{sa2sa2} & L_{sa2sb} & L_{sa2sc} & L_{sa2ra} & L_{sa2rb} & L_{sa2rc} \\ L_{sbsa1} & L_{sbsa2} & L_{sbsb} & L_{sbsc} & L_{sbra} & L_{sbrb} & L_{sbrc} \\ L_{scsa1} & L_{scsa2} & L_{scsb} & L_{scsc} & L_{scra} & L_{scrb} & L_{scrc} \\ \hdashline L_{rasa1} & L_{rasa2} & L_{rasb} & L_{rasc} & L_{rara} & L_{rarb} & L_{rarc} \\ L_{rbsa1} & L_{rbsa2} & L_{rbsb} & L_{rbsc} & L_{rbra} & L_{rbrb} & L_{rbrc} \\ L_{rcsa1} & L_{rcsa2} & L_{rcsb} & L_{rcsc} & L_{rcra} & L_{rcrb} & L_{rcrc} \end{array}\right] \left[\begin{array}{c} i_{sa} \\ i_{sa} - i_f \\ i_{sb} \\ i_{sc} \\ \hdashline i_{ra} \\ i_{rb} \\ i_{rc} \end{array}\right] \tag{3.4}$$

where the subscripts ‘ $s$ ’ and ‘ $r$ ’ denote stator and rotor, and the subscripts ‘ $a$ ’, ‘ $b$ ’and ‘ $c$ ’ denote phase ‘a’, ‘b’ and ‘c’. Therefore, $v_{sa}, v_{sb}, v_{sc}, v_{ra}, v_{rb}$ and $v_{rc}$ represent the voltages of each phase. $i_{sa}, i_{sb}, i_{sc}, i_{ra}, i_{rb}$ and $i_{rc}$ represent the currents of each phase. $i_f$ is the short circuit current. $\psi_{sa1}$ and $\psi_{sa2}$ are the magnetic fluxes for the un-shorted and shorted turns respectively. $\psi_{sb}, \psi_{sc}, \psi_{ra}, \psi_{rb}$ and $\psi_{rc}$ are the magnetic fluxes for the stator phase ‘a’, ‘b’ and rotor phases, respectively.

The parameters in above model equation can be classified into two groups, the fault-affected parameters and fault-free parameters as shown in Table 3.1, where the parameters with subscript ‘sa’ is affected by the fault and can be expressed as a function of the fault level parameter $\mu$.

Table 3.1. Parameters of model (3.3)-(3.4).

| | Fault-affected parameters | Fault-free parameters |
|---|---|---|
| Resistance | $r_{sa1} = (1-\mu)r_s$, $r_{sa2} = \mu r_s$. | $r_{sb} = r_{sc} = r_s$<br>$r_{ra} = r_{rb} = r_{rc} = r_r$ |
| Self inductance | $L_{sa1sa1} = (1-\mu)L_{\sigma s} + (1-\mu)^2 M_s$<br>$L_{sa2sa2} = \mu L_{\sigma s} + \mu^2 M_s$ | $L_{sbsb} = L_{scsc} = L_{\sigma s} + M_s$<br>$L_{rara} = L_{rbrb} = L_{rcrc} = L_{\sigma r} + M_r$ |
| Mutual inductance | $L_{sa1sa2} = L_{sa2sa1} = \mu(1-\mu)M_s$<br>$L_{sa1sb} = L_{sbsa1} = L_{sa1sc} = L_{scsa1}$<br>$= -\frac{1}{2}(1-\mu)M_s$ | $L_{rarb} = L_{rbra} = L_{rarc}$<br>$= L_{rcra} = L_{rbrc} = L_{rcrb} = -\frac{1}{2}M_r$ |

| | | |
|---|---|---|
| | $L_{sa1ra} = L_{rasa1} = (1-\mu)M_{sr}\cos(\theta_r)$<br>$L_{sa1rb} = L_{rbsa1} = (1-\mu)M_{sr}\cos(\theta_r + \frac{2\pi}{3})$<br>$L_{sa1rc} = L_{rcsa1} = (1-\mu)M_{sr}\cos(\theta_r - \frac{2\pi}{3})$<br>$L_{sa2ra} = L_{rasa2} = \mu M_{sr}\cos(\theta_r)$<br>$L_{sa2rb} = L_{rbsa2} = \mu M_{sr}\cos(\theta_r + \frac{2\pi}{3})$<br>$L_{sa2rc} = L_{rcsa2} = \mu M_{sr}\cos(\theta_r - \frac{2\pi}{3})$ | $L_{sbrb} = L_{rbsb}$<br>$= L_{rcsc} = L_{scrc} = M_{sr}\cos(\theta_r)$<br>$L_{sbrc} = L_{rcsb} = M_{sr}\cos(\theta_r + \frac{2\pi}{3})$<br>$L_{scrb} = L_{rbsc} = M_{sr}\cos(\theta_r - \frac{2\pi}{3})$ |

In this table, $r_s$ and $r_r$ represent the stator and rotor resistances. $L_{\sigma s}$ and $L_{\sigma s}$ represent the stator and rotor leakage inductances. $\theta_r$ represents the electrical angle between the stator and rotor. $M_s$ and $M_r$ represent the mutual inductances of the stator and rotor. $M_{sr}$ represents the stator-rotor mutual inductance. By referring the rotor parameters to stator side, these mutual inductances are equal:

$$M_s = M_r = M_{sr} \tag{3.5}$$

By adding the first two rows of (3.3) and (3.4), a more compact representation of the model is obtained,

$$\begin{bmatrix} \mathbf{v}_{sabc} \\ \mathbf{v}_{rabc} \\ \hline 0 \end{bmatrix} = \left[\begin{array}{cc:c} \mathbf{R}_s & \mathbf{0}_{3\times3} & -\mu\mathbf{R}_1 \\ \mathbf{0}_{3\times3} & \mathbf{R}_r & \mathbf{0}_{3\times1} \\ \hline \mu\mathbf{R}_1 & \mathbf{0}_{1\times3} & -\mu r_s \end{array}\right] \begin{bmatrix} \mathbf{i}_{sabc} \\ \mathbf{i}_{rabc} \\ \hline i_f \end{bmatrix} + \frac{d}{dt}\begin{bmatrix} \boldsymbol{\psi}_{sabc} \\ \boldsymbol{\psi}_{rabc} \\ \hline \psi_{sa2} \end{bmatrix} \tag{3.6}$$

$$\begin{bmatrix} \boldsymbol{\psi}_{sabc} \\ \boldsymbol{\psi}_{rabc} \\ \hline \psi_f \end{bmatrix} = \left[\begin{array}{cc:c} \mathbf{L}_{ss} & \mathbf{L}_{sr} & -\mu\mathbf{L}_1 \\ \mathbf{L}_{sr}^T & \mathbf{L}_{rr} & -\mu\mathbf{L}_2 \\ \hline \mu\mathbf{L}_1^T & \mu\mathbf{L}_2^T & -\mu L_{DD} \end{array}\right] \begin{bmatrix} \mathbf{i}_{sabc} \\ \mathbf{i}_{rabc} \\ \hline i_f \end{bmatrix} \tag{3.7}$$

where the bold letters denote the vectors and matrices. The variable vectors are given as

$$\mathbf{v}_{sabc} = \left[v_{sa},\ v_{sb},\ v_{sc}\right]^T,\ \mathbf{v}_{rabc} = \left[v_{ra},\ v_{rb},\ v_{rc}\right]^T.$$

$$\mathbf{i}_{sabc} = \left[i_{sa},\ i_{sb},\ i_{sc}\right]^T,\ \mathbf{i}_{rabc} = \left[i_{ra},\ i_{rb},\ i_{rc}\right]^T.$$

$$\boldsymbol{\psi}_{sabc} = \left[\psi_{sa},\ \psi_{sb},\ \psi_{sc}\right]^T,\ \boldsymbol{\psi}_{rabc} = \left[\psi_{ra},\ \psi_{rb},\ \psi_{rc}\right]^T$$

where $\psi_{sa}$ represents the total magnetic flux in stator phase 'a' which is the sum of

$\psi_{sa1}$ and $\psi_{sa2}$, and $\psi_{sa2}$ is renamed as $\psi_f$ in this model.

The parameter matrices of model (3.6)-(3.7) are given as

$$\mathbf{R}_s = r_s\mathbf{I}_3,\ \ \mathbf{R}_r = r_r\mathbf{I}_3,\ \ \mathbf{R}_1 = \begin{bmatrix} r_s & 0 & 0 \end{bmatrix}^T \tag{3.8}$$

$$\mathbf{L}_{ss} = \begin{bmatrix} L_{\sigma s}+M_s & -\frac{1}{2}M_s & -\frac{1}{2}M_s \\ -\frac{1}{2}M_s & L_{\sigma s}+M_s & -\frac{1}{2}M_s \\ -\frac{1}{2}M_s & -\frac{1}{2}M_s & L_{\sigma s}+M_s \end{bmatrix},\ \ \mathbf{L}_{rr} = \begin{bmatrix} L_{\sigma r}+M_s & -\frac{1}{2}M_s & -\frac{1}{2}M_s \\ -\frac{1}{2}M_s & L_{\sigma r}+M_s & -\frac{1}{2}M_s \\ -\frac{1}{2}M_s & -\frac{1}{2}M_s & L_{\sigma r}+M_s \end{bmatrix} \tag{3.9}$$

$$\mathbf{L}_{sr} = M_s \begin{bmatrix} \cos(\theta_r) & \cos(\theta_r+\frac{2\pi}{3}) & \cos(\theta_r-\frac{2\pi}{3}) \\ \cos(\theta_r-\frac{2\pi}{3}) & \cos(\theta_r) & \cos(\theta_r+\frac{2\pi}{3}) \\ \cos(\theta_r+\frac{2\pi}{3}) & \cos(\theta_r-\frac{2\pi}{3}) & \cos(\theta_r) \end{bmatrix} \tag{3.10}$$

$$\mathbf{L}_1 = \begin{bmatrix} L_{\sigma s}+M_s & -\frac{1}{2}M_s & -\frac{1}{2}M_s \end{bmatrix}^T\ \ \mathbf{L}_2 = \begin{bmatrix} \cos(\theta_r) & \cos(\theta_r+\frac{2\pi}{3}) & \cos(\theta_r-\frac{2\pi}{3}) \end{bmatrix}^T \tag{3.11}$$

$$L_{DD} = L_{\sigma s} + \mu M_s \tag{3.12}$$

This subsection presents an example to explain how to derive a mathematical model of DFIG with respect to the single-phase short circuit fault. A compact matrix representation of the model is obtained as in (3.6)-(3.7). This representation is employed in next subsection, based on which a general model is developed.

### 3.2.1.3 Generalized DFIG model

In this subsection, a more general model of DFIG is proposed, which allows representing the short circuit fault in any phase of the stator. The same method as described in previous subsection is employed here to derive the models for the short circuit in the other phases i.e. ‘b’ and ‘c’, respectively. The models for these two cases are with the same structure as given in (3.6)-(3.7). All the parameter matrices are still the same parameter matrices except for matrices $\mathbf{R}_1$, $\mathbf{L}_1$ and $\mathbf{L}_2$. Their expression

are different with respect to the faults in different phases ‘a’, ‘b’ and ‘c’ as given in Table 3.2.

Table 3.2. Matrices $\mathbf{R}_1$, $\mathbf{L}_1$ and $\mathbf{L}_2$ with respect to the faults in different phases ‘a’, ‘b’ and ‘c’.

| | Fault in ‘sa’ | Fault in ‘sb’ | Fault in ‘sc’ |
|---|---|---|---|
| $\mathbf{R}_1$ | $\begin{bmatrix} r_s & 0 & 0 \end{bmatrix}^T$ | $\begin{bmatrix} 0 & r_s & 0 \end{bmatrix}^T$ | $\begin{bmatrix} 0 & 0 & r_s \end{bmatrix}^T$ |
| $\mathbf{L}_1$ | $\begin{bmatrix} L_{\sigma s}+M_s \\ -\frac{1}{2}M_s \\ -\frac{1}{2}M_s \end{bmatrix}$ | $\begin{bmatrix} -\frac{1}{2}M_s \\ L_{\sigma s}+M_s \\ -\frac{1}{2}M_s \end{bmatrix}$ | $\begin{bmatrix} -\frac{1}{2}M_s \\ -\frac{1}{2}M_s \\ L_{\sigma s}+M_s \end{bmatrix}$ |
| $\mathbf{L}_2$ | $\begin{bmatrix} \cos(\theta_r) \\ \cos(\theta_r-\frac{2\pi}{3}) \\ \cos(\theta_r+\frac{2\pi}{3}) \end{bmatrix}$ | $\begin{bmatrix} \cos(\theta_r+\frac{2\pi}{3}) \\ \cos(\theta_r) \\ \cos(\theta_r-\frac{2\pi}{3}) \end{bmatrix}$ | $\begin{bmatrix} \cos(\theta_r-\frac{2\pi}{3}) \\ \cos(\theta_r+\frac{2\pi}{3}) \\ \cos(\theta_r) \end{bmatrix}$ |

The fault position parameter $\mathbf{f}_x$ (as in (3.2)) is employed here to give a unified representation of matrices $\mathbf{R}_1$, $\mathbf{L}_1$ and $\mathbf{L}_2$

$$\mathbf{R}_1 = r_s\mathbf{f}_x,\ \ \mathbf{L}_1 = \mathbf{L}_{ss}\mathbf{f}_x,\ \ \mathbf{L}_2 = \mathbf{L}_{sr}\mathbf{f}_x \tag{3.13}$$

where parameter $r_s$, $\mathbf{L}_{ss}$ and $\mathbf{L}_{sr}$ have been given in (3.9)-(3.10).

By replacing $\mathbf{R}_1$, $\mathbf{L}_1$ and $\mathbf{L}_2$ in (3.6)-(3.7) with (3.13), the generalized DFIG model can be expressed as

$$\begin{bmatrix} \mathbf{v}_{sabc} \\ \mathbf{v}_{rabc} \\ \hline 0 \end{bmatrix} = \left[\begin{array}{ccc} \mathbf{R}_s & \mathbf{0}_{3\times3} & -\mu r_s\mathbf{f}_x \\ \mathbf{0}_{3\times3} & \mathbf{R}_r & \mathbf{0}_{3\times1} \\ \hline \mu r_s\mathbf{f}_x^T & \mathbf{0}_{1\times3} & -\mu r_s \end{array}\right] \begin{bmatrix} \mathbf{i}_{sabc} \\ \mathbf{i}_{rabc} \\ \hline i_f \end{bmatrix} + \frac{d}{dt}\begin{bmatrix} \boldsymbol{\psi}_{sabc} \\ \boldsymbol{\psi}_{rabc} \\ \hline \psi_f \end{bmatrix} \tag{3.14}$$

$$\begin{bmatrix} \boldsymbol{\psi}_{sabc} \\ \boldsymbol{\psi}_{rabc} \\ \hline \psi_f \end{bmatrix} = \left[\begin{array}{ccc} \mathbf{L}_{ss} & \mathbf{L}_{sr} & -\mu\mathbf{L}_{ss}\mathbf{f}_x \\ \mathbf{L}_{sr}^T & \mathbf{L}_{rr} & -\mu\mathbf{L}_{sr}\mathbf{f}_x \\ \hline \mu\mathbf{f}_x^T\mathbf{L}_{ss}^T & \mu\mathbf{f}_x^T\mathbf{L}_{sr}^T & -\mu L_{DD} \end{array}\right] \begin{bmatrix} \mathbf{i}_{sabc} \\ \mathbf{i}_{rabc} \\ \hline i_f \end{bmatrix} \tag{3.15}$$

This is a general model for the single-phase short circuit fault, which can represent

the short circuit fault at any level in any phase, by setting appropriate values of parameters $\mu$ and $\mathbf{f}_x$ according to (3.2). For instance, with $\mu$=0.01 and $\mathbf{f}_x$=[0, 1, 0]$^T$, model (3.14)-(3.15) can represent a DFIG with a 1% short circuit fault (i.e. 1% phase winding is shorted) in stator phase 'a'.

### 3.2.1.4 Electromagnetic torque calculation

In this section, the electromagnetic torque of the DFIG under the faulty condition is provided. As mentioned earlier, a DFIG with a single-phase short circuit fault can be considered as a multi-phase induction machine. Therefore, the torque calculation formula for the multi-phase induction machine is employed here to calculate the torque under faulty condition. This formula is given as [117]

$$T_g = \frac{1}{2} p\mathbf{i}^T \frac{\partial \mathbf{L}}{\partial \theta_r}\mathbf{i} \tag{3.16}$$

where $\mathbf{i}$ represents the current vector containing all the phase currents. $\mathbf{L}$ represents the inductance matrix composed of all the self and mutual inductances. $p$ is the number of pole pairs.

By applying this formula to model (3.3)-(3.4), the electromagnetic toque for a special faulty case that the short circuit only occurs at stator 'a' can be calculated as

$$T_g = p\mathbf{i}_{sabc}^T \frac{\partial \mathbf{L}_{sr}}{\partial \theta_r}\mathbf{i}_{rabc} + pM_s\mu i_f\{\sin(\theta_r)i_{ra} + \sin(\theta_r + \frac{2\pi}{3})i_{rb} + \sin(\theta_r + \frac{2\pi}{3})i_{rc}\} \tag{3.17}$$

where $\frac{\partial \mathbf{L}_{sr}}{\partial \theta_r}$ represent the first derivative of $\mathbf{L}_{sr}$ with respect to $\theta_r$ which can be calculated as

$$\frac{\partial \mathbf{L}_{sr}}{\partial \theta_r} = -M_s \begin{bmatrix} \sin(\theta_r) & \sin(\theta_r + \frac{2\pi}{3}) & \sin(\theta_r - \frac{2\pi}{3}) \\ \sin(\theta_r - \frac{2\pi}{3}) & \sin(\theta_r) & \sin(\theta_r + \frac{2\pi}{3}) \\ \sin(\theta_r + \frac{2\pi}{3}) & \sin(\theta_r - \frac{2\pi}{3}) & \sin(\theta_r) \end{bmatrix} \tag{3.18}$$

Applying the same method, a general representation of the electromagnetic torque

for any single-phase short circuit fault is obtained as

$$T_g = p(\mathbf{i}_{sabc}^T \frac{\partial \mathbf{L}_{sr}}{\partial \theta_r} \mathbf{i}_{rabc} - \mu i_f \mathbf{f}_x^T \frac{\partial \mathbf{L}_{sr}}{\partial \theta_r} \mathbf{i}_{rabc}) \tag{3.19}$$

The influences of the short circuit fault on the electromagnetic torque can be observed from this equation. An explicit analysis of these influences is given later in Section 3.4.

## 3.2.2. Model in Stationary d-q Coordinate

The faulty DFIG model (3.14)-(3.15) developed in last section is given in two different coordinates: the stator a-b-c coordinate and rotor a-b-c coordinate. The former is stationary while the latter is rotating at an angular speed $\omega_r$ relative to the former. For this reason, the model parameters (as in (3.10) and Table 3.2) vary with the relative position $\theta_r$ between these two coordinates that leads to a coupled and time-varying expression of model (3.14)-(3.15). To simplify this model, the d-q transformation is applied to project the model into a two-axis stationary coordinate, known as stationary d-q coordinate. In this coordinate, q-axis is 90 degree ahead of the d-axis, and d-axis coincides with stator phase 'a'. The stationary d-q coordinate and its relationship with the stator a-b-c coordinate and rotor a-b-c coordinate are presented in Figure 3.2.

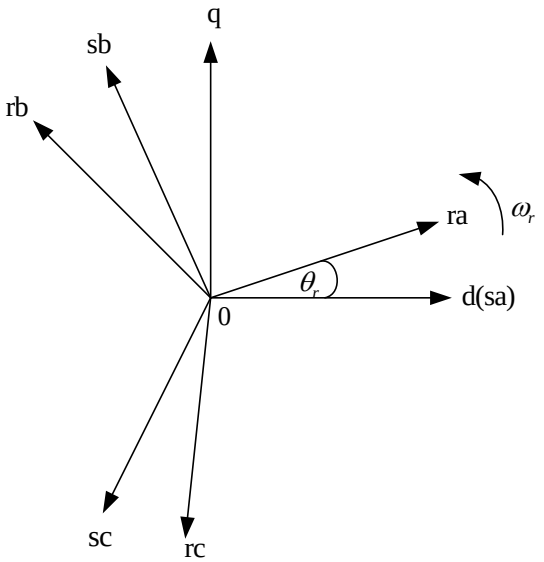


Figure 3.2. Stationary d-q coordinate and its relationship with the stator a-b-c coordinate and rotor a-b-c coordinate.

The general d-q transformation matrix $\mathbf{T}_{32}$ (from abc to dq) is given as [113]

$$\mathbf{T}_{32}=\frac{2}{3}\begin{bmatrix}\cos\theta & \cos(\theta-2\pi/3) & \cos(\theta+2\pi/3)\\ -\sin\theta & -\sin(\theta-2\pi/3) & -\sin(\theta+2\pi/3)\end{bmatrix} \tag{3.20}$$

Then the variables in the stationary d-q coordinate can be transferred from the variables in the a-b-c coordinate by following formulas.

$$\mathbf{x}_{sdq}=\mathbf{T}_{32}\big|_{\theta=0}\,\mathbf{x}_s,\ \ \mathbf{x}_{rdq}=\mathbf{T}_{32}\big|_{\theta=-\theta_r}\,\mathbf{x}_r \tag{3.21}$$

The fault variables $i_f$ and $\psi_f$ are also projected to this coordinate by using following transformation.

$$\mathbf{x}_{fdq}=\mathbf{f}_{xdq}x_f \tag{3.22}$$

where $\mathbf{f}_{xdq}$ is obtained from $\mathbf{f}_x$ and used to represent the fault position in the stationary d-q coordinate. It can take three different values which corresponding to the short circuit fault in phases ‘a’, ‘b’ and ‘c’, respectively.

$$\mathbf{f}_{adq}=\begin{bmatrix}1 & 0\end{bmatrix}^T,\ \mathbf{f}_{bdq}=\begin{bmatrix}-\frac{1}{2} & \frac{\sqrt{3}}{2}\end{bmatrix}^T,\ \mathbf{f}_{cdq}=\begin{bmatrix}-\frac{1}{2} & -\frac{\sqrt{3}}{2}\end{bmatrix}^T. \tag{3.23}$$

By applying these transformations to model (3.14) and (3.15), a d-q model of the faulted DFIG in the stationary d-q coordinate can be obtained as

Voltage equation:

$$\begin{bmatrix}\mathbf{v}_{sdq}\\ \mathbf{v}_{rdq}\\ \hdashline \mathbf{0}_{2\times1}\end{bmatrix}=\left[\begin{array}{ccc}\mathbf{R}_s^{'} & \mathbf{0}_{2\times2} & -\frac{2}{3}\mu\mathbf{R}_s^{'}\\ \mathbf{0}_{2\times2} & \mathbf{R}_r^{'} & \mathbf{0}_{2\times2}\\ \hdashline \mu r_s\mathbf{f}_{xdq}\mathbf{f}_{xdq}^T & \mathbf{0}_{2\times2} & -\mu\mathbf{R}_s^{'}\end{array}\right]\begin{bmatrix}\mathbf{i}_{sdq}\\ \mathbf{i}_{rdq}\\ \hdashline \mathbf{i}_{fdq}\end{bmatrix}+\frac{d}{dt}\begin{bmatrix}\boldsymbol{\psi}_{sdq}\\ \boldsymbol{\psi}_{rdq}\\ \hdashline \boldsymbol{\psi}_{fdq}\end{bmatrix}+\left[\begin{array}{ccc}\mathbf{0}_{2\times2} & \mathbf{0}_{2\times2} & \mathbf{0}_{2\times2}\\ \mathbf{0}_{2\times2} & -\omega_r\mathbf{J} & \mathbf{0}_{2\times2}\\ \hdashline \mathbf{0}_{2\times2} & \mathbf{0}_{2\times2} & \mathbf{0}_{2\times2}\end{array}\right]\begin{bmatrix}\boldsymbol{\psi}_{sdq}\\ \boldsymbol{\psi}_{rdq}\\ \hdashline \boldsymbol{\psi}_{fdq}\end{bmatrix} \tag{3.24}$$

Flux equation:

$$\begin{bmatrix}\boldsymbol{\psi}_{sdq}\\ \boldsymbol{\psi}_{rdq}\\ \hdashline \boldsymbol{\psi}_{fdq}\end{bmatrix}=\left[\begin{array}{ccc}\mathbf{L}_{ss}^{'} & \mathbf{L}_{sr}^{'} & -\frac{2}{3}\mu\mathbf{L}_{ss}^{'}\\ \mathbf{L}_{sr}^{'} & \mathbf{L}_{rr}^{'} & -\frac{2}{3}\mu\mathbf{L}_{sr}^{'}\\ \hdashline \mu\mathbf{f}_{xdq}\mathbf{f}_{xdq}^T\mathbf{L}_{ss}^{'} & \mu\mathbf{f}_{xdq}\mathbf{f}_{xdq}^T\mathbf{L}_{sr}^{'} & -\mu L_{DD}\mathbf{I}_2\end{array}\right]\begin{bmatrix}\mathbf{i}_{sdq}\\ \mathbf{i}_{rdq}\\ \hdashline \mathbf{i}_{fdq}\end{bmatrix} \tag{3.25}$$

where the variable vectors are given as

$\mathbf{v}_{sdq} = [v_{sd}, v_{sq}]^T$, $\mathbf{v}_{rdq} = [v_{rd}, v_{rq}]^T$, $\mathbf{i}_{sdq} = [i_{sd}, i_{sq}]^T$, $\mathbf{i}_{rdq} = [i_{rd}, i_{rq}]^T$,

$\mathbf{i}_{fdq} = [i_{fd}, i_{fq}]^T$, $\boldsymbol{\psi}_{sdq} = [\psi_{sd}, \psi_{sq}]^T$, $\boldsymbol{\psi}_{rdq} = [\psi_{rd}, \psi_{rq}]^T$, $\boldsymbol{\psi}_{fdq} = [\psi_{fd}, \psi_{fq}]^T$.

The parameter matrices are given as

$$\mathbf{R}_s^{'} = r_s \mathbf{I}_2, \quad \mathbf{R}_r^{'} = r_r \mathbf{I}_2, \tag{3.26}$$

$$\mathbf{L}_{ss}^{'} = (L_{\sigma s} + L_m)\mathbf{I}_2, \quad \mathbf{L}_{rr}^{'} = (L_{\sigma r} + L_m)\mathbf{I}_2 \text{ and } \mathbf{L}_{sr}^{'} = L_m \mathbf{I}_2 \tag{3.27}$$

$$\mathbf{J} = \begin{bmatrix} 0 & -1 \\ 1 & 0 \end{bmatrix} \tag{3.28}$$

with $L_m = \frac{3}{2} M_s$. $L_{DD}$ has been given in (3.12).

By applying the d-q transformation to torque equation (3.19), we can obtain a new representation of the electromagnetic torque in the stationary d-q coordinate.

$$T_g = \frac{3}{2} p L_m (\mathbf{i}_{sdq}^T \times \mathbf{i}_{rdq} - \frac{2}{3} \mu \mathbf{i}_{fdq}^T \times \mathbf{i}_{rdq}) \tag{3.29}$$

where $\times$ represents cross product.

It can be observed from (3.24)-(3.25)) that the time-dependent terms (i.e. $\cos(\theta_r)$ in the 3-phase model) are removed from this d-q model. Moreover, it has contains less state variables than the 3-phase model (i.e. the dimension of d-q model is six, while the dimension of 3-phase model is nine). Essentially, the d-q model is equivalent to the 3-phase, while the d-q model gives a time-invariant (assume rotor speed $\omega_r$ is invariant) and reduced-dimension representation, which is computationally more efficient for the simulation and easier for the fault analysis. Based on this d-q model, a fault diagnosis scheme for the single-phase short circuit fault is proposed later in Chapter 4.

## 3.3. Modeling of DFIG with Multiple-Phase Fault

In the previous section, we have discussed a simple fault scenario that the short circuit fault only occurs at a single phase of stator. However, as mentioned earlier in this Chapter, the fault may also occur at several phases simultaneously, sometime may even

at the rotor side. To consider such more complex fault scenario (i.e. multi-phase fault), a new DFIG model is developed in this section. Essentially, the single-phase fault can be regarded as a special case of the multi-phase fault, and thus this new model can also be used to represent the fault scenario (i.e. single-phase fault) discussed in the last section. In this new model, a group of parameters (i.e. $\mu_{sa}$, $\mu_{sb}$, $\mu_{sc}$, $\mu_{ra}$, $\mu_{rb}$, and $\mu_{rc}$) are introduced in order to represent how much percentage of the windings are shorted for each phase. By defining these six parameters properly, the short circuit fault at any levels in any phases can be quantitatively described. The model derivation in this section adopts the same procedure and methods as in the previous section. Firstly, a 3-phase model in the natural a-b-c coordinate is developed. Then, a d-q model is developed by transforming the 3-phase into the d-q coordinate.

## 3.3.1. Model in a-b-c Coordinate

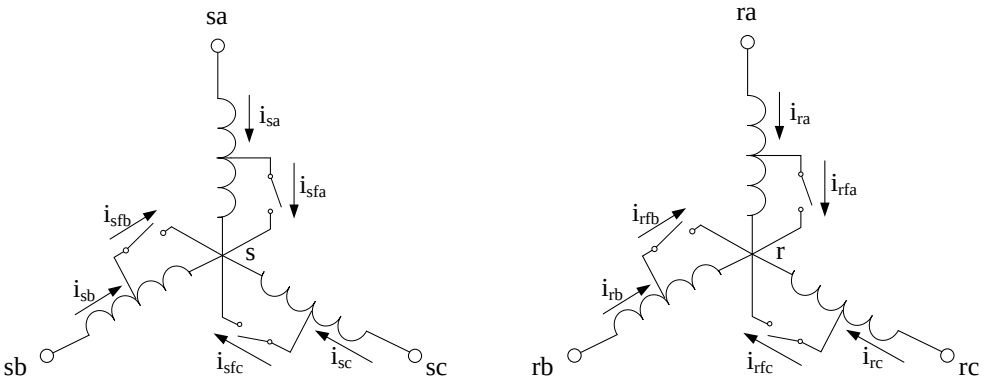


Figure 3.3. Winding configuration of the DFIG with multi-phase faults. (a) Stator winding configuration. (b) Rotor winding configuration

In order to consider all the possible positions where the faults may happen, we add the short circuit to each phase in both stator and rotor no matter it is faulted or not as depicted in Figure 3.3. The healthy and faulted phases are discriminated by setting their corresponding fault level parameters (i.e. $\mu_{sa}$, $\mu_{sb}$, $\mu_{sc}$, $\mu_{ra}$, $\mu_{rb}$, or $\mu_{rc}$). For the healthy phases their corresponding $\mu$ are set as zeros, while for the faulted phases their corresponding $\mu$ are set to some real numbers between 0 and 1.

Therefore, by setting $\mu$ for each phase appropriately, the short circuit fault at any level can be easily introduced to any phases. In addition, each phase is separated by the fault into two parts (i.e. shorted turns and un-shorted turns) which can be modeled as two independent phases. The amount of shorted turns are determined by its corresponding $\mu$, while the amount of un-shorted turns are determined by $1-\mu$. Hence this faulty DFIG can be interpreted as a multi-phase induction machine with six phases in stator and six phases in rotor. The electrical and magnetic relationship among these phases can be represented by the following equations.

Voltage equations:

$$\begin{aligned}
\mathbf{v}_s &= \mathbf{R}_{su}\mathbf{i}_s + \frac{d\boldsymbol{\psi}_{su}}{dt} \\
\mathbf{0}_{3\times1} &= \mathbf{R}_{sf}(\mathbf{i}_s - \mathbf{i}_{sf}) + \frac{d\boldsymbol{\psi}_{sf}}{dt} \\
\mathbf{v}_r &= \mathbf{R}_{ru}\mathbf{i}_r + \frac{d\boldsymbol{\psi}_{ru}}{dt} \\
\mathbf{0}_{3\times1} &= \mathbf{R}_{rf}(\mathbf{i}_r - \mathbf{i}_{rf}) + \frac{d\boldsymbol{\psi}_{rf}}{dt}
\end{aligned} \tag{3.30}$$

Flux equations:

$$\begin{aligned}
\boldsymbol{\psi}_{su} &= \mathbf{L}_{susu}\mathbf{i}_s + \mathbf{L}_{susf}(\mathbf{i}_s - \mathbf{i}_{sf}) + \mathbf{L}_{suru}\mathbf{i}_r + \mathbf{L}_{surf}(\mathbf{i}_r - \mathbf{i}_{rf}) \\
\boldsymbol{\psi}_{sf} &= \mathbf{L}_{sfsu}\mathbf{i}_s + \mathbf{L}_{sfsf}(\mathbf{i}_s - \mathbf{i}_{sf}) + \mathbf{L}_{sfru}\mathbf{i}_r + \mathbf{L}_{sfrf}(\mathbf{i}_r - \mathbf{i}_{rf}) \\
\boldsymbol{\psi}_{ru} &= \mathbf{L}_{rusu}\mathbf{i}_s + \mathbf{L}_{rusf}(\mathbf{i}_s - \mathbf{i}_{sf}) + \mathbf{L}_{ruru}\mathbf{i}_r + \mathbf{L}_{rurf}(\mathbf{i}_r - \mathbf{i}_{rf}) \\
\boldsymbol{\psi}_{rf} &= \mathbf{L}_{rfsu}\mathbf{i}_s + \mathbf{L}_{rfsf}(\mathbf{i}_s - \mathbf{i}_{sf}) + \mathbf{L}_{rfru}\mathbf{i}_r + \mathbf{L}_{rfrf}(\mathbf{i}_r - \mathbf{i}_{rf})
\end{aligned} \tag{3.31}$$

where, the subscripts '$s$' and '$r$' denote the stator and rotor, and the subscripts '$u$' and '$f$' denote the un-shorted turns and shorted turns. The flux vectors $\boldsymbol{\psi}_{su}$, $\boldsymbol{\psi}_{sf}$ $\boldsymbol{\psi}_{ru}$, and $\boldsymbol{\psi}_{rf}$ contain the fluxes in the un-shorted turns and shorted turns in the stator and rotor, respectively. The current vectors $\mathbf{i}_s$ and $\mathbf{i}_r$ contain the currents through each phase of the stator and rotor. The current vectors $\mathbf{i}_{sf}$ and $\mathbf{i}_{rf}$ contains the fault currents through the short circuit loops. All these variable vectors are given in a-b-c coordinate and can be explicitly expressed as

$$\mathbf{v}_s = \begin{bmatrix} v_{sa}, & v_{sb}, & v_{sc} \end{bmatrix}^T, \quad \mathbf{v}_r = \begin{bmatrix} v_{ra}, & v_{rb}, & v_{rc} \end{bmatrix}^T$$

$$\mathbf{i}_s = \begin{bmatrix} i_{sa}, & i_{sb}, & i_{sc} \end{bmatrix}^T, \mathbf{i}_r = \begin{bmatrix} i_{ra}, & i_{rb}, & i_{rc} \end{bmatrix}^T$$

$$\mathbf{i}_{sf} = \begin{bmatrix} i_{sfa}, & i_{sfb}, & i_{sfc} \end{bmatrix}^T, \mathbf{i}_{rf} = \begin{bmatrix} i_{rfa}, & i_{rfb}, & i_{rfc} \end{bmatrix}^T \tag{3.32}$$

$$\boldsymbol{\psi}_{su} = \begin{bmatrix} \psi_{sua}, & \psi_{sub}, & \psi_{suc} \end{bmatrix}^T, \ \boldsymbol{\psi}_{sf} = \begin{bmatrix} \psi_{sfa}, & \psi_{sfb}, & \psi_{sfc} \end{bmatrix}^T$$

$$\boldsymbol{\psi}_{ru} = \begin{bmatrix} \psi_{rua}, & \psi_{rub}, & \psi_{ruc} \end{bmatrix}^T, \ \boldsymbol{\psi}_{rf} = \begin{bmatrix} \psi_{rfa}, & \psi_{rfb}, & \psi_{rfc} \end{bmatrix}^T$$

For the simplicity of the model representation, the fault level parameters are organized into two matrices

$$\boldsymbol{\mu}_s = \begin{bmatrix} \mu_{sa} & 0 & 0 \\ 0 & \mu_{sb} & 0 \\ 0 & 0 & \mu_{sc} \end{bmatrix}, \ \boldsymbol{\mu}_r = \begin{bmatrix} \mu_{ra} & 0 & 0 \\ 0 & \mu_{rb} & 0 \\ 0 & 0 & \mu_{rc} \end{bmatrix} \tag{3.33}$$

Before introducing the model parameters in (3.30) and (3.31), two matrices $\mathbf{L}_0$ and $\mathbf{L}_{\theta_r}$ are firstly defined as

$$\mathbf{L}_0 = M_s \mathbf{g}(0), \ \mathbf{L}_{\theta_r} = M_s \mathbf{g}(\theta_r) \tag{3.34}$$

$$\mathbf{g}(0) = \begin{bmatrix} \cos(0) & \cos(0+2\pi/3) & \cos(0-2\pi/3) \\ \cos(0-2\pi/3) & \cos(0) & \cos(0+2\pi/3) \\ \cos(0+2\pi/3) & \cos(0-2\pi/3) & \cos(0) \end{bmatrix}$$

$$\mathbf{g}(\theta) = \begin{bmatrix} \cos(\theta_r) & \cos(\theta_r+2\pi/3) & \cos(\theta_r-2\pi/3) \\ \cos(\theta_r-2\pi/3) & \cos(\theta_r) & \cos(\theta_r+2\pi/3) \\ \cos(\theta_r+2\pi/3) & \cos(\theta_r-2\pi/3) & \cos(\theta_r) \end{bmatrix}$$

Based on these two matrices, the model parameter matrices in (3.30)-(3.31) are summarized in Table 3.3.

Table 3.3. Parameter matrices of model (3.30)-(3.31).

| | |
|---|---|
| Resistance matrices | $\mathbf{R}_{su} = r_s(\mathbf{I}_3 - \boldsymbol{\mu}_s), \mathbf{R}_{sf} = r_s\boldsymbol{\mu}_s, \mathbf{R}_{ru} = r_r(\mathbf{I}_3 - \boldsymbol{\mu}_r), \mathbf{R}_{rf} = r_r\boldsymbol{\mu}_r$ |
| Self-inductance matrices | $\mathbf{L}_{susu} = L_{\sigma s}(\mathbf{I}_3 - \boldsymbol{\mu}_s) + (\mathbf{I}_3 - \boldsymbol{\mu}_s)\mathbf{L}_0(\mathbf{I}_3 - \boldsymbol{\mu}_s)$<br>$\mathbf{L}_{sfsf} = L_{\sigma s}\boldsymbol{\mu}_s + \boldsymbol{\mu}_s\mathbf{L}_0\boldsymbol{\mu}_s$<br>$\mathbf{L}_{ruru} = L_{\sigma r}(\mathbf{I}_3 - \boldsymbol{\mu}_r) + (\mathbf{I}_3 - \boldsymbol{\mu}_r)\mathbf{L}_0(\mathbf{I}_3 - \boldsymbol{\mu}_r)$ |

| | |
|---|---|
| | $\mathbf{L}_{rfrf} = L_{\sigma r}\boldsymbol{\mu}_r + \boldsymbol{\mu}_r\mathbf{L}_0\boldsymbol{\mu}_r$ |
| Mutual-inductance matrices | $\mathbf{L}_{susf} = \mathbf{L}_{sfsu} = (\mathbf{I}_3 - \boldsymbol{\mu}_s)\mathbf{L}_0\boldsymbol{\mu}_s$, $\mathbf{L}_{rurf} = \mathbf{L}_{rfru} = (\mathbf{I}_3 - \boldsymbol{\mu}_r)\mathbf{L}_0\boldsymbol{\mu}_r$<br>$\mathbf{L}_{suru} = \mathbf{L}_{rusu}^T = (\mathbf{I}_3 - \boldsymbol{\mu}_s)\mathbf{L}_{\theta_r}(\mathbf{I}_3 - \boldsymbol{\mu}_r)$, $\mathbf{L}_{sfrf} = \mathbf{L}_{rfsf}^T = \boldsymbol{\mu}_s\mathbf{L}_{\theta_r}\boldsymbol{\mu}_r$<br>$\mathbf{L}_{surf} = \mathbf{L}_{rfsu}^T = (\mathbf{I}_3 - \boldsymbol{\mu}_s)\mathbf{L}_{\theta_r}\boldsymbol{\mu}_r$, $\mathbf{L}_{sfru} = \mathbf{L}_{rusf}^T = \boldsymbol{\mu}_s\mathbf{L}_{\theta_r}(\mathbf{I}_3 - \boldsymbol{\mu}_r)$ |

The parameters in this table have been defined earlier in Table 3.3.

Model (3.30)-(3.31) can be re-organized into a more compact matrix form, by adding the second equation to the first one and adding the fourth equation to the third one. In this way, a new expression of the model in terms of the phase quantities (i.e. phase currents, phase fluxes, and phase voltages) can be obtained as

$$\begin{bmatrix} \mathbf{v}_s \\ \mathbf{v}_r \\ \hdashline \mathbf{0}_{3\times1} \\ \mathbf{0}_{3\times1} \end{bmatrix} = \left[\begin{array}{cc:cc} \mathbf{R}_s & \mathbf{0}_{3\times3} & -\mathbf{R}_s\boldsymbol{\mu}_s & \mathbf{0}_{3\times3} \\ \mathbf{0}_{3\times3} & \mathbf{R}_r & \mathbf{0}_{3\times3} & -\mathbf{R}_r\boldsymbol{\mu}_r \\ \hdashline \boldsymbol{\mu}_s\mathbf{R}_s & \mathbf{0}_{3\times3} & -\mathbf{R}_s\boldsymbol{\mu}_s & \mathbf{0}_{3\times3} \\ \mathbf{0}_{3\times3} & \boldsymbol{\mu}_r\mathbf{R}_r & \mathbf{0}_{3\times3} & -\mathbf{R}_r\boldsymbol{\mu}_r \end{array}\right] \begin{bmatrix} \mathbf{i}_s \\ \mathbf{i}_r \\ \hdashline \mathbf{i}_{sf} \\ \mathbf{i}_{rf} \end{bmatrix} + \frac{d}{dt}\begin{bmatrix} \boldsymbol{\psi}_s \\ \boldsymbol{\psi}_r \\ \hdashline \boldsymbol{\psi}_{sf} \\ \boldsymbol{\psi}_{rf} \end{bmatrix} \tag{3.35}$$

$$\begin{bmatrix} \boldsymbol{\psi}_s \\ \boldsymbol{\psi}_r \\ \hdashline \boldsymbol{\psi}_{sf} \\ \boldsymbol{\psi}_{rf} \end{bmatrix} = \left[\begin{array}{cc:cc} \mathbf{L}_{ss} & \mathbf{L}_{sr} & -\mathbf{L}_{ss}\boldsymbol{\mu}_s & -\mathbf{L}_{sr}\boldsymbol{\mu}_r \\ \mathbf{L}_{sr}^T & \mathbf{L}_{rr} & -\mathbf{L}_{sr}^T\boldsymbol{\mu}_s & -\mathbf{L}_{rr}\boldsymbol{\mu}_r \\ \hdashline \boldsymbol{\mu}_s\mathbf{L}_{ss} & \boldsymbol{\mu}_s\mathbf{L}_{sr} & -(L_{\sigma s}\boldsymbol{\mu}_s + \boldsymbol{\mu}_s\mathbf{L}_0\boldsymbol{\mu}_s) & -\boldsymbol{\mu}_s\mathbf{L}_{\theta_r}\boldsymbol{\mu}_r \\ \boldsymbol{\mu}_r\mathbf{L}_{sr}^T & \boldsymbol{\mu}_r\mathbf{L}_{rr} & -\boldsymbol{\mu}_r\mathbf{L}_{\theta_r}^T\boldsymbol{\mu}_s & -(L_{\sigma r}\boldsymbol{\mu}_r + \boldsymbol{\mu}_r\mathbf{L}_0\boldsymbol{\mu}_r) \end{array}\right] \begin{bmatrix} \mathbf{i}_s \\ \mathbf{i}_r \\ \hdashline \mathbf{i}_{sf} \\ \mathbf{i}_{rf} \end{bmatrix} \tag{3.36}$$

where flux vectors $\boldsymbol{\psi}_s$ and $\boldsymbol{\psi}_r$ contain the phase fluxes in each phase of the stator and rotor, respectively. They are given as

$$\boldsymbol{\psi}_s = [\psi_{sa}, \quad \psi_{sb}, \quad \psi_{sc}]^T \tag{3.37}$$

$$\boldsymbol{\psi}_r = [\psi_{ra}, \quad \psi_{rb}, \quad \psi_{rc}]^T \tag{3.38}$$

The other variable vectors have been defined in (3.32). The parameter matrices in above model are given as $\mathbf{L}_{ss} = L_{\sigma s}\mathbf{I}_3 + \mathbf{L}_0$, $\mathbf{L}_{sr} = \mathbf{L}_{\theta_r}$ and $\mathbf{L}_{rr} = L_{\sigma r}\mathbf{I}_3 + \mathbf{L}_0$, where matrices $\boldsymbol{\mu}_s$, $\boldsymbol{\mu}_r$, $\mathbf{L}_0$ and $\mathbf{L}_{\theta_r}$ have been defined in (3.33) and (3.34).

By using the torque calculation formula (3.16), the electromagnetic torque for this model can be computed as

$$T_g = \frac{p}{2}((\mathbf{i}_s - \boldsymbol{\mu}_s\mathbf{i}_{sf})^T \frac{\partial \mathbf{L}_{sr}}{\partial \theta_r}(\mathbf{i}_r - \boldsymbol{\mu}_r\mathbf{i}_{rf})) \tag{3.39}$$

where $\frac{\partial(.)}{\partial\theta_r}$ represents the partial differential operator. $\frac{\partial \mathbf{L}_{sr}}{\partial\theta_r}$ has been given in (3.18).

Model (3.35)-(3.36) can represent the short circuit fault at any levels in any phases, by setting appropriate values of parameters $\mu_{sa}$, $\mu_{sb}$, $\mu_{sc}$, $\mu_{ra}$, $\mu_{rb}$, and $\mu_{rc}$. This model is a time-dependent system due to the existence of term $\cos(\theta_r)$. In the next section, a linear model is developed by projecting this nonlinear model into a rotating d-q coordinate.

### 3.3.2. Model in Synchronous d-q Coordinate

In this subsection, the d-q transformation is used to reduce the number of variables and remove the time-dependent term (i.e. $\cos(\theta_r)$) in model (3.35)-(3.36). All the variables of model (3.35)-(3.36) are projected to a two-axis coordinate rotating at the synchronous speed $\omega_s$ (i.e. synchronous d-q coordinate). This new coordinate and its relationship with the stator a-b-c coordinate and rotor a-b-c coordinate are given in Figure 3.4. It is worth noting that the d-q coordinate used in this section is different from the one in Section 3.2.2. The latter is stationary, while the former is rotating at the synchronous speed. By using this non-stationary coordinate, current and voltage become AC signals. This transformation will largely facilitate the controller design problem discussed in Chapter 6.

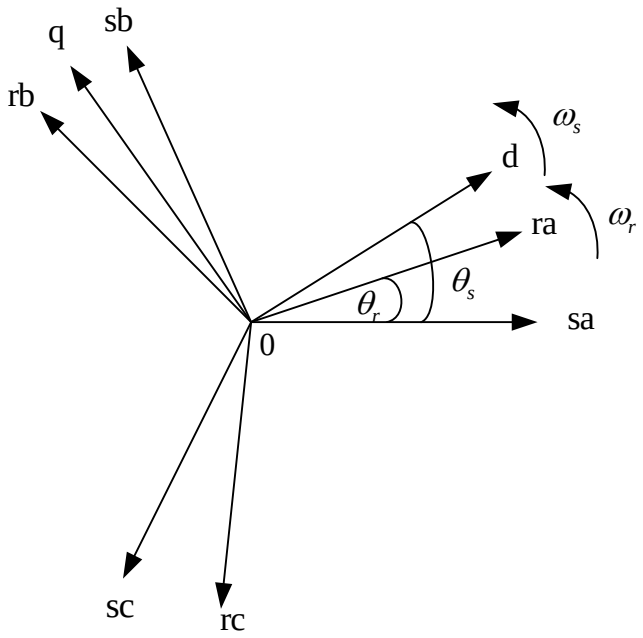


Figure 3.4. Synchronous d-q coordinate and its relationship with the stator a-b-c coordinate and rotor a-b-c coordinate.

The general d-q transformation matrix $\mathbf{T}_{32}$ (from abc to dq) and its corresponding inverse d-q transformation matrix $\mathbf{T}_{23}$ (from dq to abc) is given as follows [113]

$$\mathbf{T}_{32} = \frac{2}{3}\begin{bmatrix} \cos\theta & \cos(\theta - 2\pi/3) & \cos(\theta + 2\pi/3) \\ -\sin\theta & -\sin(\theta - 2\pi/3) & -\sin(\theta + 2\pi/3) \end{bmatrix} \tag{3.40}$$

$$\mathbf{T}_{23} = \begin{bmatrix} \cos\theta & -\sin\theta \\ \cos(\theta - 2\pi/3) & -\sin(\theta - 2\pi/3) \\ \cos(\theta + 2\pi/3) & -\sin(\theta + 2\pi/3) \end{bmatrix} \tag{3.41}$$

Then the d and q variables in the synchronous d-q coordinate can be obtained from a, b, c variables by using the following transformations.

$$\mathbf{x}_{sdq} = \mathbf{T}_{32}\,|_{\theta=\theta_s}\ \mathbf{x}_s, \quad \mathbf{x}_{rdq} = \mathbf{T}_{32}\,|_{\theta=\theta_s-\theta_r}\ \mathbf{x}_r \tag{3.42}$$

By using these transformations, a new DFIG model in the synchronous d-q coordinate is derived

$$\begin{bmatrix} \mathbf{v}_{sdq} \\ \mathbf{v}_{rdq} \\ \hline \mathbf{0}_{2\times1} \\ \mathbf{0}_{2\times1} \end{bmatrix} = \left[\begin{array}{cc:cc} \mathbf{R}_s' & \mathbf{0}_{2\times2} & -\mathbf{R}_s'\boldsymbol{\mu}_{sdq} & \mathbf{0}_{2\times2} \\ \mathbf{0}_{2\times2} & \mathbf{R}_r' & \mathbf{0}_{2\times2} & -\mathbf{R}_r'\boldsymbol{\mu}_{rdq} \\ \hdashline \boldsymbol{\mu}_{sdq}\mathbf{R}_s' & \mathbf{0}_{2\times2} & -\mathbf{R}_s'\boldsymbol{\mu}_{sdq} & \mathbf{0}_{2\times2} \\ \mathbf{0}_{2\times2} & \boldsymbol{\mu}_{rdq}\mathbf{R}_r & \mathbf{0}_{2\times2} & -\mathbf{R}_r'\boldsymbol{\mu}_{rdq} \end{array}\right] \begin{bmatrix} \mathbf{i}_{sdq} \\ \mathbf{i}_{rdq} \\ \hline \mathbf{i}_{sfdq} \\ \mathbf{i}_{rfdq} \end{bmatrix} + \frac{d}{dt}\begin{bmatrix} \boldsymbol{\psi}_{sdq} \\ \boldsymbol{\psi}_{rdq} \\ \hline \boldsymbol{\psi}_{sfdq} \\ \boldsymbol{\psi}_{rfdq} \end{bmatrix} + \left[\begin{array}{cc:cc} \mathbf{J}\omega_s & \mathbf{0}_{2\times2} & \mathbf{0}_{2\times2} & \mathbf{0}_{2\times2} \\ \mathbf{0}_{2\times2} & \mathbf{J}(\omega_s - \omega_r) & \mathbf{0}_{2\times2} & \mathbf{0}_{2\times2} \\ \hdashline \mathbf{0}_{2\times2} & \mathbf{0}_{2\times2} & \mathbf{J}\omega_s & \mathbf{0}_{2\times2} \\ \mathbf{0}_{2\times2} & \mathbf{0}_{2\times2} & \mathbf{0}_{2\times2} & \mathbf{J}(\omega_s - \omega_r) \end{array}\right] \begin{bmatrix} \boldsymbol{\psi}_{sdq} \\ \boldsymbol{\psi}_{rdq} \\ \hline \boldsymbol{\psi}_{sfdq} \\ \boldsymbol{\psi}_{rfdq} \end{bmatrix}$$

(3.43)

$$\begin{bmatrix} \boldsymbol{\psi}_{sdq} \\ \boldsymbol{\psi}_{rdq} \\ \hdashline \boldsymbol{\psi}_{sfdq} \\ \boldsymbol{\psi}_{rfdq} \end{bmatrix} = \left[\begin{array}{cc:cc} \mathbf{L}_{ss}^{'} & \mathbf{L}_{sr}^{'} & -\mathbf{L}_{ss}^{'}\boldsymbol{\mu}_{sdq} & -\mathbf{L}_{sr}^{'}\boldsymbol{\mu}_{rdq} \\ \mathbf{L}_{sr}^{'} & \mathbf{L}_{rr}^{'} & -\mathbf{L}_{sr}^{'}\boldsymbol{\mu}_{sdq} & -\mathbf{L}_{rr}^{'}\boldsymbol{\mu}_{rdq} \\ \hdashline \boldsymbol{\mu}_{sdq}\mathbf{L}_{ss}^{'} & \boldsymbol{\mu}_{sdq}\mathbf{L}_{sr}^{'} & -(L_{\sigma s}\boldsymbol{\mu}_{sdq} + \boldsymbol{\mu}_{sdq}\mathbf{L}_{sr}^{'}\boldsymbol{\mu}_{sdq}) & -\boldsymbol{\mu}_{sdq}\mathbf{L}_{sr}^{'}\boldsymbol{\mu}_{rdq} \\ \boldsymbol{\mu}_{rdq}\mathbf{L}_{sr}^{'} & \boldsymbol{\mu}_{rdq}\mathbf{L}_{rr}^{'} & -\boldsymbol{\mu}_{rdq}\mathbf{L}_{sr}^{'}\boldsymbol{\mu}_{sdq} & -(L_{\sigma r}\boldsymbol{\mu}_{rdq} + \boldsymbol{\mu}_{rdq}\mathbf{L}_{sr}^{'}\boldsymbol{\mu}_{rdq}) \end{array}\right] \begin{bmatrix} \mathbf{i}_{sdq} \\ \mathbf{i}_{rdq} \\ \hdashline \mathbf{i}_{sfdq} \\ \mathbf{i}_{rfdq} \end{bmatrix} \tag{3.44}$$

where the variable vector are given as

$\mathbf{v}_{sdq} = [v_{sd}, v_{sq}]^T$, $\mathbf{v}_{rdq} = [v_{rd}, v_{rq}]^T$,

$\mathbf{i}_{sdq} = [i_{sd}, i_{sq}]^T$, $\mathbf{i}_{rdq} = [i_{rd}, i_{rq}]^T$ $\mathbf{i}_{sfdq} = [i_{sfd}, i_{sfq}]^T$, $\mathbf{i}_{rfdq} = [i_{rfd}, i_{rfq}]^T$.

$\boldsymbol{\psi}_{sdq} = [\psi_{sd}, \psi_{sq}]^T$, $\boldsymbol{\psi}_{rdq} = [\psi_{rd}, \psi_{rq}]^T$, $\boldsymbol{\psi}_{sfdq} = [\psi_{sfd}, \psi_{sfq}]^T$, $\boldsymbol{\psi}_{rfdq} = [\psi_{rfd}, \psi_{rfq}]^T$.

Matrices $\boldsymbol{\mu}_{sdq}$ and $\boldsymbol{\mu}_{rdq}$ are transferred from matrices $\boldsymbol{\mu}_s$ and $\boldsymbol{\mu}_r$ (see in (3.33)) which is defined as

$$\boldsymbol{\mu}_{sdq} = \mathbf{T}_{32}|_{\theta=\theta_s}\ \boldsymbol{\mu}_s \mathbf{T}_{23}|_{\theta=\theta_s},\quad \boldsymbol{\mu}_{rdq} = \mathbf{T}_{32}|_{\theta=\theta_s-\theta_r}\ \boldsymbol{\mu}_r \mathbf{T}_{23}|_{\theta=\theta_s-\theta_r} \tag{3.45}$$

Correspondingly, the electromagnetic torque in the synchronous d-q coordinate is given as

$$T_g = \frac{3}{2} pL_m(\mathbf{i}_{sdq} - \boldsymbol{\mu}_{sdq}\mathbf{i}_{sfdq}) \times (\mathbf{i}_{rdq} - \boldsymbol{\mu}_{rdq}\mathbf{i}_{rfdq}) \tag{3.46}$$

The d-q model (3.43)-(3.44) is a linear model, and it has smaller dimension than the 3-phase model presented in the last section (i.e. the dimension of d-q model is eight, while the dimension of 3-phase model is twelve). Based on this d-q model, a fault diagnosis scheme for the multi-phase short circuit fault is proposed later in Chapter 4.

## 3.4. Equivalent Circuits of DFIG

As it is well known, the equivalent circuit is an important tool in analyzing the characteristics of electric machines. The complex electrical and magnetic relationships among the circuits of an electric machine can directly be observed from a simple equivalent circuit. In this Section, the equivalent circuits of the DFIG with the short circuit fault are developed in order to better understand the essential characteristic of

the short circuit fault and its effects on the DFIG (i.e. output currents and torque). This equivalent circuit is based on the d-q model proposed in Section 3.3.2. By analyzing model (3.43)-(3.44) carefully, we can find that the first two rows of these equations can be organized into a new form as

$$\begin{cases} \mathbf{v}_{sdq} = r_s(\mathbf{i}_{sdq} - \boldsymbol{\mu}_{sdq}\mathbf{i}_{sfdq}) + \dfrac{d\boldsymbol{\psi}_{sdq}}{dt} + \mathbf{J}\omega_s\boldsymbol{\psi}_{sdq} \\ \mathbf{v}_{rdq} = r_r(\mathbf{i}_{rdq} - \boldsymbol{\mu}_{rdq}\mathbf{i}_{rfdq}) + \dfrac{d\boldsymbol{\psi}_{rdq}}{dt} + \mathbf{J}(\omega_s - \omega_r)\boldsymbol{\psi}_{rdq} \end{cases} \tag{3.47}$$

$$\begin{cases} \boldsymbol{\psi}_{sdq} = L_s(\mathbf{i}_{sdq} - \boldsymbol{\mu}_{sdq}\mathbf{i}_{sfdq}) + L_m(\mathbf{i}_{rdq} - \boldsymbol{\mu}_{rdq}\mathbf{i}_{rfdq}) \\ \boldsymbol{\psi}_{rdq} = L_r(\mathbf{i}_{rdq} - \boldsymbol{\mu}_{rdq}\mathbf{i}_{rfdq}) + L_m(\mathbf{i}_{sdq} - \boldsymbol{\mu}_{sdq}\mathbf{i}_{sfdq}) \end{cases} \tag{3.48}$$

These two equations represent the characteristics (i.e. electrical and magnetic characteristics) of the stator and rotor circuits which can be elegantly expressed by a dynamic equivalent circuit as given in Figure 3.5.

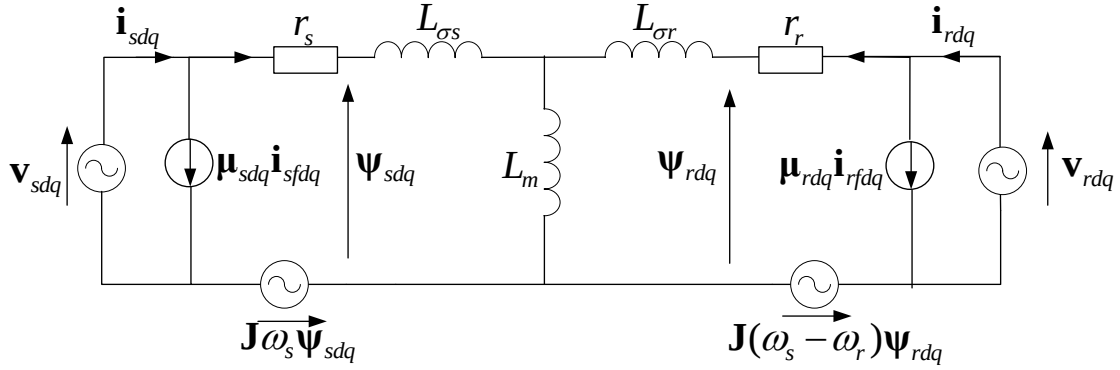


Figure 3.5. Equivalent circuit of a DFIG with short circuit fault: stator and rotor circuits.

As it is shown in this figure, when the short circuit faults occur at the stator and rotor simultaneously, the effects of the faults can be viewed as injecting two independent current sources into the stator and rotor circuits, respectively. The amplitudes of these current sources are decided by $\boldsymbol{\mu}_{sdq}$ and $\boldsymbol{\mu}_{rdq}$ (they represent the fault levels as in (3.33) and (3.45)) as well as $\mathbf{i}_{sfdq}$ and $\mathbf{i}_{rfdq}$ (they represent the fault currents). Actually, the faults only affect the output currents (i.e. $\mathbf{i}_{sdq}$ and $\mathbf{i}_{rdq}$), while other quantities (i.e. fluxes $\boldsymbol{\psi}_{sdq}$ and $\boldsymbol{\psi}_{rdq}$) inside the stator and rotor circuits are

independent from the faults. Moreover, by analyzing equation (3.46), it can be noted that the electromagnetic torque $T_g$ is also independent from the fault. This is because $T_g$ only functionally depends on $\mathbf{i}_{sdq} - \boldsymbol{\mu}_{sdq}\mathbf{i}_{sfdq}$ and $\mathbf{i}_{rdq} - \boldsymbol{\mu}_{rdq}\mathbf{i}_{rfdq}$ which are not affected by the faults. This can be easily observed from Figure 3.5.

In the next, the characteristics of the short circuit loops are investigated. Based on (3.43)-(3.44), the dynamics of the short circuit loops can be expressed by following equations.

$$\frac{d}{dt}(\boldsymbol{\mu}_{sdq}\mathbf{i}_{sfdq}) = -\frac{r_s}{L_{\sigma s}}(\boldsymbol{\mu}_{sdq}\mathbf{i}_{sfdq}) - \mathbf{J}\omega_s(\boldsymbol{\mu}_{sdq}\mathbf{i}_{sfdq}) + \frac{1}{L_{\sigma s}}\boldsymbol{\mu}_{sdq}(\mathbf{I}_2 - \boldsymbol{\mu}_{sdq})^{-1}\mathbf{v}_{sdq} \tag{3.49}$$

$$\frac{d}{dt}(\boldsymbol{\mu}_{rdq}\mathbf{i}_{rfdq}) = -\frac{r_r}{L_{\sigma r}}(\boldsymbol{\mu}_{rdq}\mathbf{i}_{rfdq}) - \mathbf{J}(\omega_s - \omega_r)(\boldsymbol{\mu}_{rdq}\mathbf{i}_{rfdq}) + \frac{1}{L_{\sigma r}}\boldsymbol{\mu}_{rdq}(\mathbf{I}_2 - \boldsymbol{\mu}_{rdq})^{-1}\mathbf{v}_{rdq} \tag{3.50}$$

Defining the flux equations as

$$\boldsymbol{\psi}_{sfdq} = L_{\sigma s}\mathbf{i}_{sfdq}, \quad \boldsymbol{\psi}_{rfdq} = L_{\sigma r}\mathbf{i}_{rfdq} \tag{3.51}$$

then the voltage equations can be obtained as

$$(\mathbf{I}_2 - \boldsymbol{\mu}_{sdq})^{-1}\mathbf{v}_{sdq} = r_s\mathbf{i}_{sfdq} + \frac{d}{dt}\boldsymbol{\psi}_{sfdq} + \mathbf{J}\omega_s\boldsymbol{\psi}_{sfdq} \tag{3.52}$$

$$(\mathbf{I}_2 - \boldsymbol{\mu}_{rdq})^{-1}\mathbf{v}_{rdq} = r_r\mathbf{i}_{rfdq} + \frac{d}{dt}\boldsymbol{\psi}_{rfdq} + \mathbf{J}(\omega_s - \omega_r)\boldsymbol{\psi}_{rfdq} \tag{3.53}$$

Based on these flux and voltage equations, the equivalent circuits of the stator short circuit loop and rotor short circuit loop can be drawn as shown in Figure 3.6.

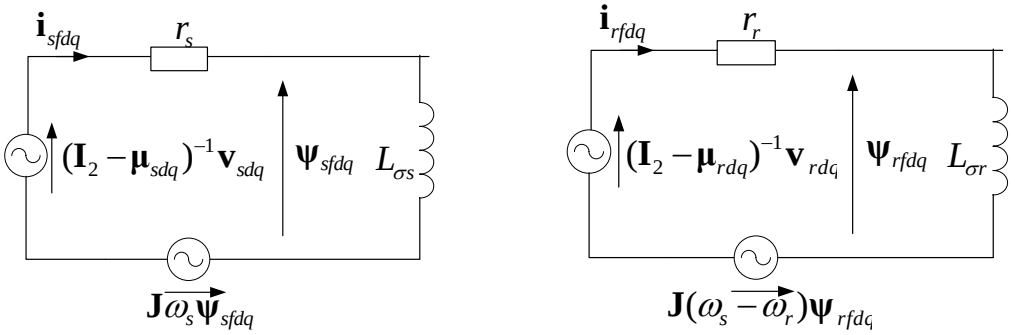


(a) (b)

Figure 3.6. Equivalent circuit of a DFIG with stator circuit fault: (a) stator short-circuit loop. (b) rotor short-circuit loop.

As it is shown in Figure 3.6, the stator short-circuit loop and rotor short-circuit loop are independent of each other and also independent of the stator and rotor circuits. Fault currents $\mathbf{i}_{sfdq}$ and $\mathbf{i}_{rfdq}$ are decided by the fault levels $\boldsymbol{\mu}_{sdq}$ and $\boldsymbol{\mu}_{rdq}$ as well as the stator and rotor voltages (i.e. $\mathbf{v}_{sdq}$ and $\mathbf{v}_{rdq}$).

Based on the above analysis, several important observations are summarized.

1. The effects of the short circuit faults can be considered as additive new currents to the existing output currents. The amplitudes of the new currents are decided by the fault levels and the input voltages.
2. The electromagnetic torque is independent of the short circuit faults.
3. The faults in one side, e.g. the stator, do not affect the current performance in the other side, e.g. the rotor, and vice verse.

These observations are further illustrated through the simulations in the following section.

## 3.5. Simulation Studies

In this section, the models proposed in above sections are simulated in order to analyze and evaluate the behaviours of DFIG in the presence of different short-circuit faults. The simulation studies in this section are carried out in the Matlab/Simulink environment, and the schematic diagram of the implemented system is given in Figure 2.1. The DFIG is rated at 2MW, and its parameters are provided in Appendix A. In this section, we only evaluate the behaviours of the DFIG under open-loop operation, and closed-loop operation is considered later in Chapter 6. The DFIG is supplied with a constant stator supply voltage ($v_{s(phase)}$ = 130 V, $f_s$ = 50 Hz) and a constant rotor control voltage ($v_{r(phase)}$ = 8.2V, $f_r$ = 4Hz). The wind turbine outputs a constant torque ($T_{wt}$ = -250Nm) to the DFIG. In the following, two important issues (i.e. effects of the short circuit faults and behaviours of the fault current $\mathbf{i}_{fdq}$) are studied, and the results of the second one will be used later in Chapter 4 in the context of fault diagnosis.

### 3.5.1. Effects of Short Circuit Fault on Currents and Torque

In this section, the 3-phase models (i.e. model in a-b-c coordinate) proposed in Section 3.2.1 and Section 3.3.1 are simulated to study the dynamic behaviours of DFIG in the presence of single-phase and multi-phase faults. The results are presented in Figure 3.7 and Figure 3.8. As it is shown in Figure 3.7(a)-(b) and Figure 3.8(a)-(b), the three phase currents become asymmetrical when the fault occurs, and an obvious increase can be observed in the current of the faulted phase. This is because the effective impedance of the faulted phase is reduced by the short circuit. Figure 3.8(a) shows that the phase with more serious fault (i.e. higher percentage short circuit) presents larger increase in its current. It also can be observed that the currents in un-faulted phases are not affected by the fault. In Figure 3.7(c) and Figure 3.8(c), we can observe that the short circuit fault induces a small disturbance in the electromagnetic toque, whereas after a short period the torque goes back to its original value. This result is consistent with the conclusions given in Section 3.4.

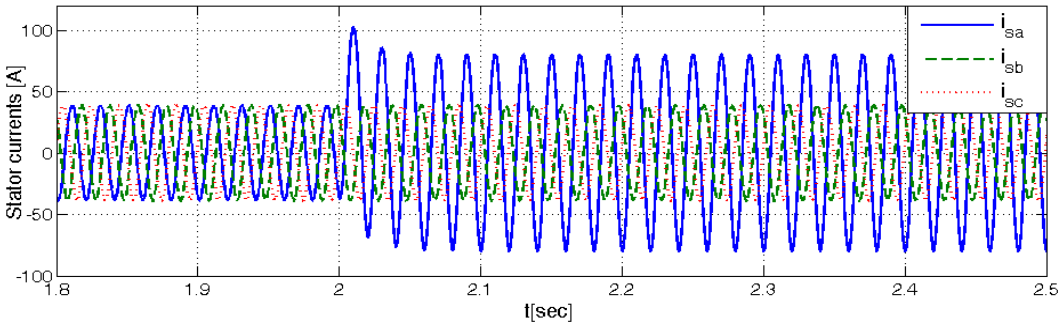


(a) Stator currents

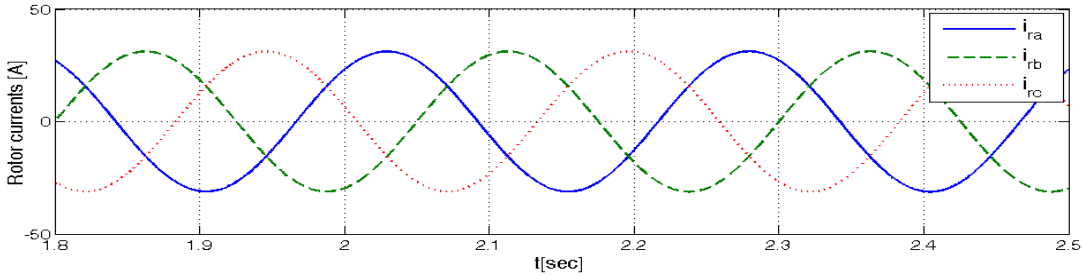


(b) Rotor currents

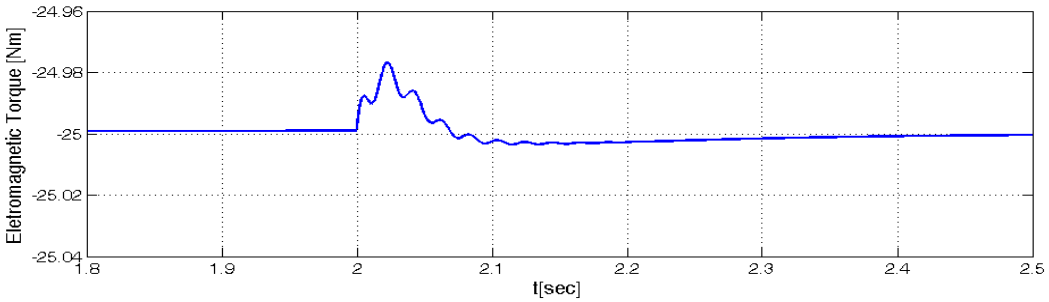


(c) Electromagnetic torque

Figure 3.7. Dynamic behavors of DFIG in the presence of single-phase short circuit fault: A 5% ( $\mu = 0.05$ ) short circuit fault is applied to stator phase 'a' at t=2 sec.

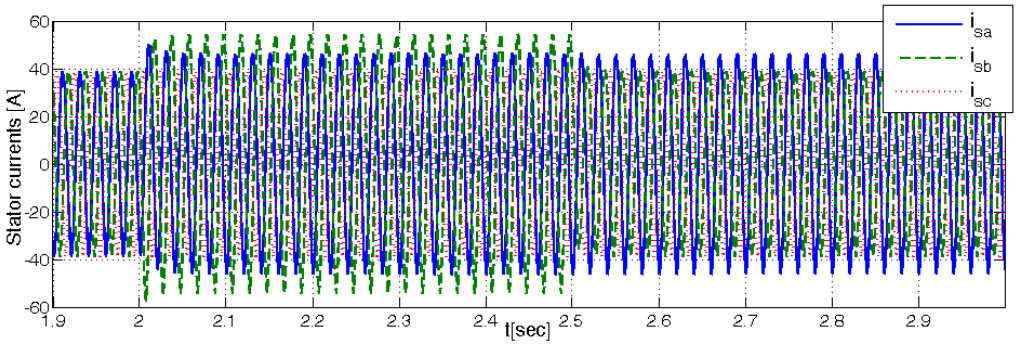


(a) Stator currents

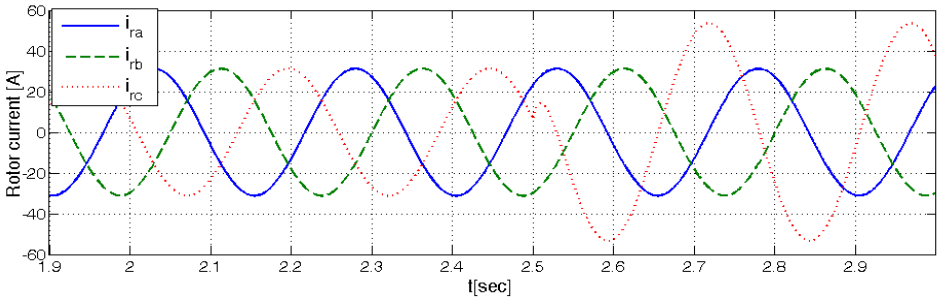


(b) Rotor currents

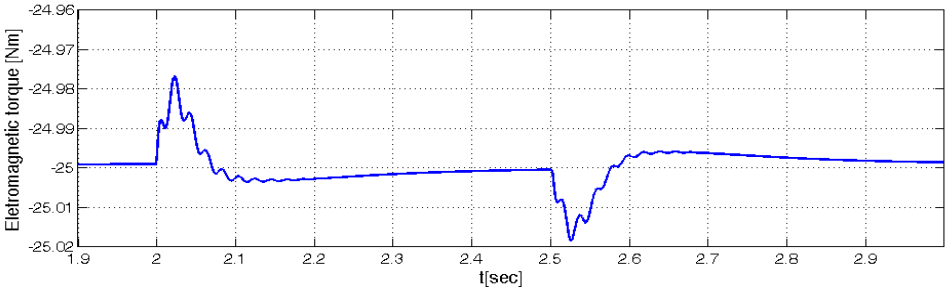


(c) Electromagnetic torque

Figure 3.8. Dynamic behaviours of DFIG in the presence of multi-phase short circuit fault: 1% ( $\mu_{sa} = 0.01$ ) and 2% ( $\mu_{sb} = 0.02$ ) short circuit faults are applied to stator phases 'a' and 'b' simultaneously at t=2sec, thereafter, 10% ( $\mu_{rc} = 0.01$ ) short circuit faults is applied to rotor phase 'c' at t=2.5sec.

## 3.5.2. Behaviour of Fault Current $\mathbf{i}_{fdq}$

In the previous subsection, the effects of short circuit faults on the currents and torque have been analyzed based on the simulations of the 3-phase models. In this subsection, we aim to analyze the behaviours of the fault current $\mathbf{i}_{fdq}$ (i.e. a vector composed of $i_{fd}$ and $i_{fq}$), which is generated from the simulations of the d-q model proposed in Section 3.2.2. The analysis results will be used later in Chapter 4 for the fault diagnosis. A short circuit fault is introduced into stator phase 'a', 'b' and 'c', respectively, and for each case the simulations results are presented in Figure 3.9.

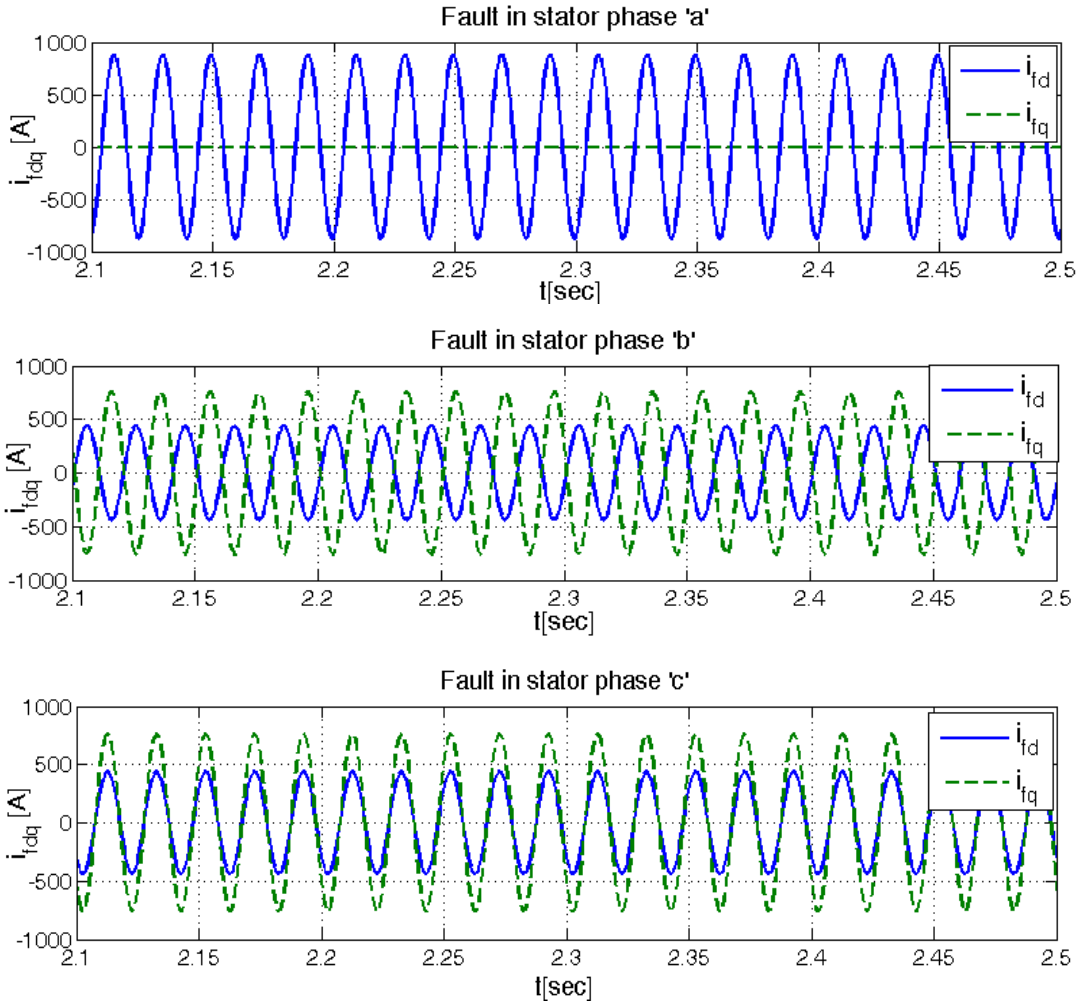


Figure 3.9. Fault current $\mathbf{i}_{fdq}$ in time domain.

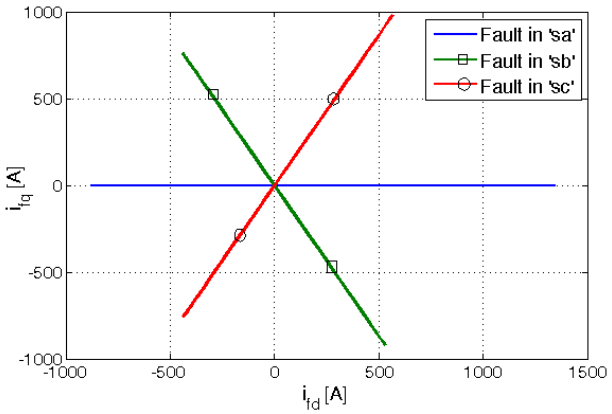


Figure 3.10. Fault current $\mathbf{i}_{fdq}$ in d-q plane.

As it is shown in this figure, fault current $\mathbf{i}_{fdq}$ has different signatures for three different fault positions (i.e. phase 'a', 'b', or 'c') in the time domain. It is essentially due to the selection of different fault position parameter $\mathbf{f}_{xdq}$ (see in (3.23)). However, it would be more convenient to identify such difference in the d-q plane as given in Figure 3.10. It can be noticed that the phase angle of $\mathbf{i}_{fdq}$ is in accordance with the physical position of the faulted phase, hence it can be used to indicate the fault position. In other words, when fault occurs in any phase, it will be reflected in the corresponding positions as indicated in Figure 3.10. This result is important as it will be employed for the fault diagnosis later in Chapter 4. However, this result can only be used to detect the fault position, for the diagnosis of the magnitude of the fault (i.e. short circuit current), other approaches need to be used as discussed in Chapter 5.

## 3.6. Summary

This chapter is concerned with the modeling of DFIG with winding short circuit faults. The single-phase short circuit and multi-phase short circuit are regarded as two different fault scenarios, and modeled separately. For them, two mathematical models are proposed, where a set of new parameters are introduced to quantitatively represent the fault. The model derivation for both of these fault scenarios follows the same procedure. Firstly, 3-phase models in the a-b-c coordinate are developed. Thereafter simplified d-q models (i.e. linear and reduced order) are derived by using d-q

transformation. Based on the model equations, the dynamic equivalent circuits of DFIG with the short circuit faults are provided. By analyzing the equivalent circuits, the characteristics of the fault and its effects on the DFIG (i.e. electromagnetic torque and phase currents) are concluded in Section 3.4 and further demonstrated via the simulation studies.

# 4. Diagnosis of Single-Phase Short Circuit Fault in DFIG

## 4.1. Introduction

In the previous chapter, the winding short circuit fault has been explicitly investigated, and two mathematical models for the single-phase and multi-phase faults have been developed. In this chapter, we focus on diagnosing the first fault (i.e. single-phase fault). A model-based fault diagnosis scheme is developed, which is based on the model proposed in Section 3.2. Since most model-based methods are based on the model represented in the state-space form, thus in this chapter, an important sinusoidal signal decomposition technique, i.e. sequence component decomposition technique [103] is applied to transform the model developed in the previous chapter (expressed by the voltage and flux equations as in (3.24)-(3.25)) into a state-space representation. In this way, the single-phase fault can be formulated as an additive term in the state space model (i.e. the additive fault). To diagnose this fault, a conventional adaptive observer [118] is firstly designed, which can provide an unbiased estimation of the fault under the assumption that no model uncertainties exist in the DFIG. However, in practice, due to the magnetic saturation and parameter variations (e.g. resistance varies with the temperature), etc., the model uncertainties may occur. In such situation, the conventional adaptive may fail to estimate the fault. Hence, a new robust adaptive observer is developed in this chapter by adding a leakage term to the adaptive law, which allows the bounded estimation errors of the states and faults. Additionally, to improve the accuracy of the fault estimation, $H_\infty$ optimization technique [104] is implemented to optimally design the parameters of the adaptive observer so as to minimize the estimation errors. The condition that

DFIG operates under varying speed is also discussed in this chapter. To ensure the stability of the adaptive observer in the presence of speed variation, a LPV adaptive observer is developed based on the self-scheduled theory [105], [106]. Its stability condition is provided by means of Linear Matrix Inequalities (LMIs).

This chapter is organized as follows. Section 4.2 introduces the principles of the sequence component decomposition, and derives the positive and negative sequence models of the DFIG with the single-phase short circuit fault. In Section 4.3, these two models are organized into a standard linear state-space representation. In Section 4.4, a conventional adaptive observer is designed to estimate the fault. To enhance the robustness of the fault estimation, in Section 4.5, a robust adaptive observer is proposed, followed by an $H_\infty$ design of the observer parameters. Based on this result, a LPV adaptive observer for the varying speed condition is proposed in Section 4.6. In Section 4.7, the simulation studies illustrate the effectiveness of the proposed fault diagnosis scheme.

## 4.2. Sequence Component Decomposition

The sequence component decomposition is a widely used technique dealing with the structural asymmetry problems of the electric machines [92], [93], [107]. In this section, this technique is employed to decompose the model of the faulty DFIG (as in Section 3.2.2) into two sub-models, namely positive-sequence model and negative-sequence model, and then organize them into the state-space representations.

### 4.2.1. Principle of Sequence Component Decomposition

According to [103], a sinusoidal vector $\mathbf{f}_{dq}$ ($\mathbf{f}_{dq}=\left[ f_d(t),\ f_q(t) \right]^T$, where $f_d(t)$ and $f_q(t)$ are the sinusoidal signals) can be represented in terms of the positive-sequence phasor ($\tilde{F}^+$) and negative-sequence phasor ($\tilde{F}^-$), which are given as

$$\mathbf{f}_{dq} = \frac{1}{2}\tilde{F}^+ e^{j\omega t} + \frac{1}{2}\tilde{F}^- e^{-j\omega t} \tag{4.1}$$

where superscripts '+' and '—' represent the positive sequence and negative sequence,

respectively. $\omega$ is the angular frequency of the sinusoidal signals. In the rectangular notation, these phasors are given as

$$\tilde{F}^{+} = F_d^{+} + jF_q^{+}, \quad \tilde{F}^{-} = F_d^{-} + jF_q^{-} \tag{4.2}$$

where $F_d^{+}$ and $F_q^{+}$ are the d and q variables in the d-q coordinate rotating at $\omega$ (or denoted as $(\mathrm{dq})^{+}$ coordinate), while $F_d^{-}$ and $F_q^{-}$ are the d and q variables in the d-q coordinate rotating at $-\omega$ (or denoted as $(\mathrm{dq})^{-}$ coordinate). Since these variables are independent of frequency $\omega$, thus in the sinusoidal steady-state they become constants.

Figure 4.1 demonstrates the basic principle of the sequence component decomposition. A sinusoidal signal is projected into two opposite rotating d-q coordinates (one is rotating at $\omega$, and the other is rotating at $-\omega$). By doing this, the signal of each channel is converted into a direct current (DC) signal corrupted with a double frequency alternating current (AC) signal. These DC signals correspond to the positive-sequence and negative-sequence phasors, which need to be preserved. Hence, the low pass filters tuned at double frequency are adopted to remove the AC signals.

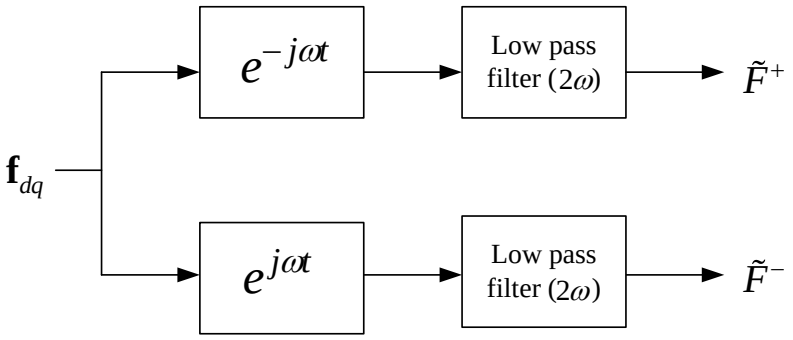


Figure 4.1 . The principle of the sequence component decomposition.

## 4.2.2. Positive-Sequence and Negative-Sequence Models

As mentioned earlier in Section 3.2.2, model (3.24)-(3.25) is given in the stationary d-q coordinate, therefore its variable vectors are the sinusoidal vectors with synchronous frequency $\omega_s$. By applying the sequence component decomposition, this model can be decomposed into two sub-models: positive-sequence model and

negative-sequence model, which are given as follows

Positive sequence model:

$$\begin{cases} \tilde{V}_s^+ = r_s(\tilde{I}_s^+ - \frac{2}{3}\mu\tilde{I}_f^+) + \frac{d}{dt}\tilde{\Psi}_s^+ + j\omega_s\tilde{\Psi}_s^+ \\ \tilde{V}_r^+ = r_r\tilde{I}_r^+ + \frac{d}{dt}\tilde{\Psi}_r^+ + j(\omega_s - \omega_r)\tilde{\Psi}_r^+ \end{cases} \tag{4.3}$$

$$\begin{cases} \tilde{\Psi}_s^+ = L_s(\tilde{I}_s^+ - \frac{2}{3}\mu\tilde{I}_f^+) + L_m\tilde{I}_r^+ \\ \tilde{\Psi}_r^+ = L_r\tilde{I}_r^+ + L_m(\tilde{I}_s^+ - \frac{2}{3}\mu\tilde{I}_f^+) \end{cases} \tag{4.4}$$

Negative sequence model:

$$\begin{cases} \tilde{V}_s^- = r_s(\tilde{I}_s^- - \frac{2}{3}\mu\tilde{I}_f^-) + \frac{d}{dt}\tilde{\Psi}_s^- - j\omega_s\tilde{\Psi}_s^- \\ \tilde{V}_r^- = r_r\tilde{I}_r^- + \frac{d}{dt}\tilde{\Psi}_r^- - j(\omega_s + \omega_r)\tilde{\Psi}_r^- \end{cases} \tag{4.5}$$

$$\begin{cases} \tilde{\Psi}_s^- = L_s(\tilde{I}_s^- - \frac{2}{3}\mu\tilde{I}_f^-) + L_m\tilde{I}_r^- \\ \tilde{\Psi}_r^- = L_r\tilde{I}_r^- + L_m(\tilde{I}_s^- - \frac{2}{3}\mu\tilde{I}_f^-) \end{cases} \tag{4.6}$$

where, subscripts ‘ *s* ’ and ‘ *r* ’ represent the stator and rotor. The variables with symbol ‘ ~ ’ are the phasors. Therefore $\tilde{V}_s^+$ , $\tilde{V}_s^-$ , $\tilde{V}_r^+$ , and $\tilde{V}_r^-$ represent the positive-sequence and negative-sequence phasors of the stator and rotor voltages, respectively. $\tilde{I}_s^+$ , $\tilde{I}_s^-$ , $\tilde{I}_r^+$ , and $\tilde{I}_r^-$ represent the positive-sequence and negative-sequence phasors of the stator and rotor currents, respectively. $\tilde{\Psi}_s^+$, $\tilde{\Psi}_s^-$, $\tilde{\Psi}_r^+$, and $\tilde{\Psi}_r^-$ are the positive-sequence and negative-sequence phasors of the stator and rotor fluxes, respectively. $\tilde{I}_f^+$ and $\tilde{I}_f^-$ are the positive-sequence and negative-sequence phasors of the fault current, respectively.

## 4.3. State Space Model Representation

To facilitate the observer design in the following sections, the models proposed in last subsection are transformed into the state-space representations. It has been mentioned

earlier that the sequence components are constants in the sinusoidal steady-state, thus we can have that $\frac{d}{dt}\tilde{I}_f^+ = 0$ and $\frac{d}{dt}\tilde{I}_f^- = 0$. In this case, model (4.3)-(4.4) and model (4.5)-(4.6) can both be rewritten into the following form, by selecting currents as the state variables.

$$\begin{cases} \dot{x}(t) = Ax(t) + Bu(t) + B_f f(t) \\ y(t) = Cx(t) \end{cases} \tag{4.7}$$

The variables and parameter matrices for these two models are defined in the following table.

Table 4.1. The variables and parameter matrices for the positive sequence and negative sequence models.

| | Positive Sequence Model | Negative Sequence Model |
|---|---|---|
| State, input, and output variables | $x^+(t) = \left[ i_{sd}^+,\ i_{sq}^+,\ i_{rd}^+,\ i_{rq}^+ \right]^T$<br>$u^+(t) = \left[ v_{sd}^+,\ v_{sq}^+,\ v_{rd}^+,\ v_{rq}^+ \right]^T$<br>$y^+(t) = \left[ i_{sd}^+,\ i_{sq}^+,\ i_{rd}^+,\ i_{rq}^+ \right]^T$ | $x^-(t) = \left[ i_{sd}^-,\ i_{sq}^-,\ i_{rd}^-,\ i_{rq}^- \right]^T$<br>$u^-(t) = \left[ v_{sd}^-,\ v_{sq}^-,\ v_{rd}^-,\ v_{rq}^- \right]^T$<br>$y^-(t) = \left[ i_{sd}^-,\ i_{sq}^-,\ i_{rd}^-,\ i_{rq}^- \right]^T$ |
| Fault variables | $f^+(t) = \left[ \mu i_{fd}^+, \mu i_{fq}^+ \right]^T$ | $f^-(t) = \left[ \mu i_{fd}^-, \mu i_{fq}^- \right]^T$ |
| Parameter matrices | $A^+ = A_r + \omega_s A_{\omega_s} - \omega_r A_{\omega_r}$<br>$B_f^+ = -\frac{2}{3}[A_1^+,\ A_2^+]$ | $A^- = A_r - \omega_s A_{\omega_s} - \omega_r A_{\omega_r}$<br>$B_f^- = -\frac{2}{3}[A_1^-,\ A_2^-]$ |
| | $B = \frac{1}{D}\begin{bmatrix} L_r\mathbf{I}_2 & -L_m\mathbf{I}_2 \\ -L_m\mathbf{I}_2 & L_s\mathbf{I}_2 \end{bmatrix},\ C = \mathbf{I}_4$ | |

In above table, the parameter or variable with superscript '+' belongs to the positive sequence model, while the one with superscript '-' belongs to the negative sequence model. $A_1$ and $A_2$ represent the first and second columns of $A$. Matrices $A_r$, $A_{\omega_s}$ and $A_{\omega_r}$ are given as

$$A_r = \frac{1}{D}\begin{bmatrix} -L_r r_s\mathbf{I}_2 & L_m r_r\mathbf{I}_2 \\ L_m r_s\mathbf{I}_2 & -L_s r_r\mathbf{I}_2 \end{bmatrix},\ A_{\omega_s} = -\begin{bmatrix} \mathbf{J} & \mathbf{0} \\ \mathbf{0} & \mathbf{J} \end{bmatrix},\ A_{\omega_r} = \frac{1}{D}\begin{bmatrix} L_m^2\mathbf{J} & L_r L_m\mathbf{J} \\ -L_s L_m\mathbf{J} & -L_s L_r\mathbf{J} \end{bmatrix} \tag{4.8}$$

where $D = L_s L_r - L_m^2$. $\mathbf{J}$ is given in (3.28). $\omega_s$ is the synchronous speed, and $\omega_r$ is the electrical rotor speed.

It can be observed that (4.7) is a linear MIMO system. Fault variables $f^+(t)$ and $f^-(t)$ are used to represent the winding short circuit fault, which is also considered as the additive faults in model (4.7). When considering the rotor speed ($\omega_r$) is a known constant, model (4.7) is simply a linear time invariant (LTI) system. Nevertheless, in practice, the DFIGs are predominately operating under the varying speed. For such case, system (4.7) becomes a linear parameter varying (LPV) system with time-varying parameter $\omega_r$, which can be measured in real-time. Essentially, LPV systems can be considered as a special class of linear time varying (LTV) systems. The main difference with LTV system is that in LPV systems the time-dependence of the system matrix (i.e. A, B, C) is not known a priori but is given only implicitly by a time varying parameter $p(t)$ which is assumed to be a priori unknown but available in real-time.

## 4.4. Conventional Adaptive Observer

The adaptive observers have made enormous achievement on diagnosing the constant or slow varying faults (some works have been reviewed in Section 2.3.1). In this section, assuming that rotor speed ($\omega_r$) is invariant and no model uncertainties exist in system (4.7), a conventional adaptive observer is designed to estimate fault variables $f^+(t)$ and $f^-(t)$, in order to diagnose the short circuit. The observer is given as follows

***Algorithm 4.1 (conventional adaptive observer)[118]:***

$$\begin{cases} \dot{\hat{x}}(t) = A\hat{x}(t) + Bu(t) + B_f \hat{f}(t) + L(y(t) - \hat{y}(t)) \\ \hat{y}(t) = C\hat{x}(t) \\ \dot{\hat{f}}(t) = \Gamma^{-1} B_f^T P(x(t) - \hat{x}(t)) \end{cases} \tag{4.9}$$

where $\hat{x}(t) \in \mathbb{R}^4$ is the state vector of the observer and $\hat{y}(t) \in \mathbb{R}^4$ is the output vector of the observer. $\hat{f}(t) \in \mathbb{R}^2$ is the estimation of the fault $f(t)$. $L \in \mathbb{R}^{4\times4}$, $P \in \mathbb{R}^{4\times4}$ and $\Gamma \in \mathbb{R}^{2\times2} > 0$ are the parameters to be designed.

With knowing that the fault $f(t)$ is constant in the sinusoidal steady-state, we can have $\dot{f}(t) = 0$. By comparing observer (4.9) with the system (4.7) and denoting

$$e_x(t) = x(t) - \hat{x}(t), \quad e_f(t) = f(t) - \hat{f}(t) \tag{4.10}$$

Then the estimation error dynamic system can be obtained as

$$\begin{cases} \dot{e}_x(t) = (A - LC)e_x(t) + B_f e_f(t) \\ \dot{e}_f(t) = -\Gamma^{-1} B_f^T P e_x(t) \end{cases} \tag{4.11}$$

**Theorem 4.1**: For a parameter matrix $\Gamma > 0$, if there exist two symmetric positive definite matrices $P$ and $Q$, such that the following condition holds

$$(A - LC)^T P + P(A - LC) = -Q \tag{4.12}$$

the adaptive observer (4.9) with gain $L$ is asymptotically stable and can ensure $\lim_{t\to\infty} e_x(t) = 0$ and $\lim_{t\to\infty} e_f(t) = 0$.

**Proof** : Select the Lyapunov function as

$$V(t) = e_x^T(t) P e_x(t) + e_f^T(t) \Gamma^{-1} e_f(t) \tag{4.13}$$

Its first derivative with respect to time is

$$\dot{V}(t) = e_x^T(t)((A - LC)^T P + P(A - LC))e_x(t) + 2e_f^T(t) B_f^T P e_x(t) + 2e_f^T(t)\Gamma^{-1}\dot{e}_f(t) \tag{4.14}$$

From the second equation of (4.11), we can have

$$e_f^T(t) B_f^T P e_x(t) + e_f^T(t)\Gamma^{-1}\dot{e}_f(t) = 0 \tag{4.15}$$

then (4.14) can be reduced as

$$\dot{V}(t) = e_x^T(t)((A - LC)^T P + P(A - LC))e_x(t) \tag{4.16}$$

According to condition (4.12), we can conclude that $\dot{V}(t) = -e_x^T(t) Q e_x(t) < 0$, which

means the estimation error system (4.11) is asymptotically stable and thus all the variables ($e_x(t), e_f(t)$) are bounded ($e_x(t) \in L_\infty$, $e_f(t) \in L_\infty$, this is according to the Lyapunov stability theory in Appendix B.1). Furthermore, we can show that

$$\int_0^\infty e_x^T(t) Q e_x(t) dt = V(0) - V(\infty) < \infty \tag{4.17}$$

This implies that $e_x(t)$ is a bounded $L^2$ signal ($e_x(t) \in L_2$). According to (4.11), we can have $\dot{e}_x(t) \in L_\infty$. Now, we have established that $e_x(t) \in L_2 \cap L_\infty$ and $\dot{e}_x(t) \in L_\infty$. According to Barbalat lemma (as in Appendix B.2 ), we can conclude $\lim_{t\to\infty} e_x(t) = 0$. Since it can be shown that

$$\int_0^\infty \dot{e}_x(t) dt = \lim_{t\to\infty} e_x(t) - e_x(0) = -e_x(0) \tag{4.18}$$

then from (4.11) it can be conclude that $\dot{e}_x(t)$ is uniformly continuous. Again, using the Barbalat lemma we can have $\lim_{t\to\infty} \dot{e}_x(t) = 0$. This means $\lim_{t\to\infty} e_f(t) = 0$. □

**Remark 4.1**: In the adaptive observer (4.9), the tuning gain $\Gamma$ for the adaptive law are usually chosen by trial and error using simulations in order to achieve a good rate of convergence. Small $\Gamma$ may result slow convergent rate whereas large $\Gamma$ may make this observer algorithm difficult to solve numerically in the simulations. In the fault vector $f(t)$, we have two elements to be estimated, therefore $\Gamma$ should be chosen properly to balance the convergence speeds between these two elements.

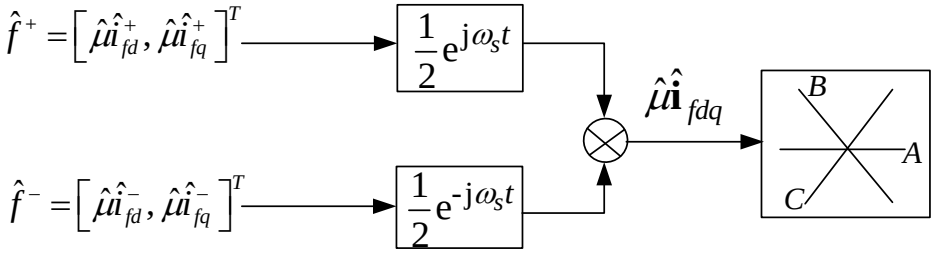


Figure 4.2. The synthesis of $\mu \mathbf{i}_{fdq}$

Two adaptive observers are required for the positive-sequence and negative-sequence models (as in Table 6) to estimate faults $f^+(t)$ and $f^-(t)$,

respectively. Once these two faults are estimated, variable vector $\mu\mathbf{i}_{fdq}$ can be obtained through the scheme given in Figure 4.2. According to the discussion in Section 3.5.2, the phase angle of fault current $\mathbf{i}_{fdq}$ is in accordance with the physical position of the faulted phase, and it thus can be used to indicate the fault position. Parameter $\mu$ (i.e. fault level parameter) is a scalar. Therefore, $\mu\mathbf{i}_{fdq}$ can be directly used to diagnose the fault position. The overall fault diagnosis scheme is given in Figure 4.3. The disadvantage of this scheme is that it is unable to diagnose the fault level, as the fault level parameter $\mu$ is unknown and can not be identified using this observer. However, this problem can be solved by using model (i.e. state-space model as in (5.8)) and the fault diagnosis scheme proposed in Chapter 5, where the unknown fault level parameter $\mu$ is formulated explicitly as a model parameter and can then be estimated, although more complicated model and observer are required.

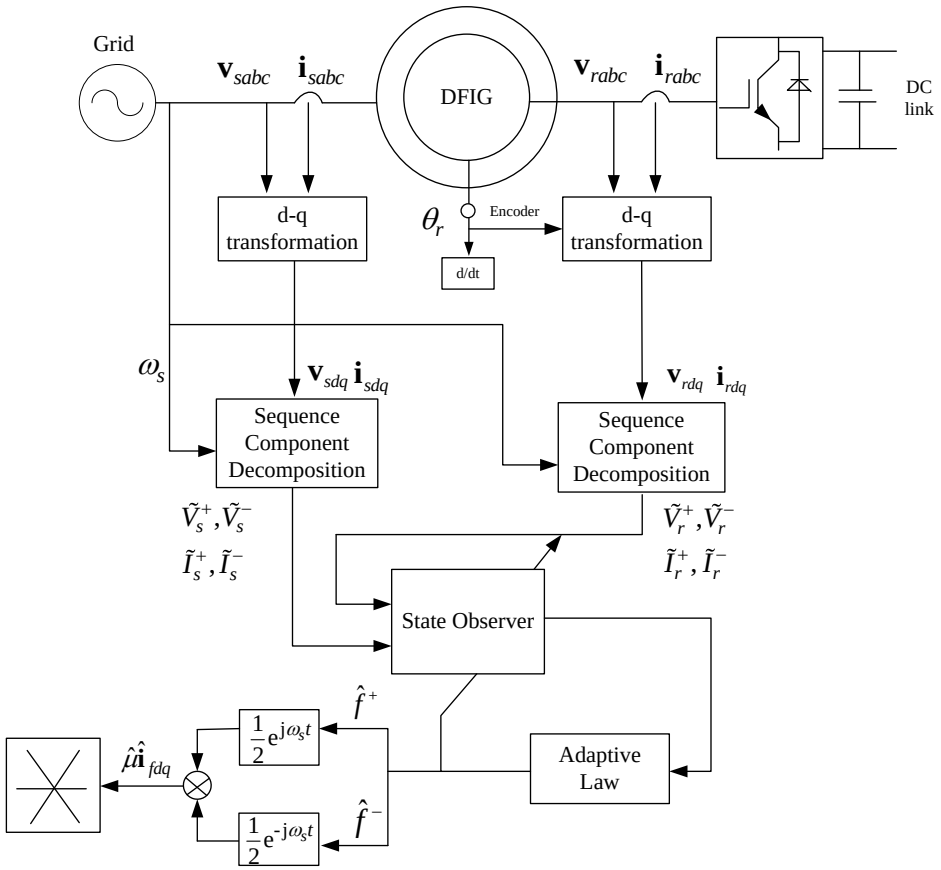


Figure 4.3. Schematic diagram of adaptive observer based fault diagnosis for single-phase short circuit fault.

## 4.5. Robust Adaptive Observer

In last section, a conventional adaptive observer is designed with the assumption that no model uncertainties exist in the DFIG (as in (4.7)). However, in practice, the model uncertainties can be caused by the magnetic saturation and parameter variations (e.g. resistance varies with the temperature), etc. As mentioned earlier in the introduction of this chapter, the conventional adaptive observer (as in last section) may give an unstable estimation of the fault in the presence of model uncertainties. To overcome this problem, several approaches have been applied to modify the observer (see [48]). An important approach is to add a leakage term (σ-modification) to the parameter adaptive law, which allows bounded estimations of the states and parameters. However, the estimation accuracy (i.e. enough small estimation errors) can not be guaranteed by this approach. In this section, the $H_\infty$ optimization technique is applied to optimally design observer gains so as to ensure the accuracy of the fault estimation.

Taking account of the model uncertainties and assuming rotor speed ( $\omega_r$ ) is invariant, the system (4.7) can be rewritten as

$$\begin{cases} \dot{x}(t) = Ax(t) + Bu(t) + B_f f(t) + w(t) \\ y(t) = Cx(t) \end{cases} \tag{4.19}$$

where the model uncertainties are represented by an unknown input $w(t) \in \mathbb{R}^4$. It is assumed that

$$\|w(t)\| \le \sigma < +\infty, \ , \ \|f(t)\| \le \tau < +\infty \tag{4.20}$$

For such a system, a modified adaptive observer is developed, which is given as follows.

### *Algorithm 4.2 (modified adaptive observer)[48]:*

$$\begin{cases} \dot{\hat{x}}(t) = A\hat{x}(t) + Bu(t) + B_f \hat{f}(t) + L(y(t) - C\hat{x}(t)) \\ \dot{\hat{f}}(t) = -\Gamma_1 \hat{f}(t) - \Gamma_2 (y(t) - C\hat{x}(t)) \end{cases} \tag{4.21}$$

where, $L \in \mathbb{R}^{4\times4}$, $\Gamma_1 \in \mathbb{R}^{2\times2} > 0$, $\Gamma_2 \in \mathbb{R}^{2\times4}$ are the parameters to be determined

By subtracting the observer with system (4.7) and considering (4.10), the estimation error dynamic system is obtained

$$\begin{cases} \dot{e}_x(t) = (A - LC)e_x(t) + B_f e_f(t) + w(t) \\ \dot{e}_f(t) = -\Gamma_1 e_f(t) + \Gamma_2 C e_x(t) + \Gamma_1 f(t) \end{cases} \tag{4.22}$$

Before presenting the main results, an important lemma the proof of theorem 4.2 is introduced

**Lemma 4.1:** Let $E$ and $F$ be real matrices of appropriate dimensions. Then for any scalar $\varepsilon > 0$ and the vectors $x, y \in \mathbb{R}^n$, we have

$$2x^T EFy \le \varepsilon^{-1} x^T EE^T x + \varepsilon y^T FF^T y \tag{4.23}$$

**Theorem 4.2**: if there exist $\Gamma_1 > 0$, $\Gamma_2$, $X$ and a symmetric positive definite matrix $P$, such that the following inequality is satisfied.

$$\Omega = \begin{bmatrix} A^T P - C^T X^T + PA - XC + I & (B_f^T P + \Gamma_2 C)^T \\ B_f^T P + \Gamma_2 C & -2\Gamma_1 + I \end{bmatrix} < 0 \tag{4.24}$$

then the adaptive observer (4.21) with gain $L = P^{-1}X$ is asymptotically stable and it can ensure $e_x(t)$ and $e_f(t)$ are uniformly ultimately bounded.

**Proof:** Selecting the Lyapunov function as

$$V(t) = e_x^T(t) P e_x(t) + e_f^T(t) e_f(t) \tag{4.25}$$

Its first derivative with respect to time is

$$\begin{aligned} \dot{V}(t) &= e_x^T(t) P e_x(t) + e_f^T(t) e_f(t) \\ &= e_x^T(t)((A - LC)^T P + P(A - LC))e_x(t) + 2e_f^T(t)(B_f^T P + \Gamma_2 C)e_x(t) - 2e_f^T(t)\Gamma_1 e_f(t) \\ &\quad + 2w^T(t) P e_x(t) + 2e_f^T(t)\Gamma_1 f(t) \end{aligned} \tag{4.26}$$

By defining $X = PL$, we have

$$\begin{aligned} \dot{V}(t) = e_x^T(t)(A^T P - C^T X^T + PA - XC)e_x(t) + 2e_f^T(t)(B_f^T P + \Gamma_2 C)e_x(t) \\ -2e_f^T(t)\Gamma_1 e_f(t) + 2w^T(t) P e_x(t) + 2e_f^T(t)\Gamma_1 f(t) \end{aligned} \tag{4.27}$$

then applying lemma 4.1 to above inequality, we can obtain

$$\begin{aligned}\dot{V}(t) \le & e_x^T(t)(A^T P - C^T X^T + PA - XC + I)e_x(t) \\ & +2e_f^T(t)(B_f^T P + \Gamma_2 C)e_x(t) + e_f^T(t)(-2\Gamma_1 + I)e_f(t) \\ & +w^T(t)PP\ w\ (t) + f^T(t)\Gamma_1\Gamma_1^T f(t)\end{aligned} \tag{4.28}$$

which can be organized into an extended form as

$$\dot{V}(t) \le \eta\ (t)^T \Omega\ \eta\ (t) + \delta \tag{4.29}$$

where $\eta\ (t) = \left[ e_x^T(t)\ \ e_f^T(t) \right]^T$, $\delta = \sigma^2 \lambda_{\max}(PP) + \tau^2 \lambda_{\max}(\Gamma_1 \Gamma_1^T)$, and

$$\Omega\ = \begin{bmatrix} A^T P - C^T X^T + PA - XC + I & (B_f^T P + \Gamma_2 C)^T \\ B_f^T P + \Gamma_2 C & -2\Gamma_1 + I \end{bmatrix} \tag{4.30}$$

From (4.24), we can conclude that

$$\dot{V}(t) \le -\left|\lambda_{\max}(\Omega)\right| \eta\ (t)^T \eta\ (t) + \delta \tag{4.31}$$

Then (4.31) implies that $\dot{V}(t)$ is negative definite if

$$\eta\ (t)^T \eta\ (t) > \delta / \left|\lambda_{\max}(\Omega)\right| \tag{4.32}$$

which indicates that the $\eta\ (t)$ is uniformly bounded. In other words, $e_x(t)$ and $e_f(t)$ are also bounded.

□

## 4.5.1. Optimal Adaptive Observer

In last subsection, a modified adaptive observer is designed to enhance the robustness of the fault estimation. Although condition (4.24) ensures that the bounded estimation errors of the faults in the presence of model uncertainties, it does not guarantee that the estimation errors are small enough in the context of the accuracy for the fault diagnosis. In this section, we aim to minimize the estimation errors by using $H_\infty$ optimization approach. Before presenting the main results, an important performance index (i.e. disturbance attenuation level) is introduced.

Estimation error dynamic system (4.22) can be organized into an augmented form as

$$\begin{cases} \dot{\bar{x}}(t) = \bar{A}\bar{x}(t) + \bar{B}d(t) \\ z(t) = \bar{C}\bar{x}(t) \end{cases} \tag{4.33}$$

where $d(t)$ represents the disturbance of this system, which is given as

$$d(t) = [w^T(t),\ f^T(t)]^T \tag{4.34}$$

and the augmented state and system matrices are given as

$$\bar{x}(t) = [e_x^T(t),\ e_f^T(t)]^T \tag{4.35}$$

$$\bar{A} = \begin{bmatrix} A - LC & B_f \\ \Gamma_2 C & -\Gamma_1 \end{bmatrix},\ \bar{B} = \begin{bmatrix} I & 0 \\ 0 & \Gamma_1 \end{bmatrix},\ \bar{C} = \begin{bmatrix} I & 0 \\ 0 & I \end{bmatrix} \tag{4.36}$$

The effect of disturbance $d(t)$ on the system output $z(t)$ can be represented by a $H_\infty$ norm.

$$\left\| T_{zd}(s) \right\|_\infty = \sup \frac{\|z(t)\|}{\|d(t)\|} \tag{4.37}$$

where $T_{zd}(s)$ is the transfer function between the disturbance $d(t)$ and the output $z(t)$. ‘sup’ represents supreme value. $\left\| T_{zd}(s) \right\|_\infty$ represents $H_\infty$ norm of transfer function $T_{zd}(s)$. $\|z(t)\|$ represents the $L_2$ norm of signal $z(t)$.

If $T_{zd}(s)$ is linear time invariant, then

$$\left\| T_{zd}(s) \right\|_\infty = \sup_\omega \bar{\sigma}(T_{zd}(j\omega)) \tag{4.38}$$

where $\bar{\sigma}$ represents maximum singular value. The objective is then to design the observer gains ($L$, $\Gamma_1$ and $\Gamma_2$), such that the system (4.33) has a guaranteed disturbance attenuation level $\gamma > 0$, which can be expressed as

$$\left\| T_{zd}(s) \right\|_\infty = \sup \frac{\|z(t)\|}{\|d(t)\|} < \gamma \tag{4.39}$$

This condition is equivalent to

$$\|z(t)\|^2 < \gamma^2 \|d(t)\|^2 \tag{4.40}$$

It is also equivalent to

$$\|e_x(t)\|^2 + \|e_f(t)\|^2 < \gamma^2 (\|f(t)\|^2 + \|w(t)\|^2) \tag{4.41}$$

If the estimation errors $e_x(t)$ and $e_f(t)$ satisfy the above inequality, we can say

that system (4.33) has a guaranteed $\gamma$ level of disturbance attenuation. The following theorem provides an analytical method for the design of observer parameters in order to guarantee this disturbance attenuation level.

**Theorem 4.3:** The estimation error dynamic system (4.33) is asymptotically stable and has a guaranteed $\gamma$ level of disturbance attenuation, if there exist a scalar $\gamma > 0$, matrices $\Gamma_1 > 0$, $\Gamma_2$, $X$ and a symmetric positive definite matrix $P$, such that the following inequality satisfied.

$$\Omega = \begin{bmatrix} A^T P - C^T X^T + PA - XC + I & (B_f^T P + \Gamma_2 C)^T & 0 & P \\ & -2\Gamma_1 + I & \Gamma_1 & 0 \\ * & & -\gamma^2 I & 0 \\ & & & -\gamma^2 I \end{bmatrix} < 0 \quad (4.42)$$

**Proof:** Firstly, the asymptotic stability of system (4.33) with $d(t) \equiv 0$ needs to be established. Select the Lyapunov equation as (4.25). Its first derivative with respect to time is calculated as

$$\begin{aligned} \dot{V}(t) = {} & e_x^T(t)(A^T P - C^T X^T + PA - XC)e_x(t) + 2e_f^T(t)(B_f^T P + \Gamma_2 C)e_x(t) \\ & + e_f^T(t)(-2\Gamma_1)e_f(t) \end{aligned} \quad (4.43)$$

Defining $\eta_0(t) = [e_x^T(t),\ e_f^T(t),\ f(t)]^T$, (4.43) can be expressed as

$$\dot{V}(t) = \eta_0(t)\Omega_0\eta_0(t) \quad (4.44)$$

with

$$\Omega_0 = \begin{bmatrix} A^T P - C^T X^T + PA - XC & (B_f^T P + \Gamma_2 C)^T \\ B_f^T P + \Gamma_2 C & -2\Gamma_1 \end{bmatrix} < 0 \quad (4.45)$$

This inequality is satisfied by (4.42). Thus, it can be concluded that $\dot{V}(t) < 0$.

To establish the $H_\infty$ performance index for system (4.22), the following performance index is defined

$$J_\infty = \int_0^\infty \phi(t)dt \quad (4.46)$$

where $\phi(t) = e_x^T(t)e_x(t) + e_f^T(t)e_f(t) - \gamma^2(f^T(t)f(t) + w^T(t)w(t))$ (4.47)

As $\dot{V}(t) < 0$, we can have

$$J_\infty < \int_0^\infty (\phi(t) + \dot{V}(t))dt \tag{4.48}$$

Then by letting $\eta(t) = [e_x^T(t),\ e_f^T(t),\ f(t),\ w(t)]^T$, we can have

$$\phi(t) + \dot{V}(t) = \eta^T(t)\Omega\eta(t) \tag{4.49}$$

where $\Omega$ is given in (4.42).

A sufficient condition for $J_\infty < 0$ is that

$$\forall t \in [0, \infty],\ \ \phi(t) + \dot{V}(t) < 0 \tag{4.50}$$

which is satisfied by (4.42). Therefore, it can be concluded that the system (4.33) has a guaranteed $\gamma$ level of disturbance attenuation. □

With the result of Theorem 4.3, the robust adaptive observer with a guaranteed disturbance attenuation level for (4.19) can be solved by testing the feasibility of the LMI (4.42). Note that any feasible solution of (4.42) yields a suitable gain for the adaptive observer(4.21). The smallest disturbance attenuation level $\gamma$ can be obtained by solving following LMI optimization problem:

$$\min_{P, X, \Gamma_1, \Gamma_2} \ \chi \tag{4.51}$$

Subject to (4.42) with $\chi = \gamma^2$

It should be noted that this is a LMI optimization problem which can be readily solved by using the MATLAB LMI toolbox.

## 4.5.2. Self-Scheduled LPV Adaptive Observer

In the above work, the DFIG rotor speed ($\omega_r$) is assumed as a known and invariant parameter. However, in practice, speed $\omega_r$ often varies in order to adapt to the wind speed and achieve a high efficiency of the wind power generation. In this situation, system (4.7) becomes a LPV system by viewing $\omega_r$ as an online measurable time-varying parameter instead of a priori. For such system, a gain-scheduled LPV adaptive observer with guaranteed $H_\infty$ performance (as in (4.39)) is developed in this

section.

Considering the time-varying parameter $\omega_r(t)$, LTI system (4.19) can be re-expressed as a LPV system, which is given as

$$\begin{cases} \dot{x}(t) = A(\omega_r(t))x(t) + Bu(t) + B_f(\omega_r(t))f(t) + w(t) \\ y(t) = Cx(t) \end{cases} \tag{4.52}$$

where matrices $A(\omega_r(t))$ and $B_f(\omega_r(t))$ affinely depend on $\omega_r(t)$ (as in Table 4.1). The rotor speed ($\omega_r$) predominately varies within $\pm 30\%$ around the synchronous speed ($\omega_s$). In other word, $\omega_r(t) \in (\omega_{r\min}, \omega_{r\max})$ with $\omega_{r\min} = 0.7\omega_s$ and $\omega_{r\max} = 1.3\omega_s$.

### *Algorithm 4.3 (LPV adaptive observer):*

For LPV system (4.52), a gain-scheduled adaptive observer is developed, which has the same structure as (4.9) but with a time-varying observer gain $L(\omega_r(t))$.

$$\begin{cases} \dot{\hat{x}}(t) = A(\omega_r(t))\hat{x}(t) + Bu(t) + B_f(\omega_r(t))\hat{f}(t) + L(\omega_r(t))(y(t) - C\hat{x}(t)) \\ \dot{\hat{f}}(t) = -\Gamma_1\hat{f}(t) - \Gamma_2(y(t) - C\hat{x}(t)) \end{cases} \tag{4.53}$$

The estimation error dynamic system is obtained by comparing (4.52) with (4.53)

$$\begin{cases} \dot{e}_x(t) = (A(\omega_r(t)) - L(\omega_r(t))C)e_x(t) + B_f(\omega_r(t))e_f(t) + w(t) \\ \dot{e}_f(t) = -\Gamma_1 e_f(t) + \Gamma_2 C e_x(t) + \Gamma_1 f(t) \end{cases} \tag{4.54}$$

The stability of this estimation error dynamic system can be proved and is given in Theorem 4.4.

**Theorem 4.4:** The estimation error dynamic system (4.54) is asymptotically stable and satisfies $H_\infty$ performance (4.39) for any $\omega_r(t)$ within $(\omega_{r\min}, \omega_{r\max})$, if there exist a scalar $\gamma > 0$, matrices $\Gamma_1 > 0$, $\Gamma_2$, $X_1$, $X_2$ and a symmetric positive definite matrix $P$, such that the following two inequalities satisfied.

$$\Omega=\begin{bmatrix} A(\omega_{\max})^T P - C^T X_1^T + PA(\omega_{\max}) - X_1 C + I & (B_f^T(\omega_{\max})P + \Gamma_2 C) & 0 & P \\ & -2\Gamma_1 + I & \Gamma_1 & 0 \\ * & & -\gamma^2 I & 0 \\ & & & -\gamma^2 I \end{bmatrix} < 0 \quad (4.55)$$

$$\Omega=\begin{bmatrix} A(\omega_{\min})^T P - C^T X_2^T + PA(\omega_{\min}) - X_2 C + I & (B_f^T(\omega_{\min})P + \Gamma_2 C)^T & 0 & P \\ & -2\Gamma_1 + I & \Gamma_1 & 0 \\ * & & -\gamma^2 I & 0 \\ & & & -\gamma^2 I \end{bmatrix} < 0 \quad (4.56)$$

The time-varying observer gain is given as

$$L(\omega_r(t)) = \big(1-\delta(t)\big) L_1 + \delta(t) L_2 \quad (4.57)$$

where $$\delta(t) = \frac{\omega_r(t) - \omega_{r\min}}{\omega_{r\max} - \omega_{r\min}} \quad (0 < \delta(t) < 1) \quad (4.58)$$

Matrices $L_1$ and $L_2$ are given as

$$L_1 = P^{-1} X_1 \quad , \quad L_2 = P^{-1} X_2 . \quad (4.59)$$

**Proof:** According to Theorem 4.3, estimation error system (4.54) is asymptotically stable and ensure $H_\infty$ performance if there exist single matrix $P > 0$ for any $\omega_r(t)$ within $\left(\omega_{r\min},\ \omega_{r\max}\right)$, such that the following LMI is satisfied.

$$\Omega=\begin{bmatrix} \big(A(\omega_r(t)) - L(\omega_r(t))\big)^T P + P\big(A(\omega_r(t)) - L(\omega_r(t))\big) + I & (B_f^T(\omega_r(t))P + \Gamma_2 C)^T & 0 & P \\ & -2\Gamma_1 + I & \Gamma_1 & 0 \\ * & & -\gamma^2 I & 0 \\ & & & -\gamma^2 I \end{bmatrix} < 0 \quad (4.60)$$

Since matrices $A(\omega_r(t))$ , $L(\omega_r(t))$ and $B_f(\omega_r(t))$ affinely depend on parameter $\omega_r(t)$ and vary within in a polytope of matrices whose vertices are the images of the vertices $\omega_{r\min}$ and $\omega_{r\max}$. In other words

$$\begin{pmatrix} A(\omega_r(t)) \\ L(\omega_r(t)) \\ B_f(\omega_r(t)) \end{pmatrix} = \big(1-\delta(t)\big) \begin{pmatrix} A(\omega_{r\max}) \\ L(\omega_{r\max}) \\ B_f(\omega_{r\max}) \end{pmatrix} + \delta(t) \begin{pmatrix} A(\omega_{r\min}) \\ L(\omega_{r\min}) \\ B_f(\omega_{r\min}) \end{pmatrix} \quad (4.61)$$

This implies for the synthesis of inequality (4.60) that we can replace the search over the whole polytope without loss of generality by the search over its extreme points. Consequently, condition (4.60) is replaced by two LMIs on vertices $\omega_{r\min}$ and $\omega_{r\max}$, which are given in (4.55) and (4.56). □

## 4.6. Simulation Studies

In this section, the adaptive observer algorithms proposed in above sections (i.e. conventional adaptive observer, optimal adaptive observer, LPV adaptive observer) are applied for the diagnosis of the single-phase short circuit fault. Their performances under various conditions (i.e. no model uncertainties, in the presence of model uncertainties, speed variation) are evaluated through simulations. In these simulations, the DFIG operates under open-loop condition, supplied with the stator supply voltage ($v_s$ = 130 V, $f_s$ = 50 Hz) and the rotor control voltage ($v_{r(phase)}$ = 8.2V, $f_r$ = 4Hz). The nominal parameters of DFIG are provided in Appendix A. Based on these parameters, the parameter matrices of model (4.7) are calculated and given in Appendix C.1.

### 4.6.1. Performance of Conventional Adaptive Observer in the Ideal Case

In this subsection, the DFIG is simulated at a constant rotor speed ($\omega_r = 289\,\text{rad/s}$), under a constant wind turbine torque ($T_{wt} = -250\,\text{Nm}$). An ideal case taking no account of model uncertainties is considered in this subsection. Two conventional adaptive observers (Algorithm 4.1) are designed as in (4.12) to estimate faults $f^+(t)$ and $f^-(t)$, respectively, whose parameters are given in Appendix C.2.

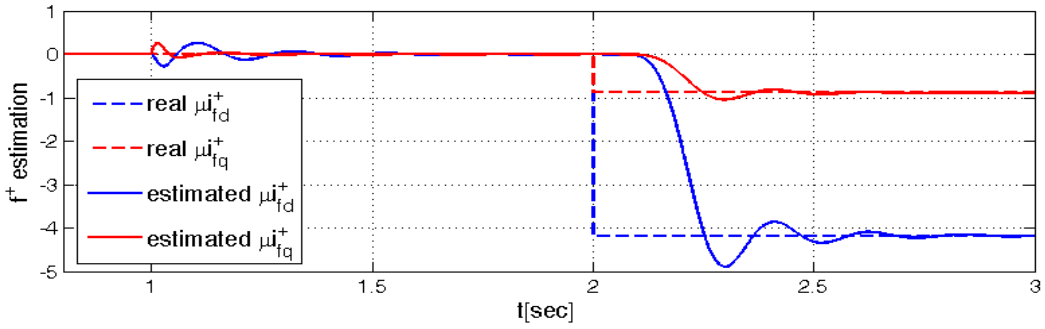


Figure 4.4. $f^+$ estimation using conventional adaptive observer.

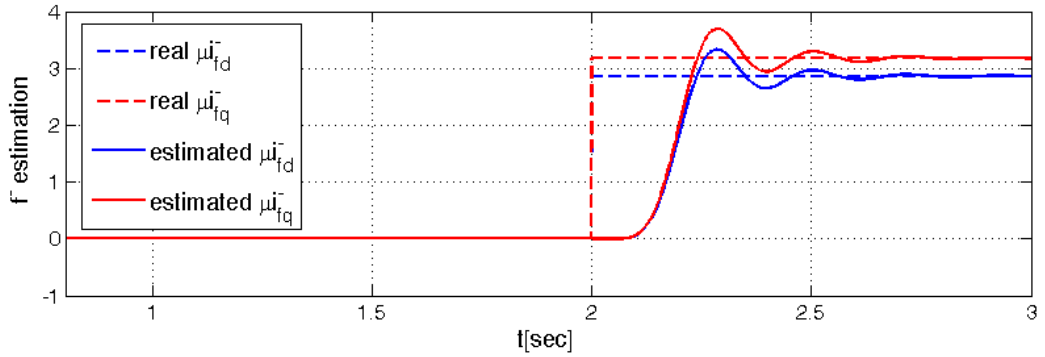


Figure 4.5. $f^-$ estimation using conventional adaptive observer.

The observer is activated at t=1sec after the DFIG reaching the steady state, and thereafter a 1% ($\mu = 0.01$) short circuit fault is applied to stator phase 'b' at t=2sec. Figure 4.4 and Figure 4.5 presents the real values of the faults ($f^+(t)$, $f^-(t)$) and their estimates. It can be observed that the conventional adaptive observer gives unbiased estimations of the faults in ideal case taking no account of the model uncertainties, while a delayed response (approximate 0.2 sec) of the estimation can be clearly observed at t=2sec, which is caused by the low filters in the sequence component decomposition (see in Figure 4.1).

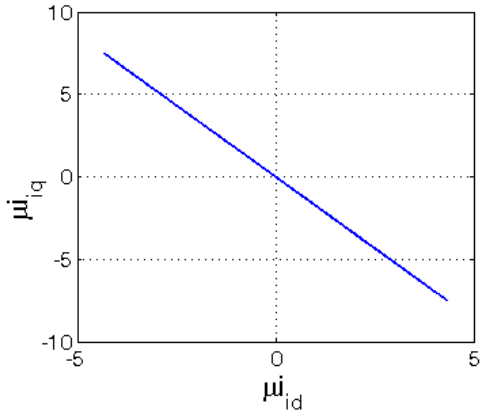


Figure 4.6. $\mu \mathbf{i}_{fdq}$ in d-q plane.

Based on the estimated $f^{+}(t)$ and $f^{-}(t)$, variable vector $\mu \mathbf{i}_{fdq}$ is synthesized according to Figure 4.2 in order to diagnose the fault position. Figure 4.6 presents $\mu \mathbf{i}_{fdq}$ in the d-q plane. As it is shown in this figure, the phase angle of the vector $\mu \mathbf{i}_{fdq}$ is $120^{\circ}$. By comparing it with Figure 3.10, it can be concluded that the short circuit fault occurs at phase 'b'.

### 4.6.2. Robustness of Optimal Adaptive Observer against Model Uncertainties

In this subsection, the performance of the proposed optimal adaptive observer (see in Section 4.5.1) in the presence of model uncertainties is evaluated via simulations. The model uncertainties are introduced by a parameter variation (i.e. an abrupt change of stator resistance $r_s$) in this simulation example. The conventional adaptive observer given in last subsection is also simulated in this subsection for the purposes of comparison. By solving the optimization problem (4.51) using Matlab LMI toolbox, a minimum disturbance attenuation level is obtained, which is $\gamma = 1.42$. The associated parameter matrices of adaptive observer (4.21) are given in Appendix C.3.

Figure 4.7 presents the maximum singular value for the transfer function $T_{zd}(j\omega)$ (as in (4.37)) versus frequency $\omega$. In this figure the horizontal dashed line

corresponds to $\gamma = 1.42$. It can be observed that the maximum singular value $T_{zd}(j\omega)$ is less then minimum value of $\gamma$. We thus can conclude that the proposed optimal adaptive observer has a guaranteed $\gamma$ level of disturbance attenuation.

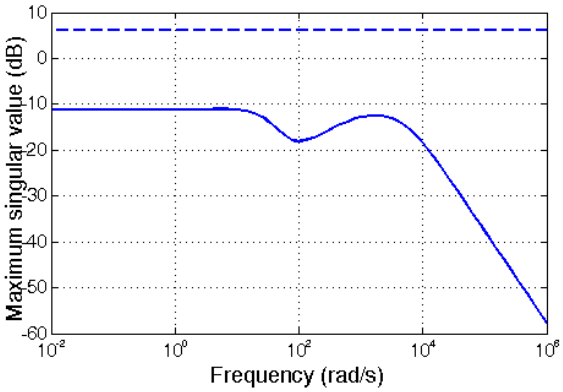


(a) Positive-sequence model.

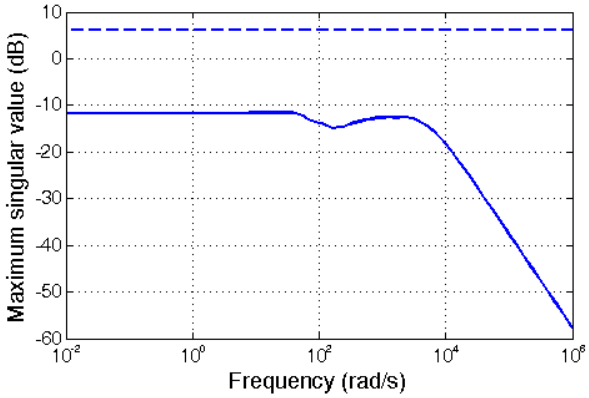


(b) Negative-sequence model.

Figure 4.7. Maximum singular value of transfer function $T_{zd}(j\omega)$.

The optimal adaptive observer resulting from $\gamma = 1.42$ is implemented to estimate faults $f^{+}(t)$ and $f^{-}(t)$. Firstly, a 1% ($\mu = 0.01$) short circuit fault is applied to stator phase 'b' at t=2sec, and then a 5% variation of the stator resistance $r_s$ is applied at t=3sec. The conventional adaptive observer designed in last subsection is also applied here for the comparison purposes and the results are given in Figure 4.8. As it shown in this figure apparently, although the conventional adaptive is able to provide unbiased fault estimations in the absence of model uncertainties (before t=3sec), it becomes unstable when model uncertainties occurs (i.e. variation of the parameter $r_s$

at t=3sec). Figure 4.9 demonstrates the fault estimation results of the optimal adaptive observer. As it is shown in this figure, when the model uncertainties occur, the estimated $f^+$ and $f^-$ are still able to track their true values in a desired accuracy. It can also be observed from this figure that the estimation errors always exist even in the absence of model uncertainties, and such biases are increased when model uncertainties are introduced. However, these small estimation biases do not affect the fault diagnosis results, which will be demonstrated in the following. In addition, when model uncertainty (i.e. variation of the parameter $r_s$) is applied at t=3s, it can be observed in Figure 4.9 that d component of the estimated fault variables (i.e. $f^+$ and $f^-$) has larger biase than q component, which domenstrates that the d component is more sensitive to the model uncertainty.

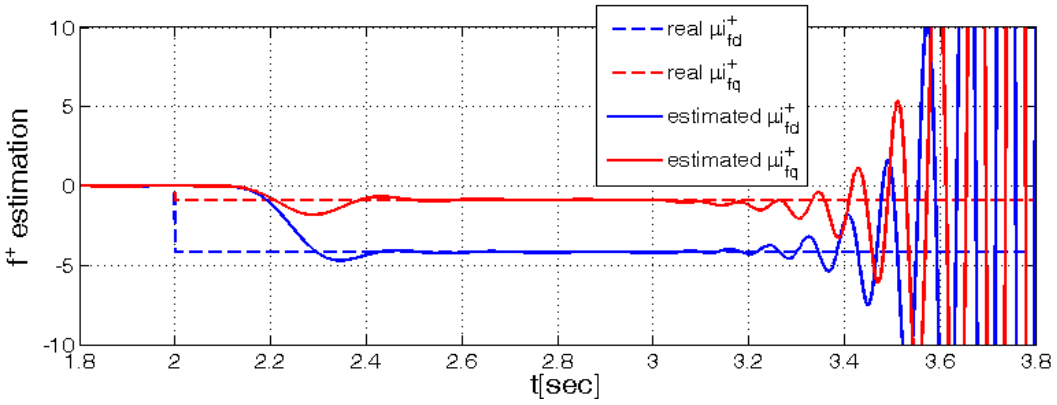


(a) $f^+$ estimation.

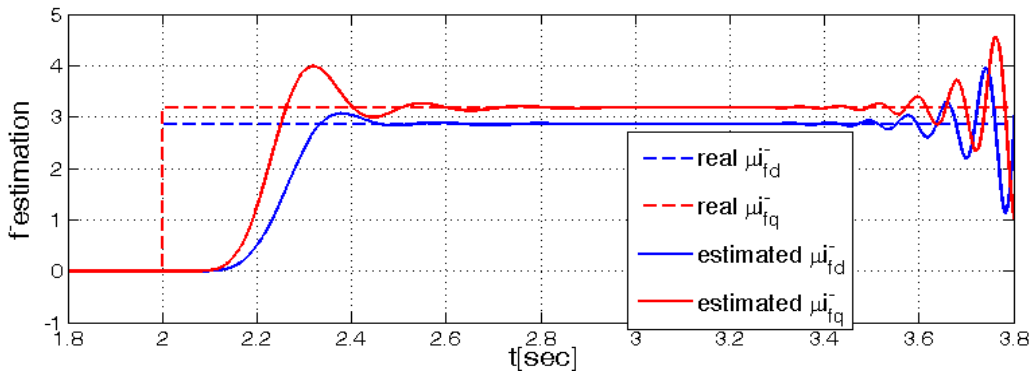


(b) $f^-$ estimation.

Figure 4.8. Performance of the conventional adaptive observer in the presence of model uncertainties. a 1% ($\mu = 0.01$) short circuit fault is applied to stator phase 'b' at t=2sec, and a 5% variation of $r_s$ is introduced at t=3sec.

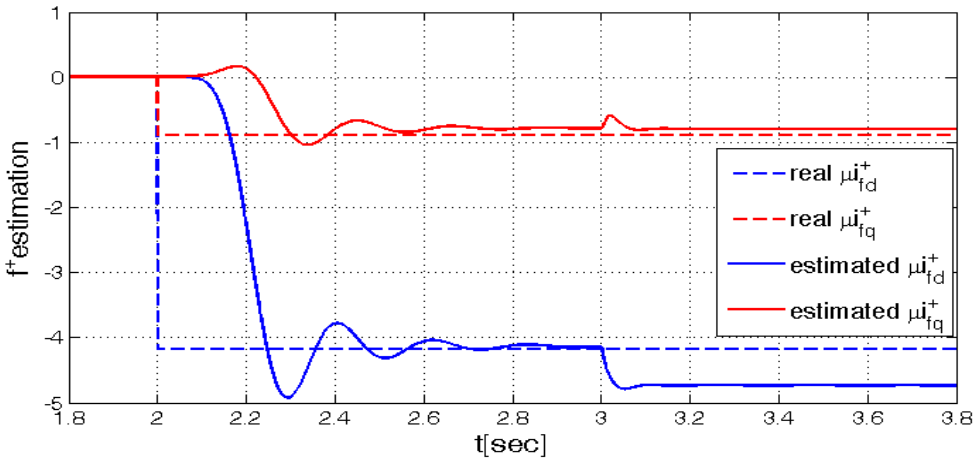


(a) $f^+$ estimation.

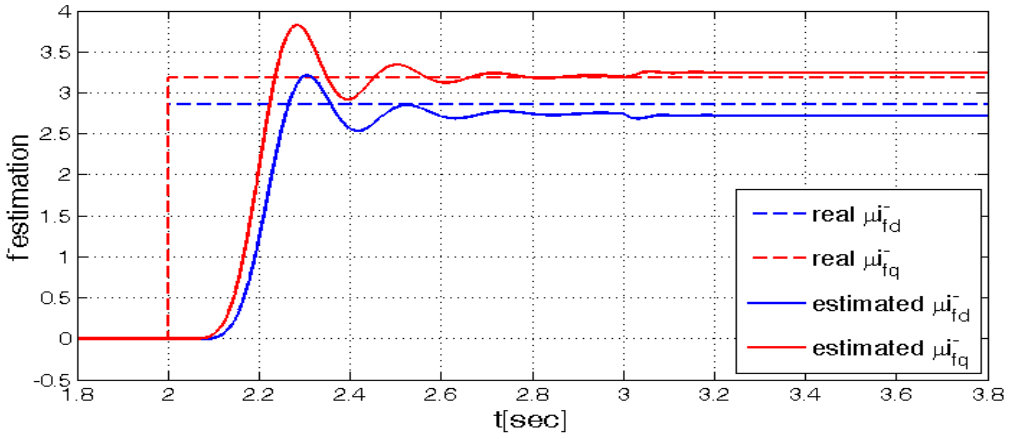


(a) $f^-$ estimation.

Figure 4.9. Performance of the optimal adaptive observer in the presence of model uncertainties. a 1% ( $\mu = 0.01$ ) short circuit fault is applied to stator phase 'b' at t=2sec, and a 5% variation of $r_s$ is applied at t=3sec.

The estimation results in Figure 4.9 are utilized to synthesize variable vector $\mu\mathbf{i}_{fdq}$ based on the scheme as in Figure 4.2. Figure 4.10 presents the estimated $\mu\mathbf{i}_{fdq}$ in the d-q plane. Due to the estimation biases, the estimated $\mu\mathbf{i}_{fdq}$ dose not presents as a straight line that perfectly overlaps with the true fault position (i.e. green line), while it exhibits as an ellipse with the main axis indicating the fault position. The area of the ellipse indicates the size of the estimation errors. Obviously, for small estimation biases, it is still able to provide clear information indicating where the fault occurs, i.e.

phase ‘b’ in this simulation.

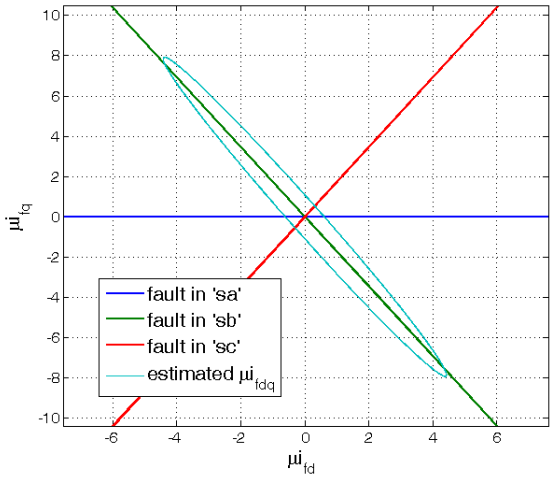


Figure 4.10. The synthesis of $\mu \boldsymbol{i}_{fdq}$ by using the optimal adaptive observer

### 4.6.3. Performance of LPV Adaptive Observer under Varying Speed

In this subsection, the proposed LPV adaptive observer (i.e. Algorithm 4.3) is applied to diagnose the short circuit fault when DFIG operates under varying speed. A sinusoidal load torque ($T_{wt} = -250 + 100\sin(20t)\text{Nm}$) is applied to the DFIG to simulate the speed variation. The model uncertainties are considered in this subsection. A 1% ($\mu = 0.01$) short circuit fault is applied to stator phase ‘b’ at t=2sec, and then a 5% variation of the stator resistance $r_s$ is applied at t=3sec. The disturbance attenuation level $\gamma$ is chosen as $1.42$. The associated parameters of the LPV adaptive observer (4.53) are given in Appendix C.4. For comparison, the LTI optimal adaptive observer designed in last subsection is also applied here to estimate the faults.

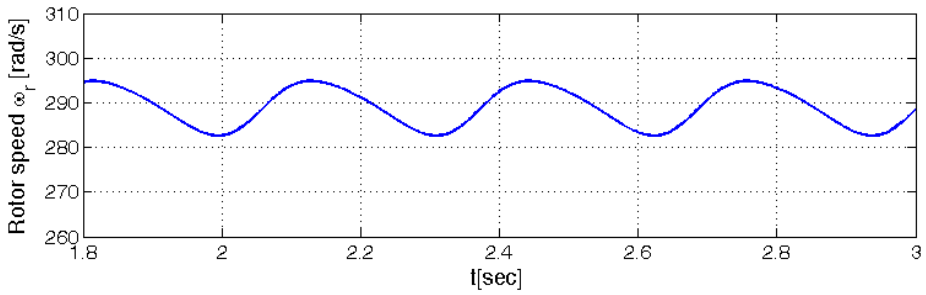


Figure 4.11. Speed variation.

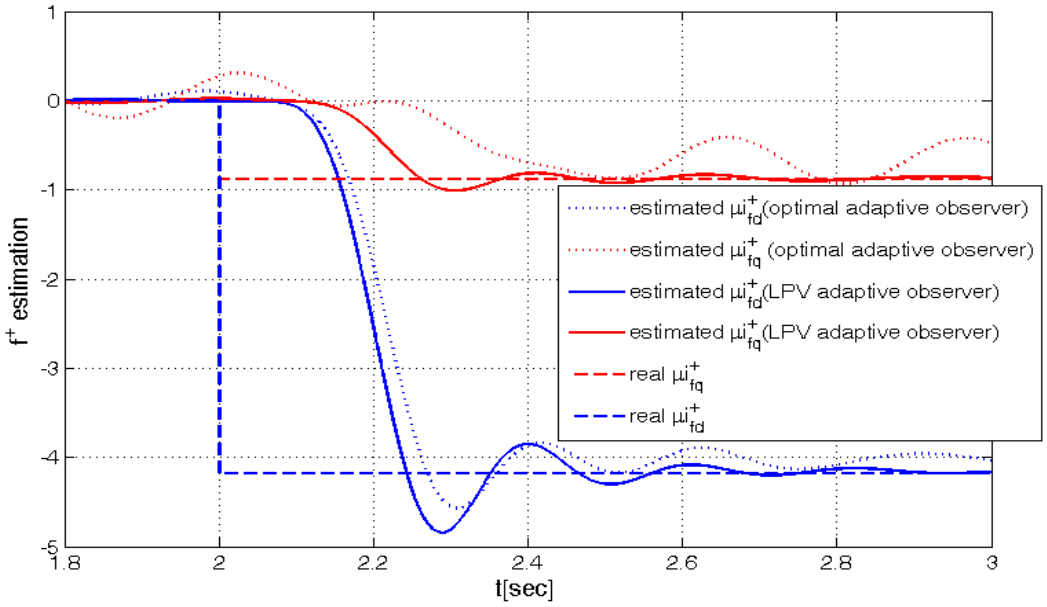


(a) $f^+$ estimation.

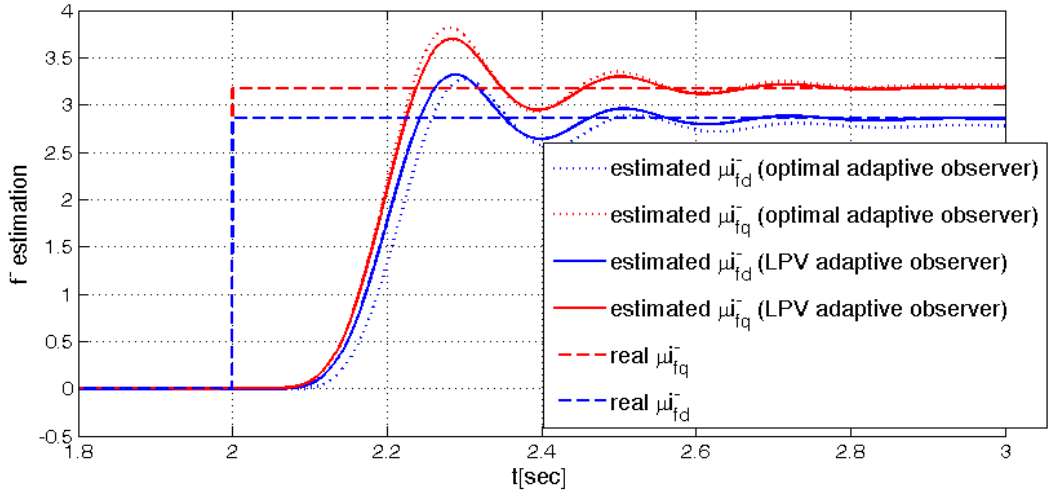


(b) $f^-$ estimation.

Figure 4.12. The comparison of the fault estimations by using LTI optimal adaptive observer and LPV adaptive observer.

The speed variation is depicted in Figure 4.11. The fault estimations by using LTI optimal adaptive observer (Algorithm 4.2) and LPV adaptive observer (Algorithm 4.3) are given in Figure 4.12. From this figure, it can be observed that under the varying speed, the asymptotic convergence of fault estimations can be both achieved using these two observer algorithms, but the LPV adaptive observer can achieve more accurate results with smaller steady state errors. This is because the LTI observer is designed based on an approximate rotor speed (e.g. $\omega_r = 289\,\text{rad/s}$), while the actual rotor speed can vary around $\omega_r$ as depicted in Figure 4.11. Nevertheless, LPV adaptive observer is based on the actual rotor speed measured in real-time, and thus it is not affected by the speed inaccuracy.

## 4.7. Summary

In this chapter, an adaptive observer based fault diagnosis scheme for the single-phase short circuit fault is proposed. To facilitate the observer design, a linear state-space representation of the faulty DFIG model is firstly derived by using the sequence component decomposition. As such, the single-phase short circuit fault is formulated into two additive faults $f^+$ and $f^-$. To estimate these faults, several adaptive observer algorithms have been developed in this chapter. Initially, a conventional adaptive observer is designed for an ideal case assuming no model uncertainties. Next, a robust adaptive observer is proposed to consider the effects of model uncertainties. The $H_\infty$ optimization technique is also applied to minimize the estimation errors for the sake of accuracy. Finally, the speed variation of the DFIG is considered. For such case a gain-scheduled LPV adaptive observer is proposed to ensure stability and performance of the fault estimation under the speed variation. The estimation results of faults $f^+$ and $f^-$ are utilized to synthesize variable vector $\mu\mathbf{i}_{fdq}$ in order to diagnose the fault position. The effectiveness of these adaptive observer algorithms on diagnosing the short circuit fault has been demonstrated through the simulations. The limitation of this fault diagnosis scheme is that it is unable to diagnose the fault level,

as the fault level parameter $\mu$ is unknown and can not be identified using the observers algorithm proposed in this chapter. This limitation is overcome by the fault diagnosis scheme in the following chapter.

# 5. Diagnosis of Multi-Phase Short Circuit Fault in DFIG

## 5.1. Introduction

Similar to the previous chapter, the adaptive observer based approaches are also applied in this chapter to diagnose the multi-phase short circuit fault. As mentioned earlier, such approaches rely on a state-space representation of the fault model. Therefore, the first objective of this chapter is to transform the proposed fault model (as in Section 3.3.2) into a state-space representation. Different from last chapter, instead of resorting to the sequence component decomposition, the fault model is directly transformed into the state-space form by using the block matrix inverse lemma. In this state-space form, the multi-phase short circuit fault is represented by a set of unknown parameters ($\mu_{sa}$, $\mu_{sb}$, $\mu_{sc}$, $\mu_{ra}$, $\mu_{rb}$, and $\mu_{rc}$) correlating to the input matrix, which can be considered as the multiplicative fault. To estimate those unknown parameters, a conventional adaptive observer is firstly designed. However, the SPR condition is required by this observer algorithm, which is difficult to be satisfied by only selecting the observer gains. To relax this condition, a modified adaptive observer is designed in this chapter, by which the SPR condition is replaced by a Lyapunov equation that it is easier to be satisfied. This observer is inspired by the work by Zhang [79], where an adaptive observer with similar structure was proposed for the parameter estimation of the MIMO linear time varying (LTV) system. In addition, the influence of model uncertainties is considered in this Chapter. In order to guarantee the convergence of the parameter estimations in the presence of model uncertainties, the high gain estimation technique is applied to redesign the observer gains of the modified adaptive observer. The DFIG speed variation is also considered in this

Chapter, for which a linear time-varying (LTV) adaptive observer is designed. This observer is suitable for the fault diagnosis under non-stationary (varying speed) condition.

This chapter is organized as follows. Section 5.2 presents the derivation of the state space model representation. In Section 5.3, a conventional adaptive observer is designed to estimate the fault parameters (i.e. $\mu_{sa}$, $\mu_{sb}$, $\mu_{sc}$, $\mu_{ra}$, $\mu_{rb}$, and $\mu_{rc}$). To relax the SPR condition required by the conventional adaptive observer, In Section 5.4 a modified adaptive observer is developed. In Section 5.5, the high observer design technique is applied to design the gain of this modified adaptive observer to enhance its robustness in the presence of model uncertainties. In Section 5.6, a LTV adaptive observer is designed by taking account of the speed variation. In Section 5.7, the simulation results illustrate the effectiveness of the proposed fault diagnosis scheme.

## 5.2. State Space Model Representation

The model for the multi-phase short circuit fault as presented in Section 3.3.2 is given by two equations: the voltage and flux equations, which can be written in a compact form as

$$\mathbf{v} = \mathbf{R}\mathbf{i} + \frac{d\boldsymbol{\psi}}{dt} + \boldsymbol{\Omega}\boldsymbol{\psi} \tag{5.1}$$

$$\boldsymbol{\psi} = \mathbf{L}\mathbf{i}$$

There are usually two methods to transform this model into a state-space representation. One is to select the currents $\mathbf{i}$ as the state variables, and the other is to select the fluxes $\boldsymbol{\psi}$ as the state variables. In this work, the first method is utilized, and the state-space representation can be obtained as

$$\frac{d\mathbf{i}}{dt} = A\mathbf{i} + B\mathbf{v} \tag{5.2}$$

where $A = -(\mathbf{L}^{-1}\mathbf{R} + \mathbf{L}^{-1}\boldsymbol{\Omega}\mathbf{L})$, $B = \mathbf{L}^{-1}$.

## 5.2.1. Inductance Matrix Inverse Calculation

As it is shown in (5.2), the inverse of the inductance matrix (i.e. $\mathbf{L}$) needs to be computed firstly in order the obtain the model parameter matrices (i.e. $A$ and $B$). From model (3.44), the inductance matrix $\mathbf{L}$ is given as

$$\mathbf{L}=\left[\begin{array}{c|c} \begin{bmatrix}\mathbf{L}'_{ss} & \mathbf{L}'_{sr}\\ \mathbf{L}'_{sr} & \mathbf{L}'_{rr}\end{bmatrix} & -\begin{bmatrix}\mathbf{L}'_{ss} & \mathbf{L}'_{sr}\\ \mathbf{L}'_{sr} & \mathbf{L}'_{rr}\end{bmatrix}\begin{bmatrix}\boldsymbol{\mu}_{sdq} & \mathbf{0}_{2\times2}\\ \mathbf{0}_{2\times2} & \boldsymbol{\mu}_{rdq}\end{bmatrix} \\ \hline \begin{bmatrix}\boldsymbol{\mu}_{sdq} & \mathbf{0}_{2\times2}\\ \mathbf{0}_{2\times2} & \boldsymbol{\mu}_{rdq}\end{bmatrix}\begin{bmatrix}\mathbf{L}'_{ss} & \mathbf{L}'_{sr}\\ \mathbf{L}'_{sr} & \mathbf{L}'_{rr}\end{bmatrix} & -\begin{bmatrix}L_{\sigma s}\mathbf{I}_2 & \mathbf{0}_{2\times2}\\ \mathbf{0}_{2\times2} & L_{\sigma r}\mathbf{I}_2\end{bmatrix}\begin{bmatrix}\boldsymbol{\mu}_{sdq} & \mathbf{0}_{2\times2}\\ \mathbf{0}_{2\times2} & \boldsymbol{\mu}_{rdq}\end{bmatrix}-\begin{bmatrix}\boldsymbol{\mu}_{sdq} & \mathbf{0}_{2\times2}\\ \mathbf{0}_{2\times2} & \boldsymbol{\mu}_{rdq}\end{bmatrix}\begin{bmatrix}\mathbf{L}'_{ss} & \mathbf{L}'_{sr}\\ \mathbf{L}'_{sr} & \mathbf{L}'_{rr}\end{bmatrix}\begin{bmatrix}\boldsymbol{\mu}_{sdq} & \mathbf{0}_{2\times2}\\ \mathbf{0}_{2\times2} & \boldsymbol{\mu}_{rdq}\end{bmatrix} \end{array}\right] \tag{5.3}$$

Before computing $\mathbf{L}^{-1}$, we need to discuss the singularity condition of $\mathbf{L}$. Note that $\mathbf{L}$ is singular whenever any of the fault level parameters ($\mu_{sa}$, $\mu_{sb}$, $\mu_{sc}$, $\mu_{ra}$, $\mu_{rb}$, and $\mu_{rc}$) equals to zero. Such singularity problem can be avoided by re-defining the state variables in model (3.44) as

$$x(t)=[\mathbf{i}_{sdq}{}^{T},\mathbf{i}_{rdq}{}^{T},(\boldsymbol{\mu}_{sdq}\mathbf{i}_{sfdq})^{T},(\boldsymbol{\mu}_{rdq}\mathbf{i}_{rfdq})^{T}]^{T} \tag{5.4}$$

Thereafter, the inductance matrix becomes

$$\mathbf{L}=\left[\begin{array}{c|c} \begin{bmatrix}\mathbf{L}'_{ss} & \mathbf{L}'_{sr}\\ \mathbf{L}'_{sr} & \mathbf{L}'_{rr}\end{bmatrix} & -\begin{bmatrix}\mathbf{L}'_{ss} & \mathbf{L}'_{sr}\\ \mathbf{L}'_{sr} & \mathbf{L}'_{rr}\end{bmatrix} \\ \hline \begin{bmatrix}\boldsymbol{\mu}_{sdq} & \mathbf{0}_{2\times2}\\ \mathbf{0}_{2\times2} & \boldsymbol{\mu}_{rdq}\end{bmatrix}\begin{bmatrix}\mathbf{L}'_{ss} & \mathbf{L}'_{sr}\\ \mathbf{L}'_{sr} & \mathbf{L}'_{rr}\end{bmatrix} & -\begin{bmatrix}L_{\sigma s}\mathbf{I}_2 & \mathbf{0}_{2\times2}\\ \mathbf{0}_{2\times2} & L_{\sigma r}\mathbf{I}_2\end{bmatrix}-\begin{bmatrix}\boldsymbol{\mu}_{sdq} & \mathbf{0}_{2\times2}\\ \mathbf{0}_{2\times2} & \boldsymbol{\mu}_{rdq}\end{bmatrix}\begin{bmatrix}\mathbf{L}'_{ss} & \mathbf{L}'_{sr}\\ \mathbf{L}'_{sr} & \mathbf{L}'_{rr}\end{bmatrix} \end{array}\right] \tag{5.5}$$

This matrix is always nonsingular for any values of $\mu_{sa}$, $\mu_{sb}$, $\mu_{sc}$, $\mu_{ra}$, $\mu_{rb}$, and $\mu_{rc}$. Therefore, its inverse can be computed by using the block matrix inverse lemma.

**Lemma 5.1 (block matrix inverse lemma):** Let a $\mathrm{m}\times\mathrm{n}$ matrix $M$ be partitioned into a block form $M=\begin{bmatrix}A & B\\ C & D\end{bmatrix}$, where $A$ and $D$ are invertible. Then we have

$$M^{-1}=\begin{bmatrix}(A-BD^{-1}C)^{-1} & -A^{-1}B(D-CA^{-1}B)^{-1}\\ -D^{-1}C(A-BD^{-1}C)^{-1} & (D-CA^{-1}B)^{-1}\end{bmatrix} \tag{5.6}$$

By applying this lemma, $\mathbf{L}^{-1}$ can be computed as

$$\mathbf{L}^{-1}=\begin{bmatrix}\begin{bmatrix}\mathbf{L}_{ss}^{'} & \mathbf{L}_{sr}^{'}\\ \mathbf{L}_{sr}^{'} & \mathbf{L}_{rr}^{'}\end{bmatrix}^{-1} & \mathbf{0}_{2\times2}\\ \mathbf{0}_{2\times2} & \mathbf{0}_{2\times2}\end{bmatrix}+\begin{bmatrix}\begin{bmatrix}L_{\sigma s}\mathbf{I}_2 & \mathbf{0}_{2\times2}\\ \mathbf{0}_{2\times2} & L_{\sigma r}\mathbf{I}_2\end{bmatrix}^{-1} & \mathbf{0}_{2\times2}\\ \mathbf{0}_{2\times2} & \begin{bmatrix}L_{\sigma s}\mathbf{I}_2 & \mathbf{0}_{2\times2}\\ \mathbf{0}_{2\times2} & L_{\sigma r}\mathbf{I}_2\end{bmatrix}^{-1}\end{bmatrix}\times$$
$$\begin{bmatrix}\begin{bmatrix}\boldsymbol{\mu}_{sdq}(\mathbf{I}_2-\boldsymbol{\mu}_{sdq})^{-1} & \mathbf{0}_{2\times2}\\ \mathbf{0}_{2\times2} & \boldsymbol{\mu}_{rdq}(\mathbf{I}_2-\boldsymbol{\mu}_{rdq})^{-1}\end{bmatrix}\begin{bmatrix}-(\mathbf{I}_2-\boldsymbol{\mu}_{sdq})^{-1} & \mathbf{0}_{2\times2}\\ \mathbf{0}_{2\times2} & -(\mathbf{I}_2-\boldsymbol{\mu}_{rdq})^{-1}\end{bmatrix}\\ \begin{bmatrix}\boldsymbol{\mu}_{sdq}(\mathbf{I}_2-\boldsymbol{\mu}_{sdq})^{-1} & \mathbf{0}_{2\times2}\\ \mathbf{0}_{2\times2} & \boldsymbol{\mu}_{rdq}(\mathbf{I}_3-\boldsymbol{\mu}_{rdq})^{-1}\end{bmatrix}\begin{bmatrix}-(\mathbf{I}_2-\boldsymbol{\mu}_{sdq})^{-1} & \mathbf{0}_{2\times2}\\ \mathbf{0}_{2\times2} & -(\mathbf{I}_2-\boldsymbol{\mu}_{rdq})^{-1}\end{bmatrix}\end{bmatrix} \tag{5.7}$$

## 5.2.2. State-Space Model

Now $\mathbf{L}^{-1}$ is used to compute the state matrix $A$ and input matrix $B$ as in (5.2) and then the state space model is derived as

$$\begin{cases}\dot{x}(t)=Ax(t)+Bu(t)\\ y(t)=Cx(t)\end{cases} \tag{5.8}$$

where the state variables $x(t)\in\mathbb{R}^8$ is given in (5.4). The input and output variables are given as

$$u(t)=[\mathbf{v}_{sdq}^T,\mathbf{v}_{rdq}^T]^T\in\mathbb{R}^4,\quad y(t)=[\mathbf{i}_{sdq}^T,\mathbf{i}_{rdq}^T]^T\in\mathbb{R}^4 \tag{5.9}$$

State, input, and output matrices are given as

$$A=A_0+A_1\omega_s+A_2\omega_r \tag{5.10}$$

$$B=B_0+B_f[\mu] \tag{5.11}$$

$$C=[\mathbf{I}_4\quad\mathbf{0}_{4\times4}] \tag{5.12}$$

where parameter matrices $A_0\in\mathbb{R}^{8\times8}$, $A_1\in\mathbb{R}^{8\times8}$, $A_2\in\mathbb{R}^{8\times8}$, $B_0\in\mathbb{R}^{8\times4}$, $B_f\in\mathbb{R}^{8\times4}$ and $C\in\mathbb{R}^{4\times8}$ are given as

$$A_0=\frac{1}{D}\begin{bmatrix}-\mathbf{R}_s^{'}\mathbf{L}_{rr}^{'} & \mathbf{R}_r^{'}\mathbf{L}_{sr}^{'} & \mathbf{R}_s^{'}\mathbf{L}_{rr}^{'} & -\mathbf{R}_r^{'}\mathbf{L}_{sr}^{'}\\ \mathbf{R}_s^{'}\mathbf{L}_{sr}^{'} & -\mathbf{R}_r^{'}\mathbf{L}_{ss}^{'} & -\mathbf{R}_s^{'}\mathbf{L}_{sr}^{'} & \mathbf{R}_r^{'}\mathbf{L}_{rr}^{'}\\ \mathbf{0}_{2\times2} & \mathbf{0}_{2\times2} & \mathbf{0}_{2\times2} & \mathbf{0}_{2\times2}\\ \mathbf{0}_{2\times2} & \mathbf{0}_{2\times2} & \mathbf{0}_{2\times2} & \mathbf{0}_{2\times2}\end{bmatrix}-\begin{bmatrix}\mathbf{0}_{2\times2} & \mathbf{0}_{2\times2} & \mathbf{R}_s^{'}L_{\sigma s}^{-1} & \mathbf{0}_{2\times2}\\ \mathbf{0}_{2\times2} & \mathbf{0}_{2\times2} & \mathbf{0}_{2\times2} & \mathbf{R}_r^{'}L_{\sigma r}^{-1}\\ \mathbf{0}_{2\times2} & \mathbf{0}_{2\times2} & \mathbf{R}_s^{'}L_{\sigma s}^{-1} & \mathbf{0}_{2\times2}\\ \mathbf{0}_{2\times2} & \mathbf{0}_{2\times2} & \mathbf{0}_{2\times2} & \mathbf{R}_r^{'}L_{\sigma r}^{-1}\end{bmatrix} \tag{5.13}$$

$$A_1 = -\begin{bmatrix} \mathbf{J} & \mathbf{0}_{2\times2} & \mathbf{0}_{2\times2} & \mathbf{0}_{2\times2} \\ \mathbf{0}_{2\times2} & \mathbf{J} & \mathbf{0}_{2\times2} & \mathbf{0}_{2\times2} \\ \mathbf{0}_{2\times2} & \mathbf{0}_{2\times2} & \mathbf{J} & \mathbf{0}_{2\times2} \\ \mathbf{0}_{2\times2} & \mathbf{0}_{2\times2} & \mathbf{0}_{2\times2} & \mathbf{J} \end{bmatrix}, \quad A_2 = \frac{1}{D}\begin{bmatrix} -L_m^2\mathbf{J} & -L_rL_m\mathbf{J} & L_m^2\mathbf{J} & L_rL_m\mathbf{J} \\ L_sL_m\mathbf{J} & L_sL_r\mathbf{J} & -L_sL_m\mathbf{J} & -L_m^2\mathbf{J} \\ \mathbf{0}_{2\times2} & \mathbf{0}_{2\times2} & \mathbf{0}_{2\times2} & \mathbf{0}_{2\times2} \\ \mathbf{0}_{2\times2} & \mathbf{0}_{2\times2} & \mathbf{0}_{2\times2} & D\mathbf{J} \end{bmatrix} \tag{5.14}$$

$$B_0 = \frac{1}{D}\begin{bmatrix} \mathbf{L}_{rr}^{'} & -\mathbf{L}_{sr}^{'} \\ -\mathbf{L}_{sr}^{'} & \mathbf{L}_{ss}^{'} \\ \mathbf{0}_{2\times2} & \mathbf{0}_{2\times2} \\ \mathbf{0}_{2\times2} & \mathbf{0}_{2\times2} \end{bmatrix}, \quad B_f = \begin{bmatrix} L_{\sigma s}^{-1}\mathbf{I}_2 & \mathbf{0}_{2\times2} \\ \mathbf{0}_{2\times2} & L_{\sigma r}^{-1}\mathbf{I}_2 \\ L_{\sigma s}^{-1}\mathbf{I}_2 & \mathbf{0}_{2\times2} \\ \mathbf{0}_{2\times2} & L_{\sigma r}^{-1}\mathbf{I}_2 \end{bmatrix} \tag{5.15}$$

The parameters in these matrices have been given in Chapter 3.

The fault level parameters ($\mu_{sa}$, $\mu_{sb}$, $\mu_{sc}$, $\mu_{ra}$, $\mu_{rb}$, $\mu_{rc}$) are all organized into a matrix $[\mu] \in \mathbb{R}^{4\times4}$

$$[\mu] = \begin{bmatrix} \boldsymbol{\mu}_{sdq}(\mathbf{I}_2 - \boldsymbol{\mu}_{sdq})^{-1} & \mathbf{0}_{2\times2} \\ \mathbf{0}_{2\times2} & \boldsymbol{\mu}_{rdq}(\mathbf{I}_2 - \boldsymbol{\mu}_{rdq})^{-1} \end{bmatrix} \tag{5.16}$$

where $\boldsymbol{\mu}_{sdq}$ and $\boldsymbol{\mu}_{rdq}$ have been given in (3.45).

To facilitate the observer design, model (5.8) is modified into the following form

$$\begin{cases} \dot{x}(t) = Ax(t) + Bu(t) + B_f\phi(t)\theta \\ y(t) = Cx(t) \end{cases} \tag{5.17}$$

where $\phi(t) \in \mathbb{R}^{4\times6}$ is a signal matrix composed of the voltage measurements.

$$\phi(t) = \begin{bmatrix} \mathbf{T}_{32}|_{\theta=\theta_s}\begin{bmatrix} v_{sa} & 0 & 0 \\ 0 & v_{sb} & 0 \\ 0 & 0 & v_{sc} \end{bmatrix} & \mathbf{0} \\ \mathbf{0} & \mathbf{T}_{32}|_{\theta=\theta_s-\theta_r}\begin{bmatrix} v_{ra} & 0 & 0 \\ 0 & v_{rb} & 0 \\ 0 & 0 & v_{rc} \end{bmatrix} \end{bmatrix} \tag{5.18}$$

where $\mathbf{T}_{32}|_{\theta=\theta_s}$ and $\mathbf{T}_{32}|_{\theta=\theta_s-\theta_r}$ are d-q transformation matrices as given in (3.42).

$\theta \in \mathbb{R}^6$ is parameter vector composed of the fault level parameters ($\mu_{sa}$, $\mu_{sb}$, $\mu_{sc}$, $\mu_{ra}$, $\mu_{rb}$, and $\mu_{rc}$) with the following structure.

$$\theta = \left[\frac{\mu_{sa}}{1-\mu_{sa}}, \frac{\mu_{sb}}{1-\mu_{sb}}, \frac{\mu_{sc}}{1-\mu_{sc}}, \frac{\mu_{ra}}{1-\mu_{ra}}, \frac{\mu_{rb}}{1-\mu_{rb}}, \frac{\mu_{rc}}{1-\mu_{rc}}\right]^T \tag{5.19}$$

$$B = B_0$$

It is can be observed that model (5.8) is a linear MIMO system, whose states $\boldsymbol{\mu}_{sdq}\mathbf{i}_{sfdq}$ and $\boldsymbol{\mu}_{rdq}\mathbf{i}_{rfdq}$ are unknown. $\theta$ is an unknown parameter vector representing the multi-phase short circuit fault. Its nonzero elements correspond to the phases where the faults occur, and the fault levels are described by the values of these nonzero elements. Therefore, the diagnosis of fault position and level can be simultaneously accomplished by estimating parameter vector $\theta$. In the following sections, several adaptive observer algorithms are proposed for joint estimation of the parameter vector $\theta$ and the unknown states (i.e. $\boldsymbol{\mu}_{sdq}\mathbf{i}_{sfdq}$, $\boldsymbol{\mu}_{rdq}\mathbf{i}_{rfdq}$). Although the state estimation is not really required for the purpose of fault diagnosis, but it will be used in the following chapter for the purpose of fault tolerant control.

## 5.3. Conventional Adaptive Observer

In this section, a conventional adaptive observer is designed to estimate the unknown parameter vector $\theta$, with the assumption that no model uncertainties exist in model (5.17).

***Algorithm 5.1(conventional adaptive observer)[118]:***

$$\begin{cases} \dot{\hat{x}}(t) = A\hat{x}(t) + Bu(t) + B_f\phi(t)\hat{\theta} + L(y(t) - C\hat{x}(t)) \\ \dot{\hat{\theta}}(t) = \Gamma\phi(t)^T(y(t) - C\hat{x}(t)) \end{cases} \tag{5.20}$$

where $\hat{x} \in \mathbb{R}^8$ and $\hat{\theta} \in \mathbb{R}^6$ are the estimates of the state $x$ and unknown parameter vector $\theta$. $L \in \mathbb{R}^{6\times 4}$ is the observer gain to be designed. $\Gamma > 0$ is a pre-specified matrix used to tune the convergence rate of parameter estimations.

As all the parameters in $\theta$ are time-invariant, it can be assumed that $\dot{\theta} = 0$.

Comparing observer (5.20) with (5.17) and denoting

$$e_x(t) = x(t) - \hat{x}(t), \quad e_\theta(t) = \theta - \hat{\theta}(t) \tag{5.21}$$

the estimation error dynamic system yields

$$\begin{cases} \dot{e}_x(t) = (A - LC)e_x(t) + B_f\phi(t)e_\theta(t) \\ \dot{e}_\theta(t) = -\Gamma\phi^T(t)Ce_x(t) \end{cases} \tag{5.22}$$

The stability of this system can be proved and the stability condition of is given in Theorem 5.1.

**Assumption 5.1:** Assume that there exists constants $\alpha > 0$, $\beta > 0$ and $T > 0$ such that for all $t$, the following inequalities hold:

$$\alpha \le \int_t^{t+T} \phi^T(t)\phi(t)d\tau \le \beta \tag{5.23}$$

This assumption is the well-known persistence of excitation condition, which is required for the parameter estimation. Also see further discussion in Remark 5.2.

**Theorem 5.1:** For a scalar $\Gamma > 0$, if there exist two symmetric positive definite matrices $P$ and $Q$ , which satisfy the following two conditions

$$(A-LC)^T P + P(A-LC) = -Q \tag{5.24}$$

$$B_f{}^T P = C \tag{5.25}$$

then for any initial condition, the adaptive observer (5.20) for system (5.17) is asymptotically stable and can ensure $\lim_{t\to\infty} e_x(t) = 0$, and under assumption 5.1 it can also ensure $\lim_{t\to\infty} e_\theta(t) = 0$.

**Proof**: The Lyapunov function is selected as

$$V(t) = e_x^T(t)Pe_x(t) + e_\theta^T(t)\Gamma^{-1}e_\theta(t) \tag{5.26}$$

The proof is similar to theorem 5.1, so the details are omitted here.

**Remark 5.1:** Conditions (5.24) and (5.25) can be also interpreted as system $\{A-LC, B_f, C\}$ with transfer function $T(s) = C(sI-(A-KC))^{-1}B_f$ is SPR (see in Appendix B.3). Actually, the parameter estimation error dynamic is governed by

$$\dot{e}_\theta(t) = -\Gamma\phi(t)^T T(s)\phi(t)e_\theta(t) \tag{5.27}$$

Therefore, under assumption 5.1, we can simply derive $e_\theta(t)$ is exponentially asymptotically stable if $T(s)$ is SPR,

**Remark 5.2:** Assumption 5.1 is the persistence of excitation condition for the estimation of unknown parameter $\theta$, which is not required by the state estimation. In

other words, the convergence of the state estimation can be achieved without this condition. However, the main objective of this adaptive observer is to estimate the unknown parameter $\theta$, therefore the persistent excitation condition has to be always satisfied. Although the matrix $\phi^T(t)\phi(t)$ may be singular for each $\tau$, (5.23) requires that $\phi(t)$ varies in such a way with time that the integral of the matrix $\phi^T(t)\phi(t)$ is uniformly positive definite over any time interval $[t, t+T]$. It is known that when DFIG is operating, the voltage signals in matrix $\phi(t)$ are always non-zero values, therefore, the assumption 5.1 can be satisfied.

Once parameter vector $\theta$ is estimated by the adaptive observer (5.20), the fault level parameters ($\mu_{sa}$, $\mu_{sb}$, $\mu_{sc}$, $\mu_{ra}$, $\mu_{rb}$, and $\mu_{rc}$) can be computed from (5.19), based on which the information of the fault position and fault level can be readily obtained. The overall fault diagnosis scheme is given in Figure 5.1. It worth mentioning that the single-phase short circuit fault can be regarded as a special case of the multi-phase fault, and thus it can be diagnosed by the scheme proposed in this chapter as well. Comparing it with the fault diagnosis scheme proposed in Chapter 4, this scheme is directly based on the d-q components of the current and voltage measurements without resorting to the sequence component decomposition, which makes it easier to be implemented. Additionally, the fault position and level can be simultaneously diagnosed online. However, the adaptive observer in this scheme is with higher dimension compared with the one in last chapter, which therefore would increase the computational cost. Besides, in practice the short circuit fault predominantly occurs at a single phase rather than several phases simultaneously. Hence, the fault diagnosis scheme proposed in last chapter is still practically significant and computationally attractive algorithm.

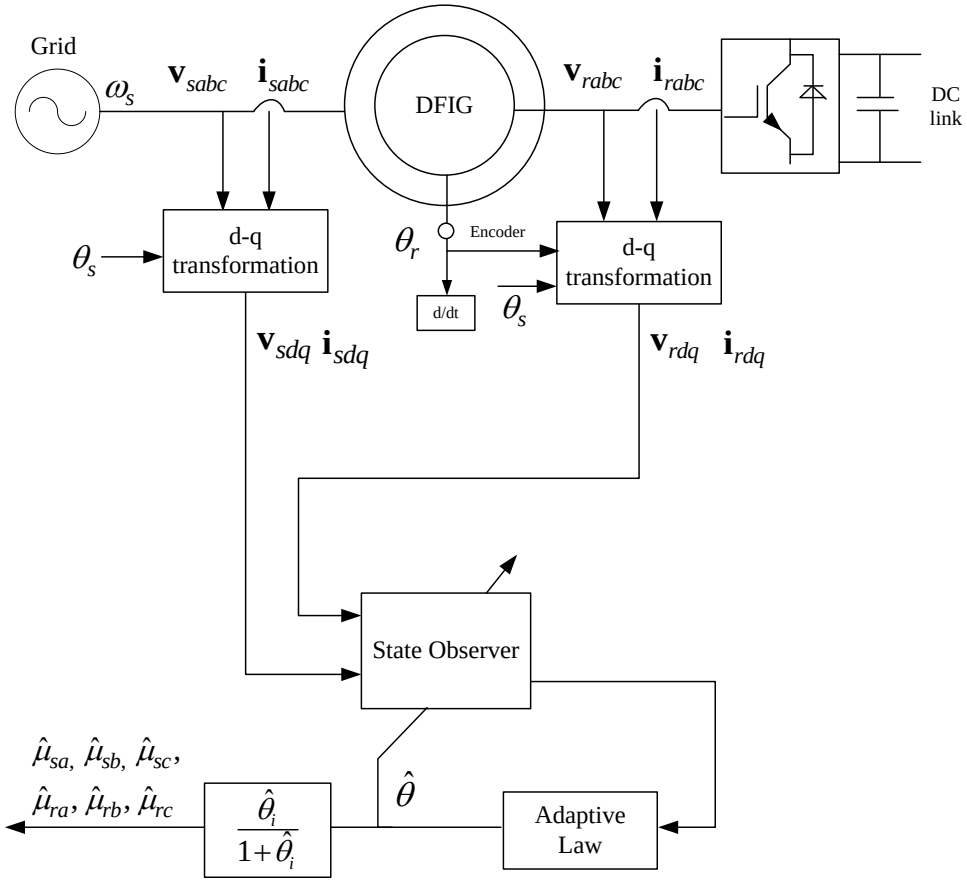


Figure 5.1. Schematic diagram of the fault diagnosis scheme for the multi-phase short circuit fault.

## 5.4. Modified Adaptive Observer

In last section, a conventional adaptive observer is designed, which can provide an unbiased estimation of parameter $\theta$ under the assumption that no model uncertainties exist in system (5.17). However, there are two limitations of this observer. Firstly, it requires SPR condition ( as in (5.24) and (5.25)), which is quite conservative and it is difficult to find an observer gain $L$ satisfy such condition. Secondly, this observer is not able to guarantee the convergence of the parameter estimations in the presence of model uncertainties. In this section, a modified adaptive observer [79] is designed to overcome these two limitations of the conventional adaptive observer. The relex of SPR condition is discussed in this section, while the robustness issue is investigated in the following section.

For system (5.17), a modified adaptive observer can be designed as follows.

***Algorithm 5.2 (modified adaptive observer)[79]:***

$$\begin{cases} \dot{\hat{x}}(t) = A\hat{x}(t) + Bu(t) + B_f\phi(t)\hat{\theta} + \left(L + \Upsilon(t)\Gamma\Upsilon^T(t)C^T\right)\left(y(t) - C\hat{x}(t)\right) \\ \dot{\hat{\theta}}(t) = \Gamma\Upsilon^T(t)C^T\left(y(t) - C\hat{x}(t)\right) \\ \dot{\Upsilon}(t) = (A - LC)\Upsilon(t) + B_f\phi(t) \end{cases} \tag{5.28}$$

where $\hat{x} \in \mathbb{R}^8$ and $\hat{\theta} \in \mathbb{R}^6$ is the estimates of the state $x$ and unknown parameter vector $\theta$. $\Upsilon(t) \in \mathbb{R}^{8\times 6}$ is a signal matrix generated from $\phi(t)$. $L \in \mathbb{R}^{8\times 4}$ is the observer gain to be designed. $\Gamma \in \mathbb{R}^{6\times 6}$ is a positive matrix tuned to balance the convergence speeds of the state and parameter estimation.

Substituting the third equation into the first one, we can have

$$\dot{\hat{x}}(t) = A\hat{x}(t) + Bu(t) + B_f\phi(t)\hat{\theta} + L\left[y(t) - C\hat{x}(t)\right] + \Upsilon(t)\dot{\hat{\theta}}(t) \tag{5.29}$$

Comparing it with system (5.17) and using the notation (5.21), the estimation error dynamic system can be obtained as

$$\begin{cases} \dot{e}_x(t) = (A - LC)e_x(t) + B_f\phi(t)e_\theta(t) + \Upsilon(t)\dot{e}_\theta(t) \\ \dot{e}_\theta(t) = -\Gamma\Upsilon^T(t)C^TCe_x(t) \end{cases} \tag{5.30}$$

Define a new variable as

$$\eta(t) = e_x(t) - \Upsilon(t)e_\theta(t) \tag{5.31}$$

then we can have, after some simple computation

$$\dot{\eta}(t) = (A - LC)\eta(t) + \left((A - LC)\Upsilon(t) + B_f\phi(t) - \dot{\Upsilon}(t)\right)e_\theta(t) \tag{5.32}$$

Then a new estimation error system in term of variables $\eta(t)$ and $e_\theta(t)$ can be expressed as

$$\begin{cases} \dot{\eta}(t) = (A - LC)\eta(t) \\ \dot{e}_\theta(t) = -\Gamma\Upsilon^T(t)C^TC\left(\eta(t) + \Upsilon(t)e_\theta(t)\right) \end{cases} \tag{5.33}$$

The stability of this system and convergence of variables $\eta(t)$ and $e_\theta(t)$ can be proved and given in the Theorem 5.2. This theorem is based on an assumption of signal $\Upsilon(t)$ which is given in assumption 5.2. The proof of this theorem requires an

important lemma which is given lemma 5.1.

**Assumption 5.2:** Assume that $\phi(t)$ is persistently exciting, so the matrix of signals $\Upsilon(t)$ generated by linearly $\phi(t)$ through the following equation

$$\dot{\Upsilon}(t) = (A - LC)\Upsilon(t) + B_f \phi(t) \tag{5.34}$$

satifies, for constants $\alpha > 0$, $\beta > 0$, $T > 0$ and all $t > t_0$, the following inequality holds:

$$\alpha I \le \int_t^{t+T} \Upsilon^T(t) C^T C \Upsilon(t) d\tau \le \beta I \tag{5.35}$$

**Lemma 5.1**[113]**:** Let $\zeta(t) \in \mathbb{R}^{m \times n}$ be a bounded and continuous matrix and $\Gamma \in \mathbb{R}^{n \times n}$ be any symmetric positive definite matrix. If there exist positive constants $\alpha > 0$, $\beta > 0$, $T > 0$ such that for all $t > t_0$

$$\alpha I \le \int_t^{t+T} \zeta^T(t)\zeta(t) d\tau \le \beta I \tag{5.36}$$

Then the following system

$$\dot{z}(t) = -\Gamma \zeta^T(t)\zeta(t) z(t) \tag{5.37}$$

is exponentially stable.

**Theorem 5.2:** For a matrix $\Gamma > 0$, if there exist two symmetric positive definite matrices $P$ and $Q$ such that the following condition holds

$$(A - LC)^T P + P(A - LC) = -Q \tag{5.38}$$

then for any initial condition, the adaptive observer (5.20) for system (5.17) is asymptotically stable and can ensure $\lim_{t \to \infty} e_x(t) = 0$, and under assumption 5.2 it can also ensure $\lim_{t \to \infty} e_\theta(t) = 0$.

**Proof:** Since condition (5.38) holds, the first equation of (5.33) is stable and variable $\eta(t)$ converges into zero as $t \to 0$. This can be easily proved according to the Lyapunov stability theorem and Barbalats lemma (as in Appendix B.1 and B.2). The parameter estimation error is governed by the following equation as given in (5.33)

$$\dot{e}_\theta(t) = -\Gamma \Upsilon^T(t) C^T C \Upsilon(t) e_\theta(t) - \Gamma \Upsilon^T(t) C^T C \eta(t) \tag{5.39}$$

As signal matrix $\phi(t)$ is bounded, $\Upsilon(t)$ generated from $\phi(t)$ is also bounded.

Under assumption 5.2 and by applying Lemma 5.1, it can be concluded that (5.39) is stable. As $\eta(t)$ converges into zero as $t \to 0$ and with the fact $\Upsilon(t)$ is bounded, we can conclude that $\lim_{t\to\infty} e_\theta(t) = 0$. From (5.31), we can have $\lim_{t\to\infty} e_x(t) = 0$. □

Comparing with the SPR condition (as in (5.24)-(5.25)) required by the conventional adaptive, condition (5.38) is easier to be satisfied and the observer gain $L$ can be simply obtained by solving (5.38)

## 5.5. High Gain Adaptive Observer

For completeness, a more realistic but complex situation is considered in this section when the system is corrupted with the model uncertainties. High gain observer is stated to be a very effective method to track the system states and attenuate the effects from unknown model uncertainties [41], [108]. In this section, we will combine this technique with the modified adaptive observer developed in last section in order to improve the robustness of this proposed adaptive observer in the presence of model uncertainties.

Taking account of the model uncertainties, system (5.17) can be modified into

$$\begin{cases} \dot{x}(t) = Ax(t) + Bu(t) + B_f \phi(t)\theta + w(t) \\ y(t) = Cx(t) \end{cases} \tag{5.40}$$

where the model uncertainties are represented by an unknown input $w(t) \in \mathbb{R}^8$. It is assumed that $w(t)$ and $\theta$ are bounded.

$$\|w(t)\| \le \sigma < +\infty, \quad \|\theta\| \le \tau < +\infty \tag{5.41}$$

To ensure bounded parameter estimation, a leakage term is added to the adaptive law, which is given as

$$\dot{\hat{\theta}}(t) = -\Gamma_1 \hat{\theta}(t) - \Gamma_2 \Upsilon^T(t) C^T \left( y(t) - C\hat{x}(t) \right) \tag{5.42}$$

where $\Gamma_1 > 0$ and $\Gamma_2 > 0$ are pre-specified parameter used to tune the convergence rate of the parameter $\theta$ estimation.

By using this modified adaptive law, the estimation error system corrupted with the

model uncertainties $w(t)$ can be obtained as

$$\begin{cases}\dot{\eta}(t)=(A-LC)\eta(t)+w(t)\\ \dot{e}_\theta(t)=-\Gamma_1 e_\theta(t)+\Gamma_1\theta+\Gamma_2\Upsilon^T(t)C^TC\left(\eta(t)+\Upsilon(t)e_\theta(t)\right)\end{cases} \tag{5.43}$$

From this equation, it can be noted that due to the existence of terms $\Gamma_1\theta$ and $w(t)$, the variables $\eta(t)$ and $e_\theta(t)$ no longer converge into zeros, while they can converge into a small bound by designing the observer gain $L$ properly. This is demonstrated in the following theorem.

**Theorem 5.5:** for two matrices $\Gamma_1>0$ and $\Gamma_2>0$, the adaptive observer in form of (5.28) with adaptive law (5.42) for system (5.40) can make the estimation errors $e_x(t)$ and $e_\theta(t)$ as small as possible to any pre-specified accuracy. Specifically, the observer gain $L$ is selected as

$$\left(\rho I+(A-LC)\right)^T P+P\left(\rho I+(A-LC)\right)=-C^TC \tag{5.44}$$

with $\rho>0$ and $P$ is a positive definite symmetric matrix.

**Proof:** The Lyapunov function is selected as in

$$V(t)=\eta(t)^T P\eta(t)+e_\theta^T(t)\Gamma_2^{-1}e_\theta(t) \tag{5.45}$$

Its time derivate is computed as

$$\begin{aligned}\dot{V}(t)=&\eta^T(t)\left((A-LC)^TP+P(A-LC)\right)\eta(t)+2\eta^T(t)Pw(t)\\&+e_\theta^T(t)\Gamma^{-1}\dot{e}_\theta(t)+\dot{e}_\theta^T(t)\Gamma^{-1}e_\theta(t)\end{aligned} \tag{5.46}$$

Substituting the second equation of (5.33) into above equation, we can obtain

$$\begin{aligned}\dot{V}(t)=&\eta^T(t)\left((A-LC)^TP+P(A-LC)\right)\eta(t)\\&-e_\theta^T(t)\Upsilon(t)^TC^TC\left(\eta(t)+\Upsilon(t)e_\theta(t)\right)-\left(\eta(t)+\Upsilon(t)e_\theta(t)\right)^TC^TC\Upsilon(t)e_\theta(t)\\&-2e_\theta^T(t)\Gamma_2^{-1}\Gamma_1e_\theta(t)+2\eta^T(t)Pw(t)+2e_\theta^T(t)\Gamma_2^{-1}\Gamma_1\theta\\=&\eta^T(t)\left((A-LC)^TP+P(A-LC)+C^TC\right)\eta(t)\\&-(\eta(t)+\Upsilon(t)e_\theta(t))^TC^TC(\eta(t)+\Upsilon(t)e_\theta(t))-e_\theta^T(t)\Upsilon^T(t)C^TC\Upsilon(t)e_\theta(t)\\&-2e_\theta^T(t)\Gamma_2^{-1}\Gamma_1e_\theta(t)+2\eta^T(t)Pw(t)+2e_\theta^T(t)\Gamma_2^{-1}\Gamma_1\theta\\\le&\eta^T(t)\left((A-LC)^TP+P(A-LC)+C^TC\right)\eta(t)\\&-2e_\theta^T(t)\Gamma_2^{-1}\Gamma_1e_\theta(t)+2\eta^T(t)Pw(t)+2e_\theta^T(t)\Gamma_2^{-1}\Gamma_1\theta\end{aligned} \tag{5.47}$$

As condition (5.44) holds, then we can have

$$\begin{aligned}
\dot{V}(t) &\le -2\rho\eta^T(t)P\eta(t) - 2e_\theta^T(t)\Gamma_2^{-1}\Gamma_1 e_\theta(t) + 2\eta^T(t)Pw(t) + 2e_\theta^T(t)\Gamma_2^{-1}\Gamma_1\theta \\
&= -2\rho\left(\eta(t) - \frac{1}{2}\rho^{-1}w(t)\right)^T P\left(\eta(t) - \frac{1}{2}\rho^{-1}w(t)\right) - 2\left(e_\theta(t) - \frac{1}{2}\theta\right)^T \Gamma_2^{-1}\Gamma_1\left(e_\theta(t) - \frac{1}{2}\theta\right) \\
&\quad + \frac{1}{2}\theta^T\Gamma_2^{-1}\Gamma_1\theta + \frac{1}{2}\rho^{-1}w^T(t)Pw(t) \\
&\le -2\rho\lambda_{\min}(P)\left(\frac{1}{2}\|\eta(t)\|^2 - \frac{1}{4}\rho^{-2}\|w(t)\|^2\right) - 2\lambda_{\min}(\Gamma_2^{-1}\Gamma_1)\left(\frac{1}{2}\|e_\theta(t)\|^2 - \frac{1}{4}\|\theta\|^2\right) \\
&\quad + \frac{1}{2}\theta^T\Gamma_2^{-1}\Gamma_1\theta + \frac{1}{2}\rho^{-1}w^T(t)Pw(t) \\
&\le -\rho\lambda_{\min}(P)\|\eta(t)\|^2 - \lambda_{\min}(\Gamma_2^{-1}\Gamma_1)\|e_\theta(t)\|^2 \\
&\quad + \frac{1}{2}\rho^{-1}\left(\lambda_{\min}(P) + \lambda_{\max}(P)\right)\sigma^2 + \frac{1}{2}\left(\lambda_{\min}(\Gamma_2^{-1}\Gamma_1) + \lambda_{\max}(\Gamma_2^{-1}\Gamma_1)\right)\tau^2
\end{aligned} \tag{5.48}$$

This implies $\dot{V}(t) < 0$ if

$$\begin{aligned}
&\rho\lambda_{\min}(P)\|\eta(t)\|^2 + \lambda_{\min}(\Gamma_2^{-1}\Gamma_1)\|e_\theta(t)\|^2 \\
&> \frac{1}{2}\rho^{-1}\left(\lambda_{\min}(P) + \lambda_{\max}(P)\right)\sigma^2 + \frac{1}{2}\left(\lambda_{\min}(\Gamma_2^{-1}\Gamma_1) + \lambda_{\max}(\Gamma_2^{-1}\Gamma_1)\right)\tau^2
\end{aligned} \tag{5.49}$$

This means the pair $(\eta(t), e_\theta(t))$ converge to the following set $D$ according to Lyapunov stability theory

$$D = \left\{ \begin{array}{l} \left(\eta(t), e_\theta(t)\right) \mid \rho\lambda_{\min}(P)\|\eta(t)\|^2 + \lambda_{\min}(\Gamma_2^{-1}\Gamma_1)\|e_\theta(t)\|^2 \\ \qquad > \frac{1}{2}\rho^{-1}\left(\lambda_{\min}(P) + \lambda_{\max}(P)\right)\sigma^2 + \frac{1}{2}\left(\lambda_{\min}(\Gamma_2^{-1}\Gamma_1) + \lambda_{\max}(\Gamma_2^{-1}\Gamma_1)\right)\tau^2 \end{array} \right\} \tag{5.50}$$

By analyzing (5.44), it is noticed that the eigenvalues of $P$ decrease as $\rho$ increases. Therefore, by increasing $\rho$, the convergence set $D$ can be made as small as desired. As $\eta(t)$ is the combination of $e_x(t)$ and $e_\theta(t)$, $e_x(t)$ thus can also be reduced. This is end of the proof.

**Remark 5.5:** The condition (5.44) can be replaced by a Lyapunov equation

$$(\rho I + A)^T P + P(\rho I + A) = C^T C \tag{5.51}$$

if the observer gain is designed as

$$L = P^{-1}C^{T} \tag{5.52}$$

In such case, $L$ can be obtained solving (5.51) and a big value of $\rho$ should be selected in order to reduce the estimation errors.

**Remark 5.6:** It is worth mentioning that in this subsection we employ high gain method to attenuate the effect of the model uncertainty instead of using $H_\infty$ method. This is due to the existence of time-varying signal matrix $\phi(t)$ in multi-phase fault model (5.40). As it is stated in Section 4.5.1, a $H_\infty$ adaptive observer with a guaranteed performance index (4.39) can be obtained by solving a LMI which is in terms of the matrix (i.e. $B_f$ in single-phase fault model (4.19)) correlated with the fault (i.e. $f$ in single-phase fault model (4.19)). In the multi-phase fault model (5.40), the matrix correlated with the fault (i.e. $\theta$) is $B_f\phi(t)$ which is a time-varying matrix. If we apply same method ($H_\infty$ method) to diagnose multi-phase fault represented by model (5.40), the time-varying matrix $B_f\phi(t)$ will result a time-varying matrix inequality which is difficult to be solved. For this reason, we use high gain method in this section to deal with the model uncertainty for multi-phase fault diagnosis problem. Even though the performance index (4.39) can not be guaranteed by using high gain method, the effect of model uncertainty can still be greatly reduced by selecting a big value of $\rho$.

## 5.6. LTV Adaptive Observer

In this section, the situation that DFIG operates under varying speed is discussed. To ensure the global convergence of the parameter and state estimations under varying speed condition, a time-varying adaptive observer is designed based on approach proposed by [43]. The model uncertainties are not considered in this section.

System (5.17) in terms of the time-varying rotor speed $\omega_r(t)$ can be expressed as a

linear time varying (LTV) system, which can be given as

$$\begin{cases} \dot{x}(t) = A(t)x(t) + Bu(t) + B_f\phi(t)\theta \\ y(t) = Cx(t) \end{cases} \tag{5.53}$$

where $A(t) = A_0 + A_1\omega_s + A_2\omega_r(t)$ (matrices $A_0$, $A_1$ and $A_2$ is given in (5.13) -(5.14), and $\omega_s$ is the synchronous speed, which is constant and known). In the following context, the dependence on *t* are omitted in order to lighten notations.

### *Algorithm 5.3 (LTV adaptive observer) [43]:*

For such system, a LTV adaptive observer is developed as follows.

$$\begin{cases} \dot{\hat{x}} = A\hat{x} + Bu + B_f\phi\hat{\theta} + \left(S_x^{-1}C^T + \Upsilon S_\theta^{-1}\Upsilon^T C^T\right)\left(y - C\hat{x}\right) \\ \dot{\hat{\theta}} = S_\theta^{-1}\Upsilon^T C^T\left(y - C\hat{x}\right) \\ \dot{\Upsilon} = (A - S_x^{-1}C^T C)\Upsilon + B_f\phi \\ \dot{S}_x = -\rho_x S_x - A^T S_x - S_x A + C^T C \\ \dot{S}_\theta = -\rho_\theta S_\theta + \Upsilon^T C^T C\Upsilon \end{cases} \tag{5.54}$$

where $\hat{x} \in \mathbb{R}^8$ and $\hat{\theta} \in \mathbb{R}^6$ are the estimates of the state $x$ and unknown parameter vector $\theta$. $\Upsilon \in \mathbb{R}^{8\times 6}$ is a signal matrix generated from $\phi$. $S_x \in \mathbb{R}^{8\times 8}$ is a symmetric signal matrix generated from $A$. $S_\theta \in \mathbb{R}^{6\times 6}$ is a symmetric signal matrix generated from $\Upsilon$. $\Gamma \in \mathbb{R}^{6\times 6}$ is a symmetric positive-definite matrix used to tune the convergence rate of the parameter estimation. $\rho_x > 0$ and $\rho_\theta > 0$ are used to tune the convergence rate of the state and parameter estimations.

Comparing observer (5.54) with system (5.17), the estimation error dynamic system can be obtained as

$$\begin{cases} \dot{e}_x = (A - S_x^{-1}C^T C)e_x + B_f\phi e_\theta + \Upsilon\dot{e}_\theta \\ \dot{e}_\theta = -S_\theta^{-1}\Upsilon^T C^T C e_x \end{cases} \tag{5.55}$$

Here a new variable $\eta$ is introduced to remove term the derivate $\Upsilon\dot{e}_\theta$, which is given as

$$\eta = e_x - \Upsilon e_\theta \tag{5.56}$$

then we can have, after some simple computation,

$$\dot{\eta} = (A - S_x^{-1} C^T C)\eta + \left((A - S_x^{-1} C^T C)\Upsilon + B_f \phi - \dot{\Upsilon}\right) e_\theta \tag{5.57}$$

Substituting the third equation of (5.54) into above equation, a new estimation error dynamic system in term of variables $\eta$ and $e_\theta$ can be obtained

$$\begin{cases} \dot{\eta} = (A - S_x^{-1} C^T C)\eta \\ \dot{e}_\theta = S_\theta^{-1} \Upsilon^T C^T C \left(\eta + \Upsilon e_\theta\right) \end{cases} \tag{5.58}$$

The stability of this estimation error dynamic system and the convergence of $e_\theta(t)$ and $\eta(t)$ can be proved and is given in Theorem 5.3.

**Theorem 5.3:** For two scalars $\rho_x > 0$ and $\rho_\theta > 0$, the adaptive observer (5.54) for system (5.53) is exponentially stable and can the estimation errors $e_x$ and $e_\theta$ tend to zero exponentially fast when $t \to 0$

**Proof:** Lyapunov function can be selected as

$$V = \eta^T S_x \eta + e_\theta^T S_\theta e_\theta \tag{5.59}$$

Its first derivative with respect to time is

$$\begin{aligned} \dot{V} = \eta^T \left([A - S_x^{-1} C^T C]^T S_x + S_x [A - S_x^{-1} C^T C]\right)\eta \\ + e_\theta^T \Upsilon^T C^T C \left(\eta + \Upsilon e_\theta\right) + \left(\eta + \Upsilon e_\theta\right)^T C^T C \Upsilon e_\theta \\ + e_\theta^T \dot{S}_\theta e_\theta + \eta^T \dot{S} \eta \end{aligned} \tag{5.60}$$

Substituting the last two equations of (5.54) into above equation, we can obtain

$$\begin{aligned} \dot{V} &= -\rho_x \eta^T S_x \eta - \rho_\theta e_\theta^T S_\theta e_\theta - \eta^T C^T C \eta \\ &\quad - e_\theta^T \Upsilon^T C^T C \eta - \eta^T C^T C \Upsilon e_\theta - e_\theta^T \Upsilon^T C^T C \Upsilon e_\theta \\ &= -\rho_x \eta^T S_x \eta - \rho_\theta e_\theta^T S_\theta e_\theta - (\eta + \Upsilon e_\theta)^T C^T C (\eta + \Upsilon e_\theta) \\ &\le -\rho_x \eta^T S_x \eta - \rho_\theta e_\theta^T S_\theta e_\theta = -\rho V \end{aligned} \tag{5.61}$$

where $\rho = \min(\rho_x, \rho_\theta)$. From above equation, we can conclude that $\eta$ and $e_\theta$ exponentially go to zero. So does $e_x$. □

Actually, this LTV adaptive is a time-varying version of the high gain adaptive observer developed in Section 5.5, where observer gain $L$ is replaced by $S_x^{-1} C^T$ and

parameter $\Gamma$ is replaced by $S_\theta$. In this LTV adaptive observer, only two parameters (i.e. $\rho_x$ and $\rho_\theta$ ) need to be pre-specified, and the other parameters (i.e. $S_x$, and $S_\theta$ ) are required to be computed online from time-varying matrices $A$ and $\phi$. These two matrices can be obtained from measured speed and voltages (as in (5.53) and (5.18)). Although this approach presents well exponential convergence in the estimation, it is based on a high dimensional model proposed in Section 5.2 (i.e. the model dimension is eight). Thus it is computationally costly which can limit its applications for practical problems.

## 5.7. Simulation Studies

In this section, three adaptive observer algorithms developed in sections 5.4, 5.5, and 5.6 are applied for the diagnosis of multi-phase short circuit fault, respectively. They are tested under different situations: no model uncertainties, in presence of model uncertainties, and speed variation, and their abilities on estimating unknown parameters ( $\mu_{sa}$, $\mu_{sb}$, $\mu_{sc}$, $\mu_{ra}$, $\mu_{rb}$, or $\mu_{rc}$ ) are demonstrated throughout the simulation studies in the following subsections. The parameters and operating condition of the DFIG in this simulation study are the same as in Section 4.6.

### 5.7.1. Performance of Conventional Adaptive Observer in Ideal Case

Firstly, an ideal case without considering model uncertainties in system (5.8) is discussed. For such a system, the modified adaptive observer (Algorithm 5.2) is implemented to estimate parameter $\theta$ so as to diagnose the short circuit fault (i.e. determine the fault level and position). The observer is constructed as in (5.28). The observer parameter is set as $\Gamma = 0.001 \times \mathbf{I}_6$ and gain $L$ is calculated from (5.38) by letting $Q = 100\mathbf{I}_4$, and the results are presented in Appendix D.2.

Two different the short circuit fault scenarios are simulated here in order to test the ability of this modified observer on diagnosing the faults on different levels and different positions..

**Fault scenario 1:** a 1% ($\mu_{sa}$=0.01) short circuit fault is applied to stator phase 'a' at t=10s, cleared at t=12s.

**Fault scenario 2:** two short circuit faults occur simultaneously in stator phase 'b' and rotor phase 'c' at t=14s: Former fault level is 2% ($\mu_{sb}$=0.02), and the latter one is 3% ($\mu_{rc}$=0.03). They are both cleared at t=16s.

As mentioned earlier, the short circuit faults are represented by the parameters ($\mu_{sa}$, $\mu_{sb}$, $\mu_{sc}$, $\mu_{ra}$, $\mu_{rb}$, or $\mu_{rc}$). For these two fault scenarios, the variations of these parameters are depicted in Figure 5.2 (red dotted lines). The fault diagnosis results of the conventional adaptive observer are also presented in this figure (blue solid lines). As it is shown in this figure, for each fault scenario, its corresponding fault parameters ($\mu_{sa}$, $\mu_{sb}$, $\mu_{sc}$, $\mu_{ra}$, $\mu_{rb}$, or $\mu_{rc}$) can be estimated accurately. Based on these estimated parameters, the fault level and fault position can therefore be precisely determined. For instance, at t=10s, parameter $\mu_{sa}$ changes to 1%, while the other parameters still remain at zeros, which means that a 1% short circuit fault occurs in stator phase 'a' and the other phases are fault-free. Some impulses can be observed in this figure (e.g. at t=10, 12, 14, and 16sec), which are caused by the parameter variations at those time instants. However, those impulses are small in magnitude and occur in very short time intervals, and thus they are not regarded as faults and do not affect the fault diagnosis results.

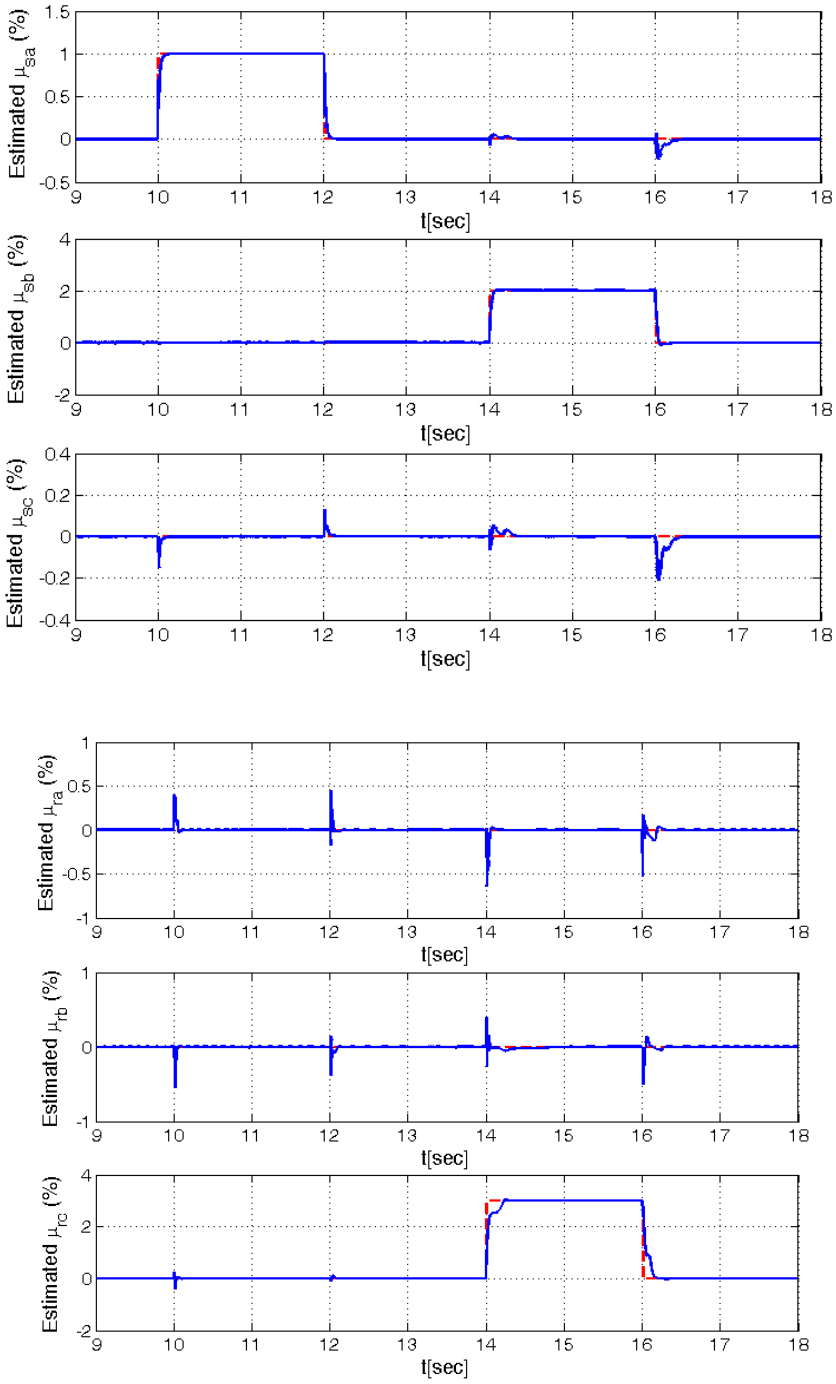


Figure 5.2. Fault diagnosis results using the modified adaptive observer.

## 5.7.2. Robustness of High Gain Adaptive Observer against Model Uncertainties

The robustness of the high gain adaptive observer (as in Section 5.4) against the model uncertainties is demonstrated in this subsection. In this simulation study, the model

uncertainties in system (5.40) is introduced by a parameter variation (i.e. an variation of stator resistance $r_s$) The observer is designed as in (5.28) with the adaptive law as in (5.42). The observer parameters used in the simulation are $\Gamma_1 = 0.0005 \times \mathbf{I}_6$, $\Gamma_2 = 0.001 \times \mathbf{I}_6$. $L$ is calculated from (5.51) by setting $\rho = 150$ and the result is given in Appendix D.3.

Firstly, the short circuit faults are simultaneously applied to each phase of the stator and rotor at t=4s, and fault level is given as follows. Thereafter, a 10% variation of resistance $r_s$ is applied later at t=5s to test the robustness of the high gain adaptive observer. The modified adaptive observer designed in last subsection is also simulated here for the comparison purposes.

**Fault scenario:**

1% ( $\mu_{sa}$ =0.01) short circuit in stator phase 'a';

2% ( $\mu_{sb}$ =0.02 ) short circuit in stator phase 'b';

3% ( $\mu_{sc}$ =0.03 ) short circuit in stator phase 'c';

1% ( $\mu_{ra}$ =0.01) short circuit in rotor phase 'a';

2% ( $\mu_{rb}$ =0.02 ) short circuit in rotor phase 'b';

3% ( $\mu_{rc}$ =0.03) short circuit in rotor phase 'c'.

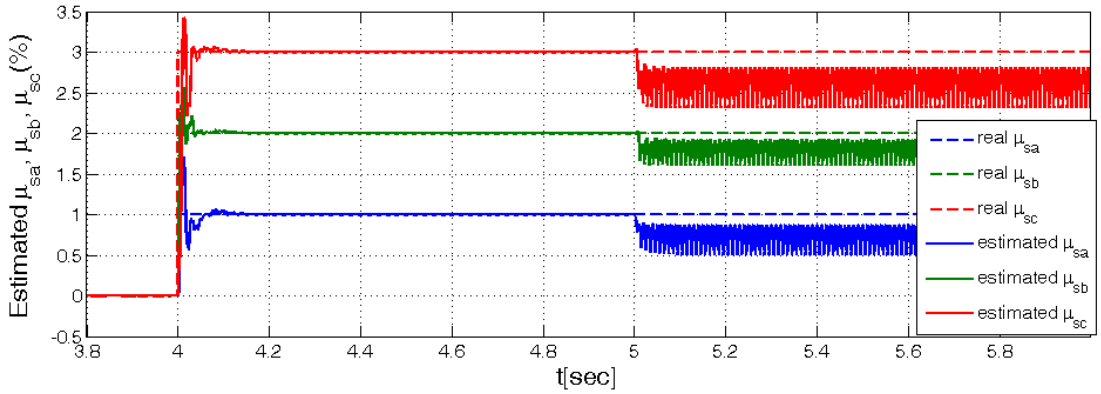


(a) Fault level parameters of the stator (i.e. $\mu_{sa}$, $\mu_{sb}$, $\mu_{sc}$).

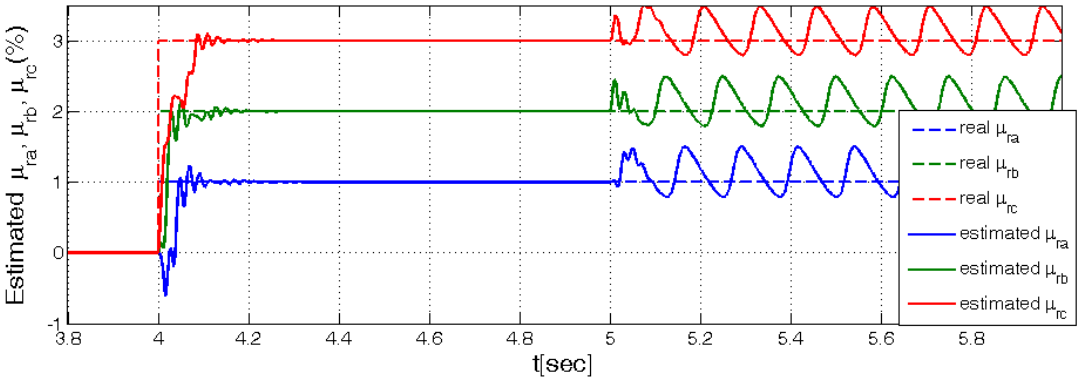


(b) Fault level parameters of the rotor (i.e. $\mu_{ra}$ , $\mu_{rb}$ , $\mu_{rc}$ ).

Figure 5.3.Performance of modified adaptive observer in the presence of model uncertainties: the short circuit faults are applied at t=4sec, and a 10% variation of $r_s$ is applied at t=5sec.

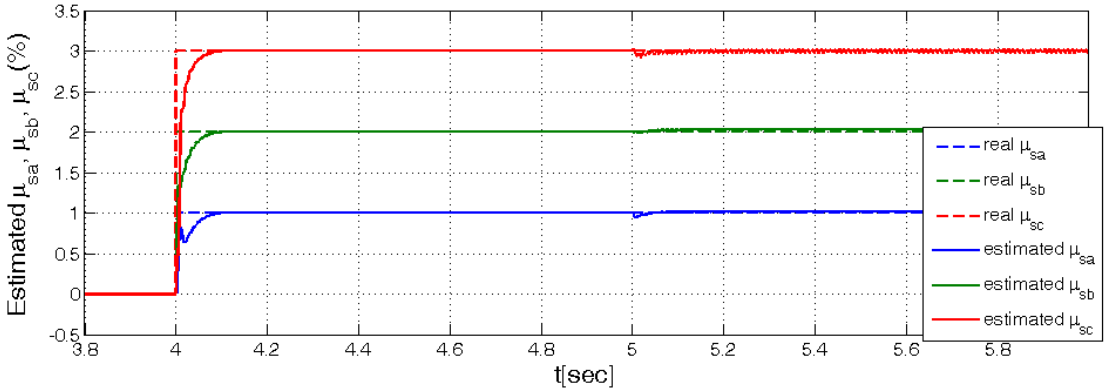


(a) Fault level parameters of the stator (i.e. $\mu_{sa}$ , $\mu_{sb}$ , $\mu_{sc}$ ).

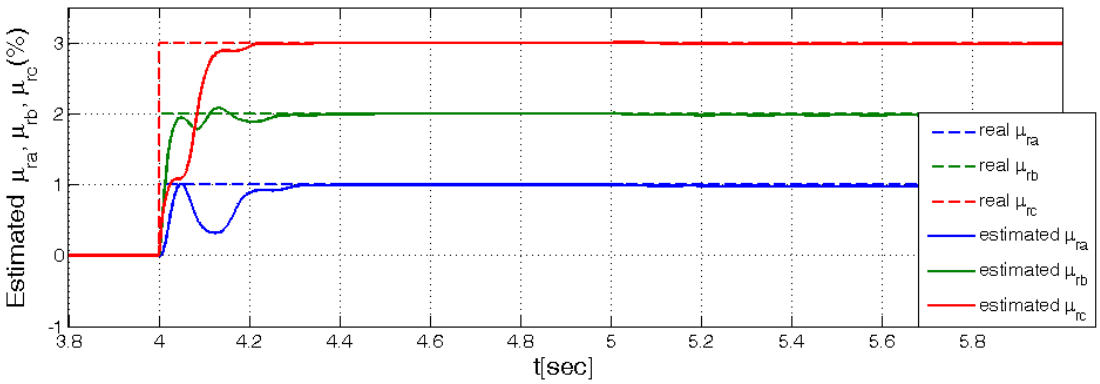


(b) Fault level parameters of the rotor (i.e. $\mu_{ra}$ , $\mu_{rb}$ , $\mu_{rc}$ ).

Figure 5.4. Performance of high adaptive observer in the presence of model uncertainties: the short circuit faults are applied at t=4sec, and a 10% variation of $r_s$ is applied at t=5sec.

The fault diagnosis results using the modified adaptive and high gain adaptive observers are provided in Figure 5.3 and Figure 5.4, respectively. As it is shown in Figure 5.3, when the model uncertainties (i.e. 10% variation of resistance $r_s$) occur at t=5s, the modified adaptive observer fails to provide acceptable estimations. The estimations start to oscillate and can not converge to their true values. It is unable to obtain accurate fault diagnosis using these estimation results. Nevertheless, as it is shown in Figure 5.4, the high gain adaptive observer can estimate the fault level parameter accurately and the estimates are almost without being affected by the model uncertainties.

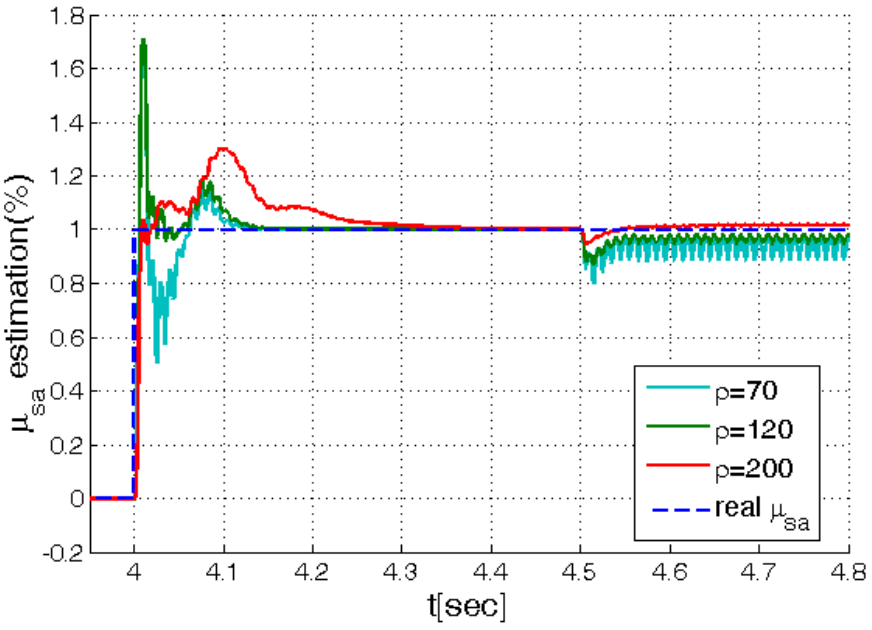


Figure 5.5. Comparison of the performances of the high gain adaptive observer with different values of $\rho$: fault is applied at t=4s; resistance $r_s$ variation occurs at t=4.5s.

As in (5.51) parameter $\rho$ is an important parameter in the design of the parameter matrices of the high gain adaptive observer. Different selections of $\rho$ correspond to different observer gains, and lead to different performances of the observer. A Comparison of the performances of the high gain adaptive observer with different values of $\rho$ is illustrated in Figure 5.5. As it shown, a large value of $\rho$ (e.g.

$\rho = 200$) present better robustness against model uncertainties, but it results a slow convergence speed. A small value of $\rho$ (e.g. $\rho = 70$) provides a faster response when fault occurs, while has weaker robustness against model uncertainties and leads larger estimation errors at the steady-state. Obviously, there is a trade-off between the convergence speed and accuracy of the estimations. Therefore $\rho$ should be chosen properly in order to achieve a desired performance, and this are usually achieved based on the simulation errors and multiple tests.

### 5.7.3. Performance of LTV Adaptive Observer under Varying Speed

In this subsection, the LTV adaptive observer (Algorithm 5.3) is applied to diagnose the short circuit fault when DFIG operates at varying speed. The speed variation is depicted in Figure 5.6 (a). The observer is designed as in (5.54), whose parameters are $\rho_x = \rho_\theta = 10$. The model uncertainties are not considered in this section. The simulations results is given in Figure 5.6 (b) and (c).

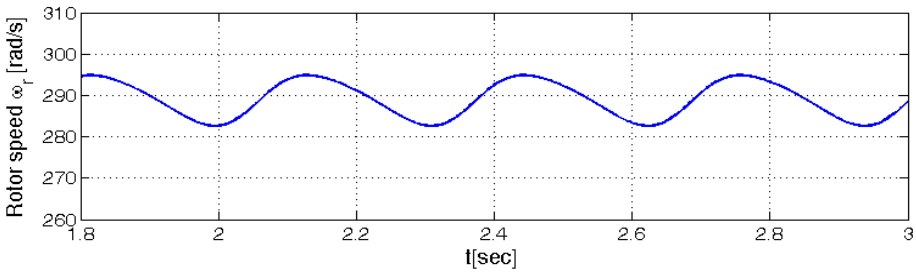


(a) Rotor Speed Variation

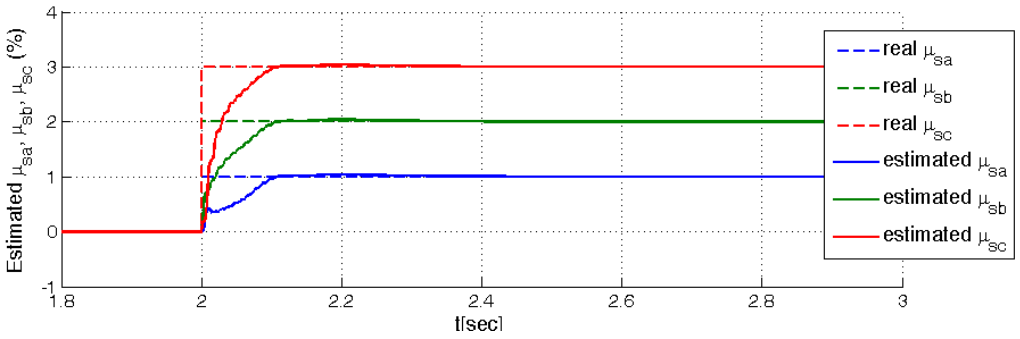


(b) Fault level parameters of the stator (i.e. $\mu_{sa}$, $\mu_{sb}$, $\mu_{sc}$).

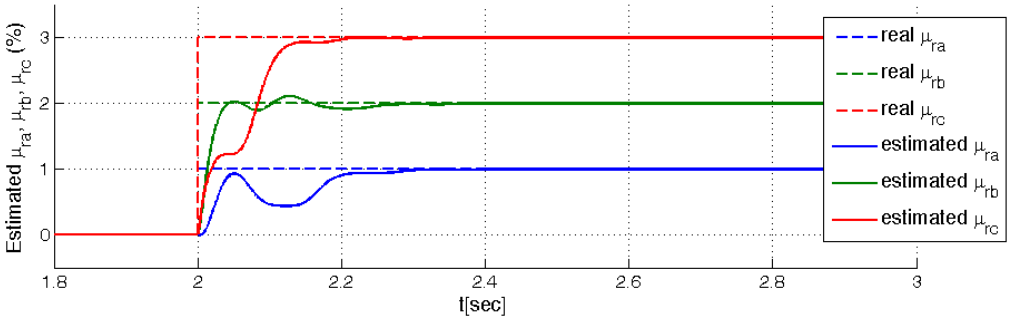


(c) Fault level parameters of the rotor (i.e. $\mu_{ra}$, $\mu_{rb}$, $\mu_{rc}$).

Figure 5.6. Fault diagnosis results using the LTV adaptive observer.

From Figure 5.6 (b) and (c), it can be observed that the LTV adaptive is able to provide a fast and unbiased estimation of the fault level parameters ($\mu_{sa}$, $\mu_{sb}$, $\mu_{sc}$, $\mu_{ra}$, $\mu_{rb}$, and $\mu_{rc}$), and estimation results are not affected by the speed variation. Based on these estimation results, an accurate fault diagnosis (i.e. level and position) can be obtained

## 5.8. Summary

In this chapter, the adaptive observers are applied for the diagnosis of the multi-phase short circuit fault. Similar to the work in Chapter 4, a state-space representation of the DFIG model with respect to the multi-phase fault is firstly derived, where a group of parameters ($\mu_{sa}$, $\mu_{sb}$, $\mu_{sc}$, $\mu_{ra}$, $\mu_{rb}$, and $\mu_{rc}$) are used to represent the faults. Several different adaptive observers are implemented to estimate these parameters online so as to diagnose the fault. Firstly, a conventional adaptive observer is designed under the SPR condition. In order to relax this condition, a modified adaptive observer is developed and the convergence of the parameter and state estimations is guaranteed by a Lyapunov equation (as in (5.38)), which can be easier be satisfied. In addition, in order to reduce the effects of model uncertainties, the high gain estimation technique is applied to redesign the modified adaptive observer. The situation that the DFIG operates under varying speed is also considered in this work, for which a LTV adaptive observer is designed.

The fault diagnosis method proposed in this chapter has many advantages over the method in last chapter. First of all, it is directly based on the voltage and current measurements without resorting to the sequence component decomposition. In addition, it can provide a precise estimation of the percentage of shorted turns ($\mu_{sa}$, $\mu_{sb}$, $\mu_{sc}$, $\mu_{ra}$, $\mu_{rb}$, and $\mu_{rc}$), which can be not realized in the method of last chapter. Moreover, it can estimate unknown states (i.e. $\boldsymbol{\mu}_{sdq}\mathbf{i}_{sfdq}$ and $\boldsymbol{\mu}_{rdq}\mathbf{i}_{rfdq}$) of system (5.8), which will be used in the following chapter to compensate the influences of winding short circuit faults.

# 6. Fault Compensation for Short Circuit Fault in DFIG Wind Turbine System

## 6.1. Introduction

As discussed in Chapter 3, for an open-loop operated DFIG wind turbine, the winding short circuit faults result asymmetries in the stator and rotor currents, while without affecting the electromagnetic torque which is a constant at steady-state. Nevertheless, for a closed-loop controlled DFIG wind turbine under the conventional control strategy, since the measured outputs (i.e. currents) are fed to the controller to adjust the system target outputs (i.e. electromagnetic torque and output power), any asymmetries in the currents can ultimately lead to the oscillations in the electromagnetic torque, and the increase in the magnitude of oscillations in the output power. This will greatly increases the mechanical stress and degrades the output power quality. In order to reduce the above mentioned effects on a closed-loop controlled DFIG wind turbine system, a fault compensator is proposed in this chapter and it is combined with a conventional controller, such that the oscillations in the torque can be removed and the oscillation amplitude in output power can be reduced. This compensator is constructed based on the estimated unknown states ($\boldsymbol{\mu}_{sdq}\mathbf{i}_{sfdq}$ and $\boldsymbol{\mu}_{rdq}\mathbf{i}_{rfdq}$) provided by the adaptive observers given in the last chapter, while when to implement the compensator depends on the whether the fault occurs that can be diagnosed using the scheme in the previous chapter. This control strategy that relies on the fault diagnosis scheme is also known as the active fault tolerant control.

This chapter is organized as follows. In Section 6.2, a conventional control strategy is implemented for the closed-loop control of the DFIG wind turbine. The control

scheme includes two parts. One is the stator flux oriented control (SFOC) algorithm for the decoupled control of the electromagnetic torque and reactive power. The other is a maximum power point tracking (MPPT) algorithm, which is implemented in order to capture the maximum wind power. In Section 6.3, a fault compensator is developed based on the adaptive observers proposed in the last chapter, and incorporated with the controller in order to eliminate the influence of short circuit faults on the closed-loop controlled system. Finally, the improvements of using the fault compensator on the output performance are demonstrated via simulations in Section 6.4.

## 6.2. Conventional Closed-Loop Control

The control of the DFIG wind turbine has two objectives: the decoupled output (i.e. electromagnetic and reactive power) control and maximum wind capture. The conventional approach for the first objective is stator flux oriented control, which can be realized by the two independent rotor current regulations on the stator flux oriented coordinate. For the second objective, a recently proposed method, maximum power point tracking (MPPT), has been extensively used in the wind power generation context. These two control strategies are always applied simultaneously to DFIG wind turbine systems. In this section, the principles of these two control algorithms are also briefly reviewed [2], [3].

### 6.2.1. MPPT

In the MPPT control, the maximum wind power capture can be obtained by setting the reference value of the torque according to the MPPT curve. This curve is determined by the output power characteristic of the wind turbine. In this subsection, such characteristic is introduced, based on which the MPPT curve is then provided.

At low wind speed, the amount of wind energy captured by the wind turbine is given as

$$P_{wt} = \frac{1}{2}\rho\pi R_{wt}^{\ 2} C_p(\lambda,\beta)\upsilon_w^{\ 3} \tag{6.1}$$

where, $\rho$ is the air density. $R_{wt}$ is the wind turbine radius. $\upsilon_w$ is the wind speed. $C_p(\lambda,\beta)$ is the power efficiency coefficient, which is a function of the tip-speed ratio ($\lambda$ ) and blade pitch angle ($\beta$). The tip-speed ratio $\lambda$ is defined as

$$\lambda = \omega_{wt} R_{wt} / \upsilon_w \tag{6.2}$$

From (6.1), it is can be observed that the power produced by the wind turbine ($P_{wt}$) is a function of the wind speed ($\upsilon_w$), blade pitch angle ($\beta$), and rotor speed of wind turbine ($\omega_{wt}$). At low wind speed, the pitch angle ($\beta$) is fixed at zero. In this case, the output power ($P_{wt}$) versus the rotor speed ($\omega_{wt}$) at different wind speed ($\upsilon_w$) is given in Figure 6.1 (curve 1). As it is shown in this figure, at a specific wind speed ($\upsilon_w$), there is a unique rotor peed ($\omega_{wt}$) to achieve the maximum output power.

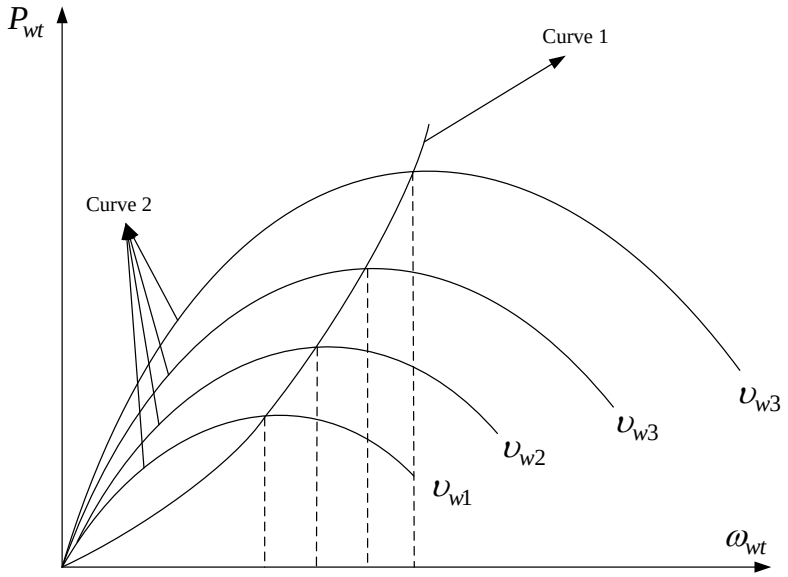


Figure 6.1. Maximum output power versus the rotor speed of wind turbine.

An important relationship between the maximum output power ($P_{wt\_opt}$) and its corresponding the turbine rotor speed ($\omega_{wt}$) is given in [3] as follows and depicted in Figure 6.1 (curve 2)

$$P_{wt\_opt} = K_{opt} \omega_{wt}^3 \tag{6.3}$$

where $K_{opt}$ is the optimal power coefficient, which is unique determined by the structure of the wind turbine and independent of the wind speed. Therefore, as long as DFIG operates following the relationship (6.3) (i.e. curve 1 in Figure 6.1), the maximum power can always be obtained, and there is no need to take account of the wind speed in the computation.

In practice, the maximum wind power capture is realized by controlling the electromagnetic torque of the DFIG. For this purpose, the maximum DFIG torque ($T_{g\_opt}$) and its corresponding the mechanical rotor speed of the DFIG ($\omega_g$) can be obtained from (6.3), which is given as

$$T_{g\_opt} = K_{opt}\omega_g^2 \tag{6.4}$$

Based on such relationship, the MPPT curve is obtained in Figure 6.2. For each measured rotor speed of the DFIG, an optimal torque can be determined according to this curve, and this optimal value is set at the reference for the torque control.

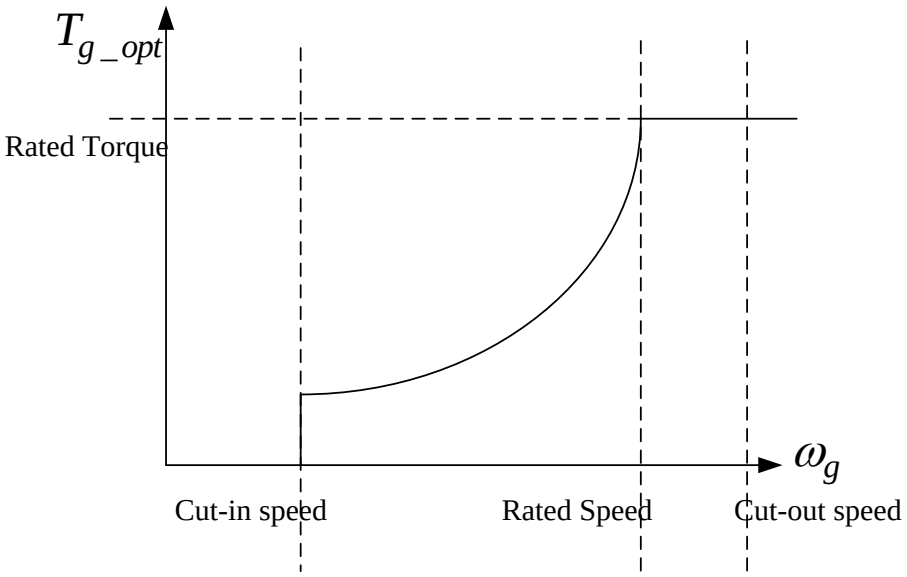


Figure 6.2. MPPT curve.

## 6.2.2. Stator Flux Oriented Control

Since the control outputs of the DFIG (i.e. the electromagnetic torque and reactive power as in (6.9)) are nonlinear in terms of the state variables (i.e. currents), an challenging task of the controller design is to deal with these output nonlinearities. The

stator flux oriented vector control is a commonly used approach to solve this problem. Another important advantage of this approach is that it allows the decoupled control of the electromagnetic torque and reactive power. In this subsection, this conventional control algorithm is briefly introduced, which is based on the following two assumptions: 1) stator resistance is negligible; 2) the amplitude of stator flux is invariant.

The stator flux oriented control is established in the stator flux oriented coordinate. In this coordinate, the dynamics of the DFIG is expressed by the following equations:

$$\begin{cases} v_{sd} = r_s i_{sd} + \dfrac{d\psi_{sd}}{dt} - \omega_s \psi_{sq} \\ v_{sq} = r_s i_{sq} + \dfrac{d\psi_{sq}}{dt} + \omega_s \psi_{sd} \end{cases}, \quad \begin{cases} v_{rd} = r_r i_{rd} + \dfrac{d\psi_{rd}}{dt} - (\omega_s - \omega_r)\psi_{rq} \\ v_{rq} = r_r i_{rq} + \dfrac{d\psi_{rq}}{dt} + (\omega_s - \omega_r)\psi_{rd} \end{cases} \tag{6.5}$$

$$\begin{cases} \psi_{sd} = L_s i_{sd} + L_m i_{rd} \\ \psi_{sq} = L_s i_{sq} + L_m i_{rq} = 0 \end{cases}, \quad \begin{cases} \psi_{rd} = L_r i_{rd} + L_m i_{sd} \\ \psi_{rq} = L_r i_{rq} + L_m i_{sq} \end{cases} \tag{6.6}$$

where $\omega_s$ is the synchronous speed. $\omega_r$ is the electrical rotor speed of DFIG and its relationship with mechanical rotor speed $\omega_g$ is given as (other parameters and variables have been defined in Chapter 3)

$$\omega_r = p\omega_g \tag{6.7}$$

It is known that in the stator flux oriented coordinate, d-axis is aligned with the stator flux vector $\psi_s$, namely, $\psi_{sd} = \psi_s$ and $\psi_{sq} = 0$. Under above two assumptions, it can be obtained from (6.5) that $v_{sq} = v_s$ and $v_{sd} = 0$. Based on these results, the stator variables ( i.e. $\psi_{sd}$, $i_{sd}$, $i_{sq}$) can be expressed in terms of the rotor current variables (i.e. $i_{rd}$, $i_{rq}$), which is given as

$$\psi_{sd} = \frac{v_s}{\omega_s},\ i_{sd} = \frac{v_s}{L_s \omega_s} - \frac{L_m}{L_s} i_{rd},\ i_{sq} = -\frac{L_m}{L_s} i_{rq} \tag{6.8}$$

By using these equations, the outputs (i.e. the electromagnetic torque and reactive power) can be formulated into linear functions in terms of the rotor currents variables, which are explained in the following.

The general expression of the electromagnetic torque and the reactive power are given as follows according to their definitions.

$$T_g = \frac{3}{2} pL_m (i_{sq} i_{rd} - i_{sd} i_{rq}), \quad Q_s = \frac{3}{2}(v_{qs} i_{ds} + v_{ds} i_{qs}) \tag{6.9}$$

By substituting (6.8) in above equations, a linear and decoupled expression of the torque and reactive power can be obtained as

$$T_g = -\frac{3}{2} p \frac{L_m}{L_s} \frac{v_s}{\omega_s} i_{rq}, \quad Q_s = \frac{3}{2}(\frac{v_s^2}{L_s \omega_s} - \frac{L_m v_s}{L_s} i_{rd}) \tag{6.10}$$

It can be noted that the electromagnetic torque ($T_g$) and reactive power ($Q_s$) are linear functions in terms of $i_{rd}$ and $i_{rq}$, and can be independently controlled via $i_{rq}$ and $i_{rd}$, respectively. Furthermore, currents $i_{rq}$ and $i_{rd}$ can be regulated by the rotor voltages $v_{rd}$ and $v_{rq}$, which is given as follows, which is obtained by substituting (6.8) into (6.5) and (6.6)

$$v_{rd} = R_r i_{rd} + \frac{D}{L_s} \frac{di_{rd}}{dt} + v_{rd\_c} \tag{6.11}$$

with $v_{rd\_c} = (\omega_s - \omega_r)\left( \frac{L_r L_m^{\ 2}}{L_s} i_{rq} \right)$

$$v_{rq} = R_r i_{rq} + \frac{D}{L_s} \frac{di_{rq}}{dt} + v_{rq\_c} \tag{6.12}$$

with $v_{rq\_c} = (\omega_s - \omega_r)\left( \frac{L_r L_m^{\ 2}}{L_s} i_{rd} + \frac{L_m}{L_s} \frac{v_s}{\omega_s} \right)$

From these equations, it can be noted that the rotor currents $i_{rd}$ and $i_{rq}$ are dominated by two first order systems, which can be independently controlled by the rotor voltages $v_{rd}$ and $v_{rq}$, respectively.

Based above analysis, the linear and decoupled control of the electromagnetic torque and reactive power can be realized by a two-stage PI controller with the first stage for the torque/power control and the second stage for the rotor current control. This control algorithm (i.e. stator flux oriented control) is incorporated with the MPPT

algorithm (as in above subsection) in order to achieve the two control objectives mentioned at the beginning of this section. The overall schematic diagram of this control algorithm is presented in Figure 6.3.

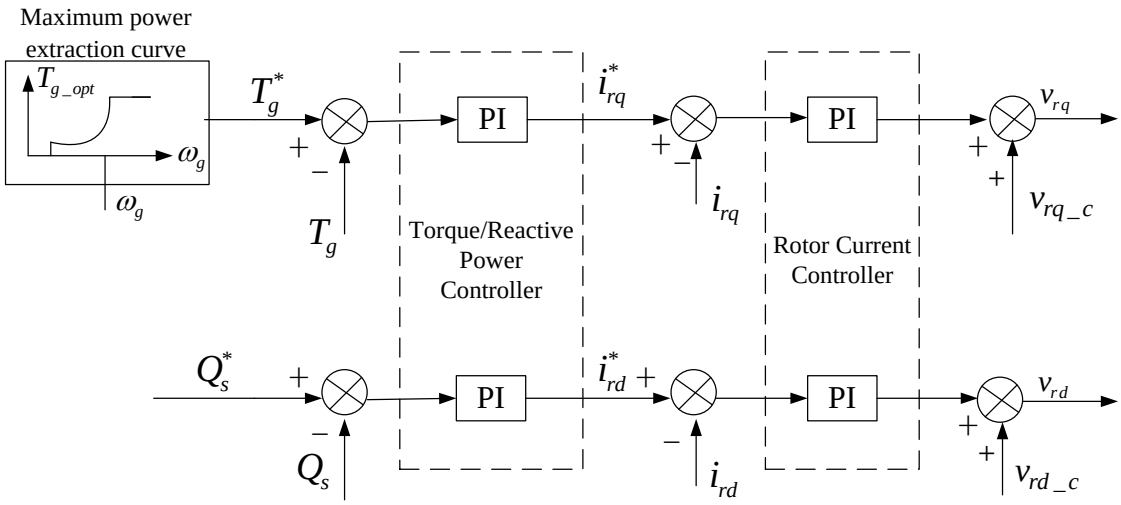


Figure 6.3. Stator flux oriented control with MPPT.

In the next, a fault compensator is developed and incorporated with this conventional control algorithm in order to eliminate the influence of short circuit faults on the closed-loop controlled system.

## 6.3. Fault Compensator

Although the aforementioned control algorithm is effective for a healthy DFIG wind turbine system, its control performance can degrade in the presence of short circuit faults. In order to maintain a normal and continued operation, a fault compensator is designed to compensate the impacts of short circuit faults on the closed-loop controlled DFIG wind turbine system. Before designing the compensator, we need to understand how the stator and rotor currents are contaminated by the short circuit faults. For this purpose, we review the model for the multi-phase short circuit fault as in (3.47)-(3.48) and the equivalent circuits Figure 3.5. It has been observed that the short circuit fault can be interpreted as an independent current source injecting into the stator or rotor output currents. Therefore, an additive relationship of the healthy and faulty system output currents can be proposed, which is given as

$$\mathbf{i}_{sdq} = \mathbf{i}^{h}_{sdq} + \boldsymbol{\mu}_{sdq}\mathbf{i}_{sfdq}, \quad \mathbf{i}_{rdq} = \mathbf{i}^{h}_{rdq} + \boldsymbol{\mu}_{rdq}\mathbf{i}_{rfdq} \tag{6.13}$$

where $\mathbf{i}^{h}_{sdq}$ and $\mathbf{i}^{h}_{rdq}$ denote the healthy currents components, and $\boldsymbol{\mu}_{sdq}\mathbf{i}_{sfdq}$ and $\boldsymbol{\mu}_{rdq}\mathbf{i}_{rfdq}$ denote the faulty current components. More importantly, the healthy current components are totally independent from the fault. Such independency can be verified by comparing the structures of faulty and healthy models. That is, by replacing the measured and faulty current components (i.e. $\mathbf{i}_{sdq}/\mathbf{i}_{rdq}$ and $\boldsymbol{\mu}_{sdq}\mathbf{i}_{sfdq}/\boldsymbol{\mu}_{rdq}\mathbf{i}_{rfdq}$) in the faulty model (3.47)-(3.48) with the proposed relationship (6.13), we can obtain the following equations

$$\begin{cases} \mathbf{v}_{sdq} = r_s\mathbf{i}^{h}_{sdq} + \dfrac{d\boldsymbol{\psi}_{sdq}}{dt} + \mathbf{J}\omega_s\boldsymbol{\psi}_{sdq} \\ \mathbf{v}_{rdq} = r_r\mathbf{i}^{h}_{rdq} + \dfrac{d\boldsymbol{\psi}_{rdq}}{dt} + \mathbf{J}(\omega_s - \omega_r)\boldsymbol{\psi}_{rdq} \end{cases} \tag{6.14}$$

$$\begin{cases} \boldsymbol{\psi}_{sdq} = L_s\mathbf{i}^{h}_{sdq} + L_m\mathbf{i}^{h}_{rdq} \\ \boldsymbol{\psi}_{rdq} = L_r\mathbf{i}^{h}_{rdq} + L_m\mathbf{i}^{h}_{sdq} \end{cases} \tag{6.15}$$

Comparing these equations with the healthy DFIG model equations (6.5) and (6.6), it can be noted that these two models are identical except that (6.14) and (6.15) are expressed in a matrix form. Hence, it can be concluded that the healthy currents components $\mathbf{i}^{h}_{sdq}$ and $\mathbf{i}^{h}_{rdq}$ are independent from the fault.

As mentioned earlier, oscillations in the electromagnetic torque and output power can be introduced in the closed-loop control when the current measurements contain faulty components. Practically, it is therefore ideal to remove such faulty current components before implementing a close-loop control strategy. Fortunately, the faulty current components $\boldsymbol{\mu}_{sdq}\mathbf{i}_{sfdq}$ and $\boldsymbol{\mu}_{rdq}\mathbf{i}_{rfdq}$ can be estimated using the adaptive observers proposed in Chapter 5, and the healthy current components $\mathbf{i}^{h}_{sdq}$ and $\mathbf{i}^{h}_{rdq}$ can thus be obtained by subtracting these estimated faulty current components from the current measurements, and used for the closed-loop control. The complete control algorithm including the fault compensator is given in Figure 6.4. This fault compensator is a sort of plug-and-play device. It is able to provide online fault

compensation and remove the effects of any possible faults, regardless their level and position, while when to implement the compensator depends on the whether the fault occurs that can be diagnosed using the scheme in Chapter 5. This compensation strategy can be generalized and incorporated into any other closed-loop controller with current measurements as control inputs, including the control algorithm given in the next Chapter.

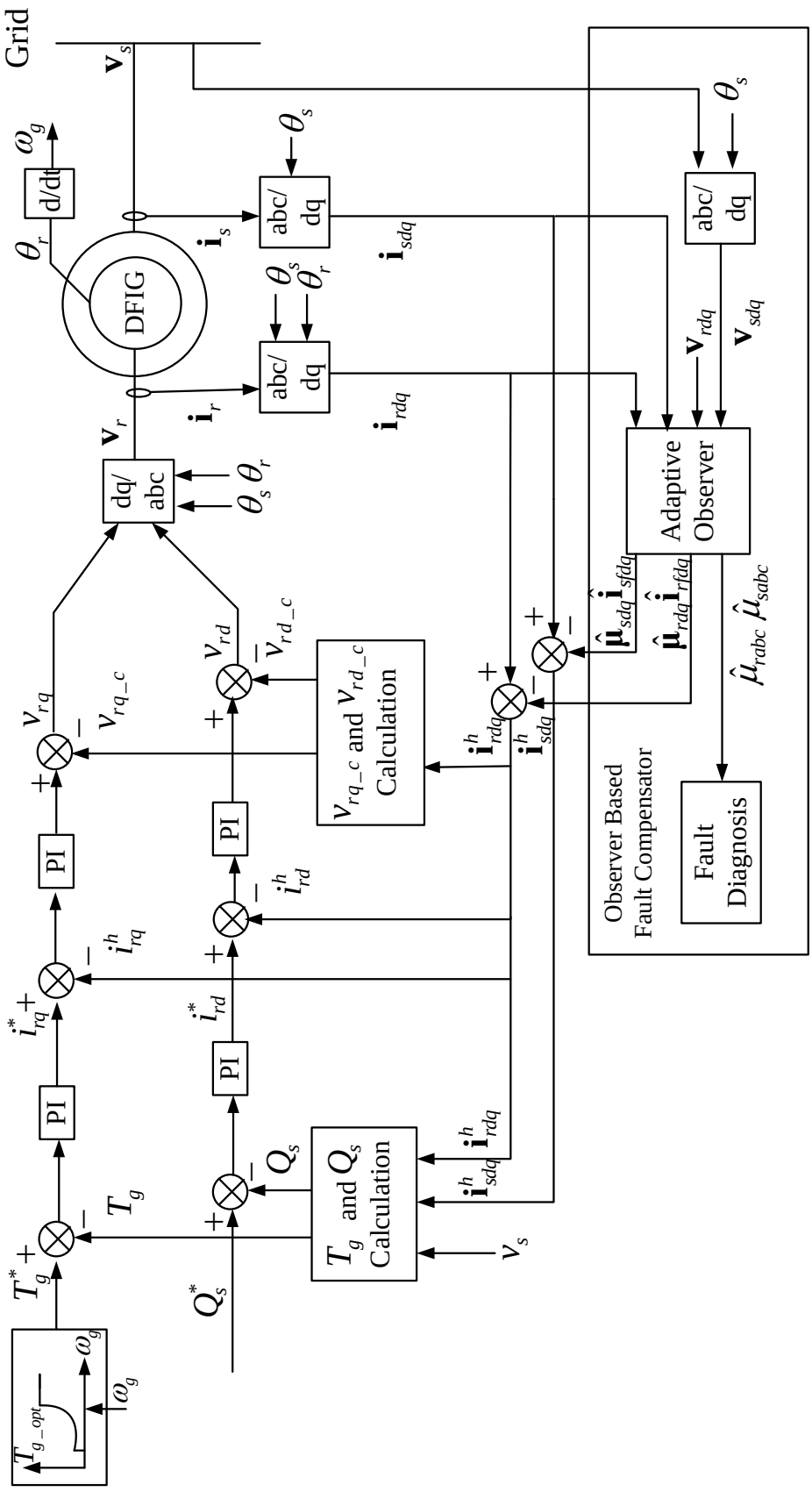


Figure 6.4. Conventional closed-loop control with the fault compensator.

## 6.4. Simulation Studies

The proposed fault compensation scheme is implemented on a closed-loop controlled DFIG wind turbine system, whose parameters are given in Appendix A. The adaptive observer based fault diagnosis scheme is firstly employed to provide online diagnosis of the short circuit faults, and meanwhile estimate faulty current components (i.e. $\boldsymbol{\mu}_{sdq}\mathbf{i}_{sfdq}$ and $\boldsymbol{\mu}_{rdq}\mathbf{i}_{rfdq}$). These components are then utilized in the fault compensator to remove the influences of the fault. The whole DFIG wind turbine system is simulated by Matlab/Simulink software. It is assumed that the wind turbine operates under the wind speed at 7m/s. DFIG is controlled by the conventional control algorithm as presented in Section 6.2. In this simulation example, we set the controller parameters as follows

1st stage PI controller parameters:

$$K_p = 1, \quad K_i = 20. \tag{6.16}$$

2nd stage PI controller parameters:

$$K_p = 0.03, \quad K_i = 10 \tag{6.17}$$

To compare the performance of the DFIG wind turbine system before and after the fault compensation, a single 2% short circuit fault is introduced stator phase ‘a’ and the fault compensator is activated at $t$=10sec. The simulation results are given in Figure 6.5.

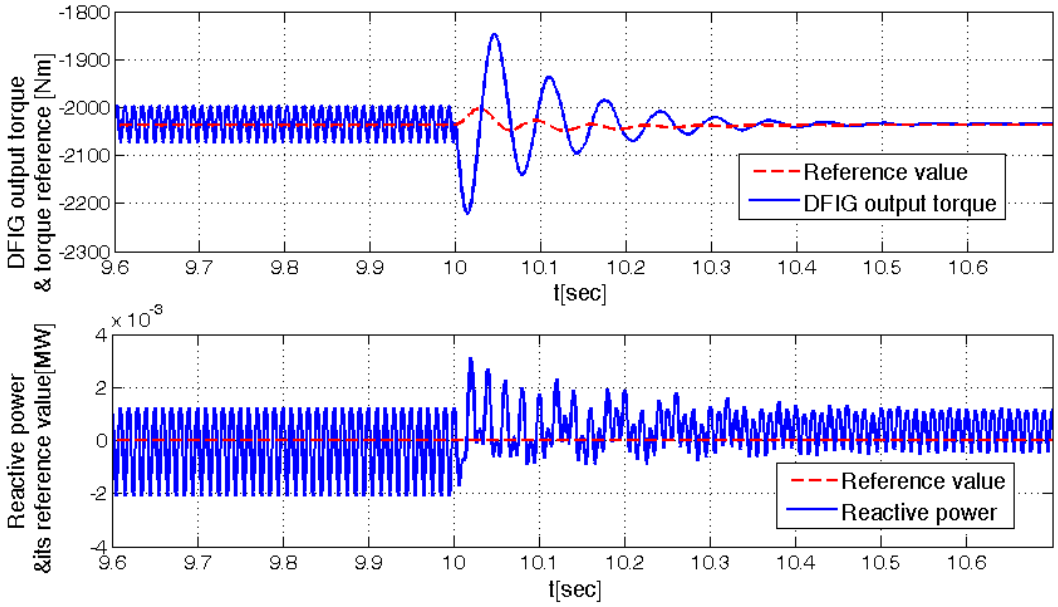


(a) Torque and reactive power reference tracking.

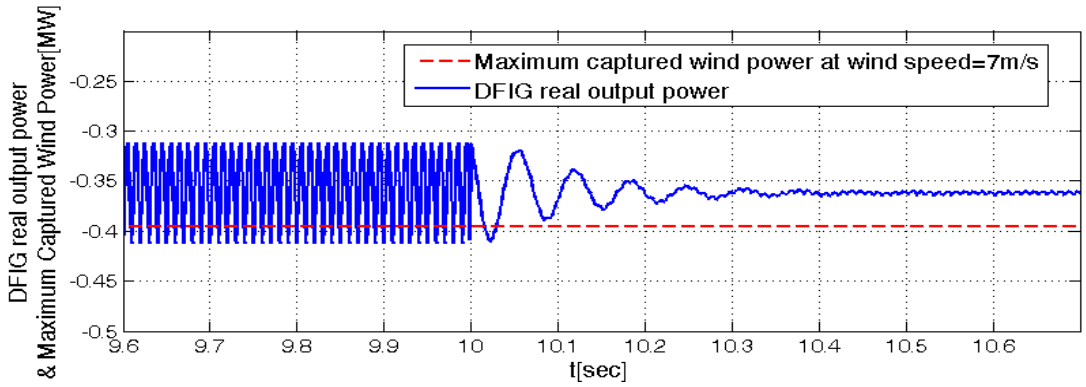


(b) DFIG output power and the maximum wind power captured at wind speed=7m/s.

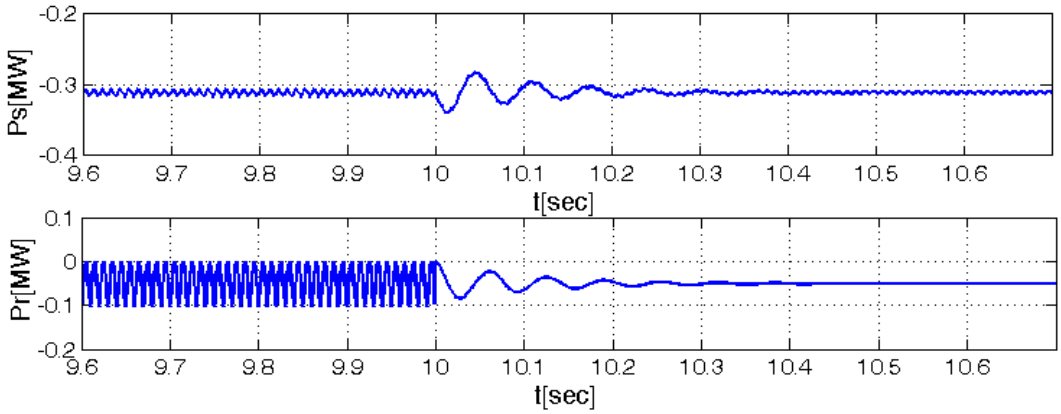


(c) Stator and rotor active power.

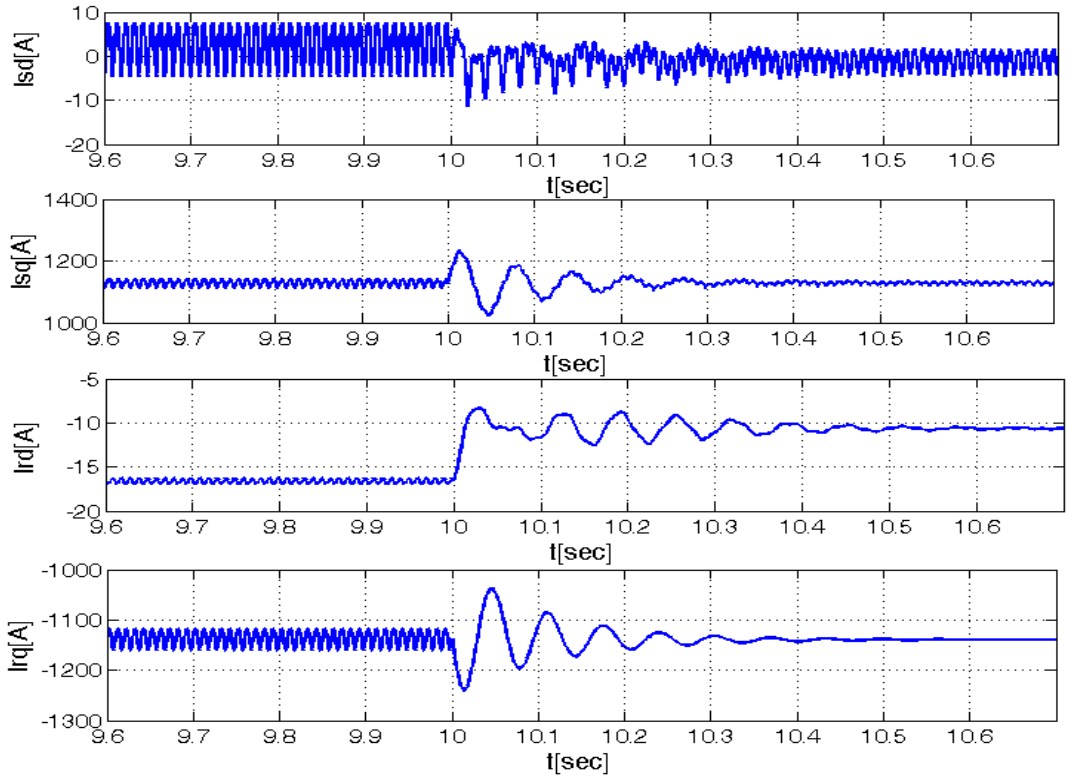


(d) Stator and rotor currents.

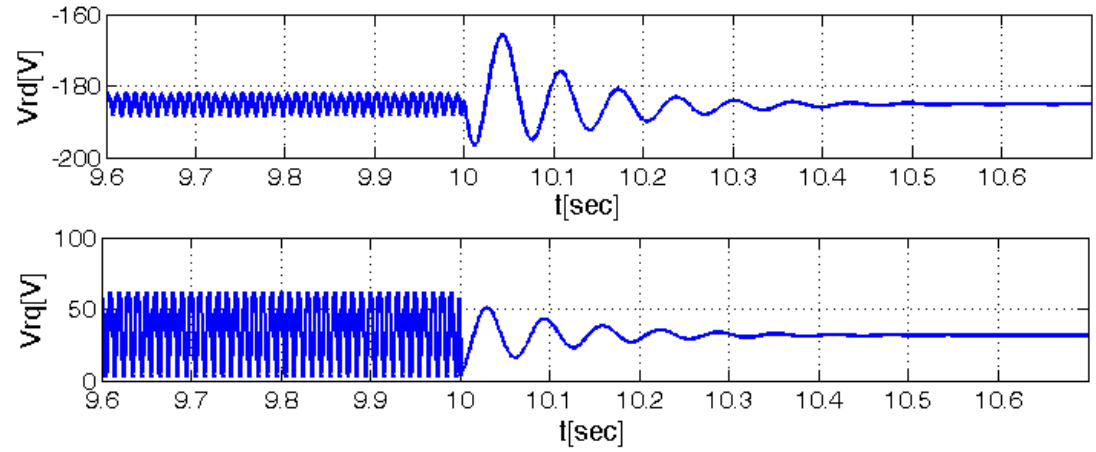


(e) Rotor control voltages.

Figure 6.5. The simulation results of fault compensation. 2% short circuit fault is applied to stator phase ‘a’, and the fault compensator is activated at t=10sec.

In Figure 6.5(a), (b) and (c), the positive power denotes the power flowing from DFIG to grid, while the negative power denotes the power flowing from gird to DFIG. As it is shown in Figure 6.5 (a), when the fault occurs, the torque and reactive power are still able to track their reference values but with strong oscillations. These oscillations are significantly reduced when the fault compensator is applied. The

actual DFIG output power (presented in Figure 6.5 (b)) is the sum of the stator and rotor active power (presented in Figure 6.5 (c)), and it is can be noted from Figure 6.5 (b) that the output power is very close to the maximum wind power captured by the wind turbine, while the difference is due to losses on the resistances. The oscillation in the output power is also reduced by the fault compensator, which is obvious as in (b). By observing Figure 6.5 (c), (d) and (e), it can be observed that when the fault compensator is applied, the oscillations in the stator quantities (i.e. stator currents $i_{sd}$ / $i_{sq}$ and active power $P_s$) are decreased, while the oscillations in the rotor quantities (i.e. rotor currents $i_{rd}$ / $i_{rq}$, active power $P_r$ and control voltages $v_{rd}$ / $v_{rq}$) are completely removed. This is due to the fault only occurs at stator in this simulation example. It is known that the oscillations in the currents and voltages are harmful for the converters. Therefore this improvement is also important in terms of the converter protection. Based on these simulation results, it can be concluded that the effects of the short circuit fault on a closed-loop controlled DFIG wind turbine system are highly reduced and the system performance is recovered by using the proposed fault compensation scheme.

## 6.5. Summary

In this chapter, a fault compensator is proposed to reduce the effects of the winding short circuit fault on a closed-loop controlled DFIG wind turbine system. The fault compensator is based on the adaptive observer proposed in last chapter. A brief introduction of a conventional control algorithm is firstly given. Thereafter, based on the estimated unknown states ($\boldsymbol{\mu}_{sdq}\mathbf{i}_{sfdq}$, $\boldsymbol{\mu}_{rdq}\mathbf{i}_{rfdq}$) provided by the adaptive observer, a fault compensator is constructed and added to the controller. The simulation studies show that this fault compensator can highly reduce the oscillations in the torque, output power and some other electrical quantities in the presence of short circuit faults.

# 7. Adaptive Nonlinear Control of DFIG Wind Turbine with Drive Train Fault

## 7.1. Introduction

The drive train is another important component of the DFIG wind turbine system. It connects the wind turbine with the DFIG and transfers the aerodynamic mechanical power to the rotor of DFIG. Due to the mechanical stress, environmental influence, etc., some mechanical faults (e.g. rotor blade broken) may occur. Such faults may result the deviation of some mechanical parameters (e.g. moment of inertia) of drive train system from their nominal values [115], [114]. Since most control strategies are designed based on the nominal system parameters, the control performance can be deteriorated (e.g. unstable or large steady state errors) under the faulty condition. The aim of this chapter is to develop an advanced control strategy, i.e. the fault tolerant control (FTC), which can provide not only the desired performance under nominal conditions, but also robust stability and acceptable performance in the presence of faults. A one-mass model is used to represent the drive train system as the control performance is dominated by the low frequency response, and the faults are presented as the unexpected change of the parameter (i.e. moment of inertia) in this model. A nonlinear control algorithm, i.e. adaptive input-output linearizing control [63], is employed here to achieve the FTC for the drive train faults. This approach has many advantages over the conventional control algorithms, e.g. the stator flux oriented control as presented in the previous chapter. Firstly, the two aforementioned assumptions, i.e. 1) the stator resistance is negligible and 2) the amplitude of the stator flux is invariant, are no longer required. This allows exact decoupled control of the torque and reactive power under both the steady state and the transient state (i.e. stator flux variations) conditions.

Moreover, this control algorithm is able to accommodate the drive train faults, by tracking the parameter variations via the parameter adaptive law. Additionally, the control performance in the presence of model uncertainties in DFIG is also discussed. A robust adaptive control algorithm (i.e. adaptive input-output linearizing control) is developed in order to achieve a desirable tracking of the torque and reactive power in the presence of faults as well as model uncertainties.

This chapter is organized as follows. In Section 7.2, the one-mass model of the drive train is presented and the faults are considered as unexpected change of moment of inertia. In Section 7.3, an adaptive input-output linearizing control algorithm is developed for the adaption of the parameter variation and the decoupled control of the torque and reactive power. In Section 7.4, a robust control algorithm is developed to ensure the desirable tracking of the torque and reactive power in the presence of model uncertainties in the DFIG. Finally, in Section 7.5, some simulation results are presented to illustrate the effectiveness of the control algorithms developed in above sections.

## 7.2. Drive Train Model and Fault Description

The drive train system comprises the low speed and high speed shafts, gearbox, bearings and other mechanical components. An explicit model of this system has been presented in Section 2.1.3. In this section, a simpler model, one-mass model, is used to describe the dynamics of this system, which is depicted in Figure 7.1

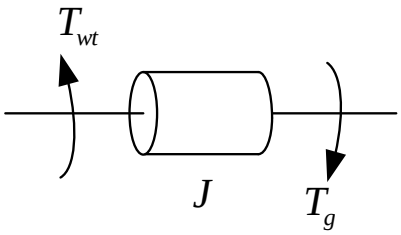


Figure 7.1. One-mass model of the drive train system.

The one-mass model of the driven train is given as

$$J\dot{\omega}_g(t) = T_{wt}(t) - T_g(t) \tag{7.1}$$

where $T_g(t)$ is the output torque of the DFIG. $T_{wt}(t)$ is the transferred wind turbine

torque on the generator side. $J$ is the equivalent moment of the inertia, which is composed of three mechanical parameters (i.e. moment of inertia of the low speed shaft $J_{wt}$, moment of inertia of the high speed shaft $J_g$, and gearbox ratio $N_g$) as given below.

$$J = \frac{J_{wt}}{N_g^2} + J_g \tag{7.2}$$

In practice, these mechanical parameters are not perfectly known and may vary when fault occurs [115], [116]. Therefore, the equivalent moment of inertia $J$ is uncertain. In this work, since we focus on the control robustness and performance in the presence of faults, one mass model is employed to represent the dynamics of the drive train as the control performance is dominated by the low frequency response, and the fault effects are only considered as the parametric uncertainties (i.e. $J$) of this model. Nevertheless, the actual behaviours of the drive train under the fault condition can be fairly complicated, it is often accompanied with the vibration and resonance which can only be modeled by some higher order, nonlinear and/or time-dependent components as investigated in some existing literatures [111], [112]. For such cases, more sophisticated methods are required for the fault diagnosis as reviewed in Chapter 2. However, this is beyond the scope of this thesis, and only the simplified model (i.e. (7.1)) is employed here to present the methodology of fault tolerance control. The extension of this work to more sophisticated models will become the future work.

## 7.3. Adaptive Input-Output Linearizing Control

In this section, an adaptive input-output linearizing control is developed to ensure the desirable performance of the DFIG wind turbine system under the faulty condition. This control algorithm contains an identification scheme (i.e. parameter adaptive law) which can asymptotically tracks the true value of parameter $J$. Once this parameter is identified, two control objectives, i.e. 1) decoupled control of the torque and reactive power, 2) desired reference tracking, are achieved by using this control algorithm. This section is organized as follows. Firstly, a third-order model of the DFIG for the purpose of control is developed, which is obtained in the stator flux oriented

coordinate. Based on this model, a non-adaptive input-output linearizing control is developed for the nominal condition under the assumption that parameter $J$ is perfectly known and invariant. Thereafter, an adaptive version of this control algorithm for the faulty condition is developed by considering parameter $J$ is an unknown constant. The MPPT control strategy presented in Section 6.2.1 is then applied to generate the reference signals for the torque control in order to achieve the maximum wind power capture. The schematic diagram of the FTC is depicted in Figure 7.2.

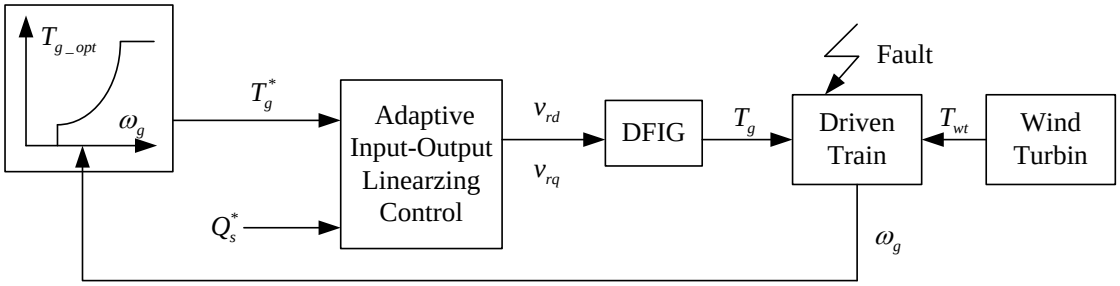


Figure 7.2. Schematic diagram of the FTC for the drive train faults.

## 7.3.1. DFIG Model for Control Purpose

In the stator flux oriented coordinate, d-axis is aligned with the stator flux vector $\psi_s$, (namely, $\psi_{sd} = \psi_s$ and $\psi_{sq} = 0$). Therefore, the mathematical model of the DFIG can be reduced into the following third-order model with neglecting the dynamics of $\psi_{sq}$.

$$\begin{cases} \dfrac{d\psi_s}{dt} = -\alpha\psi_s + \alpha L_m i_{rd} + v_{sd} \\ \dfrac{di_{rd}}{dt} = -\gamma i_{rd} + (\omega_s - \omega_r) i_{rq} + \alpha\beta\psi_s - \beta v_{sd} + \dfrac{1}{\sigma} v_{rd} \\ \dfrac{di_{rq}}{dt} = -\gamma i_{rq} - (\omega_s - \omega_r) i_{rd} + \beta\omega_r\psi_s - \beta v_{sq} + \dfrac{1}{\sigma} v_{rq} \end{cases} \tag{7.3}$$

The key parameters of this model are defined as bellow, and the other parameters and variables have been defined in Chapter 3. In the following, the dependence on *t* is omitted in order to lighten notations.

$$\alpha = \frac{R_s}{L_s},\ \ \sigma = L_r\left(1 - \frac{L_m^{\ 2}}{L_s L_r}\right),\ \ \beta = \frac{L_m}{L_s\sigma},\ \ \gamma = \frac{R_r}{\sigma} + \alpha\beta L_m,\ \ \mu = -\frac{3}{2}\frac{L_m}{L_s} p \tag{7.4}$$

The electromagnetic torque in the stator flux oriented coordinate is given as

$$T_g = \mu \psi_s i_{rq} \tag{7.5}$$

For the convenience of the controller design, model (7.3) is rewritten into a compact form as follows

$$\begin{cases} \dot{x} = f(x) + gu \\ y = h(x) \end{cases} \tag{7.6}$$

where the state and input vectors are given as

$$x = [\psi_s \ i_{rd} \ i_{rq}]^T \ , \ u = \begin{bmatrix} v_{rd} & v_{rq} \end{bmatrix}^T \tag{7.7}$$

$f(x)$ and $g$ are the smooth field vectors, which are given as

$$f(x) = \begin{bmatrix} -\alpha\psi_s + \alpha L_m i_{rd} + v_{sd} \\ -\gamma i_{rd} + (\omega_s - \omega_r) i_{rq} + \alpha\beta\psi_s - \beta v_{sd} \\ -\gamma i_{rq} - (\omega_s - \omega_r) i_{rd} + \beta\omega_r\psi_s - \beta v_{sq} \end{bmatrix} \tag{7.8}$$

$$g = \begin{bmatrix} g_d & g_q \end{bmatrix}, \ g_d = \begin{bmatrix} 0 \\ 1/\sigma \\ 0 \end{bmatrix}, \ g_q = \begin{bmatrix} 0 \\ 0 \\ 1/\sigma \end{bmatrix} \tag{7.9}$$

The control outputs of the DFIG wind turbine system are the electromagnetic torque ($T_g$) and the reactive power ($Q_s$). Therefore, the output vector is denoted as

$$y = \begin{bmatrix} T_g & Q_s \end{bmatrix}^T \tag{7.10}$$

According to the definition of the reactive power, $Q_s$ is given as

$$Q_s = v_{sd} i_{sq} + v_{sq} i_{sd} \tag{7.11}$$

In the stator flux oriented coordinate, $Q_s$ can be expressed in terms of the state variables (i.e. $x = [\psi_s \ i_{rd} \ i_{rq}]^T$), which is given as

$$Q_s = \frac{1}{L_s} v_{sq}\psi_s - \beta\sigma v_{sd} i_{rq} - \beta\sigma v_{sq} i_{rd} \tag{7.12}$$

Based on equations (7.5) and (7.12), output equation $h(x)$ is obtained as follows

$$h = \begin{bmatrix} h_1(x) & h_2(x) \end{bmatrix}^T \tag{7.13}$$

where $h_1(x) = \mu\psi_s i_{rq}$, $h_2(x) = \frac{1}{L_s} v_{sq}\psi_s - \beta\sigma v_{sd} i_{rq} - \beta\sigma v_{sq} i_{rd}$ (7.14)

It is can be noted that model (7.6) is a linear MIMO system with nonlinear outputs. For such system, a classical nonlinear control theory (i.e. input-output linearization) is applied in the following section to synthesize the nonlinear controller.

## 7.3.2. Input-Output Linearizing Control

Based on model (7.6), a nonlinear controller (i.e. input-output linearizing control) is developed for the DFIG wind turbine system to achieve the decoupled control of the torque and reactive power. This control algorithm is based on the nonlinear change of the coordinate and nonlinear redefinition of inputs to transform the nonlinear output system into an equivalent linear system in the new coordinate, and then design controller for this linear system.

Define a new coordinate as

$$\begin{aligned} z_1 &= h_1(x) \\ z_2 &= h_2(x) \end{aligned} \tag{7.15}$$

In this new coordinate, model (7.6) is given as

$$\begin{aligned} \dot{z}_1 &= L_f h_1 + L_{g_q} h_1 v_{rq} \\ \dot{z}_2 &= L_f h_2 + L_{g_d} h_2 v_{rd} + L_{g_q} h_2 v_{rq} \end{aligned} \tag{7.16}$$

where $L_f h_1$ and $L_{g_q} h_1$ are the Lie derivatives of $h_1$ with respect to $f(x)$ and $g_q$, respectively. $L_f h_2$, $L_{g_d} h_2$ and $L_{g_q} h_2$ are the Lie derivatives of $h_2$ with respect to $f(x)$, $g_d$ and $g_q$, respectively. These Lie derivatives are given as

$$L_f h_1 = -(\mu\alpha + \mu\gamma)\psi_s i_{rq} + \mu\alpha L_m i_{rd} i_{rq} - \mu(\omega_e - \omega_r)\psi_s i_{rd} + \mu\beta\omega_r {\psi_s}^2 + \mu v_{sd} i_{rq} - \mu\beta\psi_s v_{sq}$$

$$\begin{aligned} L_f h_2 = &-(\frac{\alpha}{L_s} + \beta^2\sigma\alpha) v_{sq}\psi_s - \beta^2\sigma\omega_r v_{sd}\psi_s + (\frac{\alpha L_m}{L_s} + \beta\sigma\gamma) v_{sq} i_{rd} + \beta\sigma\gamma v_{sd} i_{rq} \\ &+ \beta\sigma(\omega_g - \omega_r) v_{sd} i_{rd} - \beta\sigma(\omega_g - \omega_r) v_{sq} i_{rq} + \frac{1}{L_s} v_{sq} v_{sd} + \frac{1}{L_s}\dot{v}_{sq}\psi_s - \beta\sigma\dot{v}_{sd} i_{rq} - \beta\sigma\dot{v}_{sq} i_{rd} \end{aligned}$$

$$L_{g_q} h_1 = \frac{\mu}{\sigma}\psi_s \quad L_{g_d} h_2 = -\beta v_{sq}, \quad L_{g_q} h_2 = -\beta v_{sd} \tag{7.17}$$

Define new control inputs as

$$\begin{aligned} u_1 &= L_f h_1 + L_{g_q} h_1 v_{rq} \\ u_2 &= L_f h_2 + L_{g_d} h_2 v_{rd} + L_{g_q} h_2 v_{rq} \end{aligned} \tag{7.18}$$

The original control inputs (i.e. rotor control voltages $v_{rd}$ and $v_{rq}$) can be expressed as

$$\begin{bmatrix} v_{rd} \\ v_{rq} \end{bmatrix} = \begin{bmatrix} 0 & L_{g_q} h_1 \\ L_{g_d} h_2 & L_{g_q} h_2 \end{bmatrix}^{-1} \begin{bmatrix} u_1 - L_f h_1 \\ u_2 - L_f h_2 \end{bmatrix} \tag{7.19}$$

In this way system (7.16) becomes a linear system, which is given as

$$\begin{aligned} \dot{z}_1 &= u_1 \\ \dot{z}_2 &= u_2 \end{aligned} \tag{7.20}$$

The control objectives is to track the desired smooth reference signals $T_g^*$ and $Q_s^*$ for the electromagnetic torque $T_g$ and reactive power $Q_s$. To achieve this objective, the new-defined control inputs are designed as

$$u_1 = -k_1 (y_1 - T_g^*) + \dot{T}_g^* \tag{7.21}$$

$$u_2 = -k_2 (y_2 - Q_s^*) + \dot{Q}_s^* \tag{7.22}$$

where $k_1$ and $k_2$ are two design parameters to be determined in order to make the following linear system (7.24) asymptotically stable.

Using these new control inputs and denoting the tracking errors as

$$e_1 = y_1 - T_g^*, \;\; e_2 = y_2 - Q_s^* \tag{7.23}$$

the tracking error dynamic systems are obtained as

$$\begin{aligned} \dot{e}_1 &= -k_1 e_1 \\ \dot{e}_2 &= -k_2 e_2 \end{aligned} \tag{7.24}$$

For the purpose of the maximum wind power capture, the reference signal $T_g^*$ is set to $T_g^* = K_{opt} \omega_g^2$ according to the MPPT control strategy as presented in Section 6.2.1.

The time derivative of $T_g^*$ can be obtained based on the drive train dynamic equation (7.1).

$$\dot{T}_g^* = 2K_{opt}\omega_g\left(-\frac{1}{J}(T_{wt} - T_g)\right) \tag{7.25}$$

By substituting it into (7.21), the final representation of the control input $u_1$ is obtained as follows

$$u_1 = -k_1 e_1 + \frac{2K_{opt}}{J}\omega_g(T_g - T_{wt}) \tag{7.26}$$

According to (7.20), it can be noted that the electromagnetic torque and reactive power can be independently controlled by $u_1$ and $u_2$. Their transient responses are also decoupled when the stator flux $\psi_s$ varies. This is an important improvement over the stator flux oriented control (as in Section 6.2.2). Under the assumption that the parameters of the DFIG wind turbine including parameter $J$ remain at their nominal values and perfectly known, the control inputs $u_1$ and $u_2$ are able to ensure the perfect reference tracking of the outputs. Based on $u_1$ and $u_2$, the actual control inputs of the DFIG (i.e. rotor control voltages $v_{rd}$ and $v_{rq}$) are obtained according to (7.19). This control algorithm is essentially a full state feedback control. It requires the measurements of all the state variables. Although the stator flux $\psi_s$ (one state variable in (7.7)) can not be measured directly, it can be easily computed from the measured the stator and rotor currents.

### 7.3.3. Adaptive Control for Fault Condition

For the control algorithm given in the previous subsection, it requires the parameters of the DFIG wind turbine including parameter $J$ are perfectly known. However, as mentioned earlier, there would be unexpected change of parameter $J$, when the fault occurs. For this reason, the uncertainty of this parameter has to be considered in the

control algorithm to achieve a perfect reference tracking of the outputs.

In the section, we define a new parameter $\theta$=1/$J$ to represent $J$, and regard it as constant but unknown. The input control $u_1$ is redesigned based the estimates of these two parameters, which is given as

$$u_1 = -k_1 e_1 + \phi\,\hat{\theta} \tag{7.27}$$

where $\hat{\theta}$ is the estimate of $\theta$. $\phi$ is given as

$$\phi = 2K_{opt}\omega_g (T_g - T_{wt}) \tag{7.28}$$

Variable $\phi$ is a function of the wind turbine torque ($T_{wt}$), electromagnetic torque ($T_g$) and the rotor speed ($\omega_g$). These variables can be directly measured or computed from the measurements, i.e. $T_{wt}$ can be calculated at certain wind speed from (6.1), $T_g$ can be calculated from the measured currents according to (7.5), and $\omega_g$ can be directly measured. Therefore $\phi$ is obtainable online and also continuous and bounded. This conclusion is important for the following proof.

By substituting (7.27) into (7.20), the torque tracking error dynamic system can be obtained as

$$\dot{e}_1 = -k_1 e_1 + \phi\,\tilde{\theta} \tag{7.29}$$

where $\tilde{\theta} = \hat{\theta} - \theta$.

Based on this system, a parameter adaptive law is designed to estimate $\theta$ so as to ensure the convergence of the torque tracking error $e_1$, which are given in the following theorem.

**Theorem 7.1:** The adaptive input-output linearizing controller given by (7.18) and (7.27) together with the adaptive law

$$\dot{\hat{\theta}} = -\rho\phi e_1 \tag{7.30}$$

guarantees an unbiased tracking of the electromagnetic torque, and the adaptive law can track the true value of $J$.

**Proof:** Select the Lyapunov function as

$$V = \frac{1}{2}e_1^2 + \frac{1}{2}\rho^{-1}\tilde{\theta}^2 \tag{7.31}$$

Its first derivative with respect to time is

$$\dot{V} = -k_1 e_1^2 + \phi\tilde{\theta}e_1 + \rho^{-1}\tilde{\theta}\dot{\tilde{\theta}} \tag{7.32}$$

According to (7.30), it can be reduced as

$$\dot{V} = -k_1 e_1^2 < 0 \tag{7.33}$$

Therefore, it can be concluded that system (7.29) is asymptotically stable and thus all the variables ($e_1, \tilde{\theta}$) are bounded ($e_1 \in L_\infty$, $\tilde{\theta} \in L_\infty$, this conclusion is based on the Lyapunov stability theory in Appendix B.1). Furthermore, we can show that

$$\int_0^\infty e_1^2 dt = \frac{V(0) - V(\infty)}{k_1} < \infty \tag{7.34}$$

This implies that $e_1$ is a bounded $L_2$ signal ($e_1 \in L_2$). Since signal $\phi$ is continuous and bounded, we can have $\dot{e}_1 \in L_\infty$ according to (7.29). Now, we have established that $e_1 \in L_2 \cap L_\infty$ and $\dot{e}_1 \in L_\infty$. According to Barbalat lemma (as in Appendix B.2 ), we can have $\lim_{t\to\infty} e_1 = 0$. Since it can be shown that

$$\int_0^\infty \dot{e}_1 dt = \lim_{t\to\infty} e_1(t) - e_1(0) = -e_1(0) \tag{7.35}$$

then from (7.29) it can be conclude that $\dot{e}_1$ is uniformly continuous. Again, using the Barbalat lemma we can have $\lim_{t\to\infty} \dot{e}_1 = 0$. This means $\lim_{t\to\infty} \tilde{\theta} = 0$ under the condition that $\phi$ is persistence of excitation. □

**Remark 7.1:** variable $\phi$ is required to be persistent of excitation in order to ensure the convergence of $\tilde{\theta}$. This condition is satisfied when DFIG operates under varying speed according to (7.1).

**Remark 7.2:** This adaptive control algorithm is only developed for the torque control. Actually, there is no need to design an adaptive control for the reactive power, as the uncertainties of parameter $J$ only affect the torque control loop.

## 7.4. Robust Adaptive Input-Output Linearizing Control

In last section, the drive train faults are considered as the parametric uncertainties of drive train system, and an adaptive input-output linearizing controller is developed to ensure the desired control performances under the faulty condition by online estimating the uncertain parameters. Nevertheless, it is known that this controller is designed based on the DFIG model (as in Section 7.3.1), and thus any uncertainties in this model would also affect the control performances. In this section, this problem is considered and the control algorithm proposed in last section is modified to enhance its robustness against these model uncertainties.

By taking account of the model uncertainties, DFIG model (7.6) can be rewritten as

$$\begin{cases} \dot{x} = f(x) + gu + w \\ y = h(x) \end{cases} \tag{7.36}$$

where $w = [w_1, w_2, w_3]^T$ represents model uncertainties and it satisfies

$$\|w_1\| \le \sigma_1 < +\infty, \ \|w_2\| \le \sigma_2 < +\infty, \ \|w_3\| \le \sigma_3 < +\infty \tag{7.37}$$

Parameter $\theta$ is required to be bounded.

$$\|\theta\| \le \bar{\theta} < +\infty \tag{7.38}$$

Projecting model (7.36) to coordinate (7.15), an input-output linearizing model can be obtained as

$$\begin{aligned} \dot{z}_1 &= L_f h_1 + L_{g_q} h_1 v_{rq} + W_{T1} w_1 + W_{T2} w_3 \\ \dot{z}_2 &= L_f h_2 + L_{g_d} h_2 v_{rd} + L_{g_q} h_2 v_{rq} + W_{Q1} w_1 + W_{Q2} w_2 + W_{Q3} w_3 \end{aligned} \tag{7.39}$$

where

$$W_{T1} = \mu i_{rq}, \ W_{T2} = \mu \psi_s \tag{7.40}$$

$$W_{Q1} = \frac{v_{sq}}{L_s}, \ W_{Q2} = -\beta\sigma v_{sd}, \ W_{Q3} = -\beta\sigma v_{sq} \tag{7.41}$$

The Lie derivatives in this model has been given in (7.17)

Defining new control inputs as (7.18), model (7.39) can be reduced in a linear model as

$$\dot{z}_1 = u_1 + W_{T1} w_1 + W_{T2} w_3 \tag{7.42}$$

$$\dot{z}_2 = u_2 + W_{Q1} w_1 + W_{Q2} w_2 + W_{Q3} w_3 \tag{7.43}$$

Designing the control inputs as follows

$$u_1 = -k_1 e_1 + \phi\hat{\theta} - \frac{1}{4}\eta_{T1} e_1 W_{T1}^2 - \frac{1}{4}\eta_{T2} e_1 W_{T2}^2 \tag{7.44}$$

$$u_2 = -k_2 e_2 + \dot{Q}_s^* - \frac{1}{4}\eta_{Q1} e_2 W_{Q1}^2 - \frac{1}{4}\eta_{Q1} e_2 W_{Q1}^2 - \frac{1}{4}\eta_{Q3} e_2 W_{Q3}^2 \tag{7.45}$$

where $\eta_{T1} > 0$, $\eta_{T2} > 0$, $\eta_{Q1} > 0$, $\eta_{Q2} > 0$, and $\eta_{Q3} > 0$, which are the tuning parameters of the controller. Then the tracking error dynamic system can be obtained as

$$\dot{e}_1 = -k_1 e_1 + \phi\tilde{\theta} - \frac{1}{4}\eta_{T1} e_1 W_{T1}^2 - \frac{1}{4}\eta_{T2} e_1 W_{T2}^2 + W_{T1} w_1 + W_{T2} w_3 \tag{7.46}$$

$$\dot{e}_2 = -k_2 e_2 - \frac{1}{4}\eta_{Q1} e_2 W_{Q1}^2 - \frac{1}{4}\eta_{Q2} e_2 W_{Q2}^2 - \frac{1}{4}\eta_{Q3} e_2 W_{Q3}^2 + W_{Q1} w_1 + W_{Q3} w_3 + W_{Q3} w_3 \tag{7.47}$$

Based on this system, two modified adaptive laws are designed to estimate $\theta$ so as to ensure the convergence of tracking errors $e_1$ and $e_2$, which are given in the following theorem.

**Theorem 7.2:** The robust adaptive control (7.44) and (7.45) with adaptive law

$$\dot{\hat{\theta}} = -\delta\hat{\theta} - \rho\phi e_1 \tag{7.48}$$

where $\delta > 0$ and $\rho > 0$

guarantees that within finite time period, the torque tracking error ($e_1$), the reactive tracking error ($e_2$), and the parameter estimation error ($\tilde{\theta}$) converge to following bounds.

$$D_1 = \left\{ \left(e_1, \tilde{\theta}_1, \tilde{\theta}_2\right) \middle| k_1 {e_1}^2 + \frac{1}{2}\delta_1 {\rho_1}^{-1} {\tilde{\theta}_1}^2 + \frac{1}{2}\delta_2 {\rho_2}^{-1} {\tilde{\theta}_2}^2 < \frac{1}{\eta_{T1}} {\sigma_1}^2 + \frac{1}{\eta_{T2}} {\sigma_3}^2 + \frac{1}{2}\delta_1 {\rho_1}^{-1} {\bar{\theta}_1}^2 + \frac{1}{2}\delta_2 {\rho_2}^{-1} {\bar{\theta}_2}^2 \right\} \tag{7.49}$$

$$D_2 = \left\{ e_2 \mid k_2 e_2^{\,2} < \frac{1}{\eta_{Q1}}\sigma_1^{\,2} + \frac{1}{\eta_{Q2}}\sigma_2^{\,2} + \frac{1}{\eta_{Q3}}\sigma_3^{\,2} \right\} \tag{7.50}$$

**Proof:** Select the two Lyapunov functions as

$$V_1 = \frac{1}{2}e_1^2 + \frac{1}{2}\rho^{-1}\tilde{\theta}^2 \tag{7.51}$$

$$V_2 = \frac{1}{2}e_2^2 \tag{7.52}$$

Their first derivatives with respect to time are

$$\begin{aligned}
\dot{V}_1 &= -k_1 e_1^{\,2} - \frac{1}{4}\eta_{T1} e_1^{\,2} W_{T1}^{\,2} - \frac{1}{4}\eta_{T2} e_1^{\,2} W_{T2}^{\,2} + W_{T1} e_1 w_1 + W_{T2} e_1 w_3 + \phi\tilde{\theta} e_1 + \rho^{-1}\tilde{\theta}\dot{\tilde{\theta}} \\
&= -k_1 e_1^{\,2} - \eta_{T1}(\frac{1}{2}e_1 W_{T1} - \frac{1}{\eta_{T1}}w_1)^2 - \eta_{T2}(\frac{1}{2}e_1 W_{T2} - \frac{1}{\eta_{T2}}w_3)^2 \\
&\quad + \frac{1}{\eta_{T1}}w_1^{\,2} + \frac{1}{\eta_{T2}}w_3^{\,2} - \delta\rho^{-1}\tilde{\theta}\hat{\theta} \\
&\le -k_1 e_1^{\,2} + \frac{1}{\eta_{T1}}w_1^{\,2} + \frac{1}{\eta_{T2}}w_3^{\,2} - \delta\rho^{-1}\tilde{\theta}(\tilde{\theta} + \theta) \\
&\le -k_1 e_1^{\,2} - \frac{1}{2}\delta\rho^{-1}\tilde{\theta}^2 + \frac{1}{\eta_{T1}}\sigma_1^{\,2} + \frac{1}{\eta_{T2}}\sigma_3^{\,2} + \frac{1}{2}\delta\rho^{-1}\bar{\theta}^2
\end{aligned} \tag{7.53}$$

$$\begin{aligned}
\dot{V}_2 &= -k_2 e_2^{\,2} - \frac{1}{4}\eta_{Q1} e_2^{\,2} W_{Q1}^{\,2} - \frac{1}{4}\eta_{Q1} e_2^{\,2} W_{Q2}^{\,2} - \frac{1}{4}\eta_{Q3} e_2^{\,2} W_{Q3}^{\,2} + W_{Q1} e_2 w_1 + W_{Q2} e_2 w_2 + W_{Q3} e_2 w_3 \\
&= -k_2 e_2^{\,2} - \eta_{Q1}(\frac{1}{2}e_2 W_{Q1} - \frac{1}{\eta_{Q1}}w_1)^2 - \eta_{Q2}(\frac{1}{2}e_2 W_{Q2} - \frac{1}{\eta_{Q2}}w_2)^2 - \eta_{Q3}(\frac{1}{2}e_2 W_{Q3} - \frac{1}{\eta_{Q3}}w_3)^2 \\
&\quad + \frac{1}{\eta_{Q1}}w_1^{\,2} + \frac{1}{\eta_{Q2}}w_2^{\,2} + \frac{1}{\eta_{Q3}}w_3^{\,2} \\
&\le -k_2 e_2^{\,2} + \frac{1}{\eta_{Q1}}\sigma_1^{\,2} + \frac{1}{\eta_{Q2}}\sigma_2^{\,2} + \frac{1}{\eta_{Q3}}\sigma_3^{\,2}
\end{aligned} \tag{7.54}$$

By analyzing (7.53) and (7.54), it can be concluded that $\dot{V}_1 < 0$ and $\dot{V}_2 < 0$ if $\left\{e_1, \tilde{\theta}\right\} \notin D_1$ and $e_2 \notin D_2$. which means that the tracking errors (i.e. $e_1$ and $e_2$) and the parameter estimation error (i.e. $\tilde{\theta}$) ultimately converge into bounds $D_1$ and $D_2$

□

# 7.5. Simulation Studies

In this section, the control algorithms proposed in Section 7.3.3 and Section 7.4 are applied to control the DFIG wind turbine in the presence of drive train fault. Their

performances are evaluated through the simulations in the following subsections. Firstly, the adaptive input-output linearizing control (proposed in Section 7.3.3 ) is applied assuming no model uncertainties in the DFIG (presented in Section 7.3.1). In the next, these model uncertainties are taken into account and the robust adaptive control (proposed in Section7.4) is applied to control the DFIG wind turbine. The nominal value of $J$ is set as 2 kg.m$^2$ (an unrealistically low value) in order to reduce the simulation time required to reach a steady-state operation condtion. A drive train fault is implemented by considering an abrupt change of $J$.

$$J = \begin{cases} 2; & t < 5\text{sec} \\ 2.5; & t \geq 5\text{sec} \end{cases} \tag{7.55}$$

In this simulation, a varying wind speed (i.e. $\upsilon_{w\_rat} = 7 + 0.5\text{rand[m/s]}$) is applied to the wind turbine to ensure the DFIG operates under varying speed so as to estimate parameter $J$.

## 7.5.1. Performance of Adaptive Input-Output Linearizing Control

In this subsection, under the assumption of no uncertainties in the DFIG model, adaptive input-output linearizing control is applied for the reference tracking of the torque and reactive power in the presence of fault. The controller parameters are set as follows and the control performance is given in Figure 7.3

$$k_1 = 20,\ k_2 = 50,\ \rho = 0.2 \tag{7.56}$$

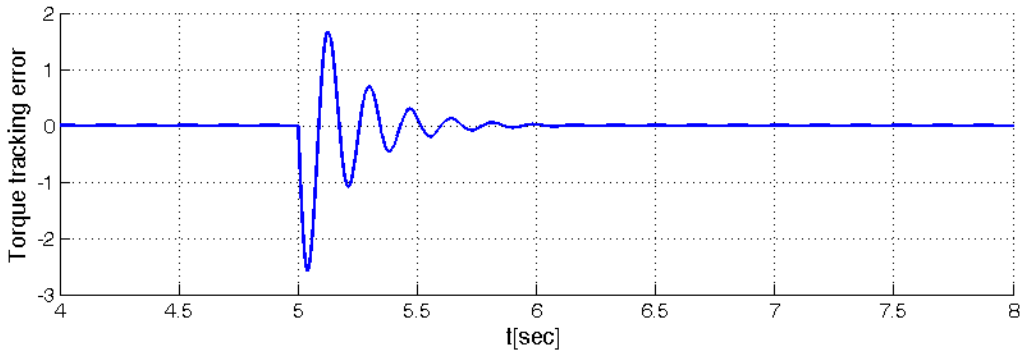


(a)Torque reference tracking error.

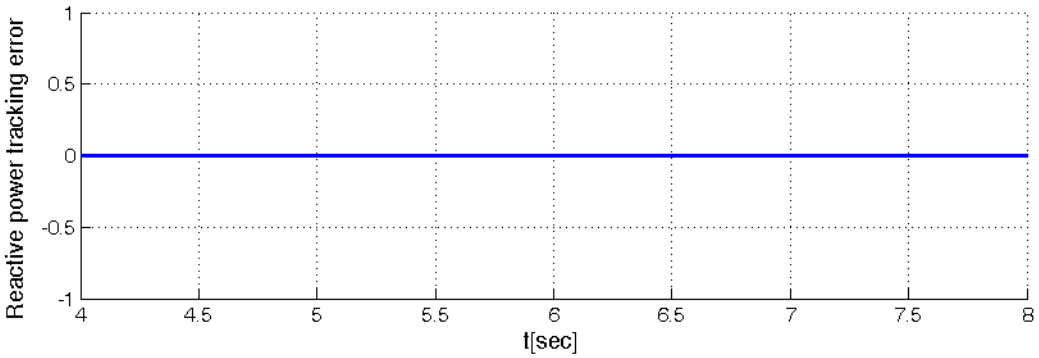


(b) Reactive power reference tracking error.

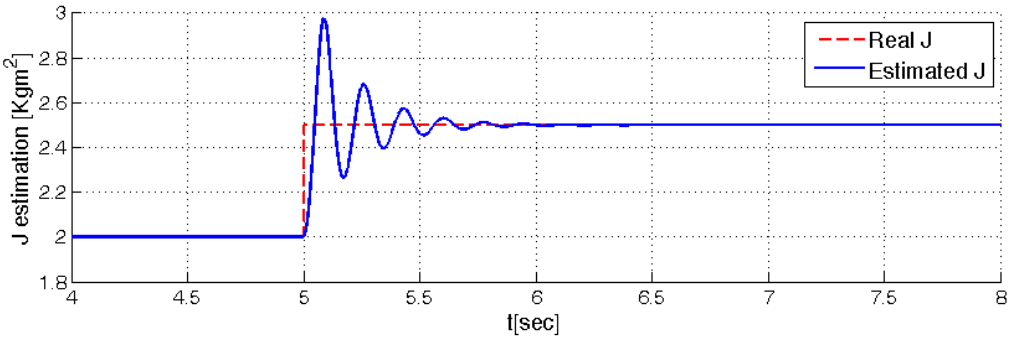


(c) Estimation of the moment of shaft inertia $J$.

Figure 7.3. Performance of adaptive input-output linearizing control.

It can be observed from Figure 7.3(a), when the fault occurs at t=5sec, due to variation of parameter $J$, a small torque tracking error occurs. Nevertheless, as it is shown in Figure 7.3(c), this error quickly disappears when parameter $J$ is accurately estimated. In addition, as it is shown in Figure 7.3(c), no reactive power tracking error occurs during the fault. This verifies that the torque control and reactive power control are completely decoupled, and the fault only influences the torque control. Also the true value of parameter $J$ can be accurately estimated.

### 7.5.2. Performance of Robust Adaptive Input-Output Linearizing Control

In this subsection, the presence of model uncertainties in the DFIG is considered, and the robust adaptive control algorithm (proposed in Section 7.4) is applied to deal with the effects of these model uncertainties. To test this control algorithm, the model

uncertainties is set as follows

$$w_1 = w_2 = w_3 = n(t) \tag{7.57}$$

where $n(t)$ is a white noise with zero mean and variance 0.1. Here, we use this model uncertainties as an example to verify the proposed control algorithm. Actually, the white noise model uncertainties rarely exist in the pratical system.

The controller is designed as (7.44)-(7.45), whose parameters are set as

$$k_1 = 10,\ \ k_2 = 10,\ \ \delta = 0.05,\ \ \rho = 0.2.$$

$$\eta_{T1} = \eta_{T2} = 0.01,\ \ \eta_{Q1} = \eta_{Q2} = \eta_{Q3} = 0.02 \tag{7.58}$$

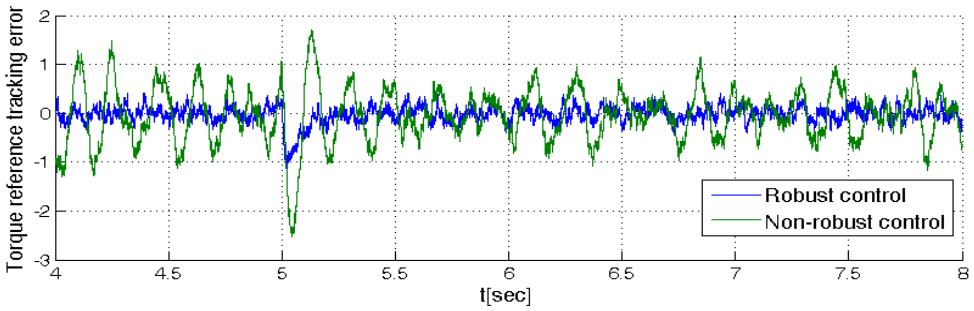


(a) Torque reference tracking error.

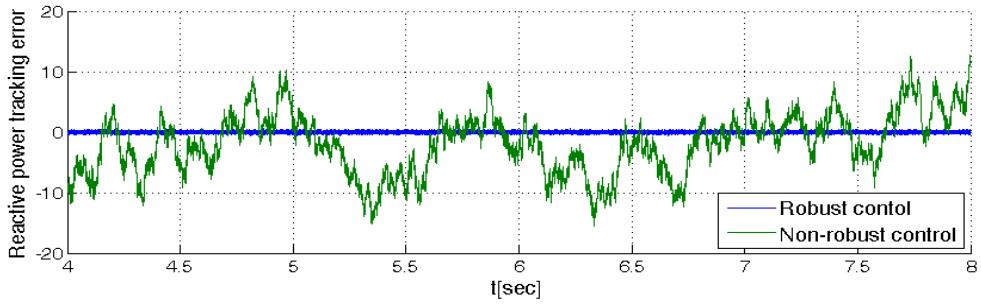


(b) Reactive power reference tracking error.

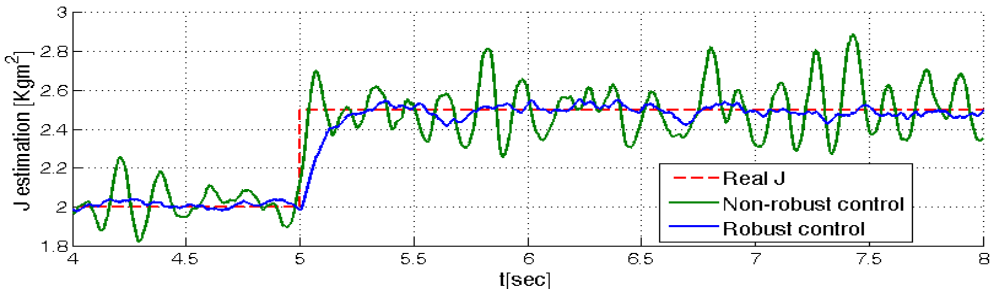


(c) $J$ estimation

Figure 7.4. Performance of robust adaptive input-output linearizing control.

For the purpose of comparison, the non-robust control designed in last subsection is also implemented in this subsection. The simulation results of these two control algorithms (i.e. robust control and non-robust control) are presented in Figure 7.4. As it is shown in Figure 7.4(a) and Figure 7.4(b), the tracking errors of the torque and reactive power are highly reduced by using the robust control algorithm, specially the reactive power tracking error. As illustrated in last subsection, the torque tracking relies on the estimation of parameter $J$, and any inaccurate estimation would increase the torque tracking error, while the reactive power tracking is totally independent of this estimation. Also, it can be observed from Figure 7.4(c) that the estimation error of parameter $J$ always exists even by using the robust control. This explains why the torque presents larger tracking error than the reactive power. Again from Figure 7.4(c), it can be observed that robust control is able to track the true value of $J$ in a desired accuracy, while the non-robust control almost loses the tracking.

## 7.6. Summary

This chapter is concerned with the FTC of the DFIG wind turbine against the drive train fault. The fault is considered as the parametric uncertainty (i.e. equivalent moment of inertia $J$) of the drive train system (i.e. represented by one-mass model). With this consideration, an adaptive nonlinear control algorithm (i.e. adaptive input-output linearizing control) is developed. With its adaptive law, it can online estimates the uncertain parameter (i.e. $J$) and adjusts the control input so as to ensure the system performance in the presence of fault. This control algorithm is based on a third-order DFIG model. Under the assumption of no uncertainties in this model, the decoupled and unbiased tracking of the torque and reactive power are achieved, and parameter $J$ can be accurately estimated. Furthermore, a robust adaptive input-output linearizing control algorithm is proposed to take account of these model uncertainties. The simulation results show that it provides smaller tracking errors and more accurate estimation of parameter $J$ than the non-robust control algorithm.

# 8. Conclusion

This chapter provides some general overall comments and discusses possible directions for future work.

## 8.1. Summary and Conclusions

In this thesis, a model-based fault diagnosis and fault tolerant control scheme was developed for improving the reliability of DFIG based wind turbine systems. A literature survey indicated that little study on this problem has been done on the model-based approaches. An electrical and a mechanical fault scenarios, the DFIG winding short circuit and drive train fault, are considered due to their high occurrence rates. For the DFIG winding short circuit fault, an online fault diagnosis scheme was proposed by using adaptive observer based approaches. Then, an active fault tolerant scheme was synthesized based the fault information provided by the fault diagnosis scheme. For the drive train fault, the work focused on fault tolerance rather than diagnosis. The fault is represented by the unexpected change of moment of inertia, and is accommodated by adapting parameter variations using parameter adaptive control algorithms. This control scheme is also a kind of active FTC.

A realistic simulation model of DFIG based wind turbine systems was designed to test the proposed algorithms, which consists of three sub-models, a static aerodynamics model of the wind turbine, a one-mass model of the drive train, and an electrical model of the DFIG. Among these sub-models, the DFIG model is explicitly designed, which allow the simulation of both nominal and faulty conditions. The results achieved for these two faults are summarized below.

### *DFIG winding short circuit fault:*

Two mathematical models of the DFIG with respect to two types of faults, single-phase and multi-phase faults, were proposed which can represent the short circuit fault at any levels in any phases. These models were initially developed in the

a-b-c coordinate, and then transformed into the d-q coordinate, based on which the equivalent circuits of DFIG with faults were also provided. A model simulation study was conducted to demonstrate the influences of short circuit faults on an open-loop operated DFIG wind turbine system. Three main conclusions one can draw from the simulation results are:

1. The effects of short circuit faults can be considered as additive new currents to the existing output currents. The amplitudes of the new currents are decided by the fault level.
2. The electromagnetic torque is independent of short circuit faults.
3. The faults in one side, e.g. the stator, do not affect the current performance in the other side, e.g. the rotor, and vice verse.

To facilitate the synthesis of model-based fault diagnosis and FTC schemes, these proposed fault models were reorganized into linear state-space representations. As such the single-phase and multi-phase faults were formulated into two general system faults, i.e. additive and multiplicative faults, respectively. The adaptive observers were then implemented to diagnose these two faults. Several important issues in adaptive observer design were considered. The first issue considered is the robustness against model uncertainties. In this thesis, $\sigma$-modification was applied to guarantee bounded fault estimations. However, by using this method, large estimation errors may still exist, which can not meet the accuracy requirement of the fault diagnosis. To solve this problem, two robust adaptive observers were proposed by using $H_\infty$ optimization and high-gain observer techniques, respectively, in order to reduce estimation errors. The simulation study showed that these observers are robust against model uncertainties and they can provide more accurate fault estimations than the conventional adaptive observer algorithms. Another important issue considered is the effects of rotor speed variations, for which a self-scheduled LPV adaptive observer was developed. The simulation study showed it can ensure desired fault estimations in presence of speed variations. Generally speaking, the proposed fault diagnosis scheme for multi-phase fault is superior to the one for single-phase fault, because the former can be applied to deal with more general fault cases including single-phase fault as well as multi-phase

fault. In addition, it provided state estimations, which are required to synthesize FTC schemes.

In the context of FTC, a fault compensator was designed, which was used to correct the current measurements and reference signals based on the information provided by fault diagnosis schemes. This enabled the FTC scheme to be designed independent of the nominal controller and without affecting the nominal performance of the system. For this reason, this fault compensator can cooperate with many control algorithms, not only confined to the classical algorithm (i.e. stator flux oriented control) presented in Chapter 6. This fault compensator was validated on a closed-loop controlled DFIG wind turbine system, and the simulation results showed that it can highly reduce the oscillations in the electromagnetic torque, output power and other output electrical quantities aroused by winding short circuit faults.

***Drive Train Fault:***

This work more focused on fault tolerant control rather than diagnosis, and the faults are considered as unexpected change of moment of inertia. An adaptive input-output linearizing control was designed to adapt the parameter variatons so as to accommodate the fault. This control algorithm was designed directly based a nonlinear model of DFIGs, and it was able to achieve complete decoupled control of the torque and reactive power, and the parameter variation was adapted by the adaptive law. In addition, a robust version of this control algorithm was developed to cope with the effects of model uncertainties. Its robustness against model uncertainties and fault has been demonstrated via simulations.

## 8.2. Future Work

The following is proposed to be future work:

- For the mechanical fault, we only considered a simplified model of the drive train system to facilitate our illustration of the fault tolerance control scheme, and consider the fault simply as unexpected change of moment of inertia. In the future work, more realistic and complicated models would be investigated and modified

fault tolerant control sheme need to be developed.

- In this thesis, we only discussed two types of faults, DFIG winding short circuit and drive train faults. A further study for other fault scenarios of wind turbine systems need be conducted, such as grid fault and pitch control failure.

- The methods presented in this thesis are only applicable to the fault diagnosis and FTC of subsystems. However, if several faults in different subsystems occur simultaneously, the cooperation between these methods is not discussed in this work, which can be selected as a possible research direction in the future. An alternative way is to develop a supervisory FDD and FTC system for the whole system, which also forms another important work in the future.

- Of course, the most important future work is to test the developed fault diagnosis and FTC schemes on a real wind turbine system. All the presented work in this thesis is based on Matlab simulation, which begs the question how good will it be applied to real systems. For this reason, some further experimental investigations need to be conducted in the future.

# Bibliography

[1] M. Tazil, V. Kumar, R. C. Bansal, S. Kong, Z. Y. Dong, W. Freitas, H. D. Mathur, "Three-Phase doubly fed induction generators: an overview," *IET Electr Power Appl*., vol. 4, issue. 2, pp. 75-89, 2010.

[2] J. Ekanayake, L. Holdsworth, N. Jenkins, "Control of DFIG wind turbines," *Power Engineer*, vol. 17, issue 1, pp. 28-32, Feb. 2003.

[3] L. Holdsworth, X.G. Wu, J. Ekanayake and N. Jenkins, "Comparison of fixed speed and doubly-fed induction wind turbines during power system disturbances," *IEE Proc.-Gener.Transm. Distrib.*, vol. 150, no. 3, pp. 343-352, May 2003.

[4] M. Kalantar and S. M. Mousavi, "Dynamic behaviour of a stand-alone hybrid power generation system of wind turbine, microturbine, solar array and battery storage," *Applied Energy*, vol. 87, pp. 3051-3064, 2010.

[5] W. Qian, W. Zhou, J. M. Aller, and R. G. Harley, "Wind speed estimation based sensorless output maximum control for a wind turbine driving a DFIG," *IEEE Trans. Power Eletron*. vol. 23, no. 3, May, 2008.

[6] F. Iov, A. D. Hansen, P. Sorensen, F. Blaabjerg, *Wind turbine blockset in Matlab/Simulink,* Aalborg University, March 2004.

[7] C. Koroneos, T. Spachos, and N. Moussiopoulos, "Exergy analysis of renewable energy sources," *Renewable Energy*, vol. 28, issue. 2, pp. 295-310, Feb, 2003.

[8] M. Aktarujjaman, M. E. Haque, K. M. Muttaqi, M. Negnevisky, and G. Ledwich, "Control Dyanmics of a doubly fed induction generator under sub-and super-synchronous modes of operation, " *In Proc. IEEE PES GM 2008*, Pittsburgh, PA, Jul. 2008.

[9] S. M. Muyeen, M. H. Ali, R. Takahashi, T. Murata, J. Tamura, Y. Tomaki, A. Sakahara, and E. Sasano, "Comparative study on transient stability analysis of

wind turbine generator system using different drive train models," *Renewable Power Generation, IET,* vol. 1, issue. 2, pp. 131-141, Jun. 2007.

[10] R. Pena, J.C. Clare, and G. M. Asher, "Doubly fed induction generator using back-back PWM converter and its application to variable-speed wind energy generation," *IEE Proceedings of Eletric Power Applications*, vol. 143, issue. 3, pp. 231-241, May, 1996.

[11] Y. Amirat, M. Benbouzid, E. Al-Ahmar, B. Bensaker and S. Turri, "A brief status on condition monitoring and fault diagnosis in wind energy conversion systems," *Renewable and Sustainable Engergy Reviews*, vol. 13, issue 9, pp. 2629-2636, Dec. 2009.

[12] Z. Hammeda, Y. Honga, Y.Choa, S.Ahnb, and C.Song, "Condition monitoring and fault detection of wind turbines and related algorithms: A review," *Renewable and Sustainable Energy Reviews*, vol. 13, issue 1, pp. 1-39, Jan. 2009.

[13] B. Lu, Y. Li, X. Wu, and Z. Yang, "A review of recent advances in wind turbine condition monitoring and fault diagnosis," *In Proc. IEEE Conference on Power Electronics and Machnies in Wind Applications*, pp.1-7, 2009.

[14] D. U. Campos-Delgado, D. R. Espinoza-Trejo, and E. Palacios, "Fault tolerant control in variable speed drives: a survery," *IET Electr. Power Appl.*, vol. 2, no. 2, pp. 121-134, August 2007.

[15] J. Nilsson and LM. Bertling, "Survey of failures in wind power systems with focus on Swedish wind power plant during 1997-2005," *IEEE Transactions on Energy Conversion*, vol. 22, issue 1, pp.167-173, March 2007.

[16] S. Grubic, J. M. Aller, B. Lu, and T. G. Habetler, "A survey on testing and monitoring methods for stator insulation systems of low-voltage induction machines focusing on turn insulations problems," *IEEE Trans. Ind. Electron.*, vol. 55, no. 12, pp. 4127-4136, Dec. 2008.

[17] Q. Huang, D. Jiang, L. Hong and Y. Ding, "Application of wavelet neural networks on vibration fault diagnosis for wind turbine gearbox," *Lecture Notes in*

*Computer Science*, vol. 5264 LNCS, Part2, Advances in Neural Networks, pp. 313-320 [Proc. 5th Int. Symposium on Neural Networks, 2008].

[18] P. M. Frank, S. X. Ding, and T. Marcu, "Model-based fault diagnosis in technical process," *Transaction of the Institute of Measurement and Control*, vol. 22, issue. 1, pp. 57-101, 2000.

[19] R. J. Patton, J. Chen, and S. B. Nielsen, "Model-based methods for fault diagnosis: Some guidelines," *Transactions of the Institute of Measurement and Control*, vol. 17, issue. 2, pp, 73-81, 1995.

[20] R. J. Patton and J. Chen, "Observer-based fault detection and isolation: robustness and applications," *Control Engineering Practice*, vol. 5, issue. 5, pp. 671-682, May, 1997.

[21] J. Chen, R. J. Patton, and H. Y. Zhang, "Design of unknown input observer and robust fault detection filters," *International Journal of Control*, vol. 63, no. 1, pp. 85-105, 1996.

[22] S. Dash and V. Venkatasubramanian, " Challenges in the industrial applications of fault diagnostic system," *Computer and Chemical Engineering*, vol. 24, issue. 3, pp.785-791, 2000.

[23] V. Venkatasubramanian, R. Rengaswamy, K. Yin, and S. N. Kavuri, "A review of process of fault detection and diagnosis. Part I. Quantitive model-based methods," *Comupters and Chemical Engineering*, vol.27, issue 3, pp. 293-311, 2003.

[24] V. Venkatasubramanian, R. Rengaswamy, and S. N. Kavuri, "A review of process of fault detection and diagnosis. Part II. Qualitative models and search strategies," *Comupters and Chemical Engineering*, vol.27, issue 3, pp. 313-326, 2003.

[25] V. Venkatasubramanian, R. Rengaswamy, S. N. Kavuri, and K. Yin, "A review of process of fault detection and diagnosis. Part III. Process history based methods," *Comupters and Chemical Engineering*, vol.27, issue 3, pp. 327-346, 2003.

[26] R. Isermann, “Process fault detection based on modeling and estimation methods-a survey,” *Automatica*, vol. 30, pp. 397-404, 1984.

[27] R. Isermann, “Fault diagnosis of machines via parameter estimation and knowledge processing-tutorial paper,” *Automatica*, vol. 29, issue. 4, pp. 815-835, 1993.

[28] R. Isermann. “Supervision, fault-detection and fault-diagnosis methods- an introduction,” *Control Engineering Practice,* vol. 5, issue. 5, pp. 637-719, 1997.

[29] R. Isermann. “Special section of papers on supervision, fault detection and diangosis of technical systems,” *Control Engineering Practice*, vol. 5, issue. 5, pp. 639-652, 1997.

[30] R. Isermann, “Model-based fault detection and diagnosis status and applications,” *Annual Review in Control*, vol. 29, issue. 1, 2005.

[31] R. Iserman, *Fault diagnosis systems: An introduction from fault detection to fault tolerance*, Springer, Berlin, 2006.

[32] X. Ding, Steven, *Model-based fault diagnosis techniques: design schemes, algorithm, and tools*, Springer, Berlin, 2008.

[33] J. Chen and R. J. Patton. *Robust Model-Based Fault Diagnosis for Dynamic Systems*, Boston: Kluwer Academic Publisher, 1999.

[34] P. M. Frank and X. Ding, “Survey of robust residual generation and evaluation methods in observer based fault detection system,” *Journal of Process Control*, vol. 7, issue. 6, pp. 403-424, Dec. 1997.

[35] K. Watanabe and D. M. Himmeblau, “Instrument fault detection is systems with uncertainties, ” *International Journal of System Science*, vol. 13, issue. 2, pp. 137-158, 1982.

[36] L. Guo, Y. M. Zhang, H. Wang, and J. C. Fang, “Observer-based optimal fault detection and diagnosis using conditional probability distuributions,” *IEEE Trans. Signal Processing*, vol. 54, no. 10, Otc. 2006.

[37] Y. Zhang, Q. G. Wang, and K. Y. Lum, "A H-infinity fault detection and diagnosis scheme for discrete nonlinear system using output probability density estimation," *Intelligent Systems and Automation: 2nd Mediterranean Conference on Interlligent Systems and Automation (CISA'09)*, vol. 1107, pp. 79-84, Mar. 2009.

[38] G. Besancon, *Paramter/fault estimation in nonlinear systems and adaptive observer: Nonliear Observer and Applications. Lecture Notes in Control and Information Science*, vol. 363, pp. 211-222, 2007.

[39] D. Miljković, "Fault detection methods: A literature survey," *MIPRO, 2011 Proceedings of the 34th International Convention*, pp. 750-755, Opatija, May 2011.

[40] L. Ljung, "Asymptotic behaviour of the extended kalman filter as paramter estimator for linear system," *IEEE Transactions on Automatic Control*, vol. 24, issue. 1, pp. 36-50, Feb, 1979.

[41] Z. Gao, T. Breikin and H. Wang, "High gain estimator and fault tolerant design with application to gas turbine dynamic system," *IEEE Transactions on Control Systems Technology*. vol. 15, issue. 4, pp. 740-753, 2007.

[42] A. Ticlea and G. Besancon, "On the state and parameter simultaneous estimation problem in induction motors," *In Proceeding of the 17th World Congress on The International Federation of Automatic Control*, pp.11184-11189, Seoul, Korea, July, 2008.

[43] G. Besancon, J. De León-Morales, and O. Huerta-Guevara, "On adaptive observer for state affine systems," *International Journal of Control*, vol. 79, no. 6, pp. 581-591, June 2006.

[44] X. Ding and P. M. Frank, "An adaptive observer based fault detection scheme for nonlinear systems," *In Proceedings of 12th IFAC Wold Congress*, pp. 307-312, Syndney, 1993.

[45] K. Zhang, B. Jiang, and V. Cocquempot, "Adaptive Observer based fast fault estimation," *International Journal of Control, Automation, and Systems*, vol. 6, no. 3, pp. 320-326, June 2008.

[46] H. Wang, Z. J. Huang, and S. Daley, “On the use of adaptive updating rules for acutator and sensor fault diagnosis,” Automatica, vol. 33, no. 2, pp. 217-225, 1997.

[47] S. S. Haykin, *Adaptive Filter Theory*, Englewood Cliffs, N.J., London : Prentice Hall, 1995

[48] P. A. Ioannou and J. Sun, *Robust Adaptive Control*, PTR Prentice-Hall, 1996.

[49] J. Jung, K, Huh, H. K. Fathy, and J. L. Stein, “Optimal robust adaptive observer design for a class of nonliear systems via an H-infinity approach,” *In Proceedings of the 2006 Americal Control Conference*, pp. 3637-3642, Minneapolis, Minnesota, USA, June 2006.

[50] R. J. Patton, “Fault tolerant control systems: the 1997 situation,” *In Proceedings of the IEE Colloquium on Fault Diagnosis and Control System Reconfiguration*, pp. 1033-1054, London, UK, May, 1993.

[51] Y. Zhang and J. Jiang, “Bibliographical review on reconfigurable fault tolerant control systems,” *Annual Reviews in Control*, vol. 32, pp. 229-252, 2008.

[52] J. Jiang, “Fault tolerant control systems-An introductory overview,” *Automatica* vol. 31, issue. 1, pp. 161-174. 2005.

[53] M. Blanke, M. Kinnaert, J. Lunze, and M. Staroswiecki, *Diagnosis and Fault tolerant Control (2nd ed.)*, Berlin, Germany: Springer.

[54] G. Tao, S. Chen, S. M. Joshi, and X. Tang, *Adaptive control of systems with actuator failures*. Berlin, Germany: Springer.

[55] D. Ye and G. H. Yang, “Adaptive fault tolerant tracking control against actator faults with application to fight control,” *IEEE Transactions on Control System Technology*, vol. 4, issue. 6, pp. 1088-1096, Nov. 2006.

[56] R. J. Veillette, “Reliable linear-quadratic state-feedback control,” *Automatica*, vol. 31, no. 1, pp. 137-143, 1995

[57] R. J. Veillette, J. V. Medanić, and W. R. Perkins, “Design of reliable control systems,” *IEEE Trans. Automat. Contr.*, vol. 37, pp 290-304, Mar. 1992.

[58] G. H. Yang and K. Y. Lum, “Fault tolerant flight tracking control with stuck faults, ” *In Proc. Amer. Contr. Conf.*, pp 521-526, 2003.

[59] F. Liao, J. L. Wang, and G. H. Yang, “Reliable robust flight tracking control: an LMI approach,” *IEEE Trans. Contr. Syst. Tech.*, vol. 10, no. 1, Jan. 2002.

[60] G. Tao, S. M. Joshi, and X. L. Ma, “Adaptive state feedback and tracking control of system with actuator failures,” *IEEE Trans. Autom. Contr.*, vol. 46, no.1, pp. 78-95, Jan. 2001.

[61] G. Tao, S. Chen, and S. M. Joshi, “An adaptive actuator failure compensation controller using output feedback,” *IEEE Trans. Autom. Contr.*, vol. 47, no. 3, pp. 506-511, March 2002.

[62] G. H. Yang and D. Ye, “Adaptive fault tolerant $H_\infty$ control via dyanmic output feedback for linear system against actuator faults,” *In Proceedings of the 45$^{th}$ IEEE Conference on Decision & Control*, pp. 3524-3529, San Diego, CA, USA, Dec. 2006.

[63] R. Marino, S. Peresada, and P. Valigi, “Adaptive input-output linearizing control of induction motors,” *IEEE Trans. Autom. Contr.*, vol. 38, no. 2, pp. 208-221, Feb. 1993.

[64] A. Fekin and F. N. Chowdhury, “A fault tolerant control design for induction motors,” *2005 IEEE Int. Conf Systems Man. and Cybernetics*, vol. 2, pp. 1320-1325. Oct. 2005.

[65] J. A. Farooq, A. Djerdir and A. Miraoui, “Modeling and simulation of stator winding inter-turn faults in permanent magnet synchronous motors,” *COMPEL-Int. J. Comput. Math. Elect. Eletron. Eng.*, vol. 27, no. 4, pp. 887-896,2008.

[66] Jesper S. Thomsen and Carsten S. Kallesøe, “ Stator fault modeling of induction motors,” *IEEE Int. Symposium on Power Electronics, Eletrical Drives, Automation and Motion*, pp.1275-1280, 2006.

[67] X. Cheng, V. Cocquempot and C. Christophe, “A model of asynchronous machine for stator fault detection and isolation,” *IEEE Trans. Ind. Eletron.*, vol. 50, no. 3, pp. 578-584, Jun. 2003.

[68] M. Arkan, D. Kostic-Perovic and P. J. Unworth, "Modeling and simulation of induction motors with inter-turn faults for diagnostics," *Eletr. Power Sys. Res.*, vol. 75, no. 1, pp. 57-66, Jul. 2005.

[69] Q. F. Lu, Z. T. Cao and E. Ritchie, "Modeling of stator inter-turn short circuit fault in doubly-fed induction generators for wind turbine," *35th Annual IEEE Power Electronics Specialists Conference*, Aachen, Germany, 2004, pp. 932-937.

[70] H. Douglas, P. Pillay, P. Barendse, "The detection of inter-turn stator faults in doubly-fed induction generators," *In Proceeding of IEEE Industry Applications Conference*, vol. 2, pp. 1097-1102, Oct. 2003.

[71] G. Joksimovic and J. Penman, "The detection of inter-turn short circuit in stator windings of operating motors," *IEEE Trans. Ind. Eletron.*, vol. 47, no. 5, Oct. 2000.

[72] Y. Gritli, A. Stefani, F. Filippetti and A. Chatti, "Stator fault analysis based on wavelet technique for wind turbines equipped with DFIG," *In Proceeding of IEEE International Conference on Clean Electrical Power*, Capri, Italy, June 2009, pp. 485-491.

[73] S. Bachir et al., "Diagnosis by parameter estimation of stator and rotor fault occuring induction machines, " *IEEE Trans. Ind. Eletron.*, vol. 53, no. 3, pp. 963-973, Jun. 2006.

[74] F. Bagheri, H. Khaloozaded, K. Abbaszadeh, "Stator fault detection in induction machnies by parameter estimation, using adaptive kalman filter," *In Proceding of the 15$^{th}$ Mediterranean Conference on Control & Automation*, July 2007, Athens, Greece.

[75] C. S. Kallesøe, H. Rasmussen, P. Vadstrup, and R. Izadi-Zamanabadi, "Estimation of stator winding faults in induction motors using an adaptive observer scheme," *Proceedings of the IEEE 39$^{th}$ IAS Annual Meeting*, Seattle, Washington, 2004.

[76] C. H. De Angelo, G. R. Bossio, S. J. Giaccone, M. I. Valla, J. A. Solsona, and G. O. Garcia, "Online model based stator fault detection and identification in

induction motors," *IEEE Trans. Ind. Electron.*, vol. 56, no. 11, pp. 4671-4680, Nov. 2009.

[77] V. Dinkhauser and F. W. Fuchs, "Detection of rotor turn-to-turn faults in doubly fed induction generator in wind energy plants by means of observers," *Power Electronics and Motion Control Conference, 2008. EPE-PEMC 2008.* 13th, pp. 1819-1826, Spet. 2008.

[78] H. Wang and S. Daley, "Actuator fault diagnosis: an adaptive observer based technique," *IEEE Trans. Automat. Contr.*, vol. 41, no. 7, July 1996.

[79] Q. Zhang, "Adaptive observer for multiple-input-multiple output (MIMO) linear time-varying systems," *IEEE Transaction on Automatic Control*, vol. 47, issue 3, pp. 525-529, 2002.

[80] J. Cusido, L. Romeral, J.A. Ortega, J.A. Rosero, and A. Garcia Espinosa, "Fault detection in induction machines using power spectral density in wavelet decomposition," *IEEE Trans. Ind. Electron.*, vol. 55, no. 2, pp. 633-643, Feb. 2008.

[81] W. Q. Wilson, F. Ismail and M. F. Golnaragh, "Assessment of gear damage monitoring techniques using vibration measruements," *Mechanical Systems and Signal Processing*, vol. 15, pp. 905-922, 2001.

[82] Z. K. Peng and F. L. Chu, "Application of the wavelet transform in machnie condition monitoring and fault diagnositics: a review with bibliography," *Mechanical System and Signal Processing*, vol. 18, pp. 199-221, 2004.

[83] A. R. Mohanty and C. Kar, "Fault detection in a multistage gearbox by demodulation of motor curent waveform," *IEEE Transanction on Industrial Electronics*, vol. 53, issue. 4, pp. 1285-1297, Aug. 2006.

[84] L. Eren and MJ, Devaney, "Bearing damag detection via wavelet packet decomposition of stator current," *IEEE Transactions on Instrumentation & Measurement*, vol. 53, issue. 2, pp. 431-436, April, 2004.

[85] M. Benbouzid, "A review of induction motors signature analysis as a medium for faults detection," *IEEE Transaction on Industrial Electronics*, vol.47, issue. 5, pp. 984-993, Oct. 2006.

[86] M. Benbouzid and G. Kliman, "What stator current processing based techinique to use for induction motor rotor fault diagnosis?," *IEEE Transactions on Energy Conversion*, vol. 18, issue. 2, pp. 238-244, June, 2003.

[87] D. Casadei, F. Filippetti, A. Stefani, C. Rossi, A. Yazidi, and GA. Capolino, "Diagnostic technique based on rotor modulating signals signature analysis for doubly fed induction machnies in wind generator system, " *In Proceeding of IEEE IAS'06*, pp. 1525-1532, 2006.

[88] D. Casadei, F. Filippetti, A. Stefani, C. Rossi , A. Yazidi, and GA. Capolino, "Experimental fault characterization of doubly fed induction machine for wind power generation," *In Proceedings of IEEE SPEEDAM'06*, pp. 281-286, 2006.

[89] S. F. Legowski, A.H.M. Sadrul Ula, A. M. Trzynadlowski, "Instantaneous power as a medium for the signature analysis of induction motors," *IEEE Transactions on Industry Applications*, vol. 32, no. 4, Julu/August, 1996.

[90] M. Arkan, D.K. Perovic, and P. Unsworth, "Online stator fault diagnosis in induction motor, " *Prc. Inst. Elect. Eng.—Elect. Power Appl.*, vol. 148, no. 6, pp. 632-637, Nov, 2001.

[91] R. M. Tallam and T. G. Habetler, "Transient model for induction machines with stator winding turn faults," *IEEE Trans. on Application*. vol. 38, pp. 632-637, June 2002.

[92] S.B. Lee, R. Tallam, and T. Habetler, "A robust, online turn fault detection technique for induction machnies based on monitoring the sequence component inpendance matrix," *IEEE Trans. Power Electron.*, vol. 18, no.3, pp. 865-872, May 2003.

[93] S. Cruz and A Cardoso, "Multiple reference frames theory: A new method for the diagnosis of stator fautls in three-phase induction motors," *IEEE Trans. Energy Convers*., vol. 20, no. 3, pp. 611-619, Spe. 2005.

[94] S. Cruz and A Cardoso, "Diagnosis of Stator Inter-Turn Short Circuits in DTC Induction motor Drives," *IEEE Trans. Ind. Appl*., vol. 40, no. 5, pp. 1349-1360, Sep./Oct. 2004

[95] K. S. Gaeid and H. W. Ping, " Wavelet fault diagnosis and tolerant of induction motor: A review," *International Journal of the Physical Science*, vol. 6, no. 3, pp.358-376, Feb. 2011.

[96] M. B. K. Bouzis, G. Champenois, N. M. Bellaaj, L. Signax, and K. Jelassi, "An effective neural approach for the automatic location of stator interturn faults in induction motor," *IEEE Trans. Ind. Electron*., vol. 55, no. 12, pp. 4277-4289, Dec. 2008.

[97] M. S. Ballal, Z. J. Khan, H. M. Suryawanshi, and R. L. Sonolikar, "Adaptive neural fuzzy inference system for the detection of interturn insulation and bearing wear faults in induction motor," *IEEE Trans. Ind. Electron.*, vol. 54, no. 1, pp250-258, Feb. 2007.

[98] M. C. Garcia, M. A. Sanz-Bobi, and J. Pico, "SIMAP: Intelligent System for Predictive Maintenance: Application to the health condition monitoring of a wind turbine gearbox," *Computers In Industry*, vol. 57, issue. 6, pp. 552-568, Aug. 2006.

[99] C. Bonivento, A. Isidori, L. Marconi, and A. Paoli, "Implicit fault tolerant control: application to idncution motors," *Automatica*, vol. 40, issue. 3, pp. 355-371, March 2004.

[100] V. Kešić, M. Vašak, N. Perić, T. Wolbank, and G. Joksimović, "Fault tolerant control of a blade-pitch wind turbine with inverter-fed generator," *Proceedings of IEEE International Symposium on Industrial Electronics*, ISIE, Jun. 2011.

[101] K. Rothenhagen and F. W. Fuchs, "Doubly fed induction generator model-based sensor fault detection and control loop reconfiguration," *IEEE Trans. Ind. Electron.* vol. 54, no. 10, Oct. 2009.

[102] K. Rothenhagen and F. W. Fuchs, "Current sensor fault detection by bilinear observer for a doubly fed induction generator," *IECON'06*, Paris, France. CD-ROM Paper

[103] D. W. Novotny and T. A. Lipo, *Vector Control and Dynamics of AC Drives*, New York: Oxford Univ, Press, 1996.

[104] P. Gahinet and P. Apkarian, "A linear matrix inequality approach to $H_\infty$ Control," *Int. J. Robust and Nolinear Contr.*, vol. 4, pp. 421-448, 1994.

[105] P. Apkarian, P. Gahinet and G. Becker, "Self-scheduled $H_\infty$ Control of linear parameter –varying systems: a design example," *Automatica*, vol. 31, no. 9, pp. 1251-1261, 1995.

[106] M. O. Abdalla, E. G. Nobrega, and K. M. Grigoriadis, "Fault detection and isolation filter design for linear parameter varying systems," *Proceedings of Americal Control Conference*, Arlington, VA, June 2001.

[107] L. Xu and Y. Wang, "Dynamic modeling and control of DFIG based wind turbines under unbalanced network conditions," *IEEE Trans. Power Systems*, vol. 22, no. 1, Feb. 2007.

[108] A. Xu and Q. Zhang, "Nonlinear system fault diagnosis based on adaptive estimation," *Automatica*, vol. 40, issue. 7, pp. 1181-1193, July 2004.

[109] H. Hammouri and J. D. Leon-Morales, "Observer synthesis for the state affine system, ", *In Proc. of the 29th IEEE Conf. Dec. and Control*, Honolulu, HI, pp. 784-785, 1990.

[110] G. Beasancon, H. Hammouri and G. Bornard, "Observer synthesis for a class of nonlinear control system," *Eurpean Journal of Control*, vol. 2, pp. 176-192, 1996.

[111] I. Howard, S. Jia, and J. Wang, "The dynamic modeling of a spur gear in mesh including friction and a crack," *Mechanical System and Signal Processing*, vol. 15, issue. 5, pp. 831-853, 2001.

[112] C. D. Begg, T. Merdes, C. Byington, and K. Maynard, "Dyanmic modeling for mechanical fault diagnostics and prognostics," *Maintenance and Reliability Conference, 1999. MARCON99.*

[113] B. D. Anderson, R. R. Bitmead, C. R. Johnson, P.V. Kokotovic, R. L. Kosut, I. M. Mareels, L. Praly, and B. D. Riedle, *Stability of Adaptive Aystems: Passivity and Averaging Analysis*, ser. Signal Processing, Optimization, and Control. Cambridge, MA: MIT Press, 1986.

[114] M. L. Benloucif and H. Balaska, “Robust detection for an induction machine,” *World Automation Congress WAC’06*, Budapest, 2006.

[115] G. G. Rigatos, *Modelling and control for intelligent industrial systems*, Springer-Verlag Berlin, 1998

[116] W. Yang, P.J. Tavner, M. R. Wilkinson, “Condition monitoring and fault diagnosis of a wind turbine synchronous generator drive train,” *IET Renewable Power Generation*, vol. 3, no. 1, pp. 1-11, Mar. 2009.

[117] Y. Zhao and T. A. Lipo, “Modeling and control of a multi-phase induction machine with structural unbalance,” *IEEE Transactions on Engergy Conversion*, vol. 3, no. 3, September, 1996.

[118] G. Lüders and K. S. Narendra, “An adaptive observer and identifier for a linear system,” *IEEE Trans. Automat. Contr.*, vol. AC-18, pp. 496-499, Oct. 1973.

# Appendix A. DFIG Wind Turbine Parameters

## Wind Turbine Parameters

Rated power: 2MW;

moment of the inertia: $J$ = 2 kg.m$^2$

Wind turbine radius: $R_{wt}$ = 35m

Gear box ratio: $N_g$ = 120

Air density: $\rho$ = 1.25 kg/m$^3$

Cut-in wind speed: $\upsilon_{w\_cin}$ = 3.8 m/s

Cut-out wind speed: $\upsilon_{w\_cout}$ = 25 m/s

Rated wind speed: $\upsilon_{w\_rat}$ = 12 m/s

the power coefficient $C_p(\lambda,\beta)$ is given as

$$C_p(\lambda,\beta) = 0.5176\left(\frac{116}{\lambda_i} - 0.4\beta - 5\right)e^{\frac{-21}{\lambda_i}} + 0.0068\lambda$$

with

$$\frac{1}{\lambda_i} = \frac{1}{\lambda + 0.08\beta} - \frac{0.035}{\beta^3 + 1}$$

## DFIG Parameters

Rated power: 2MW

Rated stator frequency: $f_s$ = 50 Hz

Rated stator phase voltage: $v_s$ = 130 V

Mutual inductance: $L_m$ = 44.2 mH

Stator leakage inductance: $L_{s\sigma}$ = 673.97 μH

Rotor leakage inductance: $L_{r\sigma}$ = 490.60 μH

Stator resistance: $r_s$ = 45 mΩ

Rotor resistance: $r_r$ = 66.5 mΩ

Number of pole pairs: $p$ = 2

# Appendix B. Theorem and Lemma

## B.1 Lyapunov Stability Theory:

Lyapunov stability theroy or called Lyapunov sencond method is the most powerful approach for analyzing the stability of the dyanmic system. This approach is a generalization of the engery concepts associated with a mechanical system. Before presenting the central theorem, some important definitions are introduced firstly.

**Definition 1:** The equilibrim point $x = 0$ of system $\dot{x} = f(x)$ is said to be stable if, for each $\varepsilon > 0$, there is $\delta = \delta(\varepsilon)$ such that

$$\|x(0)\| < \delta \Rightarrow \|x(t)\| < \varepsilon, \forall t \geq 0$$

**Definition 2:** An equilibrium point $x = 0$ of system $\dot{x} = f(x)$ is asymptotically stable if it is stable and $\delta$ can be chosen such that

$$\|x(0)\| < \delta \Rightarrow \lim_{t\to\infty} x(t) = 0$$

**Theorem:** Let $x = 0$ be an equilibrium point for $\dot{x} = f(x)$ and $D \subset R^n$ be a domain containing $x = 0$. Let $V : D \to R$ be a continously differentiable function such that

$$V(0) = 0 \text{ and } V(x) > 0 \text{ in } D - \{0\}$$

$$\dot{V}(x) \leq 0 \text{ in } D$$

Then, $x(0)=0$ is stable. Moreover, if

$$\dot{V}(x)<0 \text{ in } D-\{0\}$$

Then $x(0)=0$ is asymptotically stable.

## B.2. Barbalat's Lemma:

If a function $f(t)$ is uniformly continous for $t\in[0,\infty]$, and $\int_0^\infty f(t)dt$ exists, then $\lim_{t\to\infty} f(t)=0$.

## B.3. SPR Condition and Kalman -Yakubovic Lemma:

**Definination 3:** Positive Real Systems:

Consider a dynamic system

$$\dot{x}=Ax+bu$$
$$y=c^Tx$$

with its transfer function matrix is given by

$$G(s)=c^T(sI-A)^{-1}b$$

Such system is said to be positve real if

$$\Re\big(G(s)\big)\geq 0 \text{ for all } \Re\big(s\big)\geq 0$$

It is strictly positive real if $G(s-\varepsilon)$ is positive real for some $\varepsilon>0$

## Kalman -Yakubovic Lemma:

This system given above is strictly positve real if and only if there exist positive defiinte $P$ and $Q$ such that

$$A^TP+PA=-Q$$

$$Pb=C$$

# Appendix C. Simulation Parameters of Chapter 4

## C.1 Model Parameter Matrices:

Positive-Sequence Model

$$A^{+}=\begin{bmatrix} -21 & 9044.3 & 53.9 & 8928.4 \\ -9044.3 & -21 & -8928.4 & 53.9 \\ 20.5 & -8818.9 & -54.4 & -8705.0 \\ 8818.9 & 20.5 & 8705.0 & -54.4 \end{bmatrix},\quad B_f{}^{+}=\begin{bmatrix} 14 & -6029.5 \\ 6029.5 & 14 \\ -13.7 & 5879.3 \\ -5879.3 & -13.7 \end{bmatrix}$$

Negative-Sequence Model

$$A^{-}=\begin{bmatrix} -21 & 8416.0 & 53.9 & 8928.4 \\ -8416.0 & -21 & -8928.4 & 53.9 \\ 20.5 & -8818.9 & -54.4 & -9333.3 \\ 8818.9 & 20.5 & 9333.3 & -54.4 \end{bmatrix},\quad B_f{}^{-}=\begin{bmatrix} 14 & -5610.7 \\ 5610.7 & 14 \\ -13.7 & 5879.3 \\ -5879.3 & -13.7 \end{bmatrix}$$

The input and output matrices for both of these models are the same

$$B^{+(-)}=\begin{bmatrix} 465.9 & 0 & -455.6 & 0 \\ 0 & 465.9 & 0 & -455.6 \\ -455.6 & 0 & 460.3 & 0 \\ 0 & -455.6 & 0 & 460.3 \end{bmatrix},\quad C^{+(-)}=\mathbf{I}_4$$

## C.2. Parameters of Conventional Adaptive Observer

The observer parameters for the positive-sequence model

$$L=\begin{bmatrix} 29.0 & 9044.3 & 53.9 & 8928.4 \\ -9044.3 & 29.0 & -8928.4 & 53.9 \\ 20.5 & -8818.9 & -4.4 & -8705.0 \\ 8818.9 & 20.5 & 8705.0 & -4.4 \end{bmatrix},\quad \Gamma=0.001\times\mathbf{I}_2$$

The observer parameters for the negative-sequence model

$$L=\begin{bmatrix} 29.0 & 8416.0 & 53.9 & 8928.4 \\ -8416.0 & 29.0 & -8928.4 & 53.9 \\ 20.5 & -8818.9 & -4.4 & -9333.3 \\ 8818.9 & 20.5 & 9333.3 & -4.4 \end{bmatrix},\quad \Gamma=0.005\times\mathbf{I}_2$$

## C.3. Parameters of Optimal Adaptive Observer

The observer parameters for the positive-sequence model

$$P=\begin{bmatrix} 0.4730 & -0.000 & 0.4636 & -0.000 \\ -0.000 & 0.4730 & -0.000 & 0.4636 \\ 0.4636 & -0.000 & 0.4744 & -0.000 \\ -0.000 & 0.4636 & -0.000 & 0.4744 \end{bmatrix},$$

$$X=\begin{bmatrix} 47.7437 & -0.0088 & -6.0847 & 125.7217 \\ 0.0088 & 47.7437 & -125.6516 & -7.2768 \\ -8.4132 & -125.7859 & 46.9856 & 0.0260 \\ 125.7157 & -7.2212 & -0.0260 & 46.9856 \end{bmatrix}$$

$$L=\begin{bmatrix} 2.8000 & 6.1494 & -2.6016 & 6.2888 \\ -6.1460 & 2.7417 & -6.2853 & -2.6613 \\ -2.7540 & -6.2744 & 2.6414 & -6.1454 \\ 6.2709 & -2.6945 & 6.1420 & 2.6997 \end{bmatrix}\times 10^{3}$$

$$\Gamma_1=\begin{bmatrix} 2.0041 & 0.000 \\ 0.000 & 2.0041 \end{bmatrix},\ \Gamma_2=\begin{bmatrix} -0.3019 & -137.7699 & 0.0909 & 31.3197 \\ 137.7699 & -0.3019 & -31.3197 & 0.0909 \end{bmatrix}$$

The observer parameters for the negative-sequence model

$$P=\begin{bmatrix} 0.4730 & -0.000 & 0.4636 & -0.000 \\ -0.000 & 0.4730 & -0.000 & 0.4636 \\ 0.4636 & -0.000 & 0.4744 & -0.000 \\ -0.000 & 0.4636 & -0.000 & 0.4744 \end{bmatrix},$$

$$X=\begin{bmatrix} 47.7437 & 0.0776 & -14.1395 & 126.0484 \\ -0.0776 & 47.7437 & -125.9417 & -2.0898 \\ -0.3584 & -125.4958 & 46.9856 & 0.1047 \\ 125.3891 & -12.4082 & -0.1047 & 46.9856 \end{bmatrix}$$

$$L=\begin{bmatrix} 2.4062 & 6.1396 & -3.0046 & 6.3013 \\ -6.1343 & 2.9953 & -6.2959 & -2.4017 \\ -2.3521 & -6.2642 & 3.0352 & -6.1575 \\ 6.2589 & -2.9532 & 6.1523 & 2.4461 \end{bmatrix}\times 10^{3}$$

$$\Gamma_1=\begin{bmatrix} 2.0041 & 0.000 \\ 0.000 & 2.0041 \end{bmatrix},\ \Gamma_2=\begin{bmatrix} -0.3019 & 60.3658 & 0.0909 & 225.5079 \\ -60.3658 & -0.3019 & -225.5079 & 0.0909 \end{bmatrix}$$

## C.4. Parameters of LPV Adaptive Observer:

The observer parameters for the positive-sequence model are

$$P=\begin{bmatrix} 0.8543 & 0.000 & 0.8455 & 0.000 \\ 0.000 & 0.8543 & 0.000 & 0.8455 \\ 0.8455 & 0.000 & 0.8372 & 0.000 \\ 0.000 & 0.8455 & 0.000 & 0.8372 \end{bmatrix},$$

$$X_1=\begin{bmatrix} 394.7737 & 0.0019 & 29.1506 & 2.2511 \\ -0.0019 & 394.7737 & -2.2502 & 28.5731 \\ 28.0659 & -2.2522 & 394.7700 & 0.0033 \\ 2.2513 & 28.6434 & -0.0033 & 394.7700 \end{bmatrix}$$

$$X_2 = \begin{bmatrix} 394.7737 & 0.005 & 28.4748 & 4.1837 \\ -0.005 & 394.7737 & -4.1726 & 28.7648 \\ 28.7417 & -4.1890 & 394.7700 & 0.0033 \\ 4.1778 & 28.4517 & -0.0017 & 394.7700 \end{bmatrix}$$

$$L_1 = \begin{bmatrix} 7.6390 & 0.0475 & -7.7033 & 0.0469 \\ -0.0474 & 7.6269 & -0.0468 & -7.7154 \\ -7.7141 & -0.0479 & 7.7840 & -0.0473 \\ 0.0479 & -7.7018 & 0.0473 & 7.7962 \end{bmatrix} \times 10^5$$

$$L_2 = \begin{bmatrix} 7.6248 & 0.0882 & -7.7174 & 0.0872 \\ -0.0880 & 7.6309 & -0.0870 & -7.7114 \\ -7.6997 & -0.0891 & 7.7983 & -0.0880 \\ 0.0889 & -7.7059 & 0.0878 & 7.7922 \end{bmatrix} \times 10^5$$

$$\Gamma_1 = \begin{bmatrix} 2.0246 & -0.000 \\ -0.000 & 2.0246 \end{bmatrix}, \quad \Gamma_2 = \begin{bmatrix} -0.3870 & -180.9491 & -0.3739 & -174.8402 \\ 180.9491 & -0.3870 & 174.8402 & -0.3739 \end{bmatrix}$$

The observer parameters for the negative-sequence model are

$$P = \begin{bmatrix} 0.8543 & 0.000 & 0.8455 & 0.000 \\ 0.000 & 0.8543 & 0.000 & 0.8455 \\ 0.8455 & 0.000 & 0.8372 & 0.000 \\ 0.000 & 0.8455 & 0.000 & 0.8372 \end{bmatrix},$$

$$X_1 = \begin{bmatrix} 394.7737 & 0.0061 & 29.19097 & 2.2647 \\ -0.0061 & 394.7737 & -2.2504 & 28.3519 \\ 28.1068 & -2.2520 & 394.7700 & -0.0005 \\ 2.2377 & 28.8646 & -0.0005 & 394.7700 \end{bmatrix}$$

$$X_2 = \begin{bmatrix} 394.7737 & 0.0005 & 28.3735 & 4.1832 \\ -0.0005 & 394.7737 & -4.1772 & 28.0037 \\ 28.8431 & -4.1843 & 394.7700 & -0.0029 \\ 4.1783 & 28.2128 & 0.0029 & 394.7700 \end{bmatrix}$$

$$L_1 = \begin{bmatrix} 7.6382 & 0.0475 & -7.7042 & 0.0472 \\ -0.0474 & 7.6269 & -0.0469 & -7.7200 \\ -7.7132 & -0.0480 & 7.7849 & -0.0477 \\ 0.0477 & -7.6971 & 0.0474 & 7.8008 \end{bmatrix} \times 10^5$$

$$L_2 = \begin{bmatrix} 7.6227 & 0.0881 & -7.7195 & 0.0873 \\ -0.0880 & 7.6149 & -0.0871 & -7.7272 \\ -7.6975 & -0.0890 & 7.8004 & -0.0881 \\ 0.0889 & -7.6897 & 0.0880 & 7.8082 \end{bmatrix} \times 10^5$$

$$\Gamma_1 = \begin{bmatrix} 2.0246 & -0.000 \\ -0.000 & 2.0246 \end{bmatrix}, \quad \Gamma_2 = \begin{bmatrix} -0.3870 & -176.9057 & -0.3739 & 179.3195 \\ -176.9057 & -0.3870 & -179.3195 & -0.3739 \end{bmatrix}$$

# Appendix D. Simulation Parameters of Chapter 5

## D.1 Model Parameter Matrices

$$A=\begin{bmatrix} -0.0210 & 9.0443 & 0.0539 & 8.9284 & -0.0458 & -8.7302 & -0.0539 & -8.9284 \\ -9.0443 & -0.0210 & -8.9284 & 0.0539 & 8.7302 & -0.0458 & 8.9284 & -0.0539 \\ 0.0205 & -8.8189 & -0.0544 & -8.7050 & -0.0205 & 8.8189 & -0.0241 & 8.7302 \\ 8.8189 & 0.0205 & 8.7050 & -0.0544 & -8.8189 & -0.0205 & -8.7302 & -0.0241 \\ 0 & 0 & 0 & 0 & -0.0668 & 0.3142 & 0 & 0 \\ 0 & 0 & 0 & 0 & -0.3142 & -0.0668 & 0 & 0 \\ 0 & 0 & 0 & 0 & 0 & 0 & -0.0785 & 0.0252 \\ 0 & 0 & 0 & 0 & 0 & 0 & -0.0252 & -0.0785 \end{bmatrix}\times 10^{3}$$

$$B=\begin{bmatrix} 465.9745 & 0 & -455.6284 & 0 \\ 0 & 465.9745 & 0 & -455.6284 \\ -455.6284 & 0 & 460.2600 & 0 \\ 0 & -455.6284 & 0 & 460.2600 \\ 0 & 0 & 0 & 0 \\ 0 & 0 & 0 & 0 \\ 0 & 0 & 0 & 0 \\ 0 & 0 & 0 & 0 \end{bmatrix}$$

$$B_f=\begin{bmatrix} 1.4838 & 0 & 0 & 0 \\ 0 & 1.4838 & 0 & 0 \\ 0 & 0 & 0.6642 & 0 \\ 0 & 0 & 0 & 0.6642 \\ 1.4838 & 0 & 0 & 0 \\ 0 & 1.4838 & 0 & 0 \\ 0 & 0 & 0.6642 & 0 \\ 0 & 0 & 0 & 0.6642 \end{bmatrix}\times 10^{3},\quad C=[\mathbf{I}_4 \quad \mathbf{0}_{4\times 4}]$$

## D.2. Parameters of Modified Adaptive Observer

$$L = \begin{bmatrix} 255.3225 & -0.0000 & 258.8691 & -1.7369 \\ -0.0000 & 255.3225 & 1.7369 & 258.8691 \\ 258.8691 & 1.7369 & 262.5263 & -0.0000 \\ -1.7369 & 258.8691 & -0.0000 & 262.5263 \\ -127.5714 & 62.2275 & -130.9402 & 64.7242 \\ -62.2275 & -127.5714 & -64.7242 & -130.9402 \\ -25.1876 & -25.4748 & -24.0889 & -25.1501 \\ 25.4748 & -25.1876 & 25.1501 & -24.0889 \end{bmatrix}$$

## D.3. Parameters of High Gain Adaptive Observer

$$L = \begin{bmatrix} 960.6761 & 0.0000 & -72.9386 & -1.4108 \\ 0.0000 & 960.6761 & 1.4108 & -72.9386 \\ -72.9386 & 1.4108 & 997.9687 & -0.0000 \\ -1.4108 & -72.9386 & -0.0000 & 997.9687 \\ 455.1090 & -677.8991 & 538.6715 & -758.8843 \\ 677.8991 & 455.1090 & 758.8843 & 538.6715 \\ 436.5899 & 691.6251 & 398.7353 & 733.3644 \\ -691.6251 & 436.5899 & -733.3644 & 398.7353 \end{bmatrix}$$